Mogens Blanke, Michel Kinnaert,
Jan Lunze and Marcel Staroswiecki

Diagnosis and Fault-Tolerant Control

Figures

September 2015

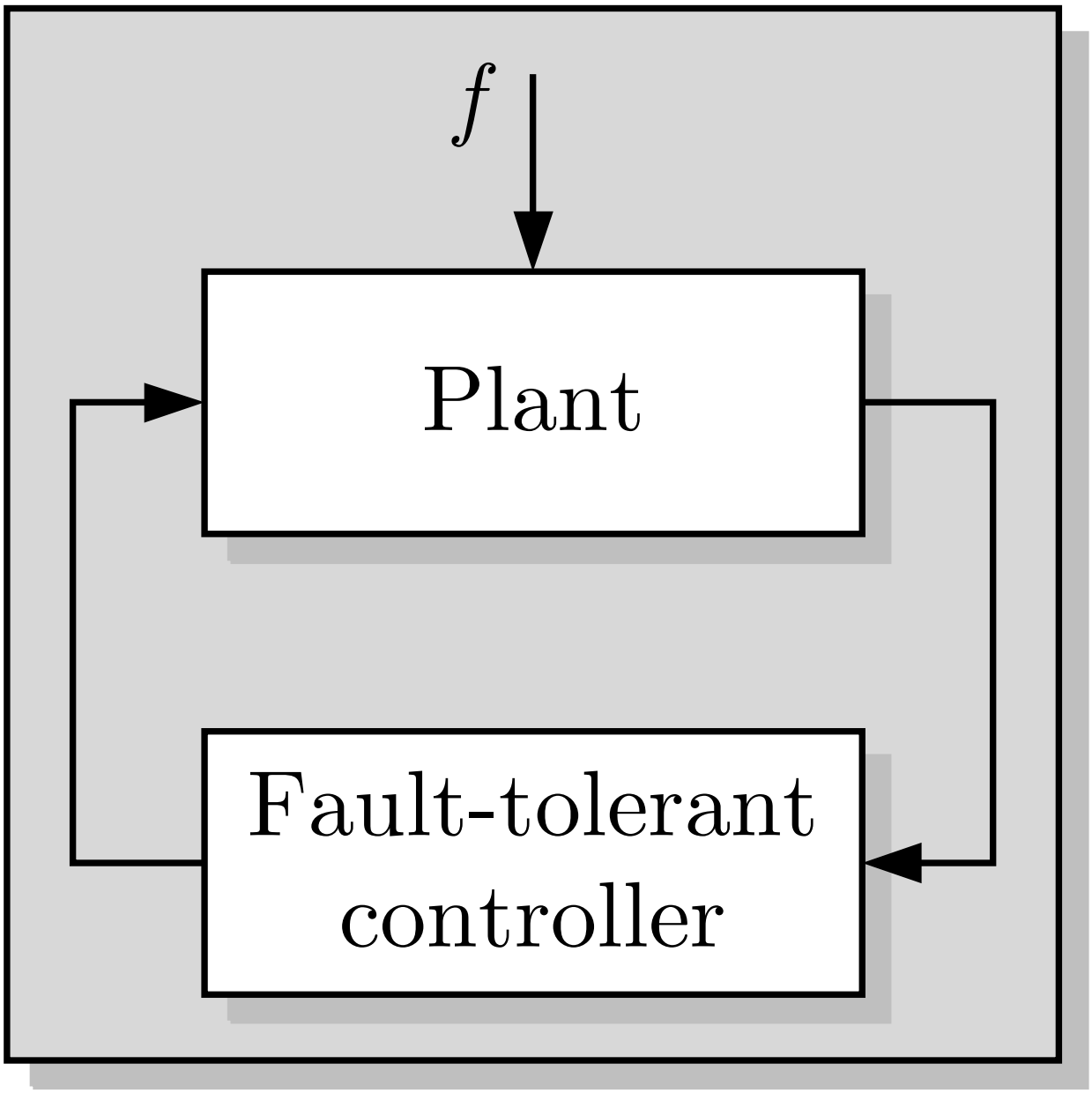

Fig. 1.1. Fault-tolerant system

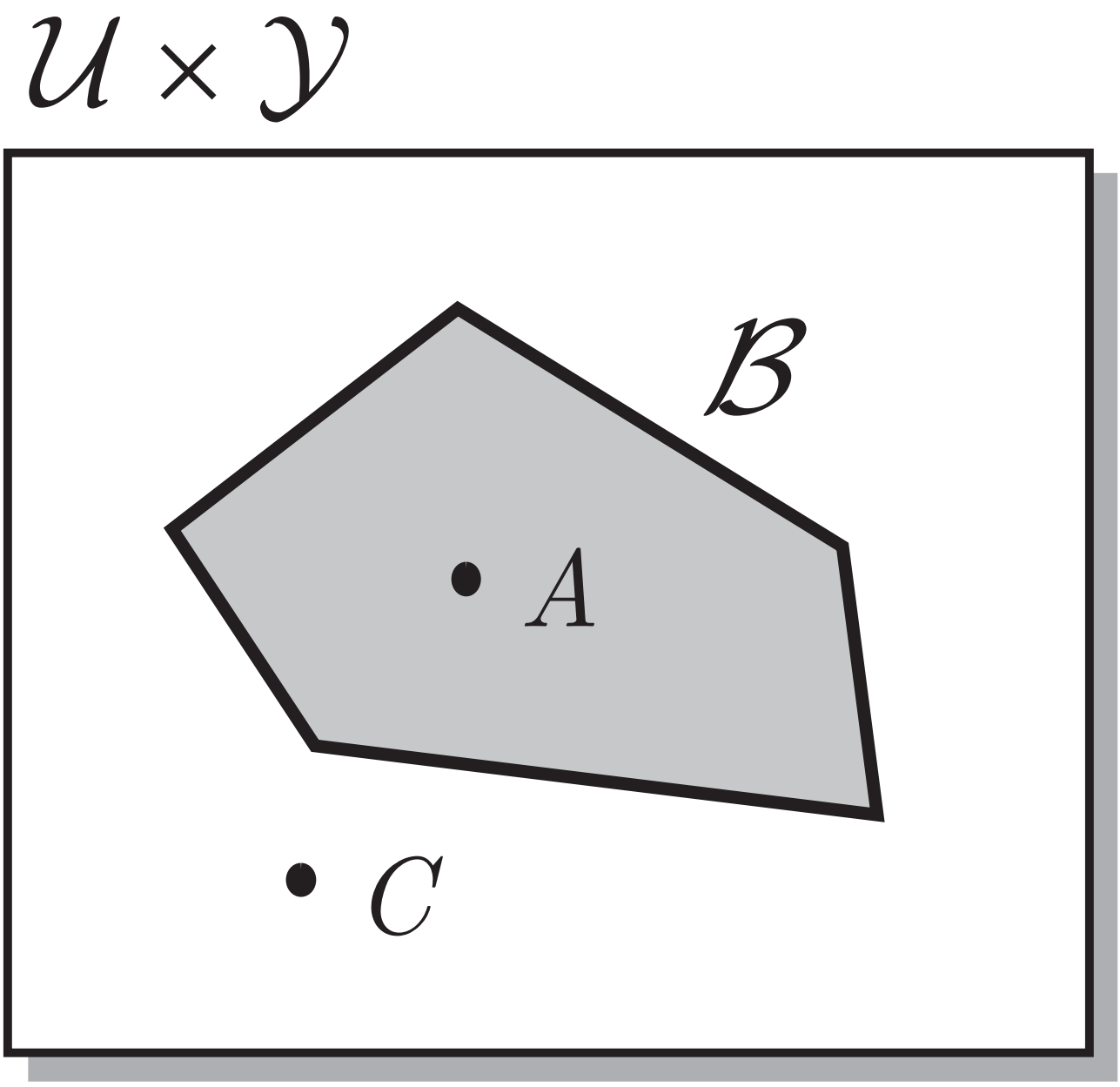

Fig. 1.2. Graphical illustration of the system behaviour

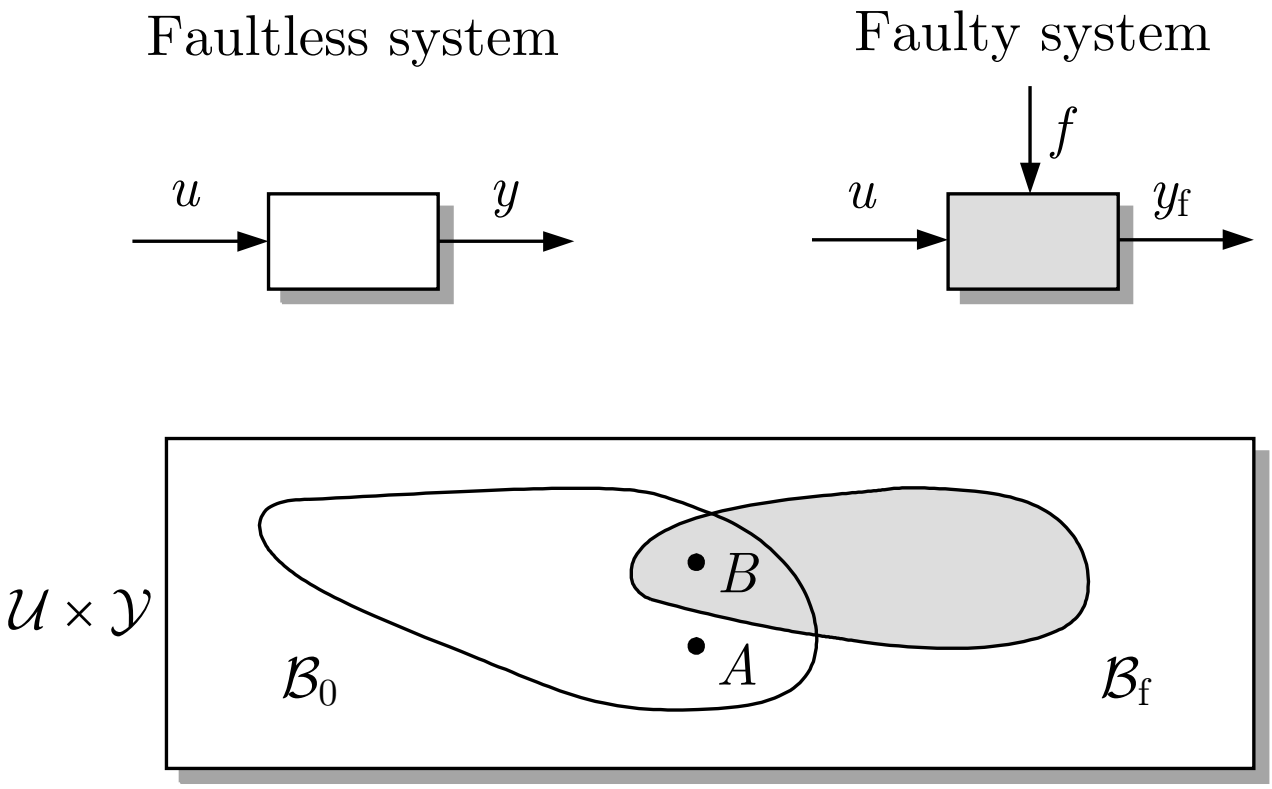

Fig. 1.3. System subject to faults

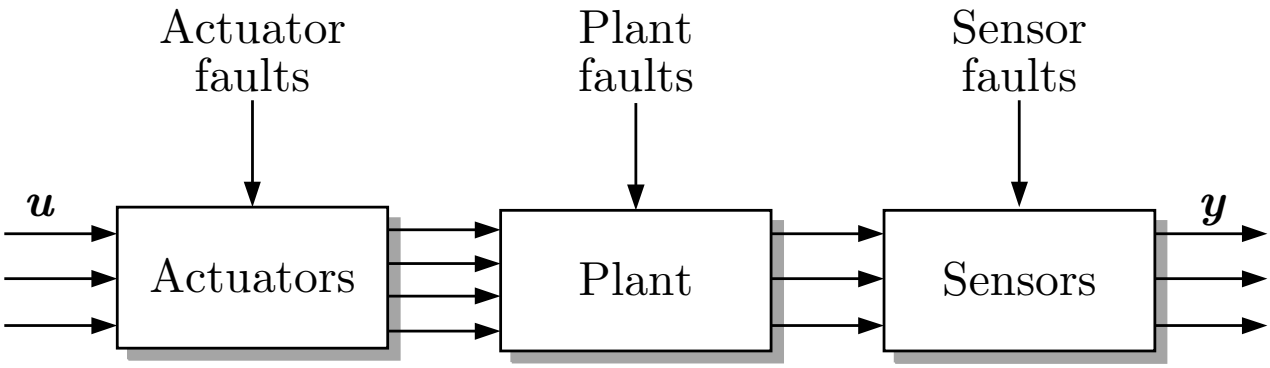

Fig. 1.4. Distinction between actuator faults, plant faults and sensor faults

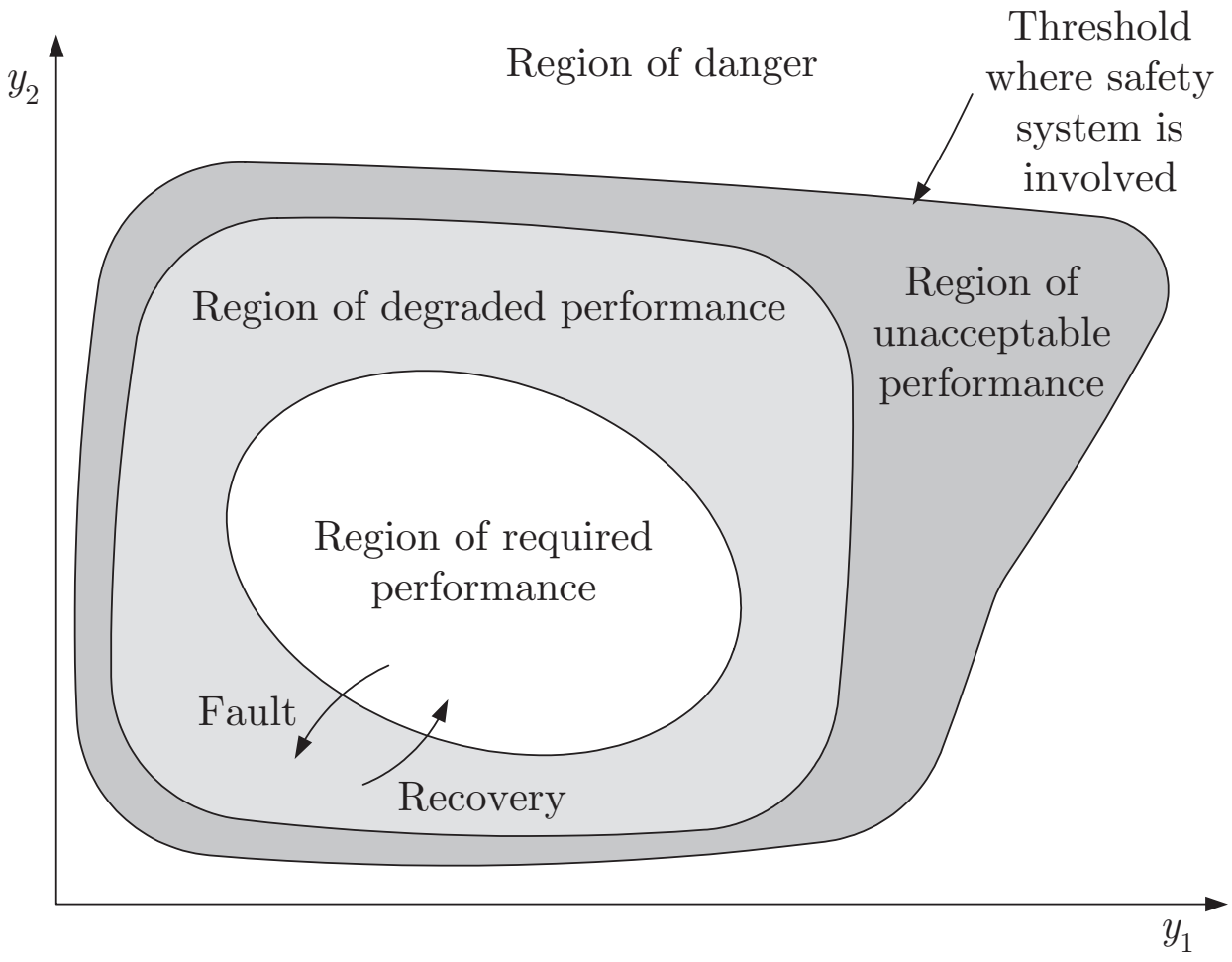

Fig. 1.5. Regions of required and degraded performance

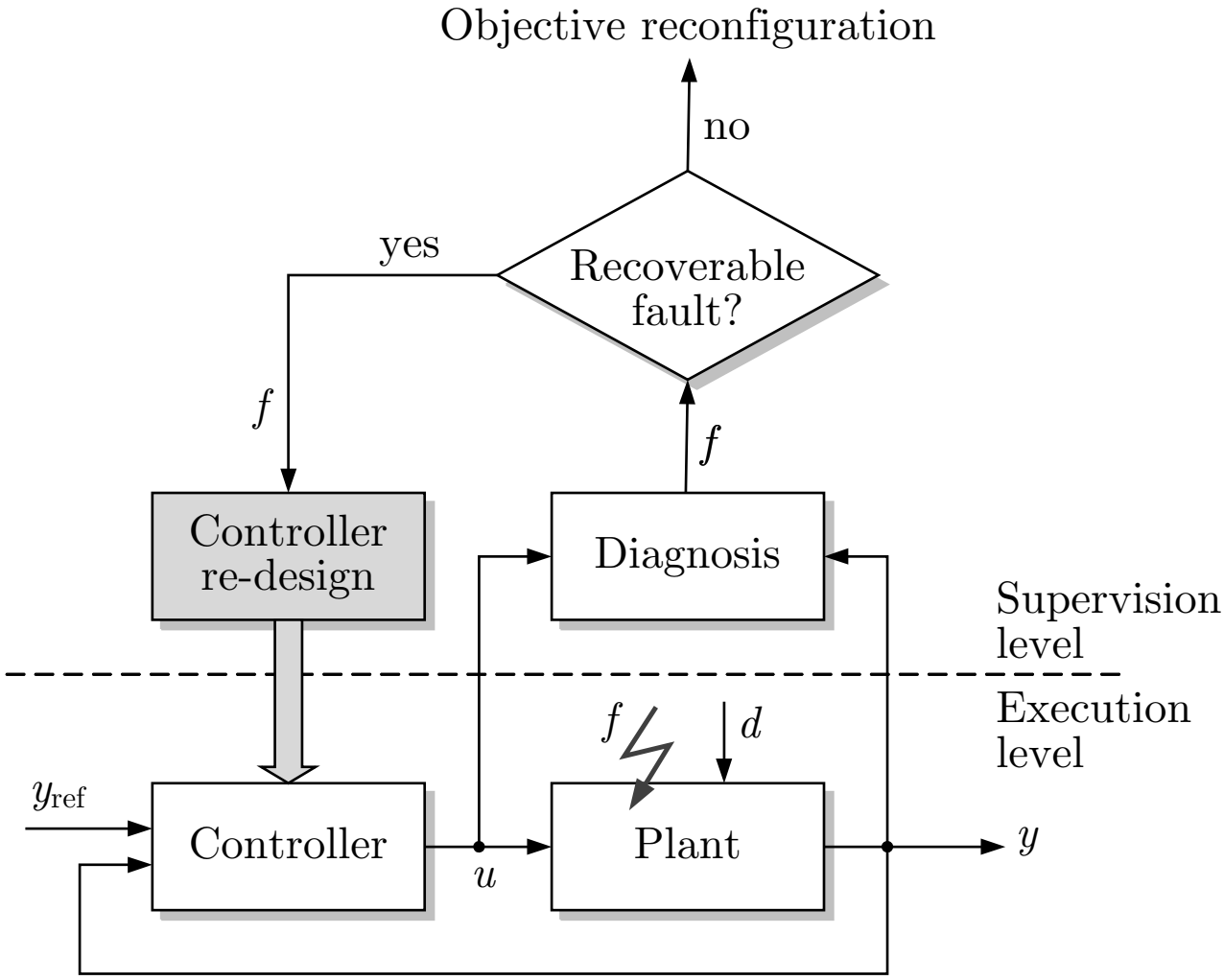

Fig. 1.6. Architecture of fault-tolerant control

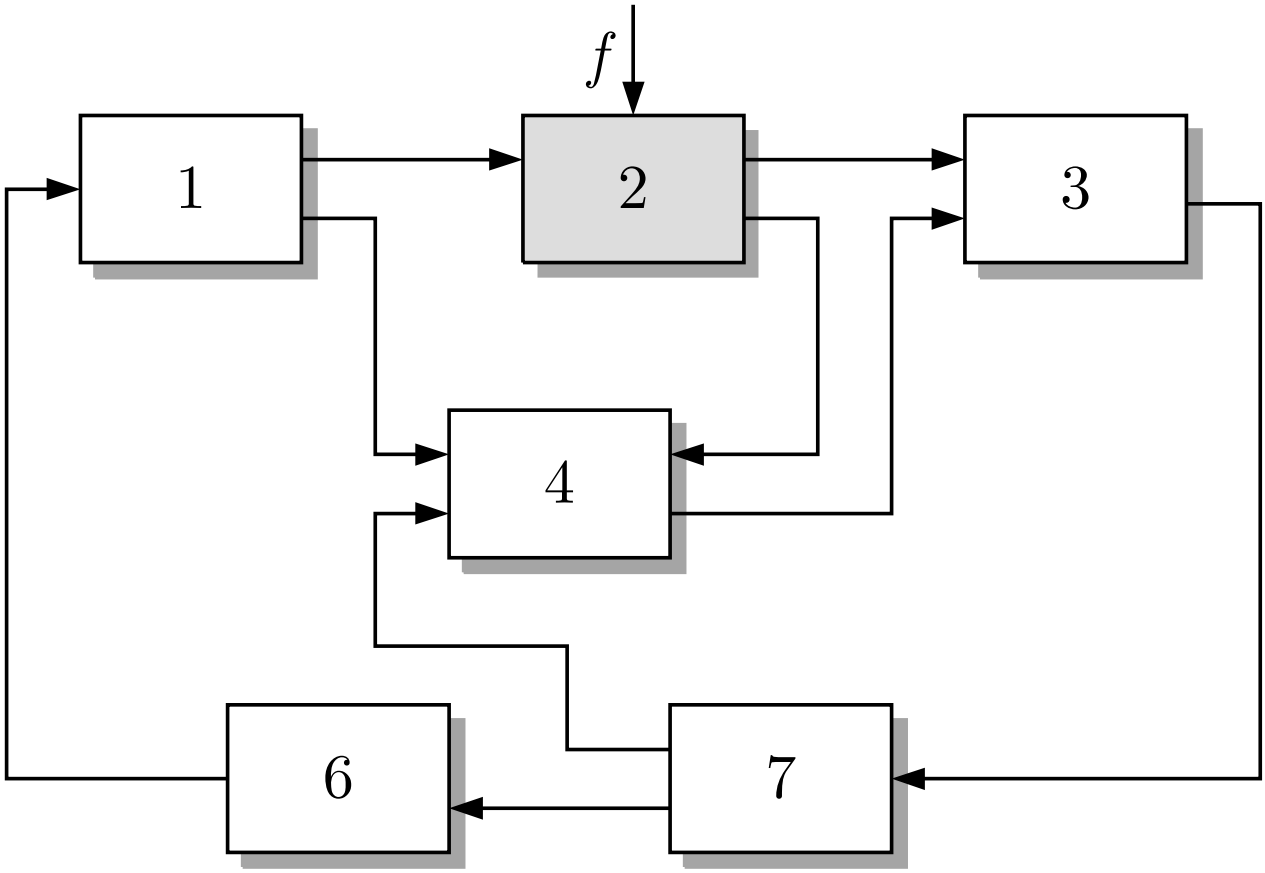

Fig. 1.7. Fault propagation in interconnected systems

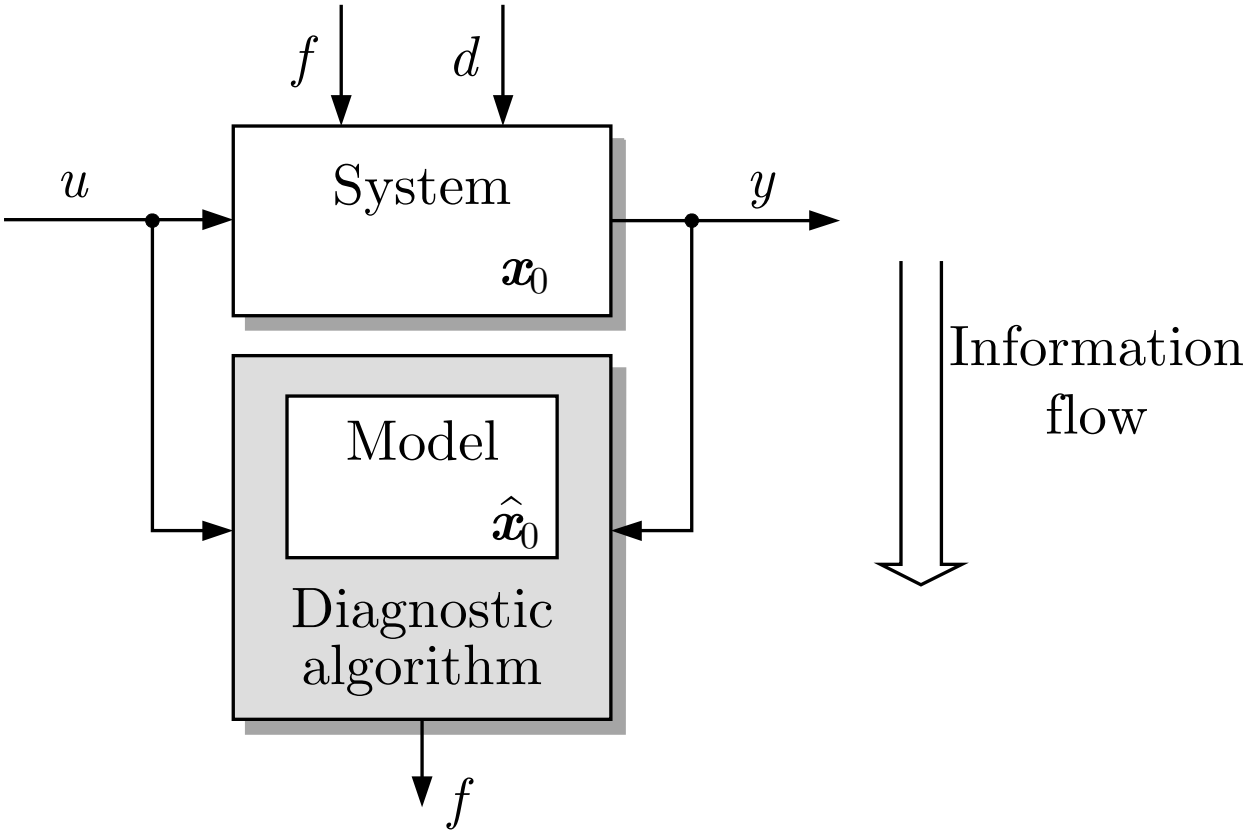

Fig. 1.8. Fault diagnosis

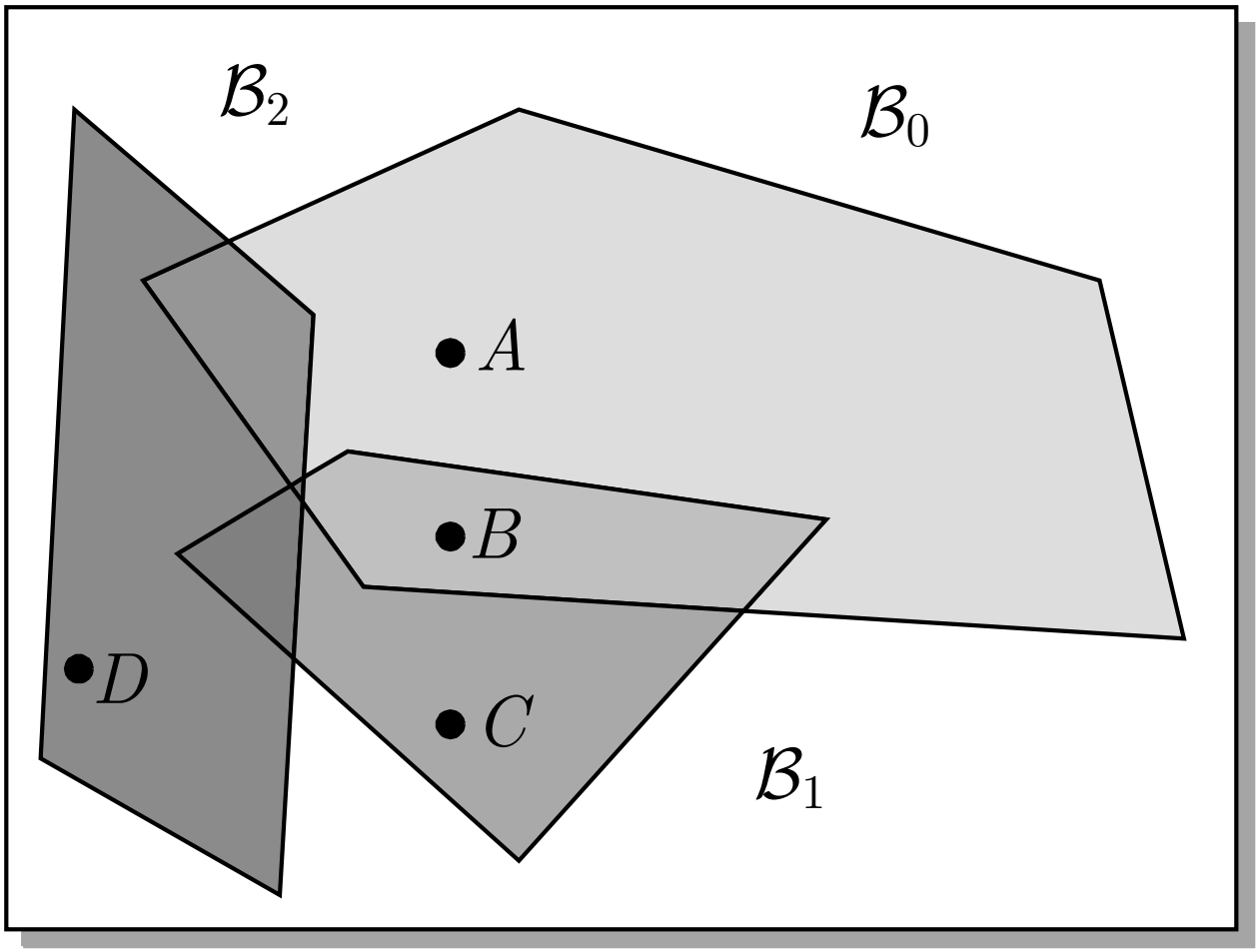

Fig. 1.9. Behaviour of the faultless and the faulty system

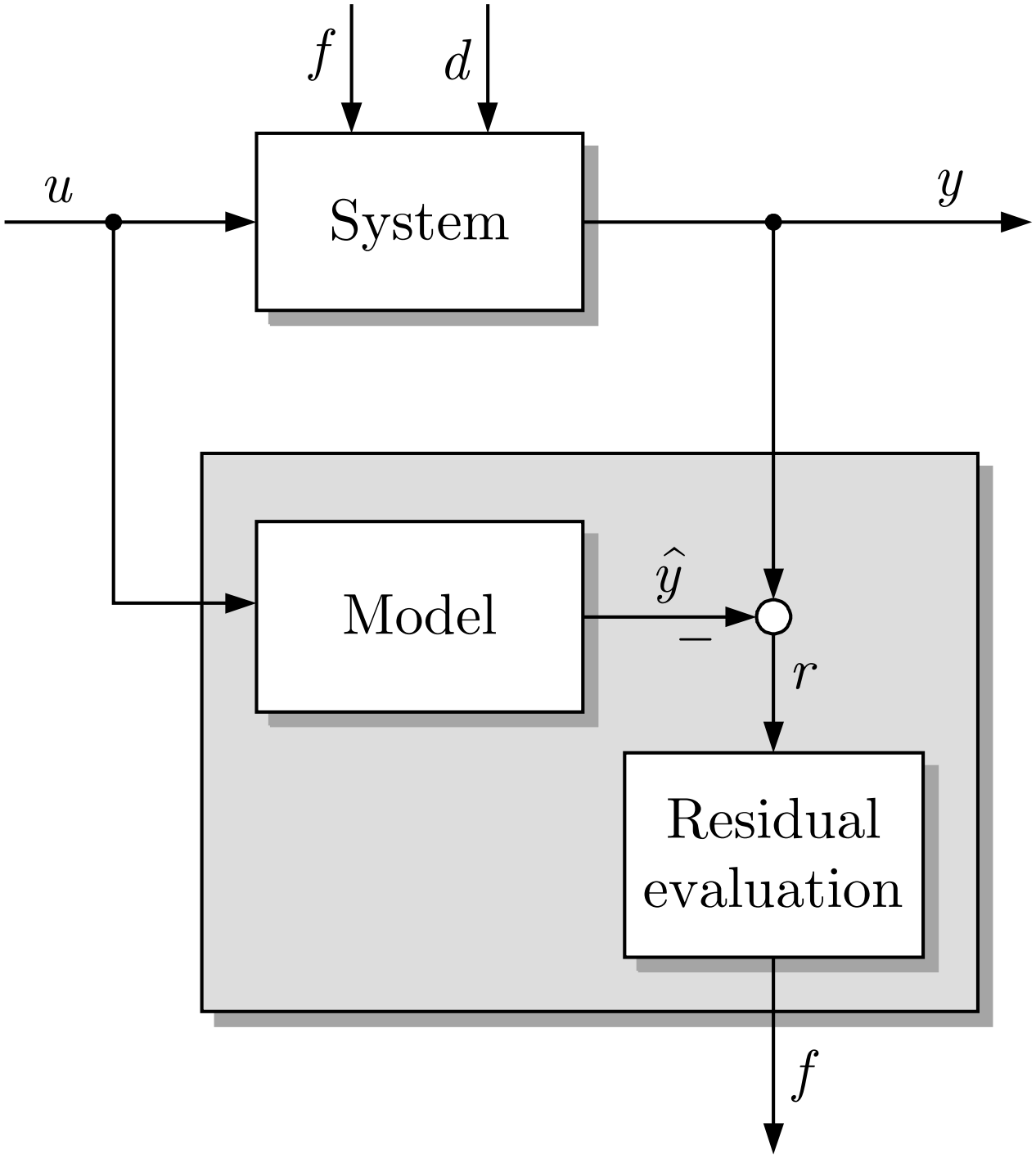

Fig. 1.10. Diagnosis of continuous-variable systems

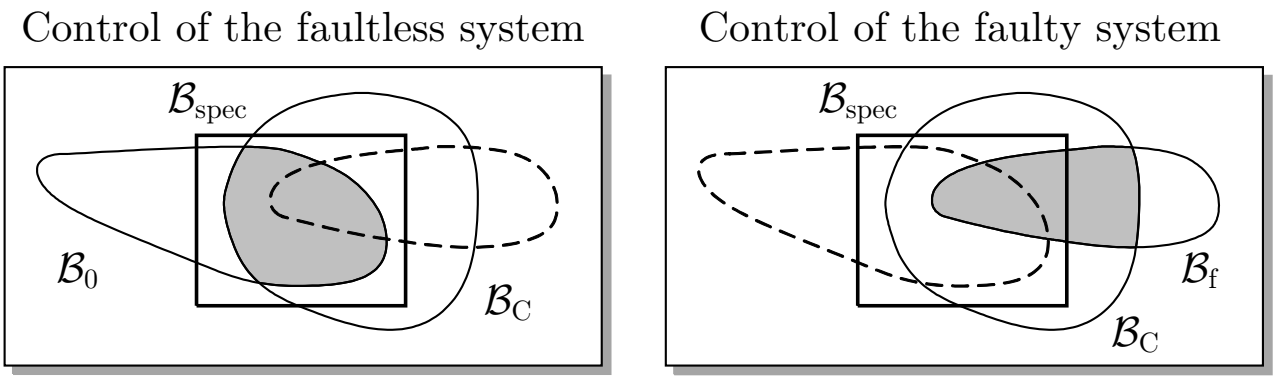

Fig. 1.11. Behaviour of the faultless and the faulty closed-loop system

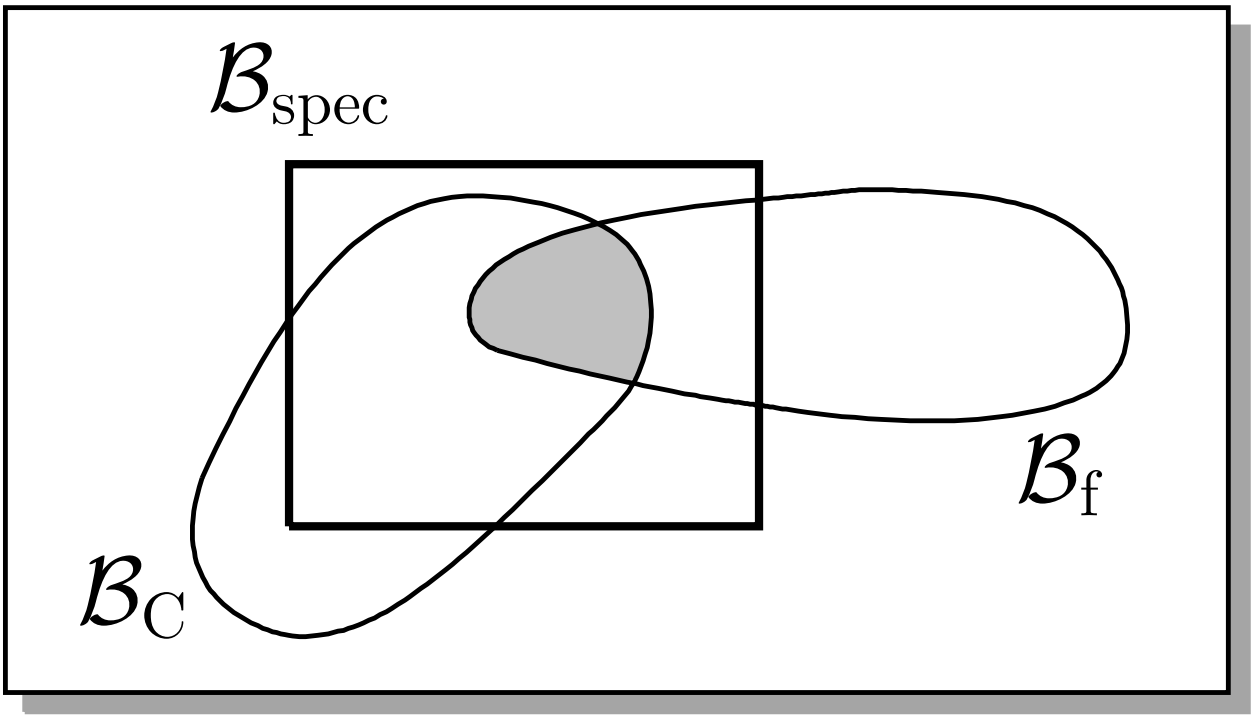

Fig. 1.12. Behavioural representation of fault accommodation

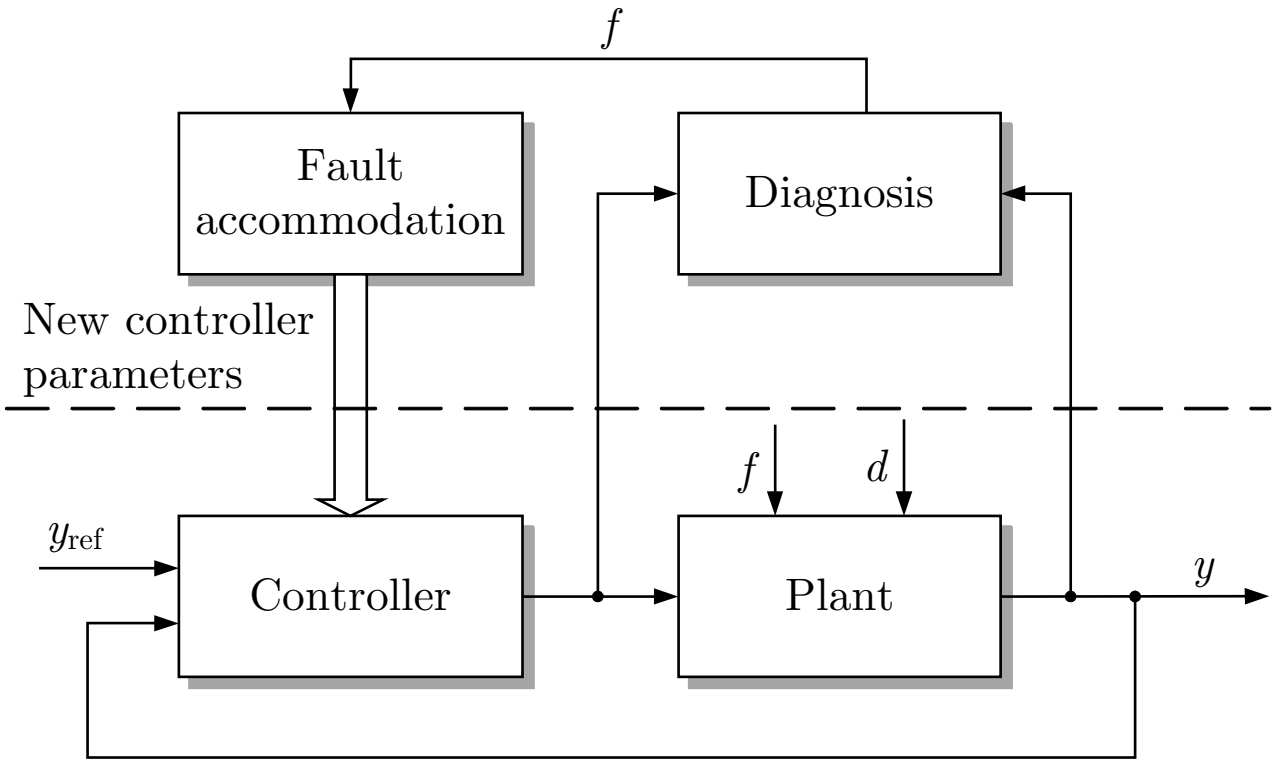

Fig. 1.13. Fault accommodation

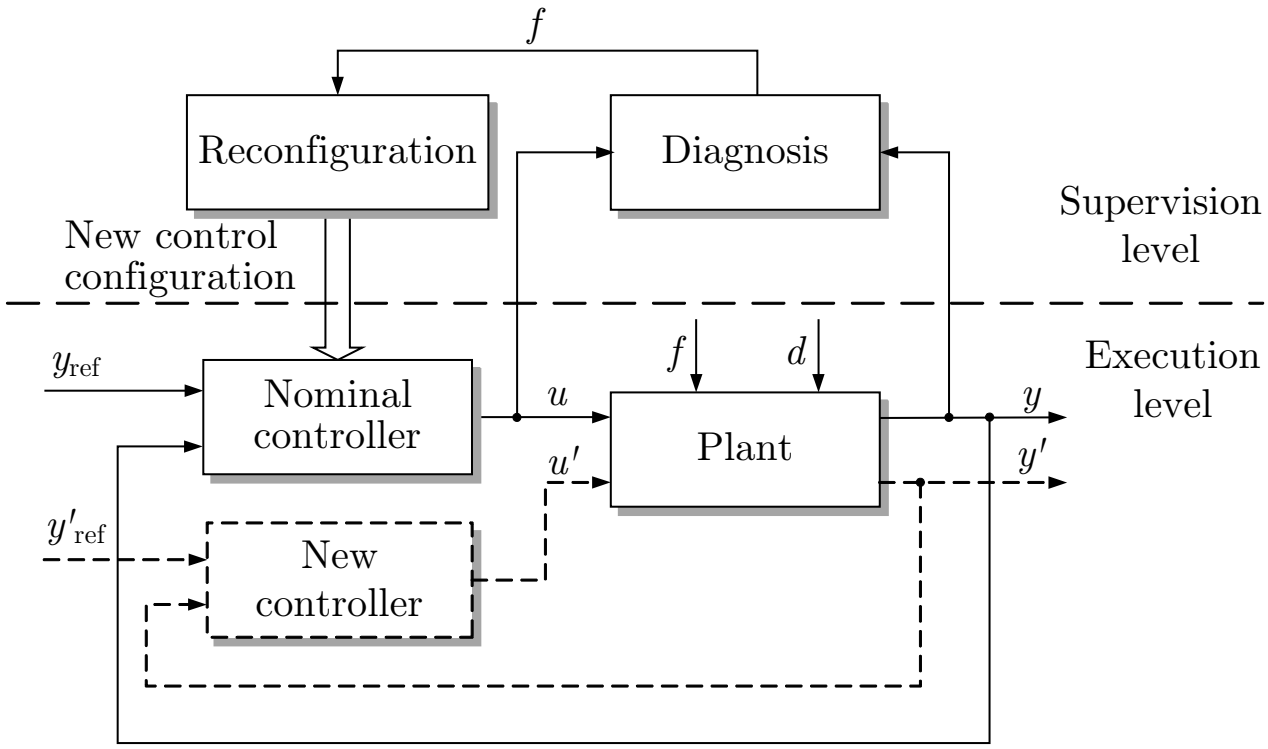

Fig. 1.14. Control reconfiguration

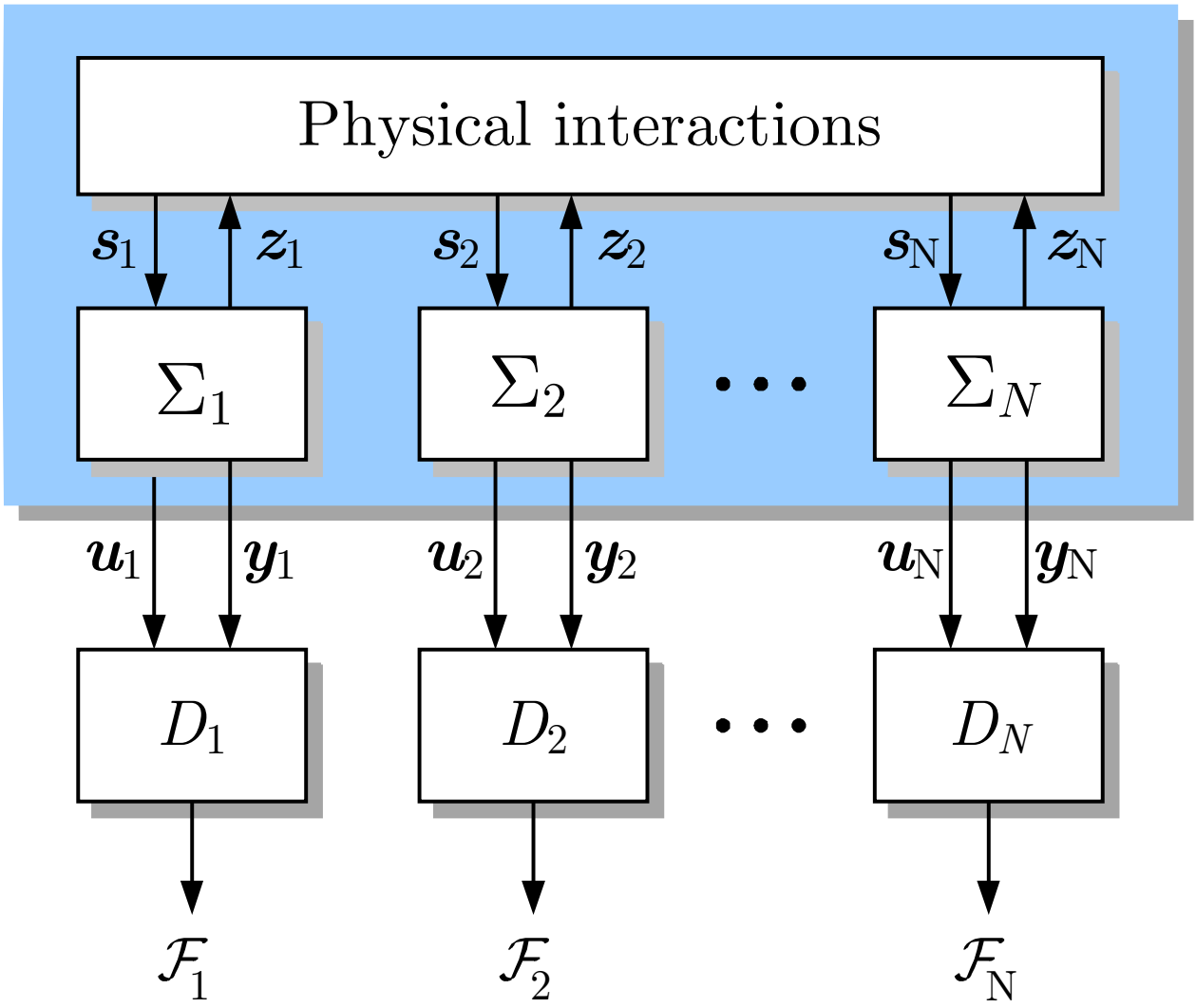

Fig. 1.15. Decentralised diagnosis

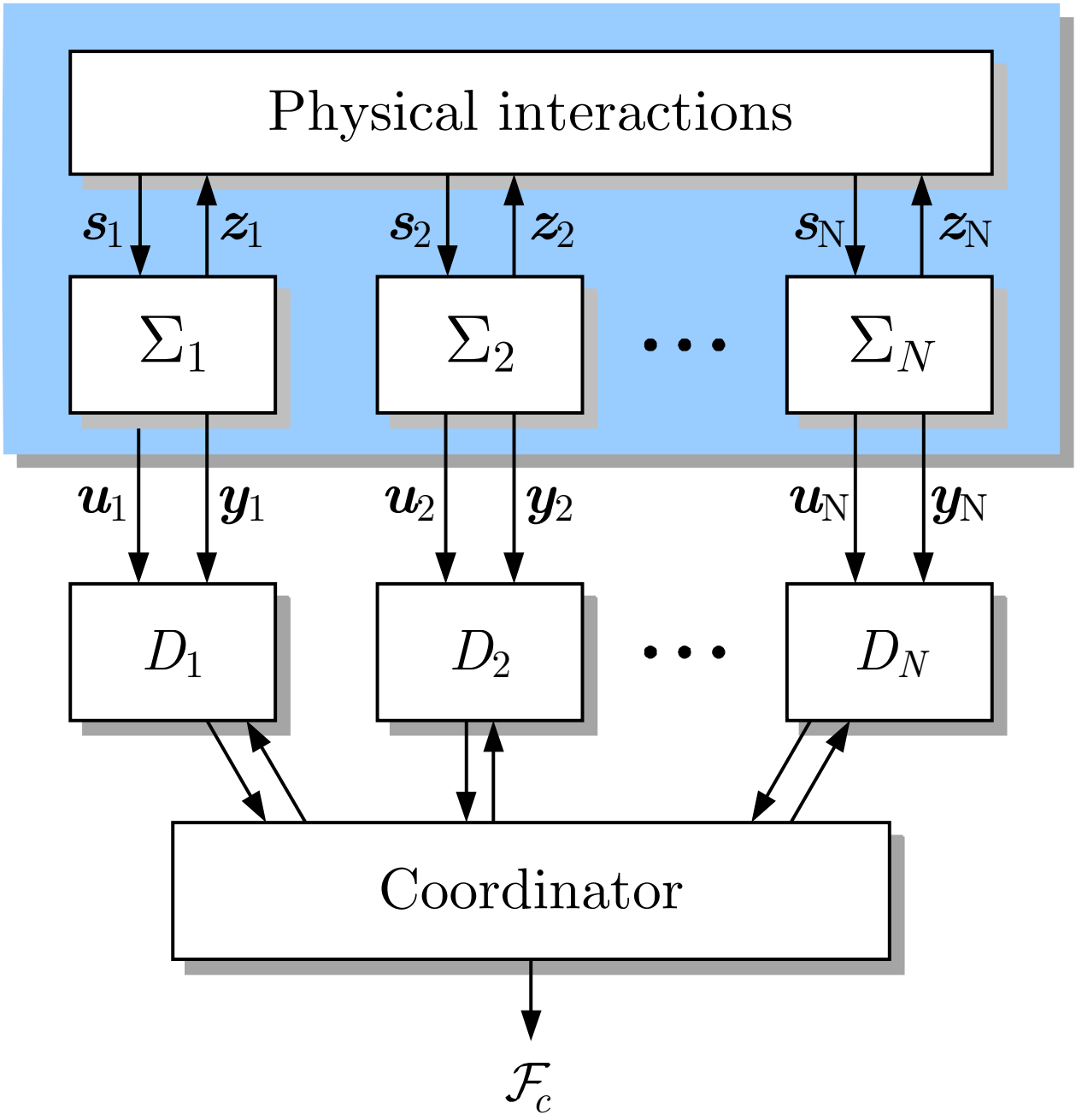

Fig. 1.16. Coordinated diagnosis

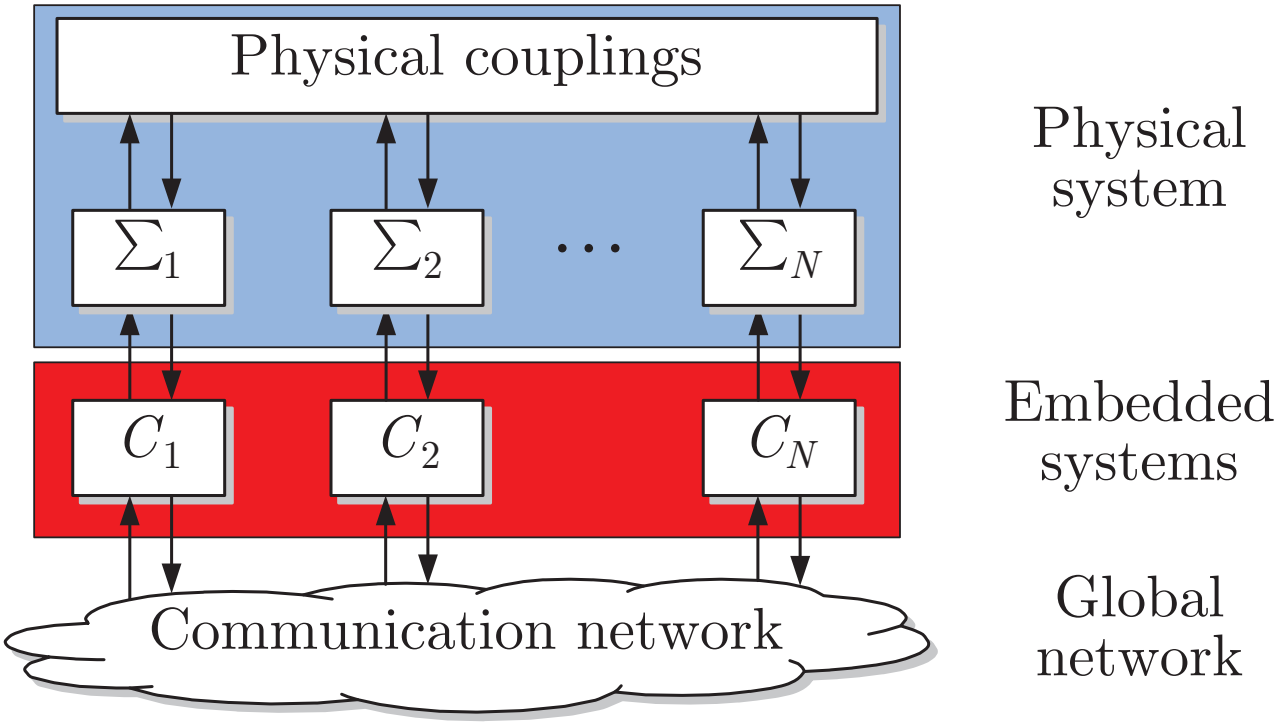

Fig. 1.17. Structure of a cyberphysical system

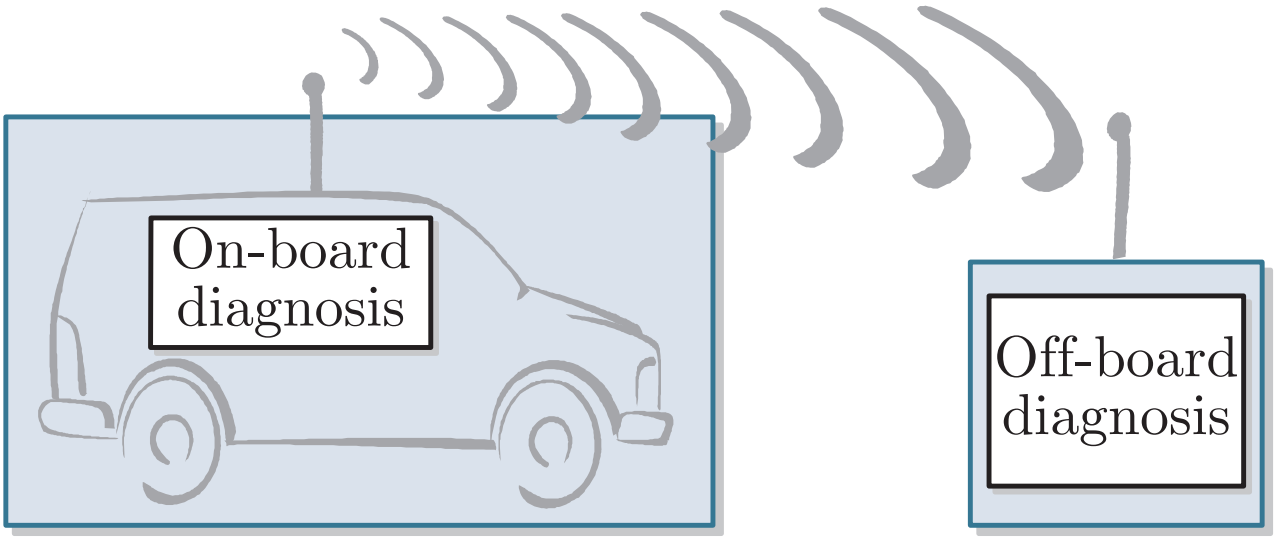

Fig. 1.18. Remote diagnosis

Blanke/Kinnaert/Lunze/Staroswiecki:
Diagnosis and Fault-Tolerant Control, (3rd edition), Springer-Verlag 2015

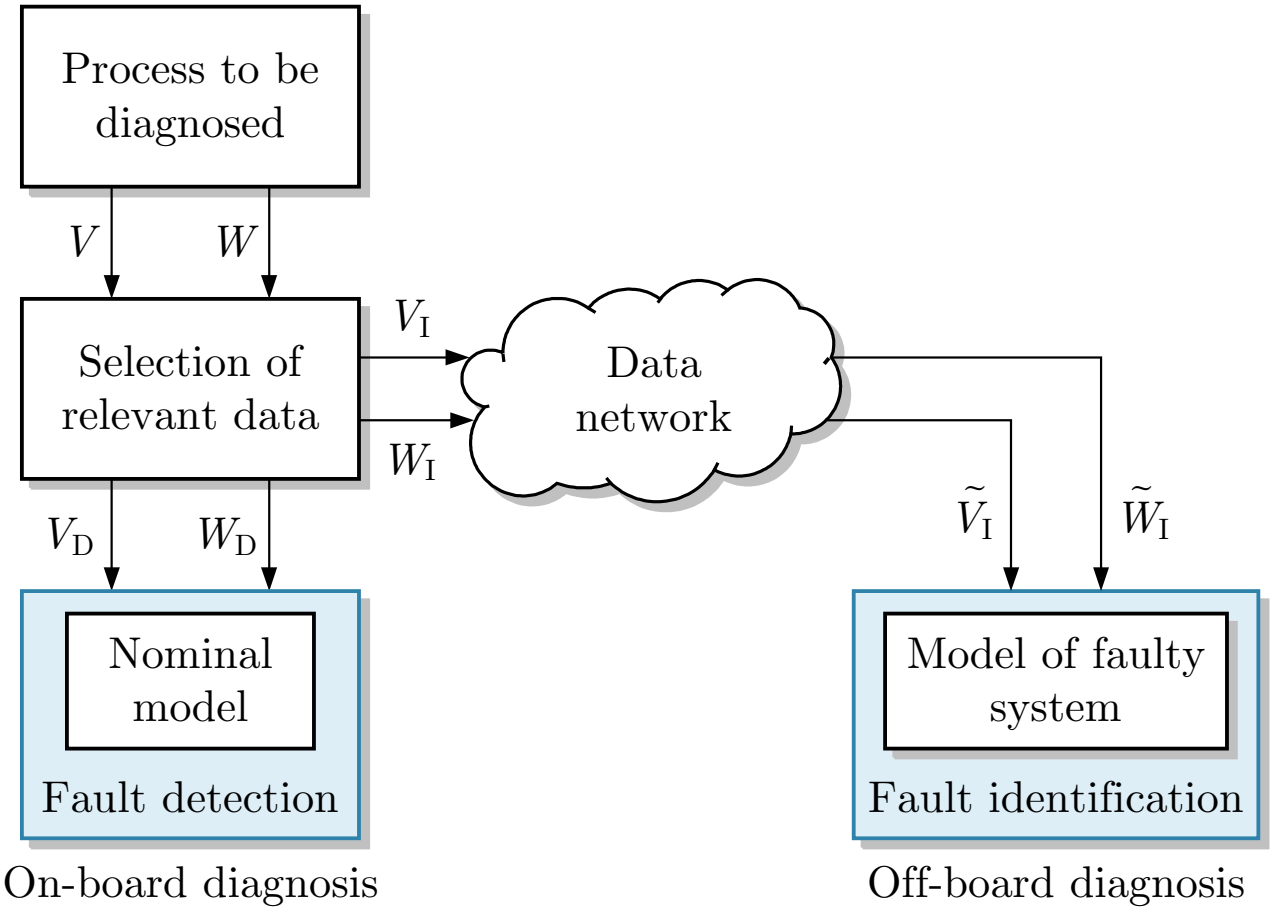

Fig. 1.19. Decomposition of the diagnostic task

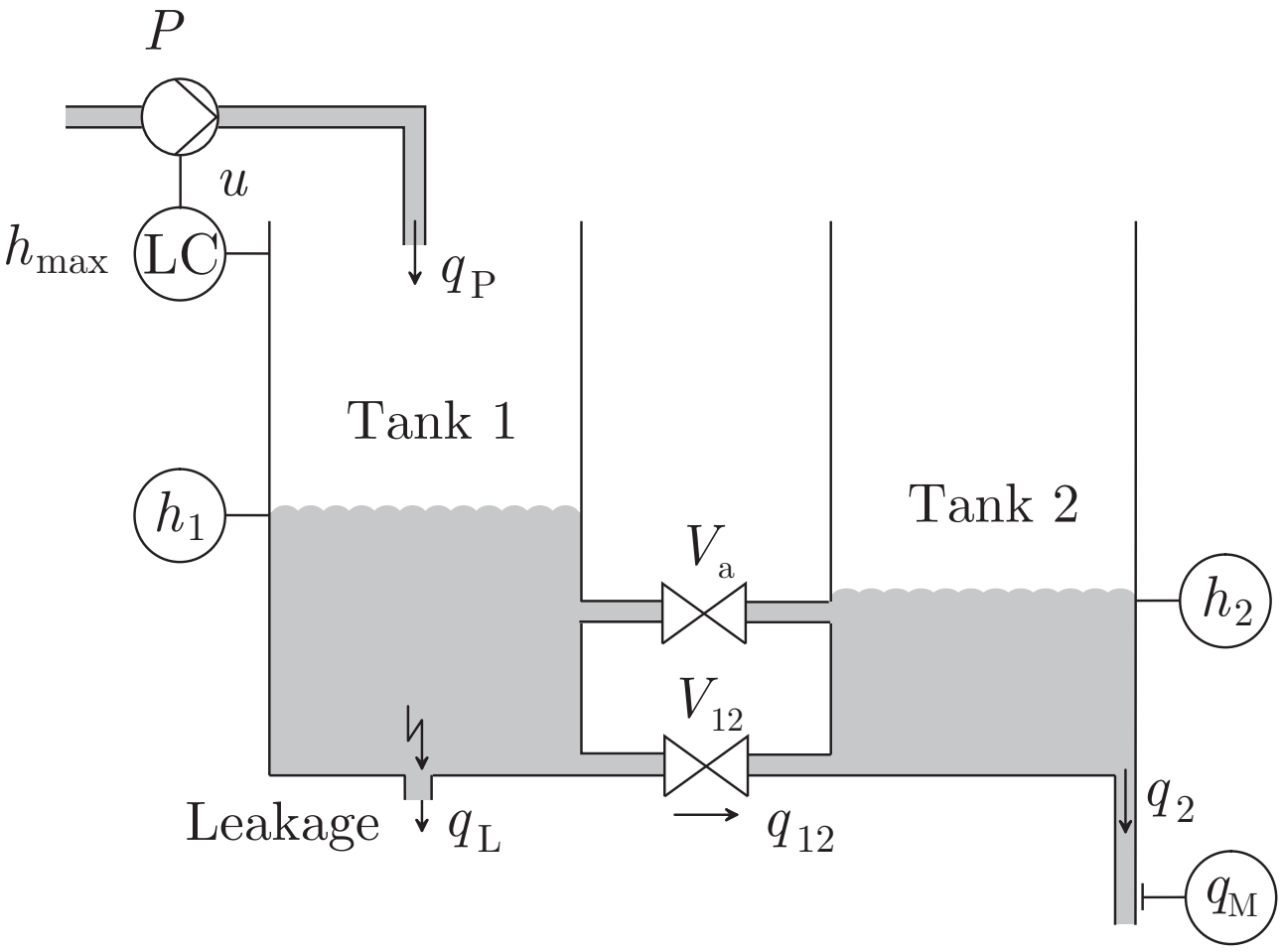

Fig. 2.1. Two-tank system

Blanke/Kinnaert/Lunze/Staroswiecki:
Diagnosis and Fault-Tolerant Control, (3rd edition), Springer-Verlag 2015

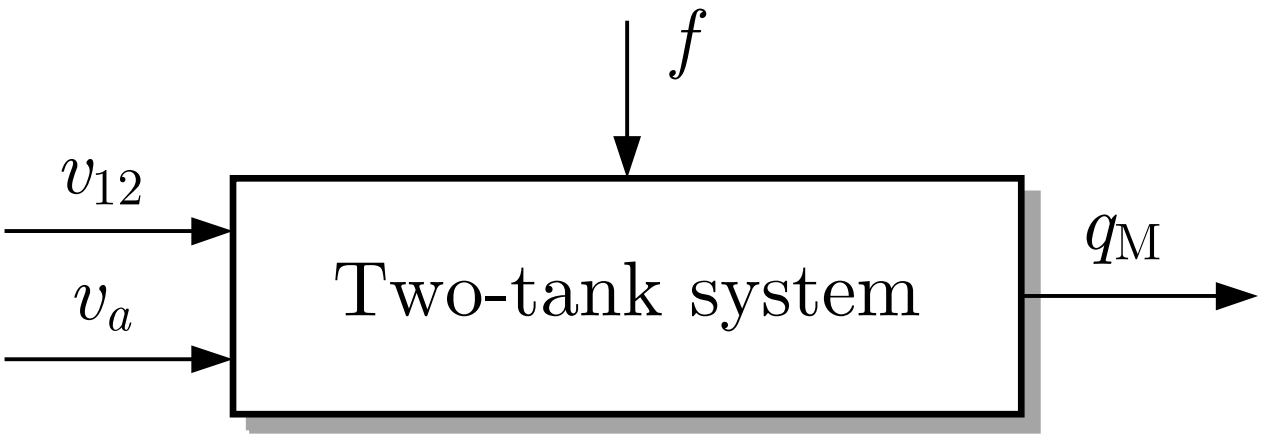

Fig. 2.2. Block diagram of the tank system

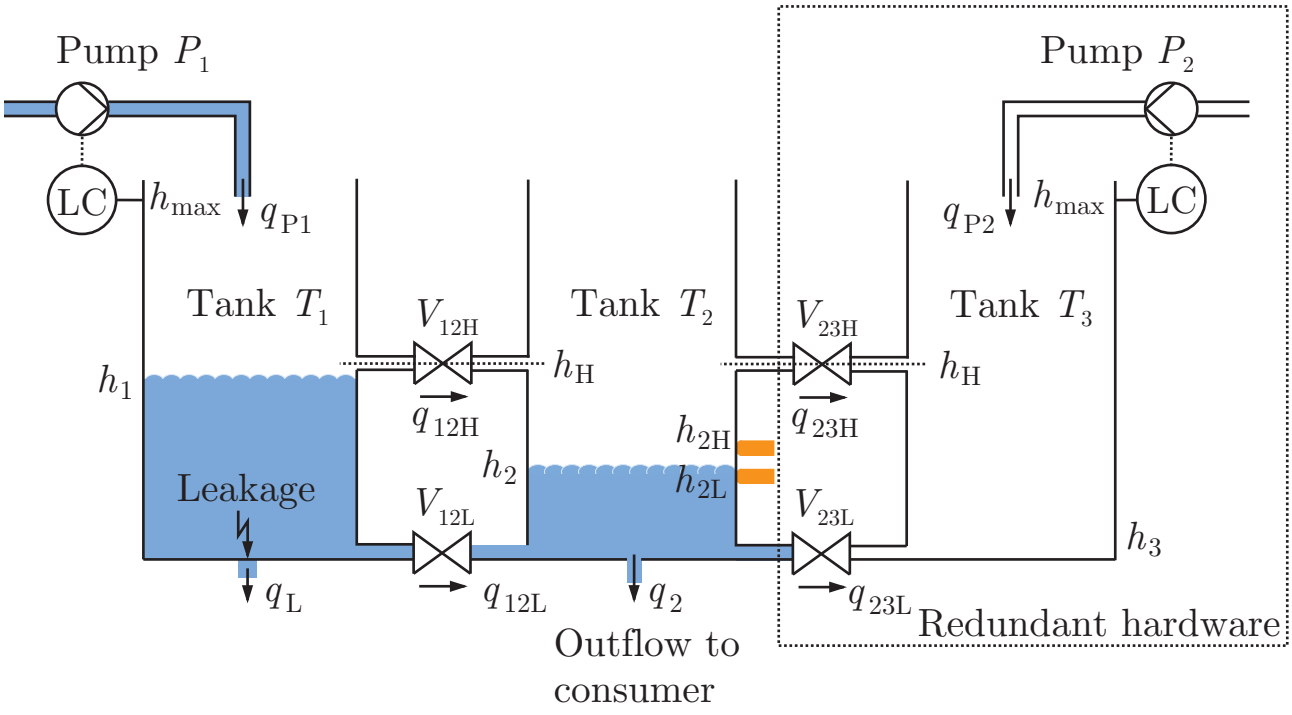

Fig. 2.3. Three-tank system

Blanke/Kinnaert/Lunze/Staroswiecki:
Diagnosis and Fault-Tolerant Control, (3rd edition), Springer-Verlag 2015

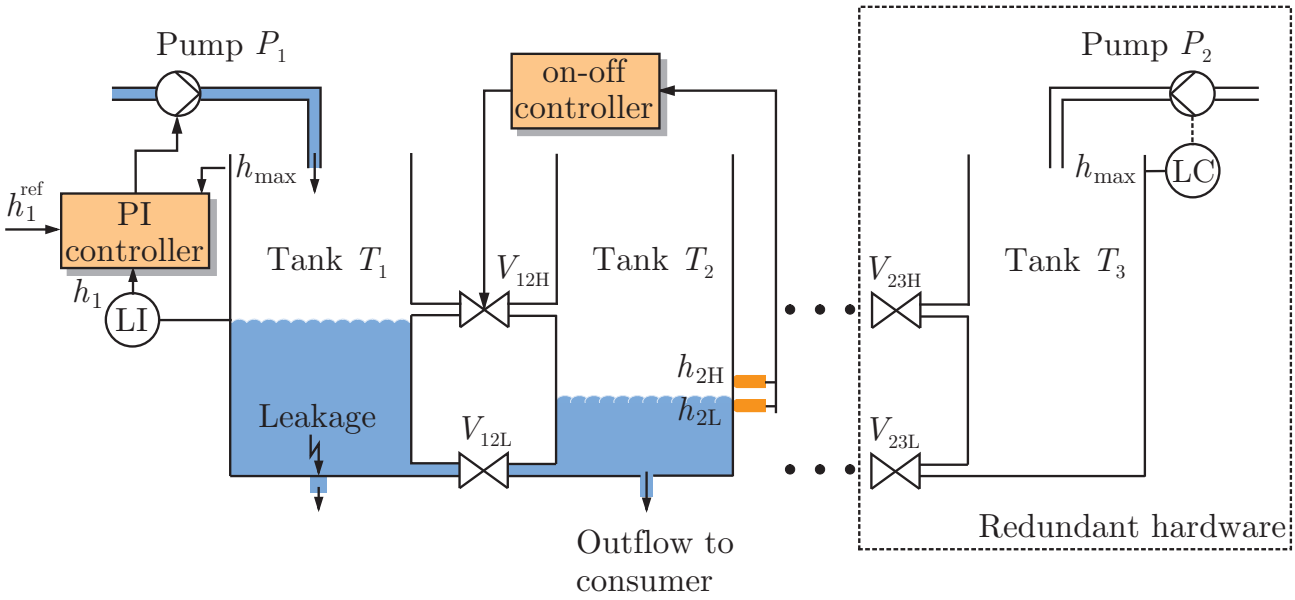

Fig. 2.4. Nominal configuration of the three-tank system

Blanke/Kinnaert/Lunze/Staroswiecki:
Diagnosis and Fault-Tolerant Control, (3rd edition), Springer-Verlag 2015

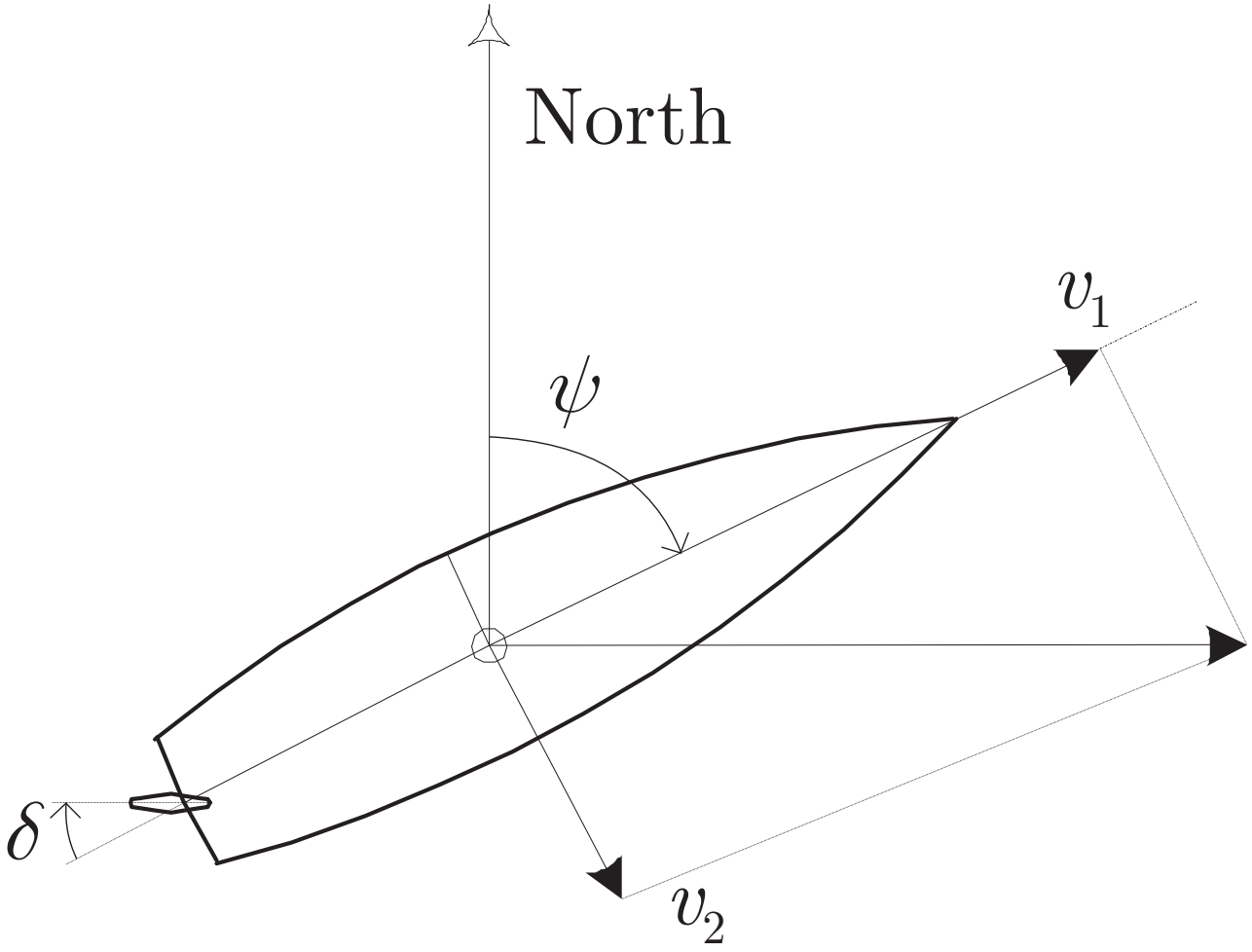

Fig. 2.5. Motion of a ship steered by its rudder

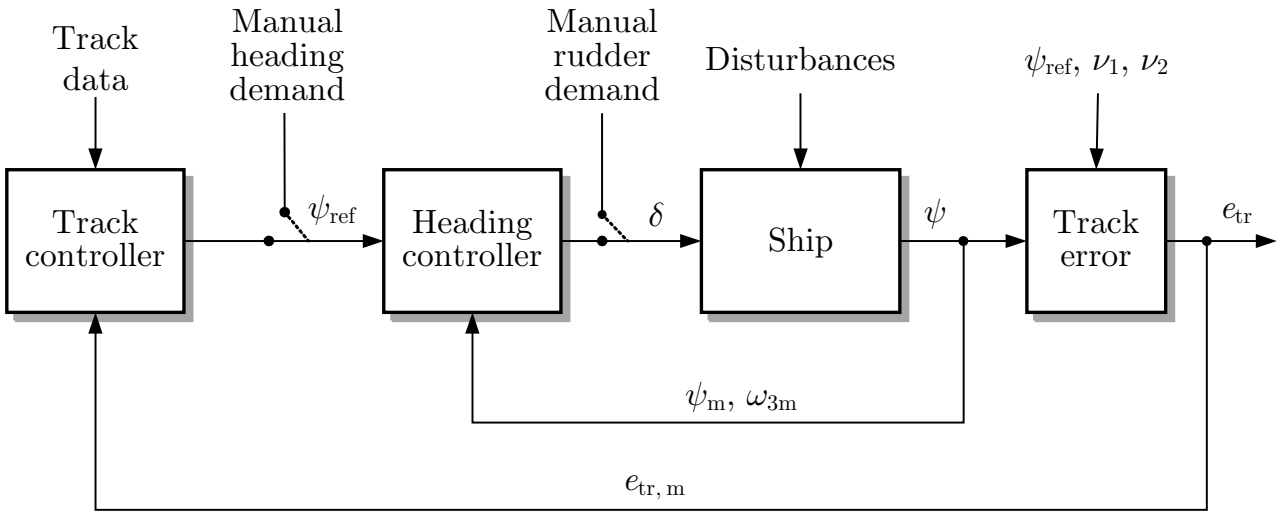

Fig. 2.6. Cascaded architecture of controllers for ship steering

Blanke/Kinnaert/Lunze/Staroswiecki:
Diagnosis and Fault-Tolerant Control, (3rd edition), Springer-Verlag 2015

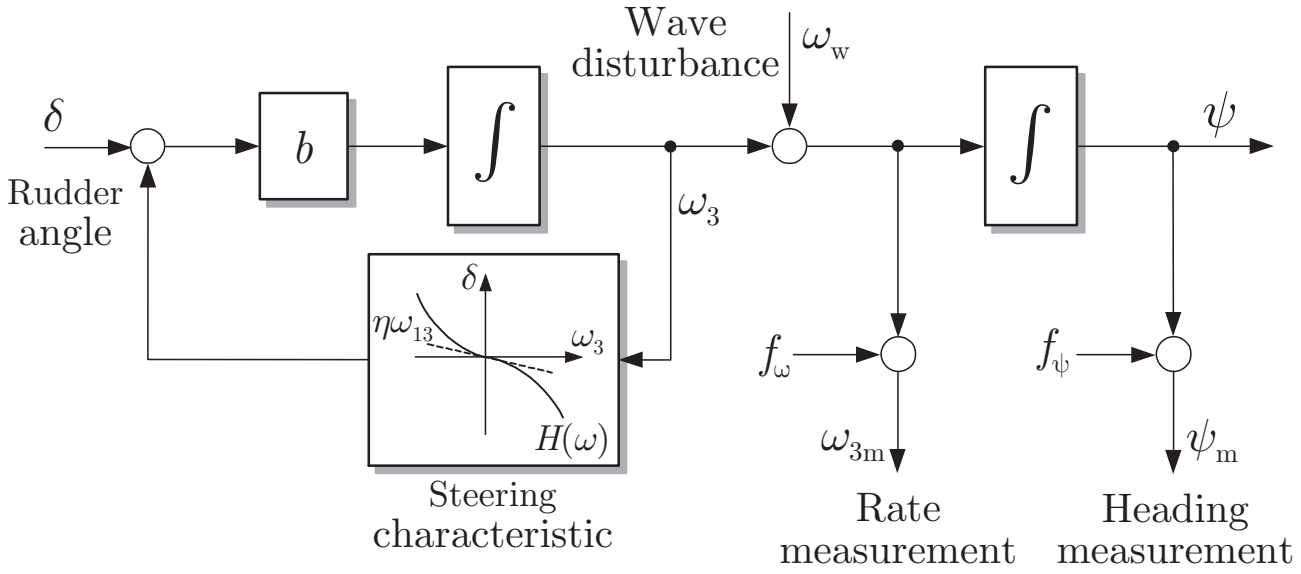

Fig. 2.7. A simple dynamical model of a ship steered by the rudder

Blanke/Kinnaert/Lunze/Staroswiecki:
Diagnosis and Fault-Tolerant Control, (3rd edition), Springer-Verlag 2015

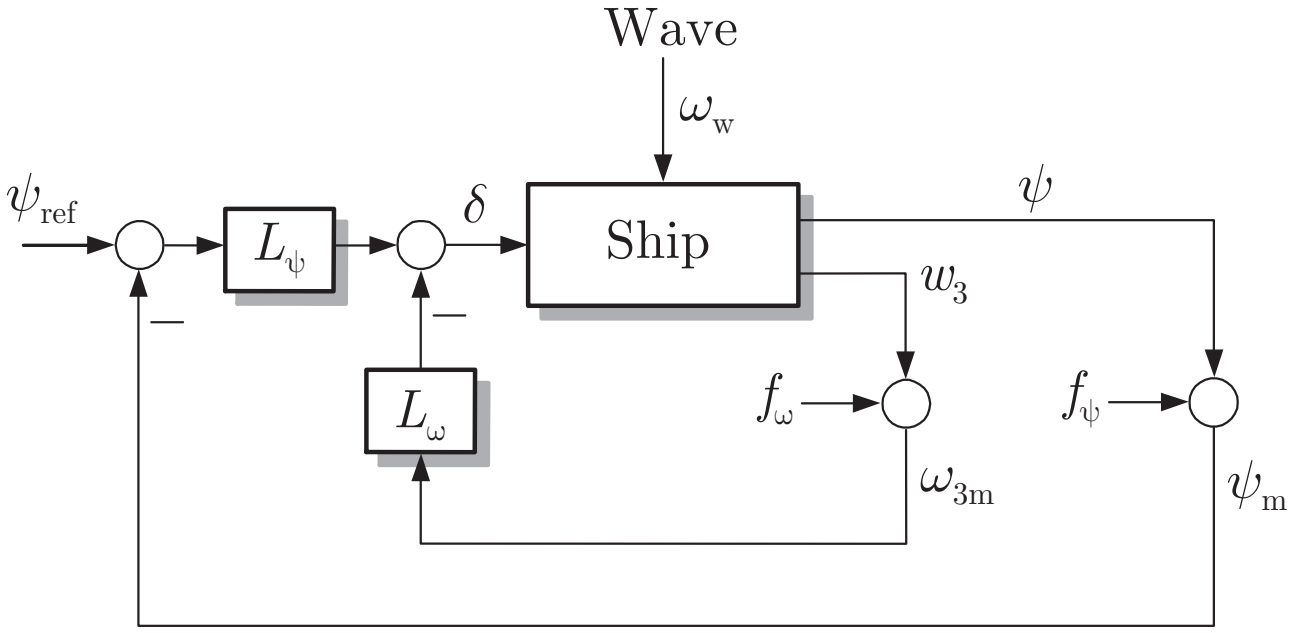

Fig. 2.8. Simple heading controller (autopilot) for the ship example

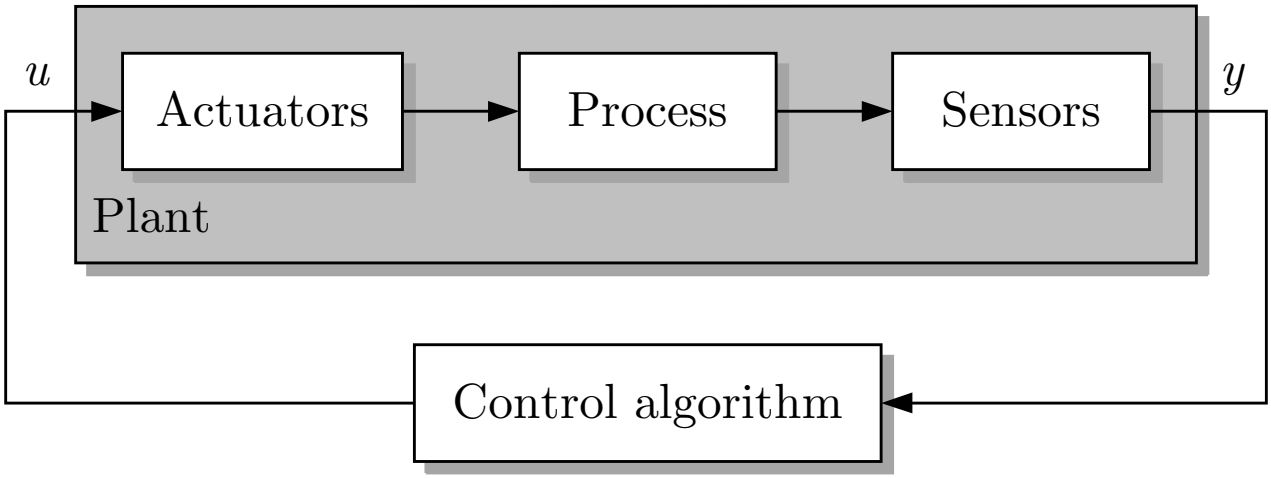

Fig. 3.1. Controlled system

Blanke/Kinnaert/Lunze/Staroswiecki:
Diagnosis and Fault-Tolerant Control, (3rd edition), Springer-Verlag 2015

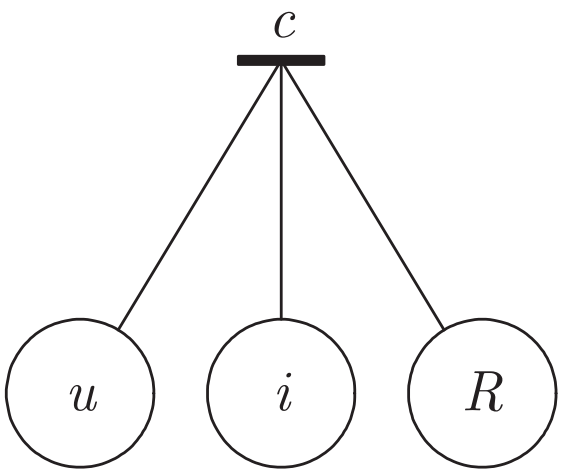

	u	i	R
c	1	1	1

Fig. 3.2. Structure of Ohm's law

Blanke/Kinnaert/Lunze/Staroswiecki:
Diagnosis and Fault-Tolerant Control, (3rd edition), Springer-Verlag 2015

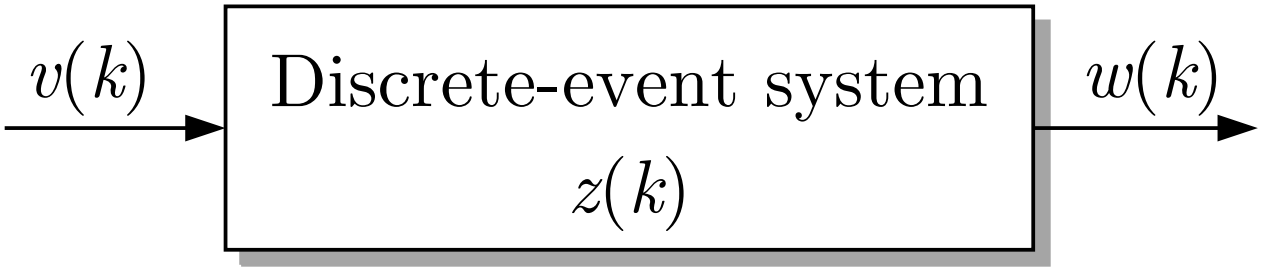

Fig. 3.3. Discrete-event dynamical system

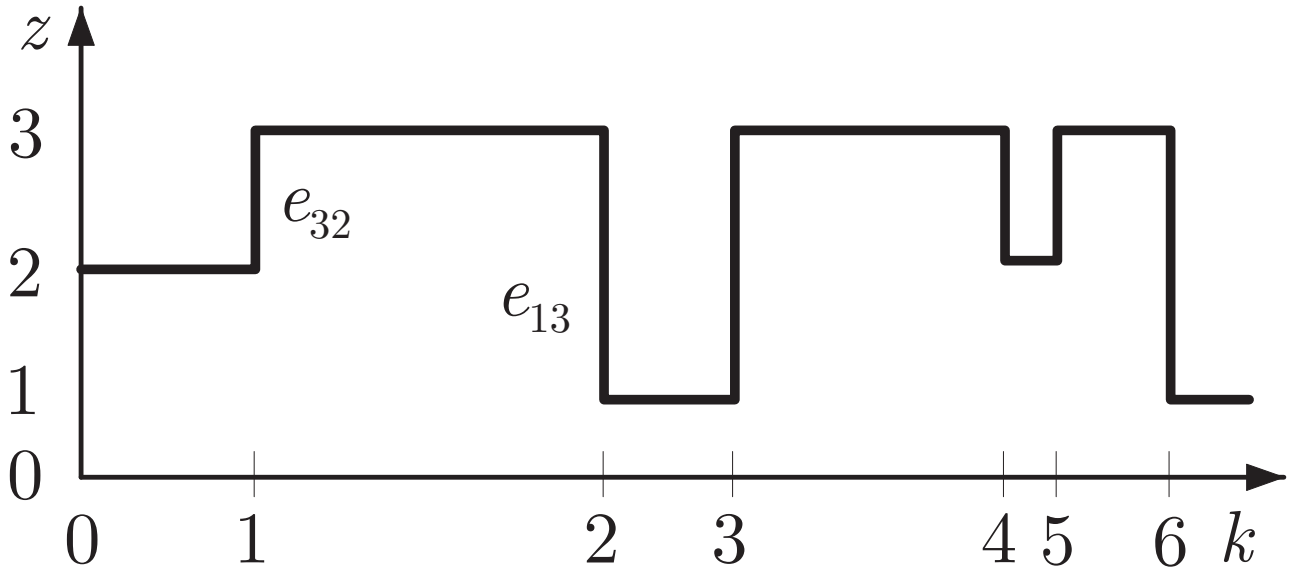

Fig. 3.4. Symbolic signal values and event sequence

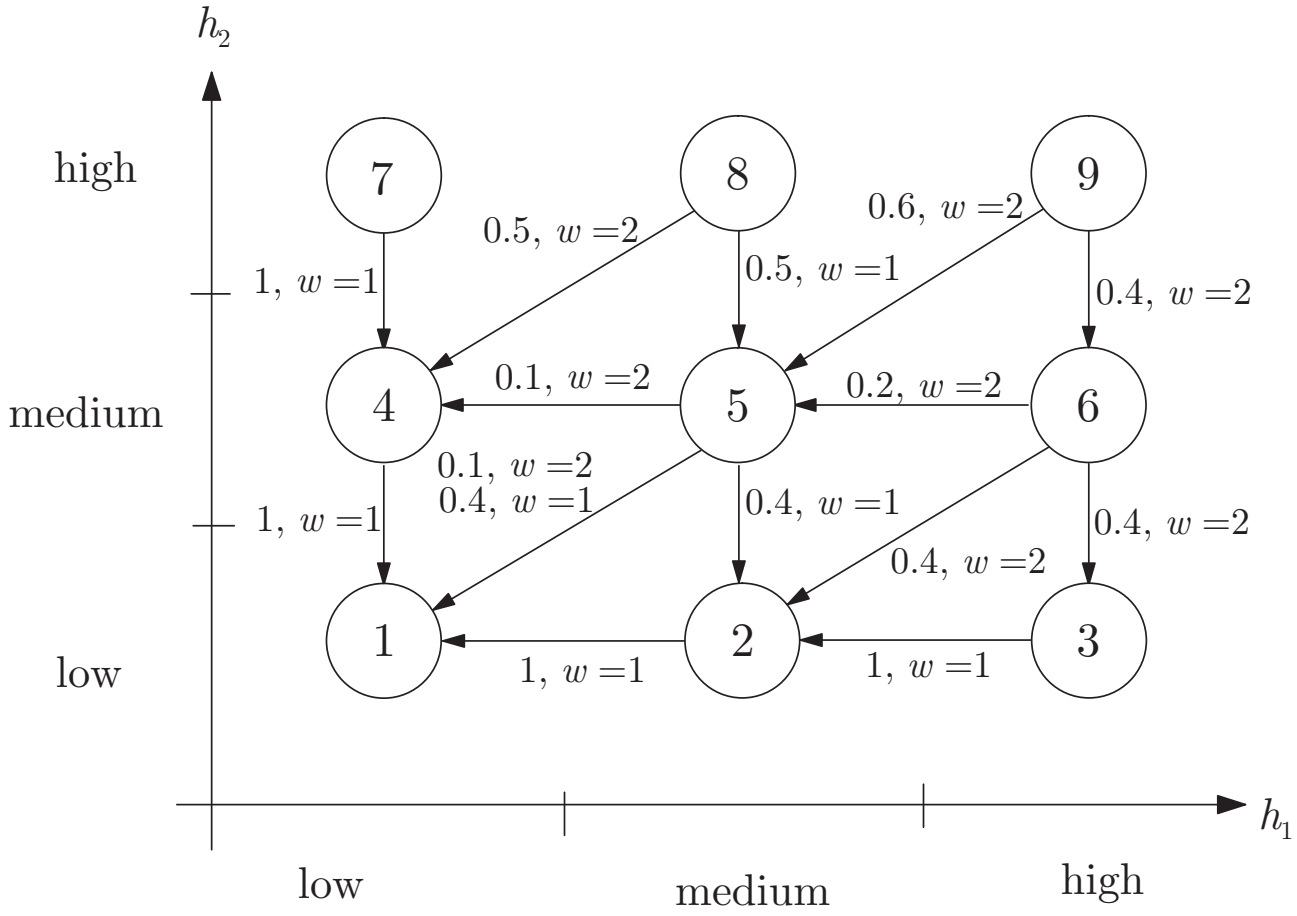

Fig. 3.5. Stochastic automaton describing the tank system for faulty pump $(q_{\mathrm{P}} = 0)$

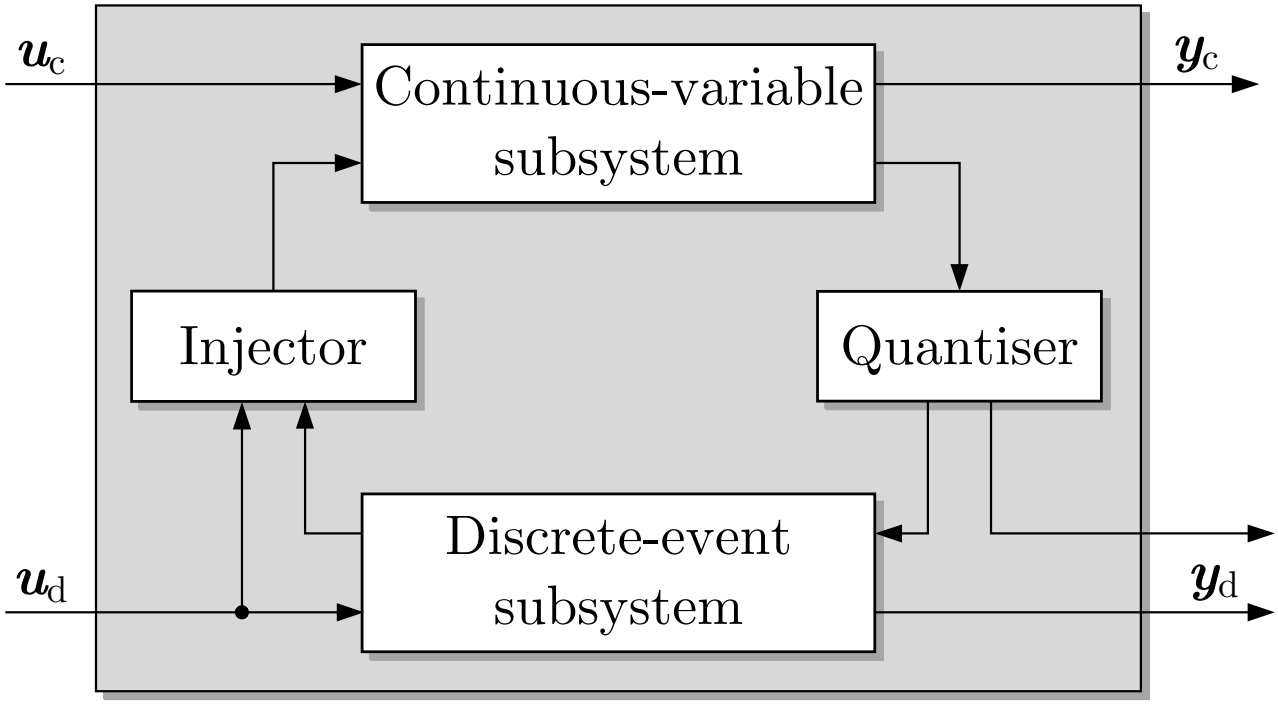

Fig. 3.6. Hybrid dynamical system

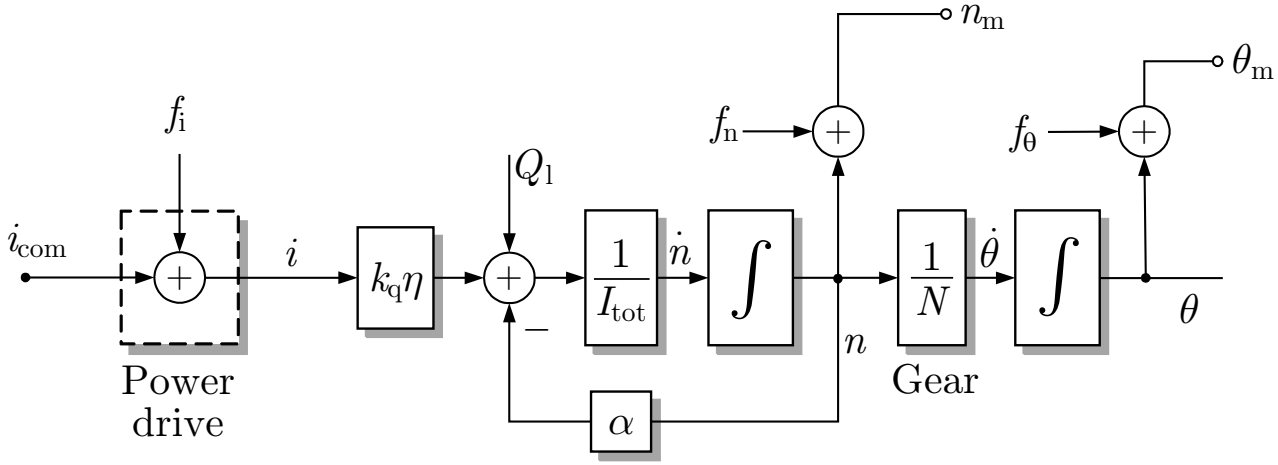

Fig. 3.7. Block diagram of actuator with additive faults - open loop

Blanke/Kinnaert/Lunze/Staroswiecki:
Diagnosis and Fault-Tolerant Control, (3rd edition), Springer-Verlag 2015

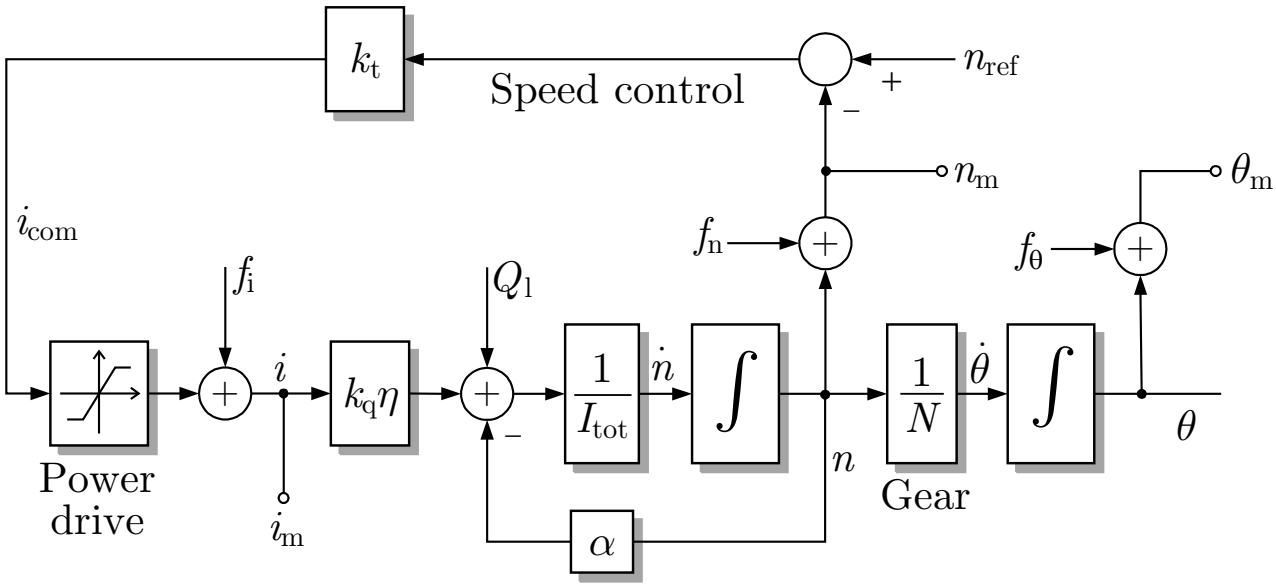

Fig. 3.8. Actuator with angular velocity feedback

Blanke/Kinnaert/Lunze/Staroswiecki:
Diagnosis and Fault-Tolerant Control, (3rd edition), Springer-Verlag 2015

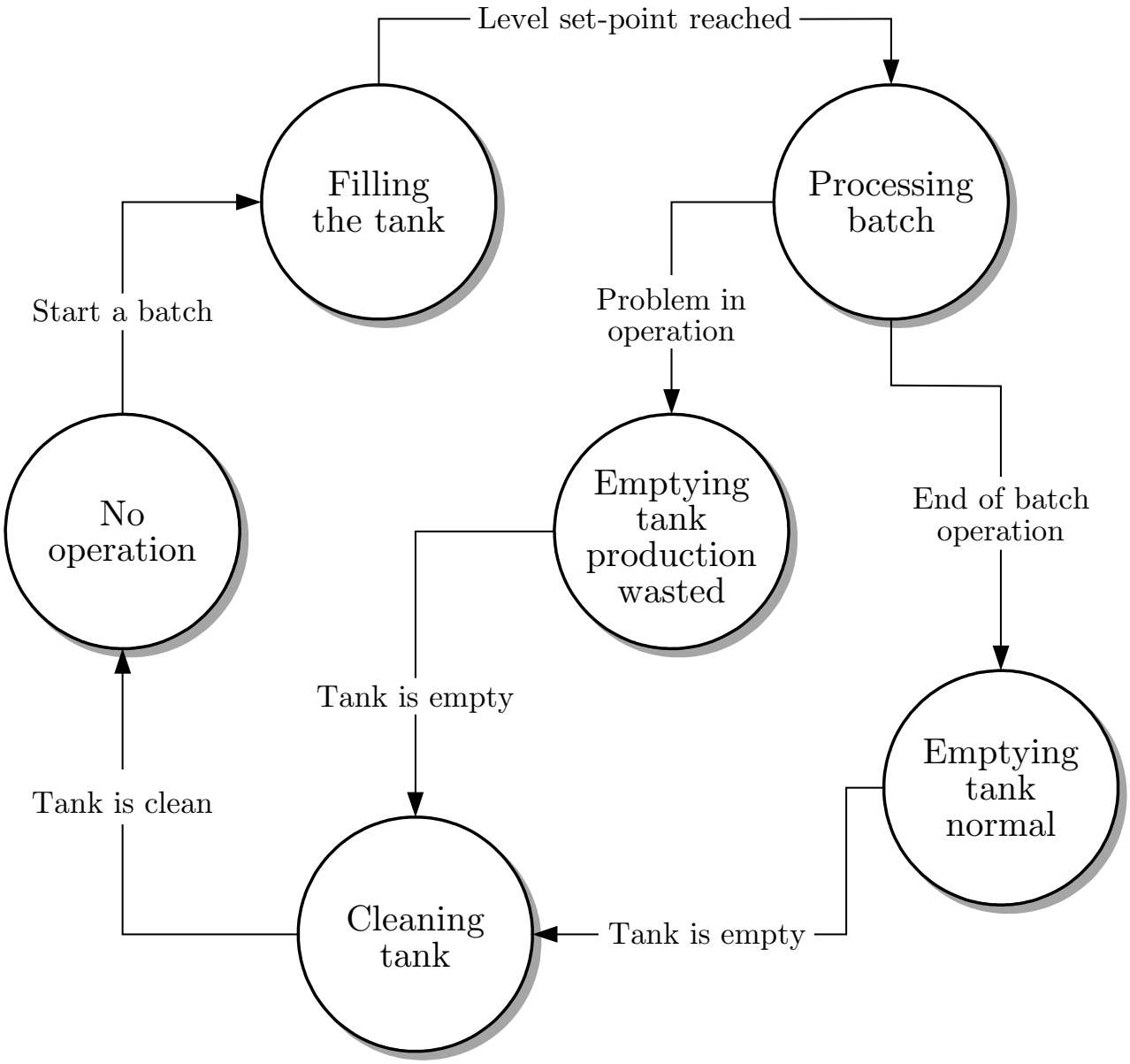

Fig. 4.1. Automaton of a batch process illustrated through use-modes

Blanke/Kinnaert/Lunze/Staroswiecki:
Diagnosis and Fault-Tolerant Control, (3rd edition), Springer-Verlag 2015

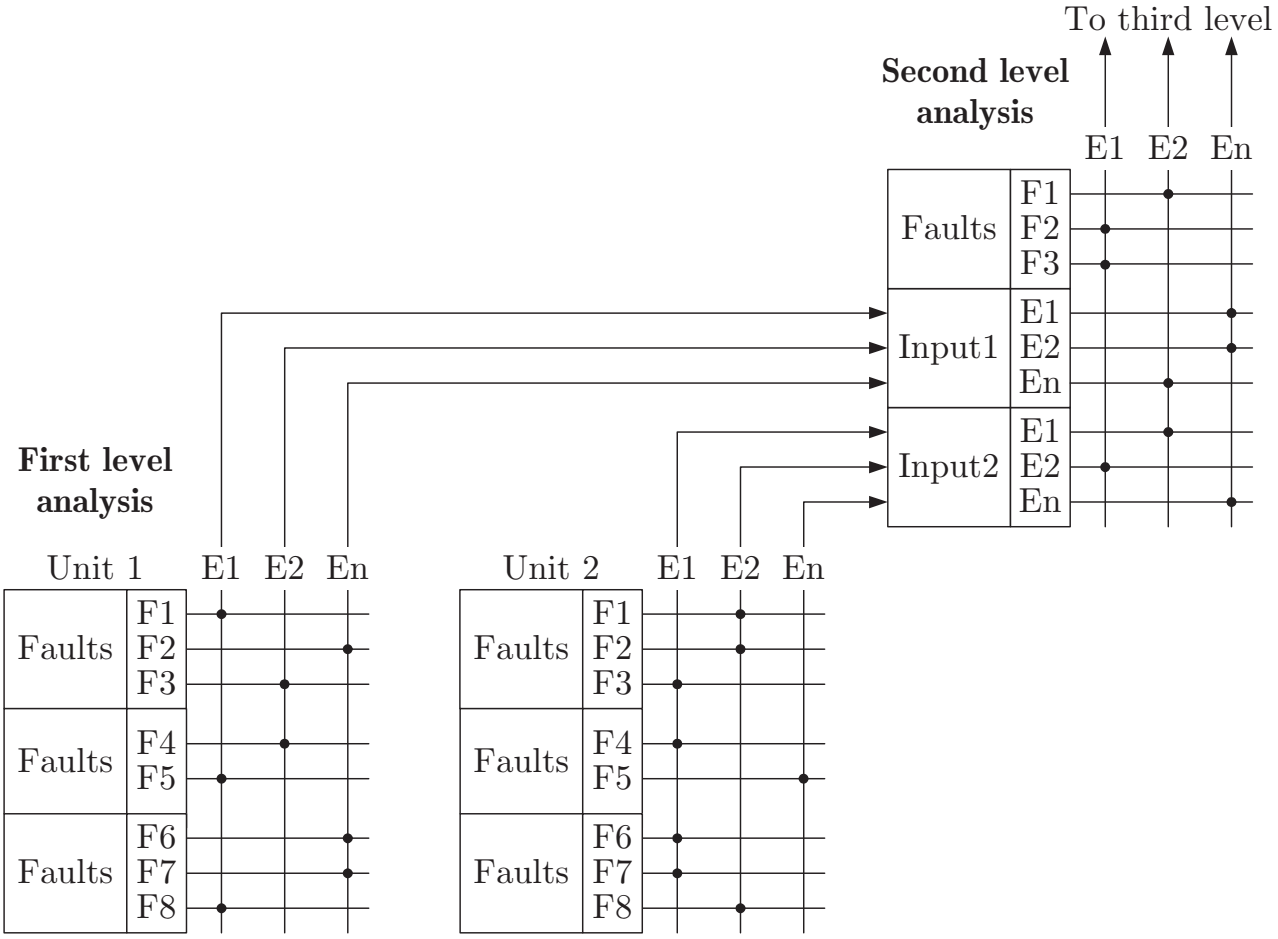

Fig. 4.2. Traditional failure modes and effects analysis scheme illustrated graphically for two component levels

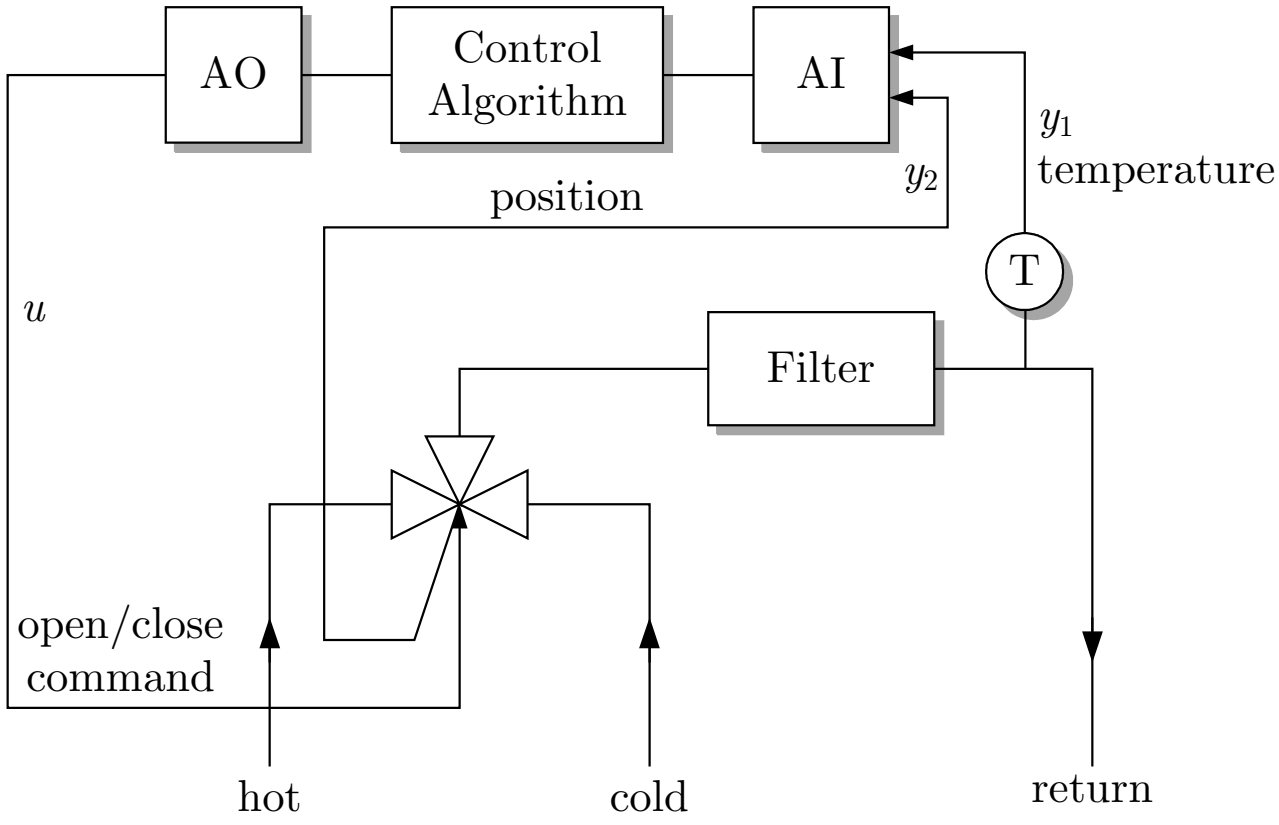

Fig. 4.3. Piping and instrumentation diagram representation of a temperature control loop with 3-way valve

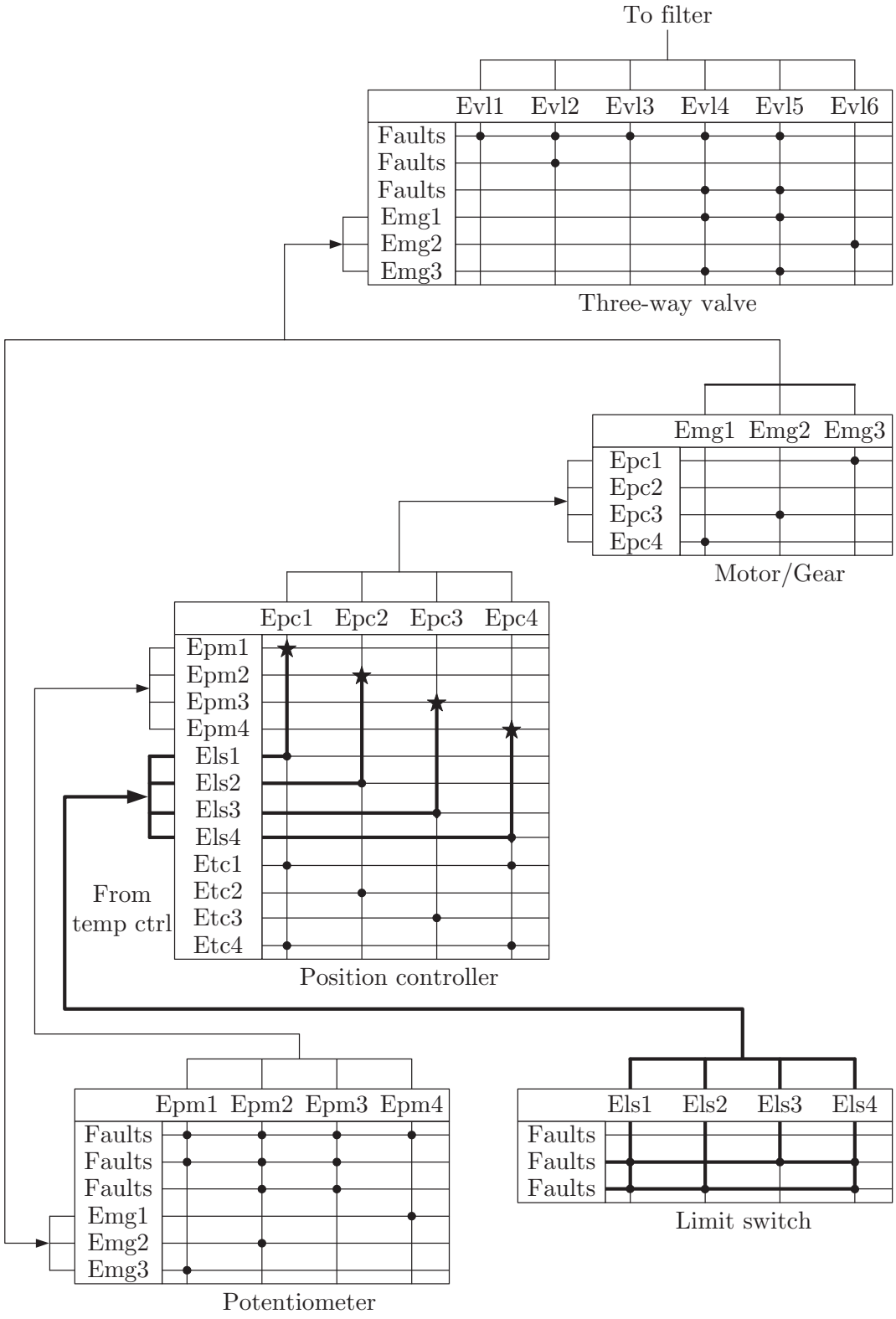

Fig. 4.4. Propagation of fault effects in closed-loop control of 3-way valve

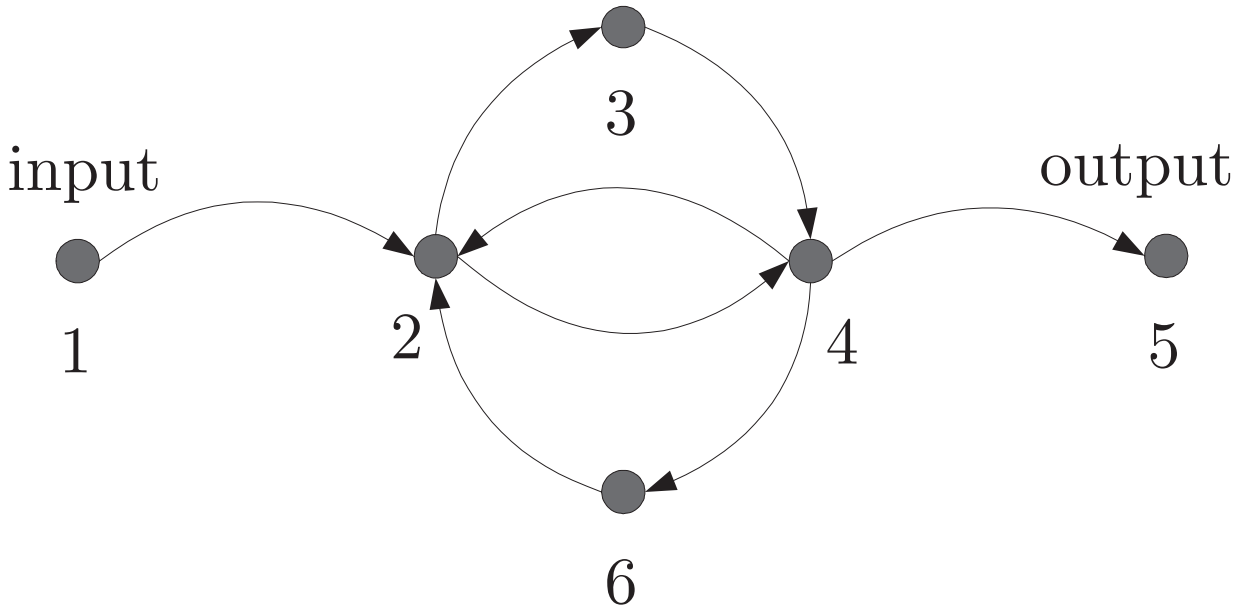

Fig. 4.5. A fault propagation graph example. One vertice is input (1), another is output (5).

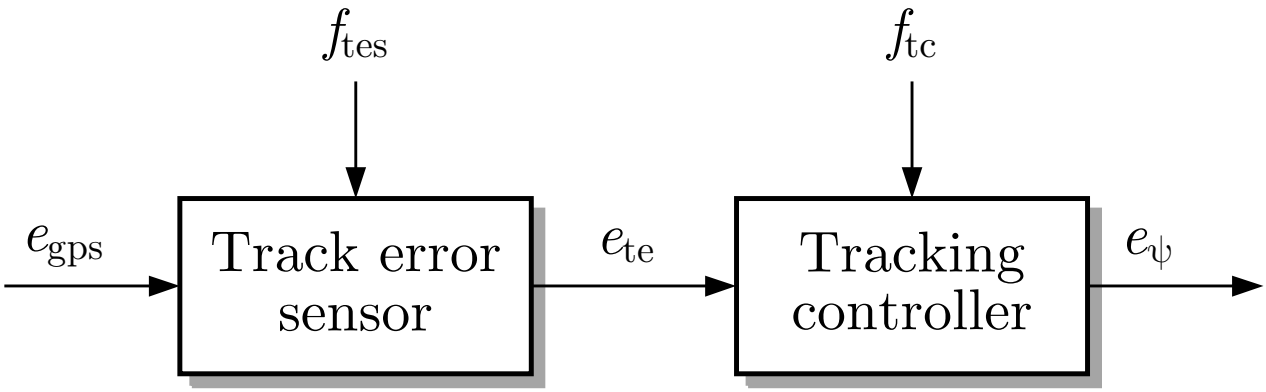

Fig. 4.6. Propagation of faults through the track error sensor and track controller

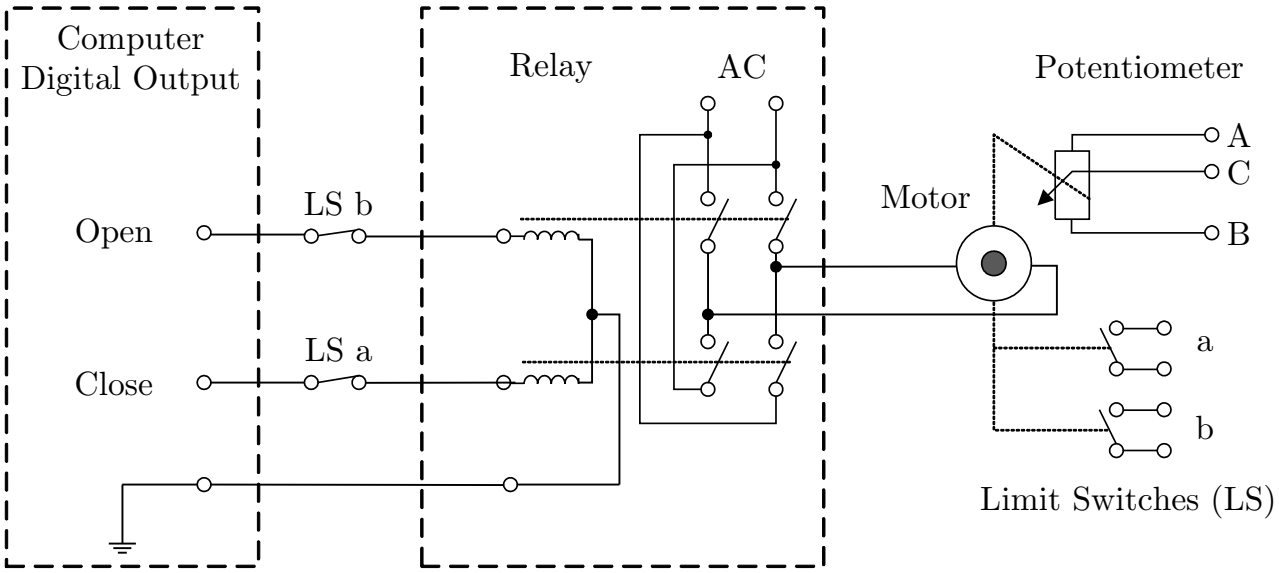

Fig. 4.7. Operation of 3-way valve actuator with relay operated induction motor. (Abbreviations: o:open, c:close, LS:Limit switch, AC: Alternating Current)

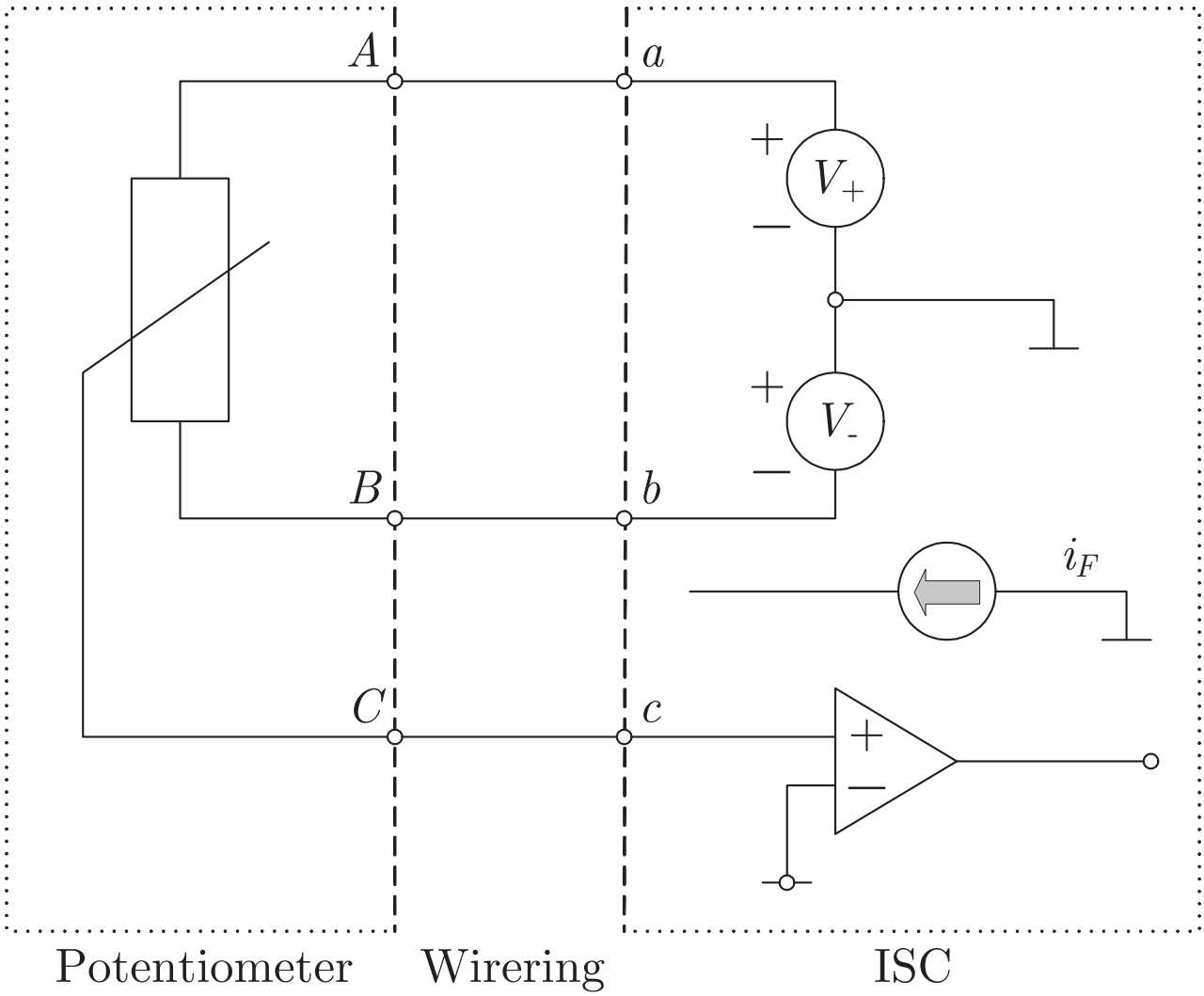

Fig. 4.8. Electrical diagram of potentiometer and computer interface to enable fault detection at the single sensor level

Blanke/Kinnaert/Lunze/Staroswiecki:
Diagnosis and Fault-Tolerant Control, (3rd edition), Springer-Verlag 2015

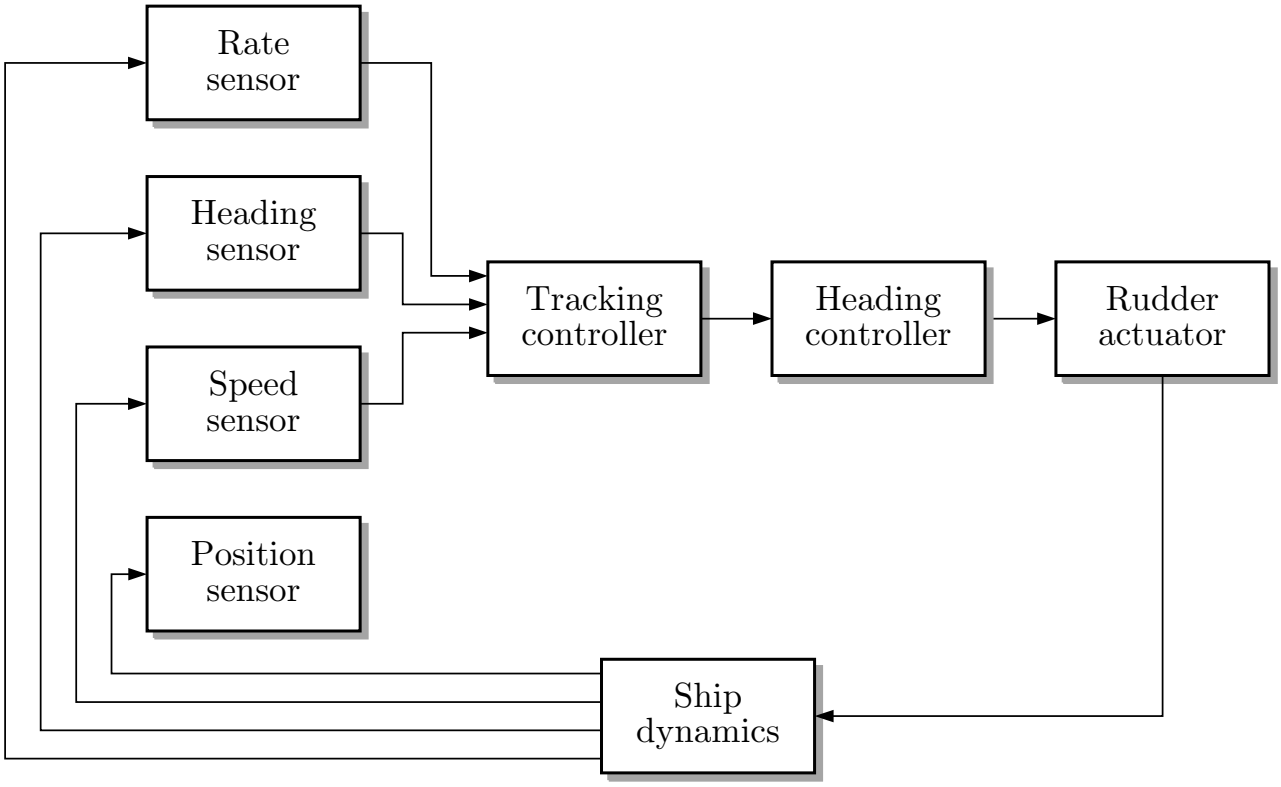

Fig. 4.9. Fault propagation in the ship steering problem

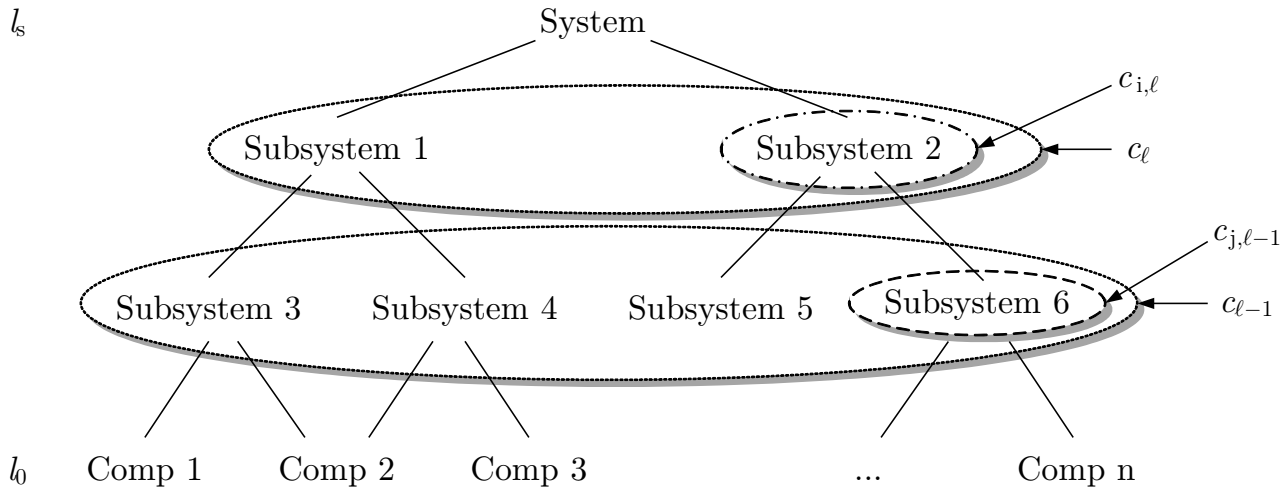

Fig. 4.10. Aggregation of low-level components into high-level ones

Blanke/Kinnaert/Lunze/Staroswiecki:
Diagnosis and Fault-Tolerant Control, (3rd edition), Springer-Verlag 2015

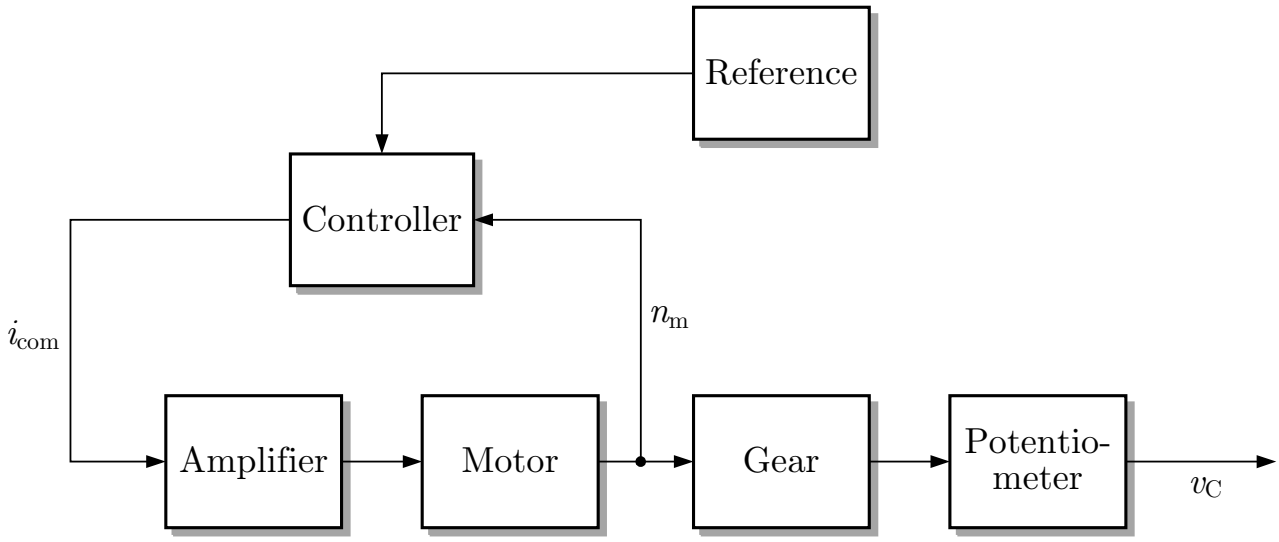

Fig. 4.11. Component diagram for speed loop part of the industrial actuator

Blanke/Kinnaert/Lunze/Staroswiecki:
Diagnosis and Fault-Tolerant Control, (3rd edition), Springer-Verlag 2015

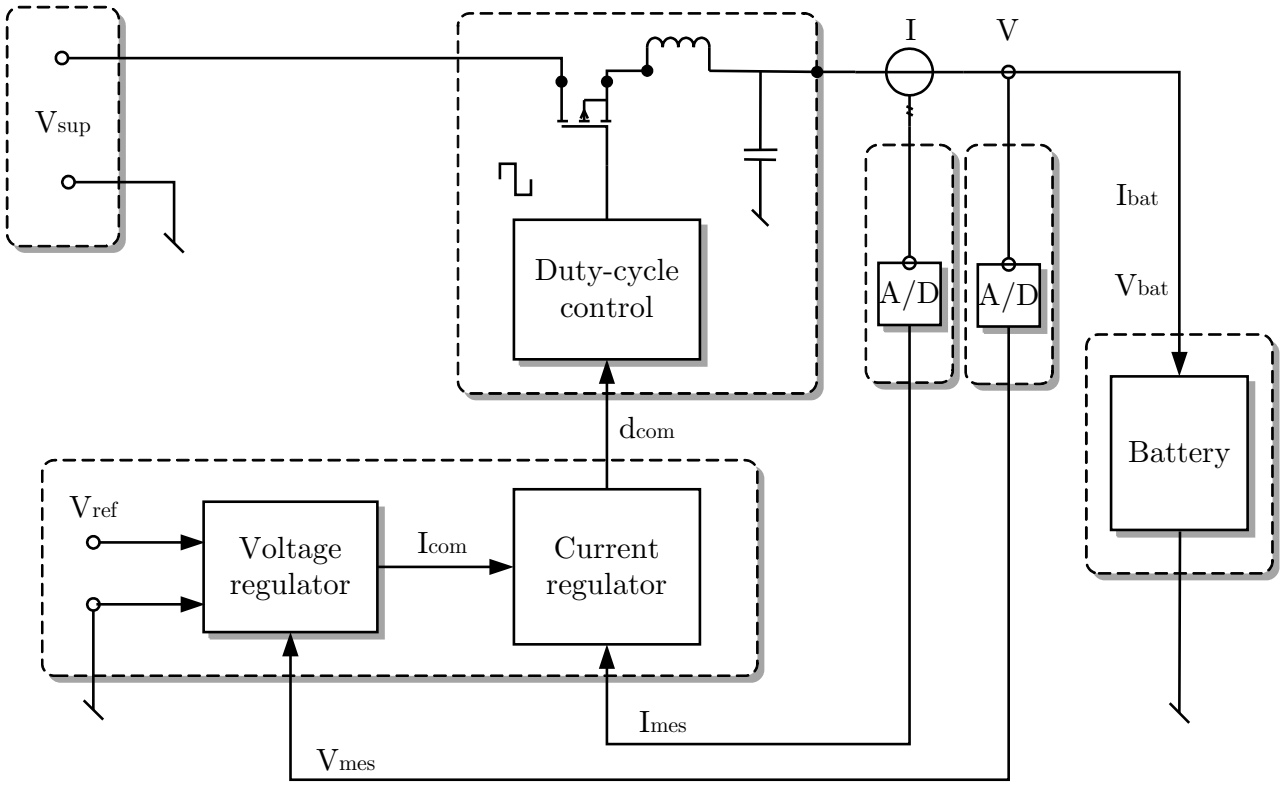

Fig. 4.12. Component diagram of battery charger

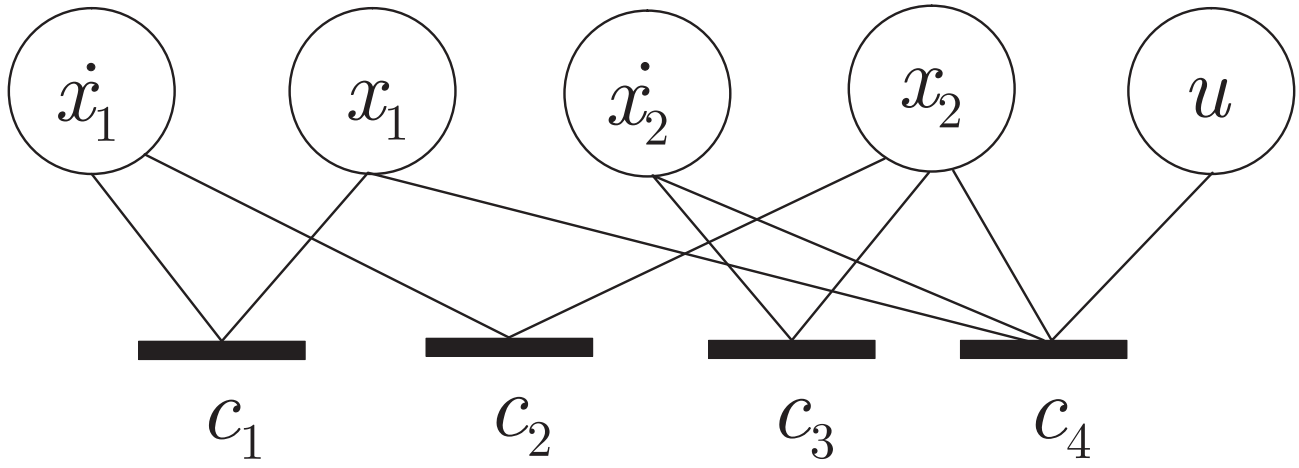

Fig. 5.1. Bi-partite graph of the linear system

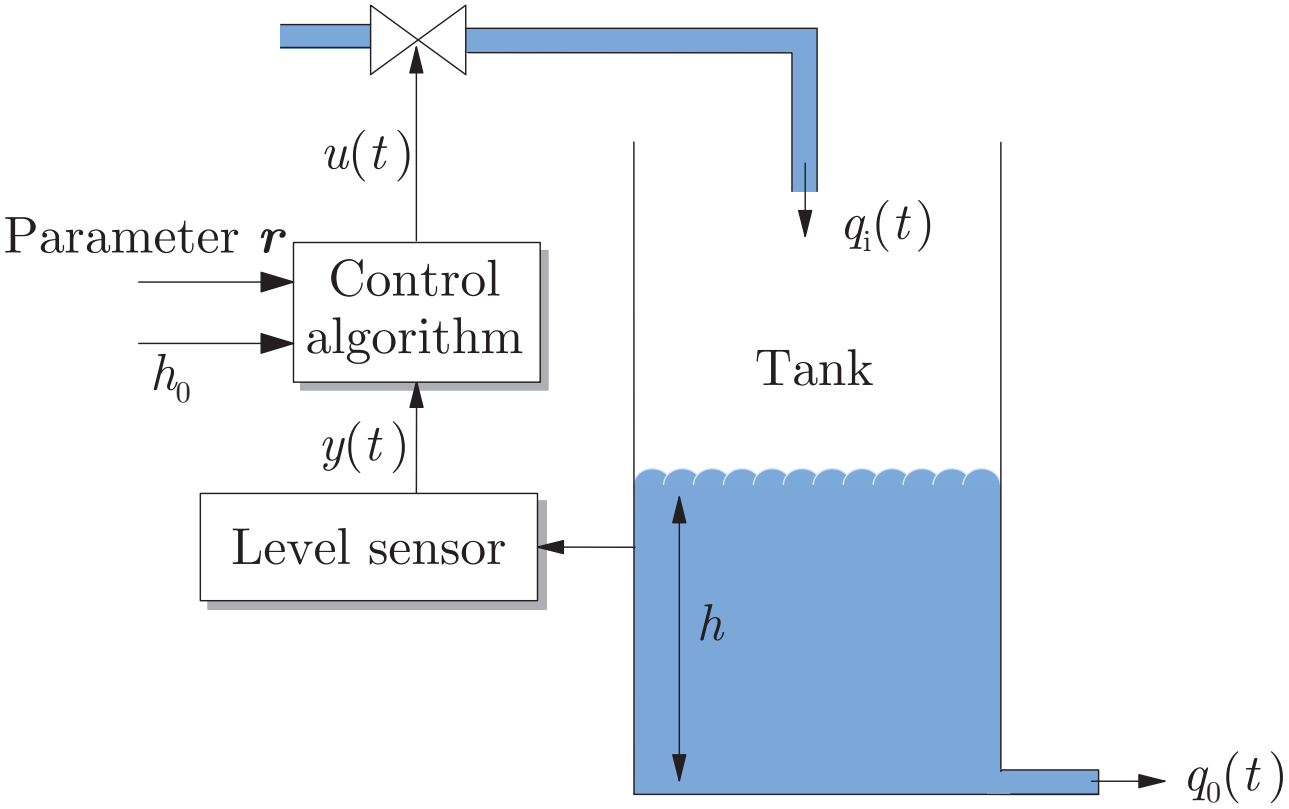

Fig. 5.2. Single-tank system

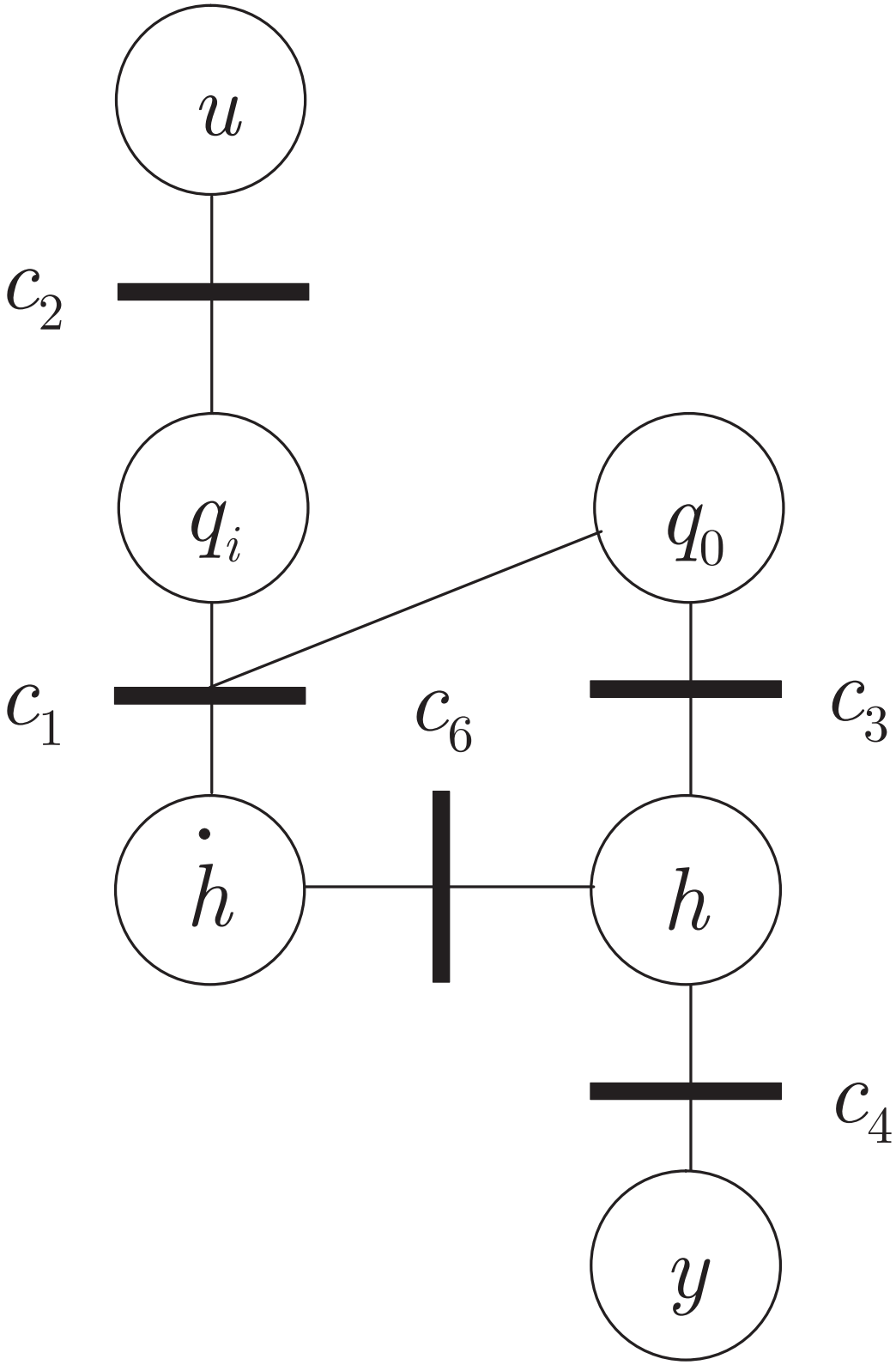

Fig. 5.3. Structure graph of the single-tank system without controller

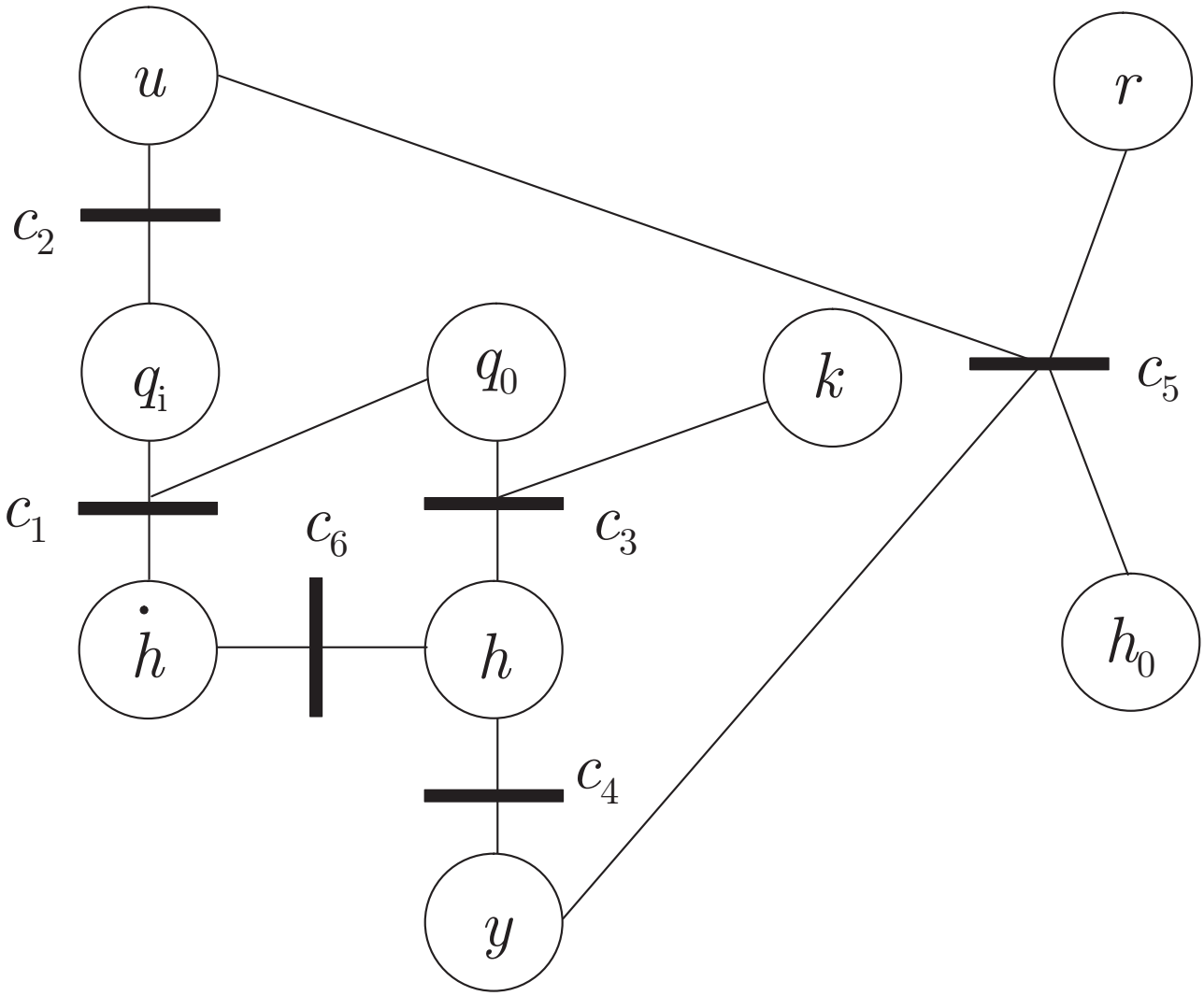

Fig. 5.4. Structure graph of the controlled tank

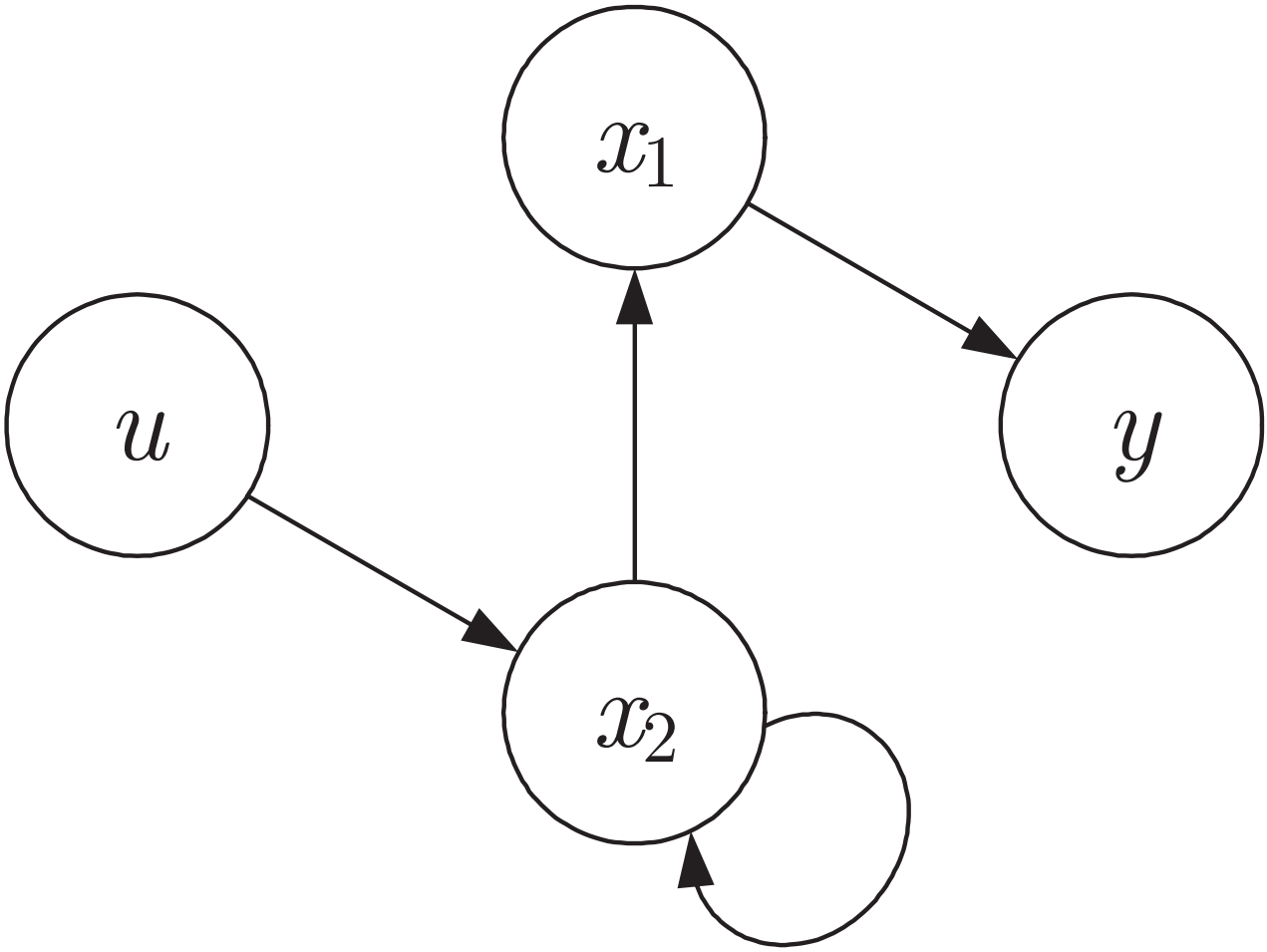

Fig. 5.5. Digraph of the linear system

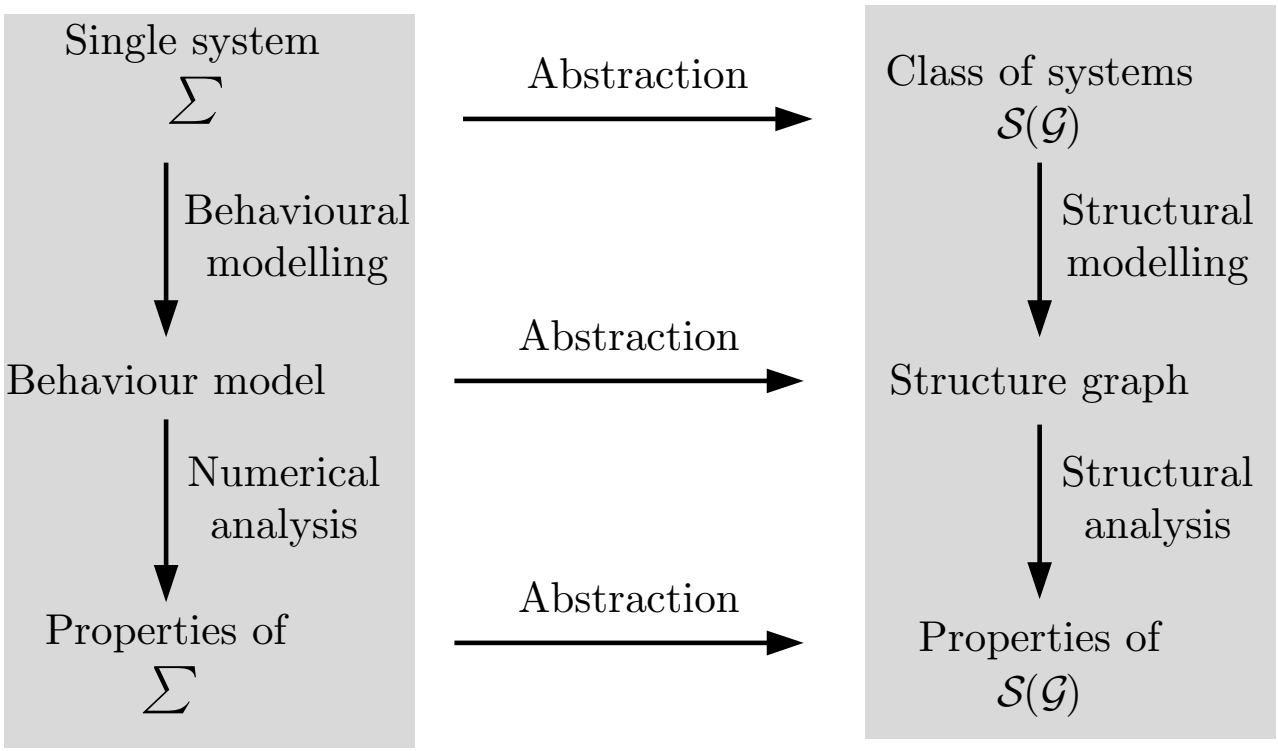

Fig. 5.6. Numerical and structural analysis of dynamical systems

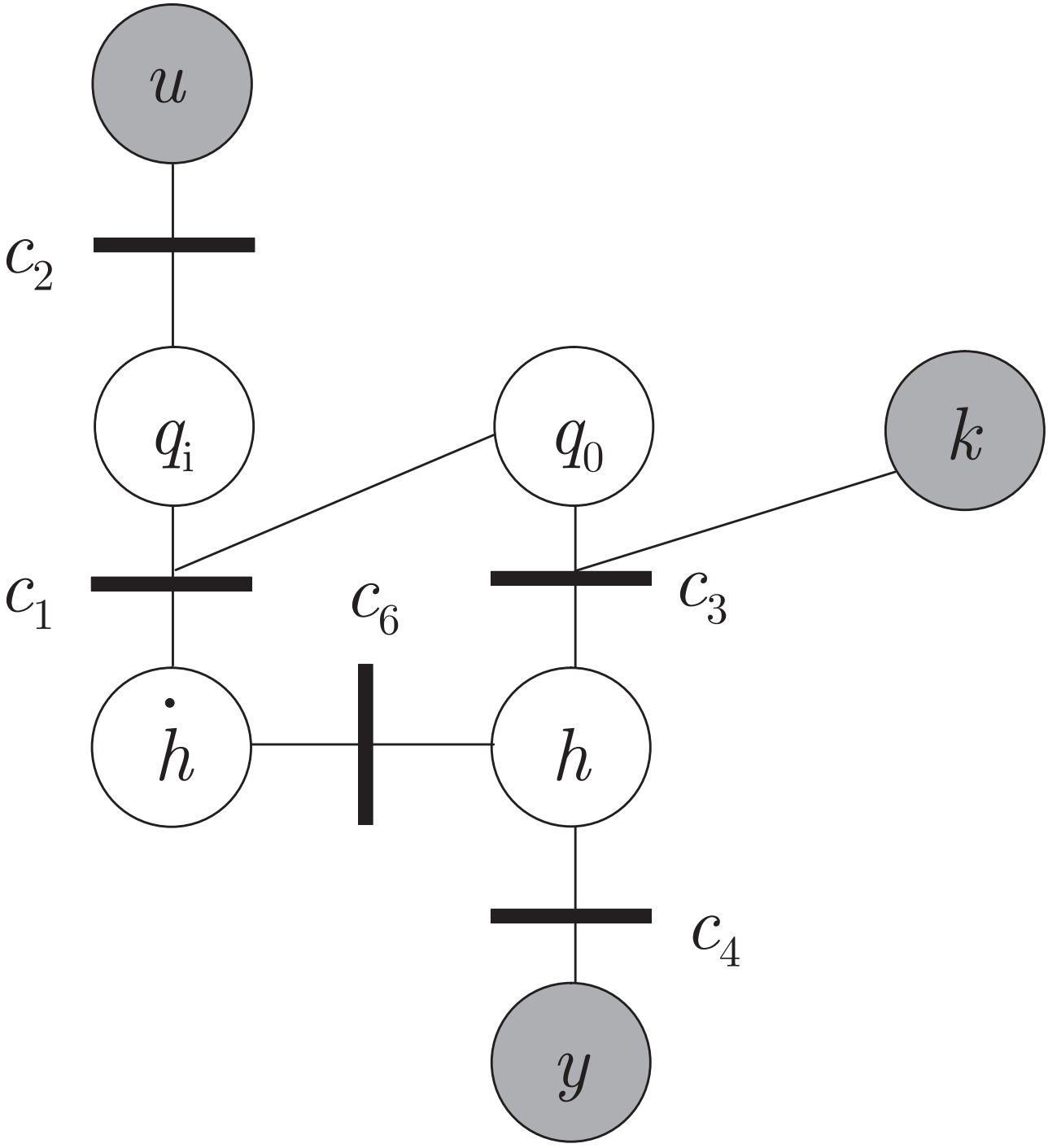

Fig. 5.7. Reduced structure graph of the tank system

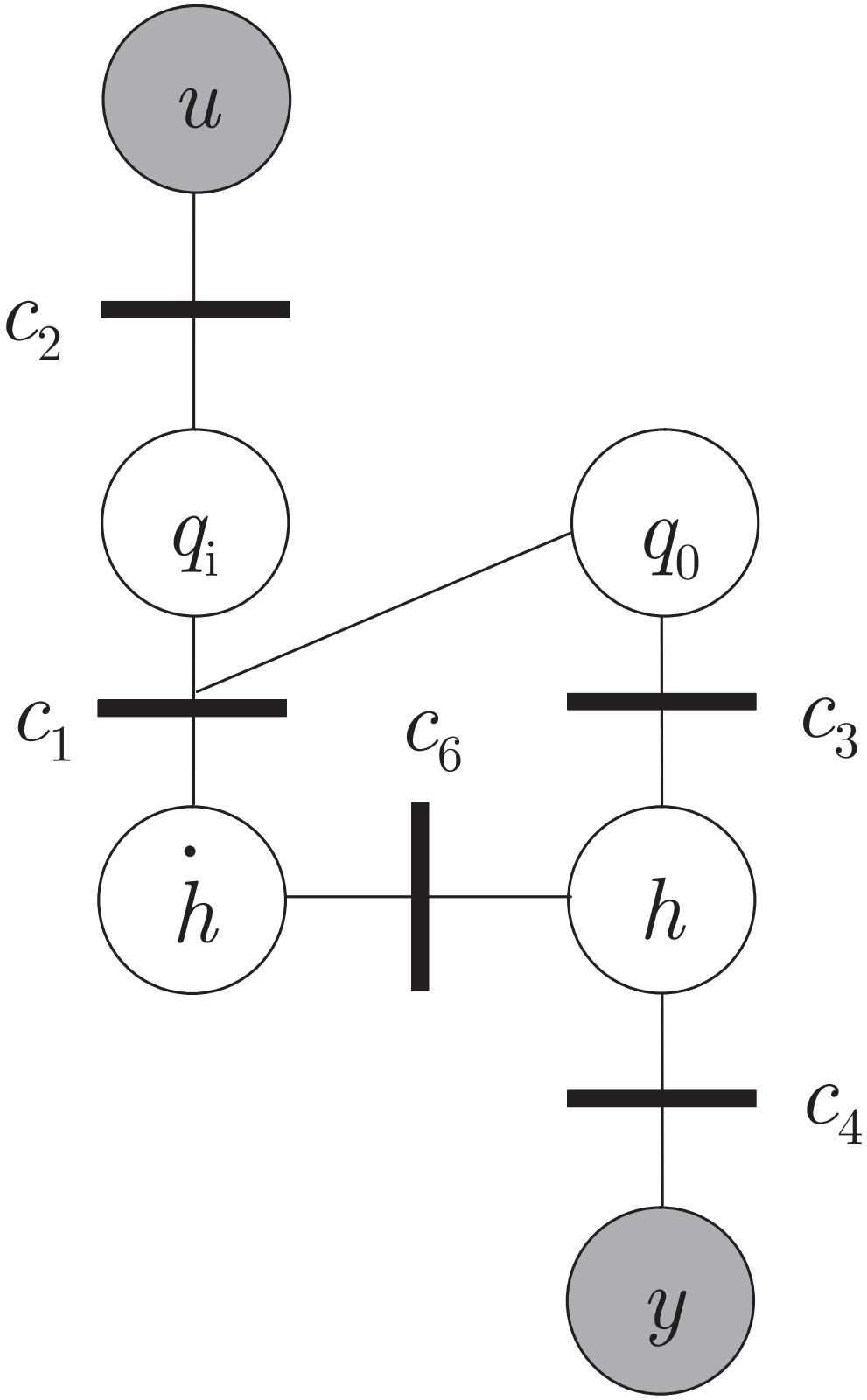

Fig. 5.7. Structure graph used in diagnosis

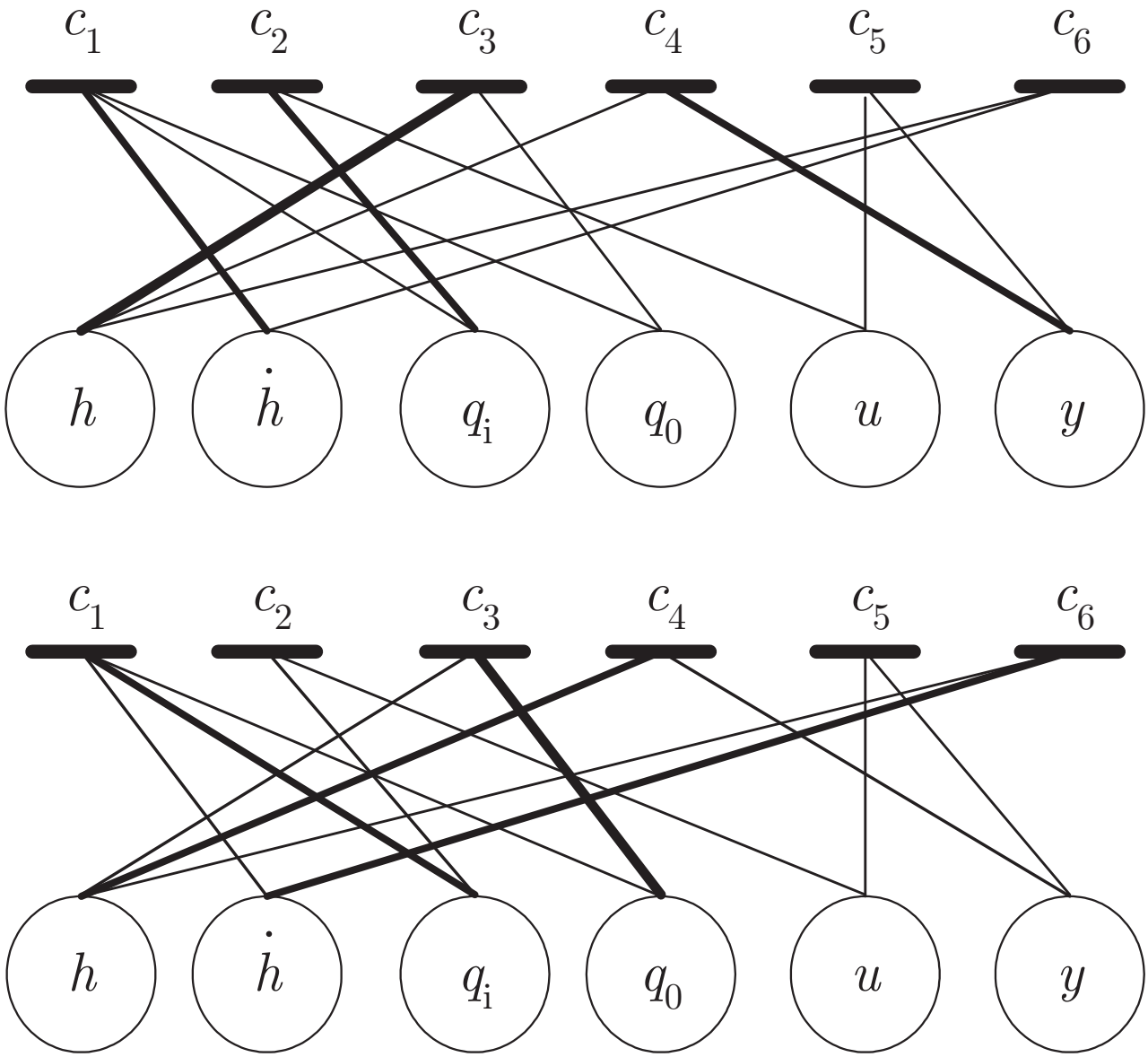

Fig. 5.8. Two matchings for the tank system: The edges $e \in \mathcal{M}$ are drawn by thick lines.

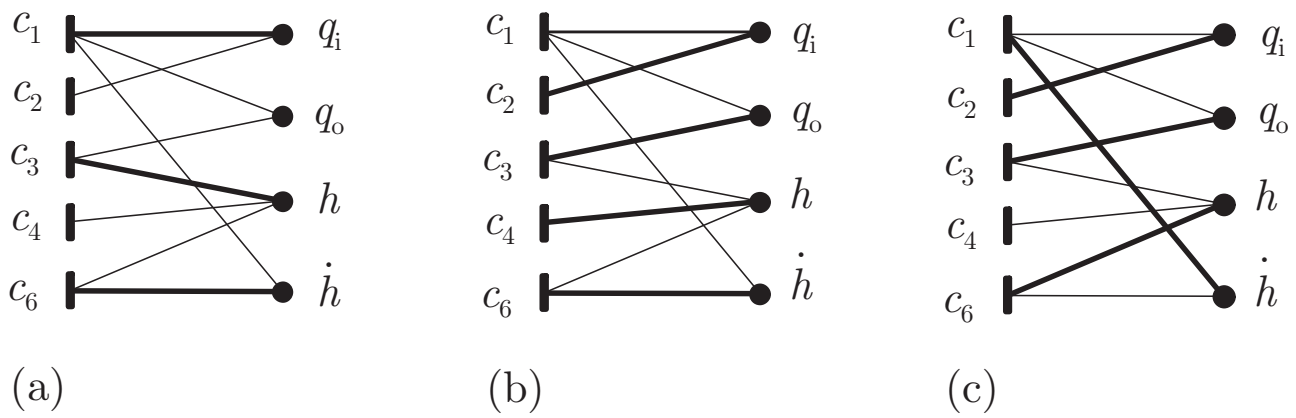

Fig. 5.9. An incomplete matching (a) and two matchings (b), (c) that are complete with respect to $\mathcal{Z}$

Blanke/Kinnaert/Lunze/Staroswiecki:
Diagnosis and Fault-Tolerant Control, (3rd edition), Springer-Verlag 2015

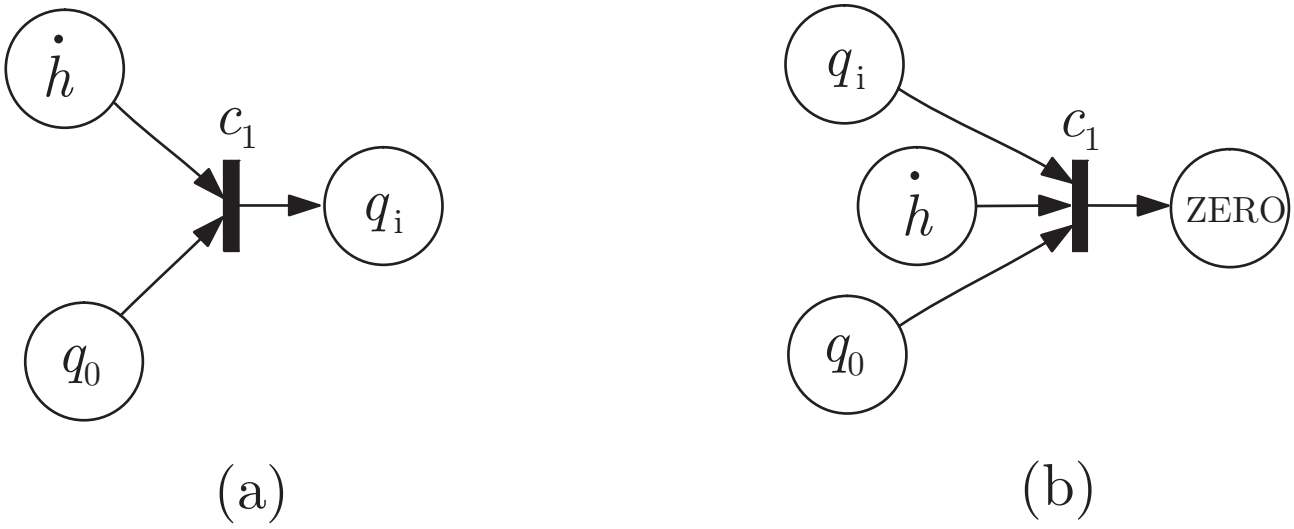

Fig. 5.10. Matched (a) and a non-matched constraint (5.13) (b)

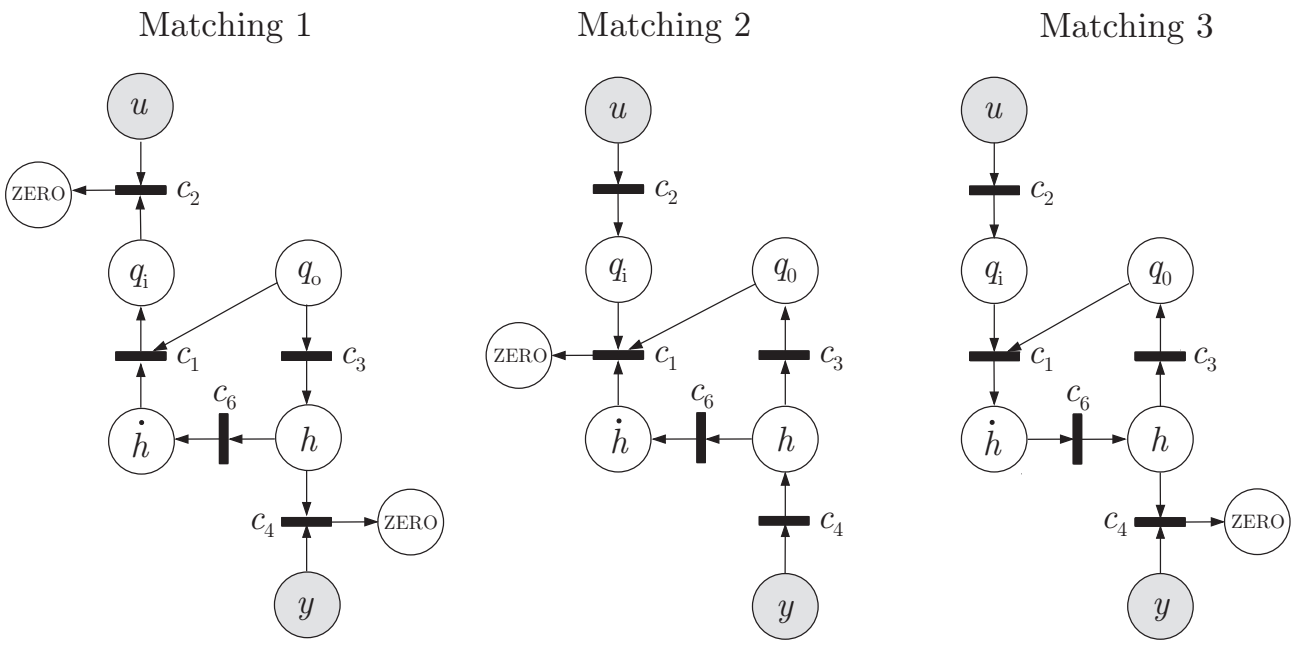

Fig. 5.11. Directed graphs corresponding to the three matchings

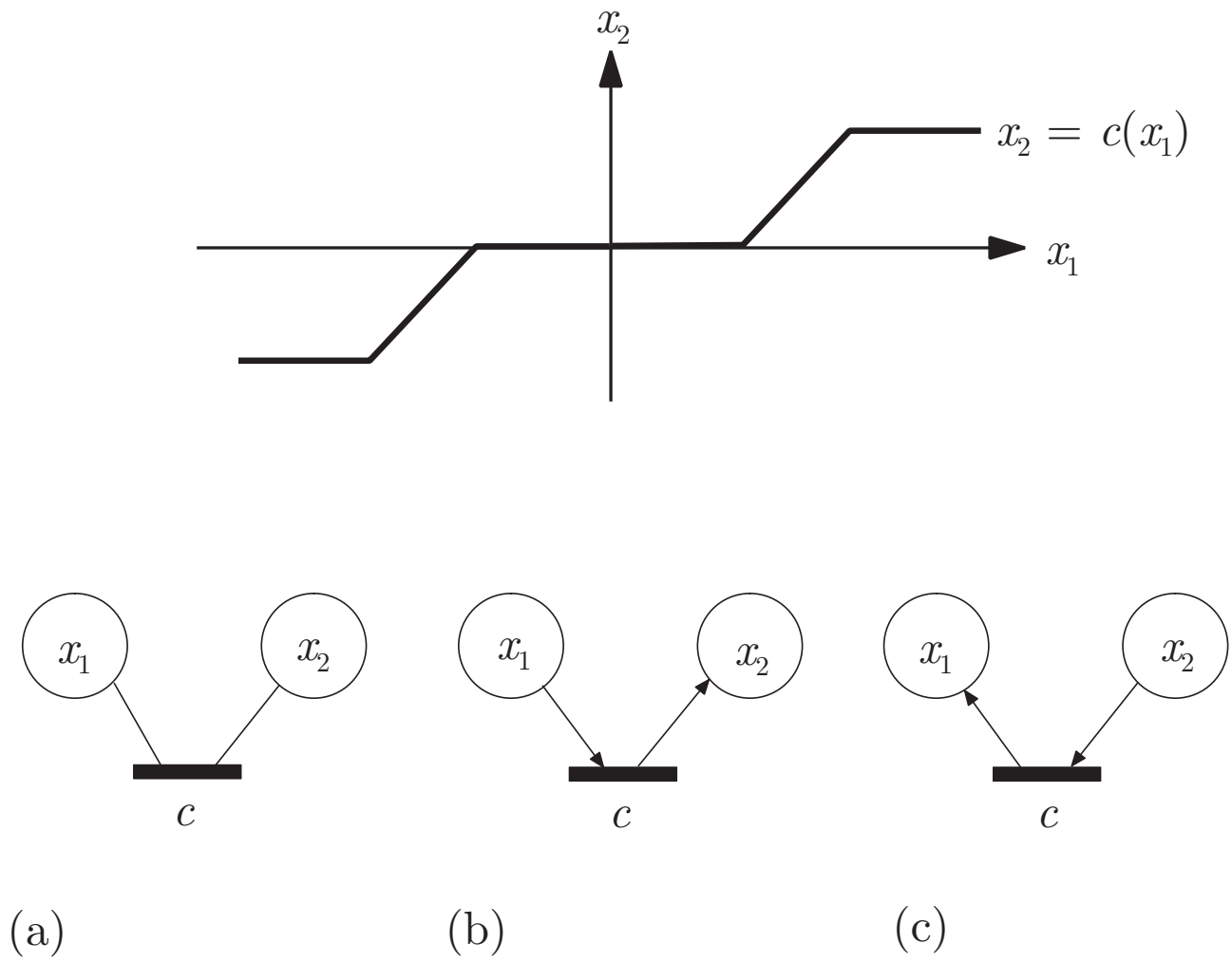

Fig. 5.12. Structure graph (a), possible (b) and impossible matching (c)

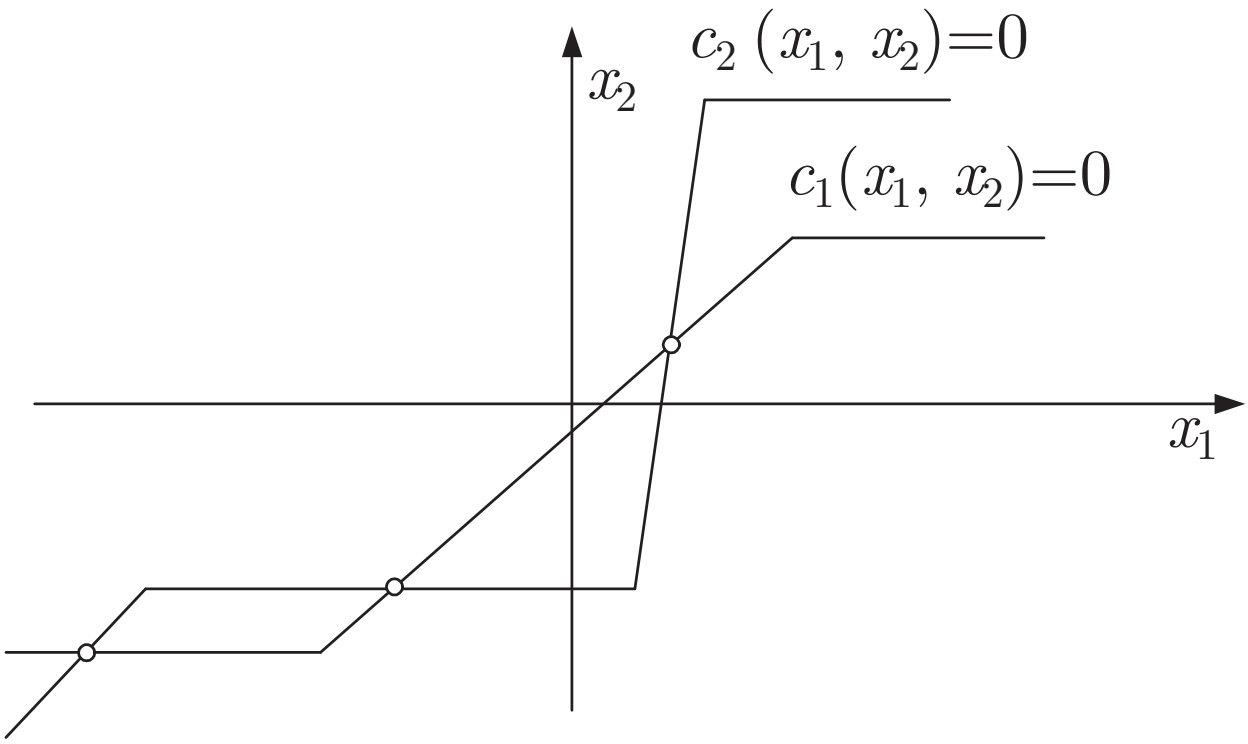

Fig. 5.13. Two algebraic constraints with two unknowns

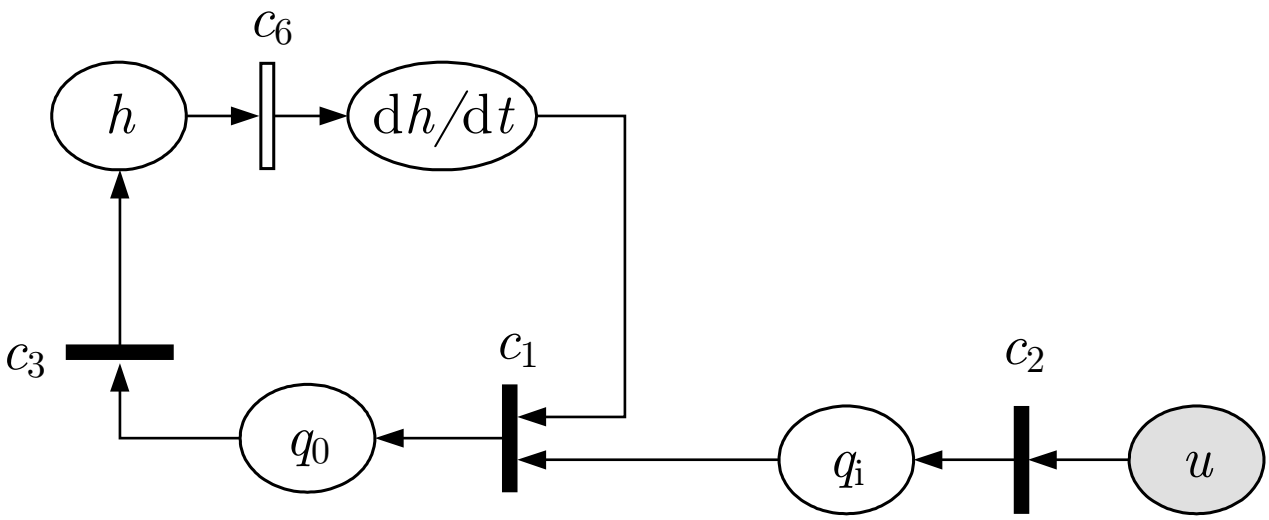

Fig. 5.14. A matching with a differential loop

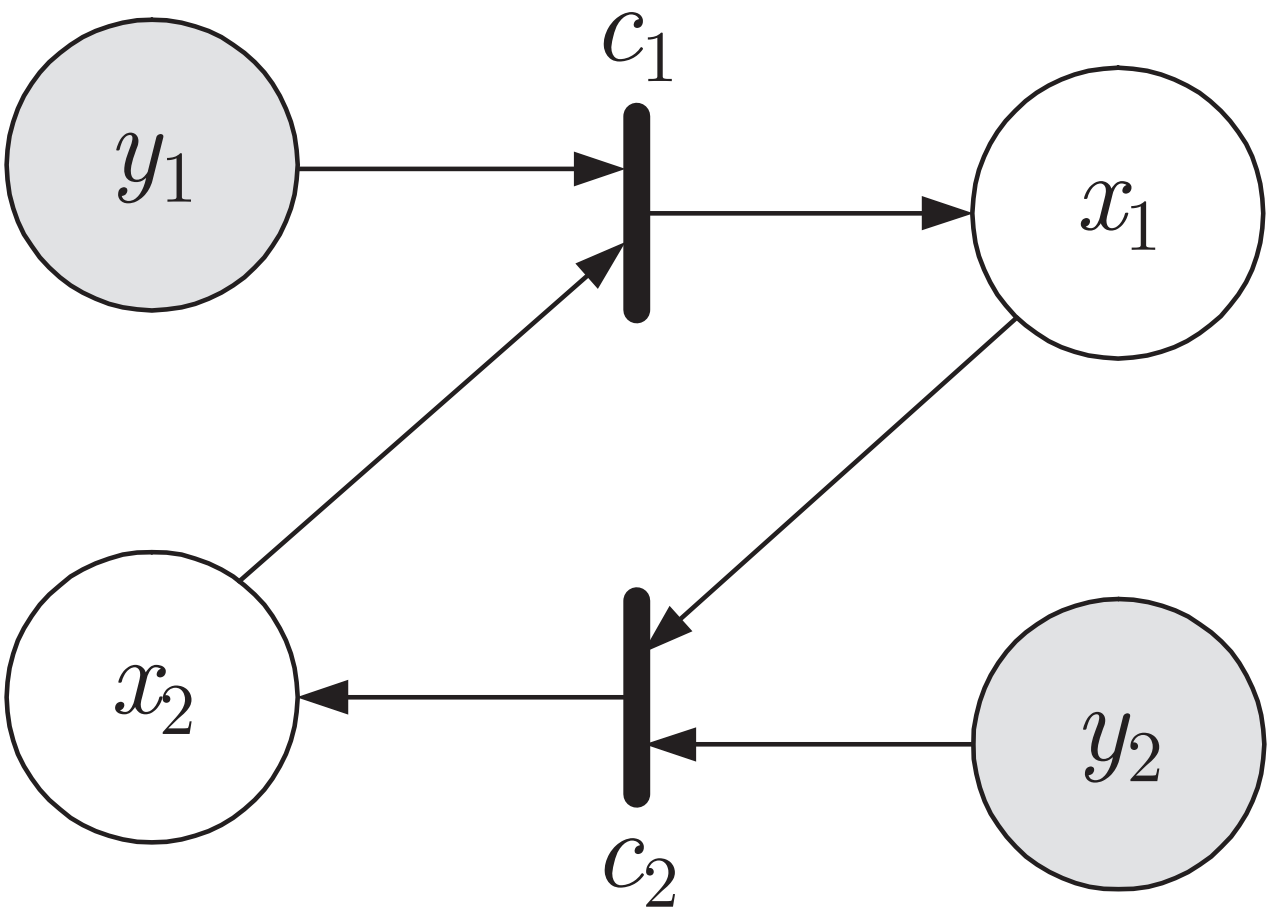

Fig. 5.15. An algebraic loop (Part 1)

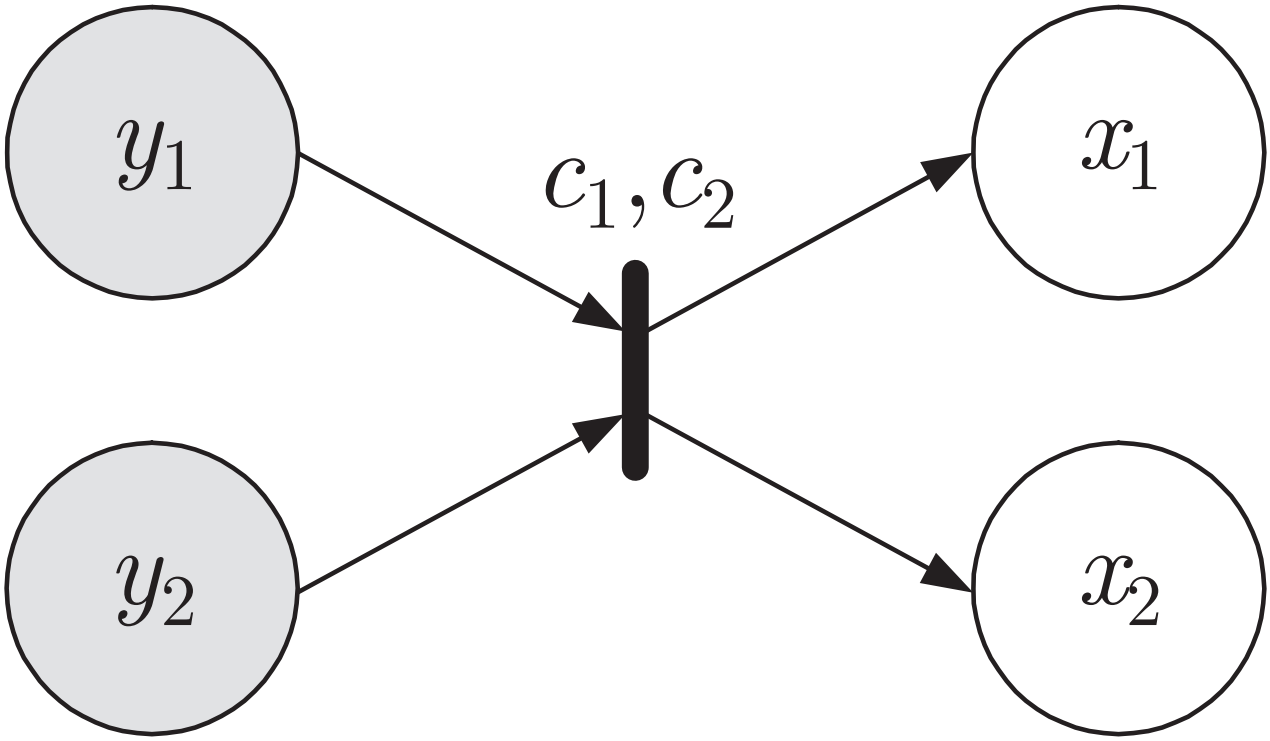

Fig. 5.15. An algebraic loop (Part 2)

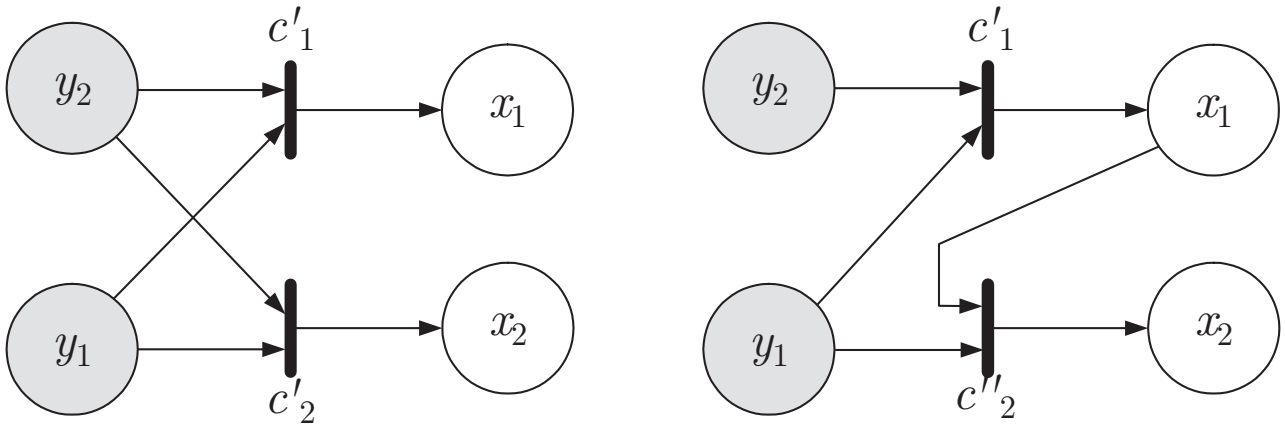

Fig. 5.16. Two equivalent loop-free oriented graphs

Blanke/Kinnaert/Lunze/Staroswiecki:
Diagnosis and Fault-Tolerant Control, (3rd edition), Springer-Verlag 2015

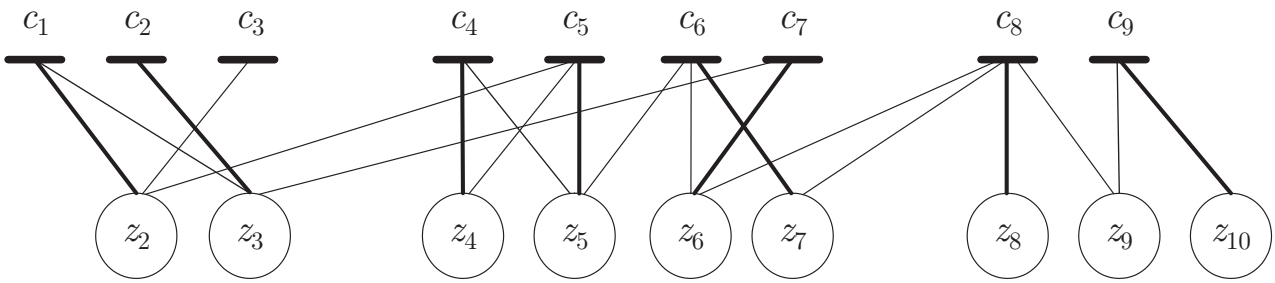

Fig. 5.17. Example of the canonical decomposition of a bi-partite graph

Blanke/Kinnaert/Lunze/Staroswiecki:
Diagnosis and Fault-Tolerant Control, (3rd edition), Springer-Verlag 2015

Page 151

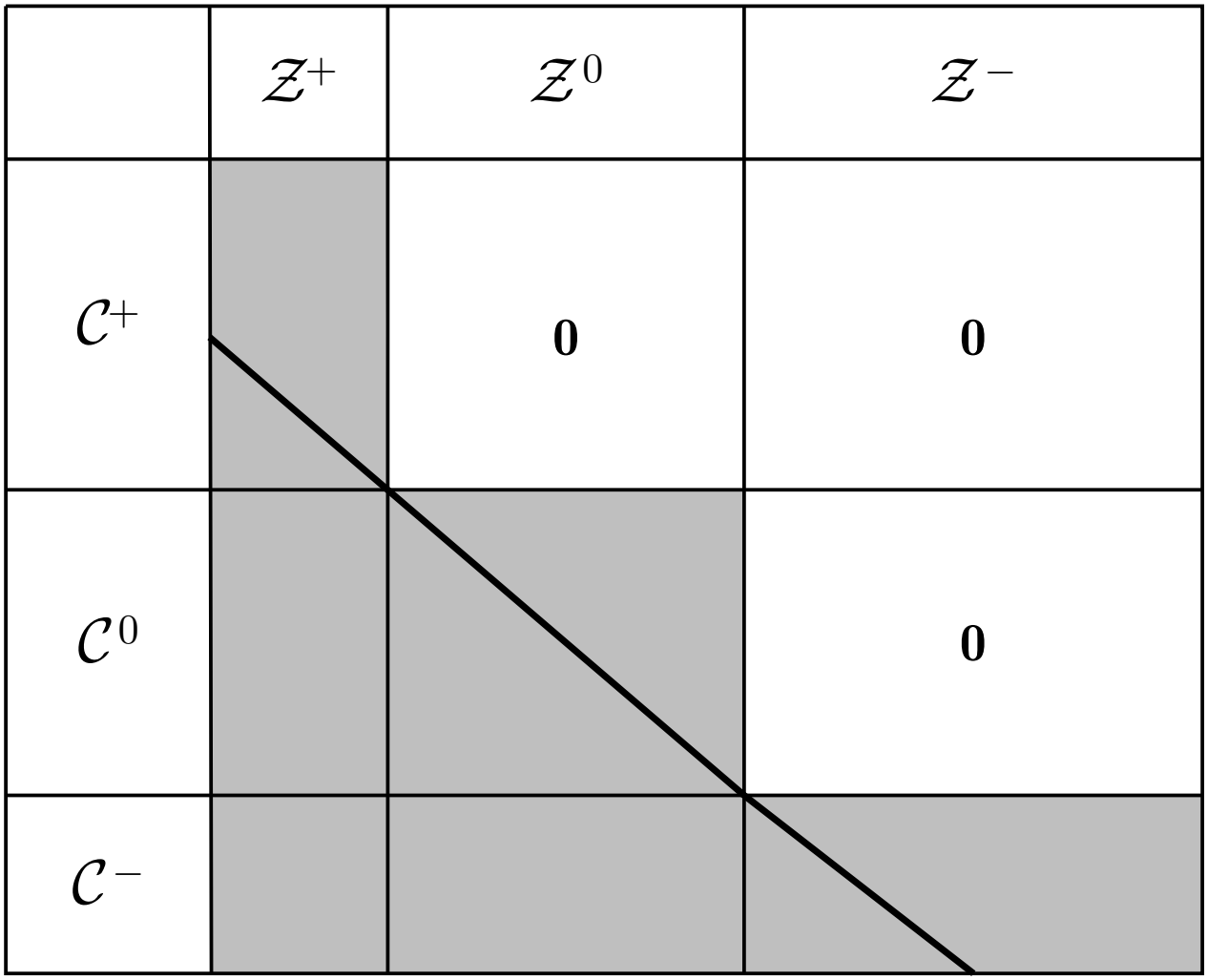

Fig. 5.18. Canonical decomposition of the structure graph

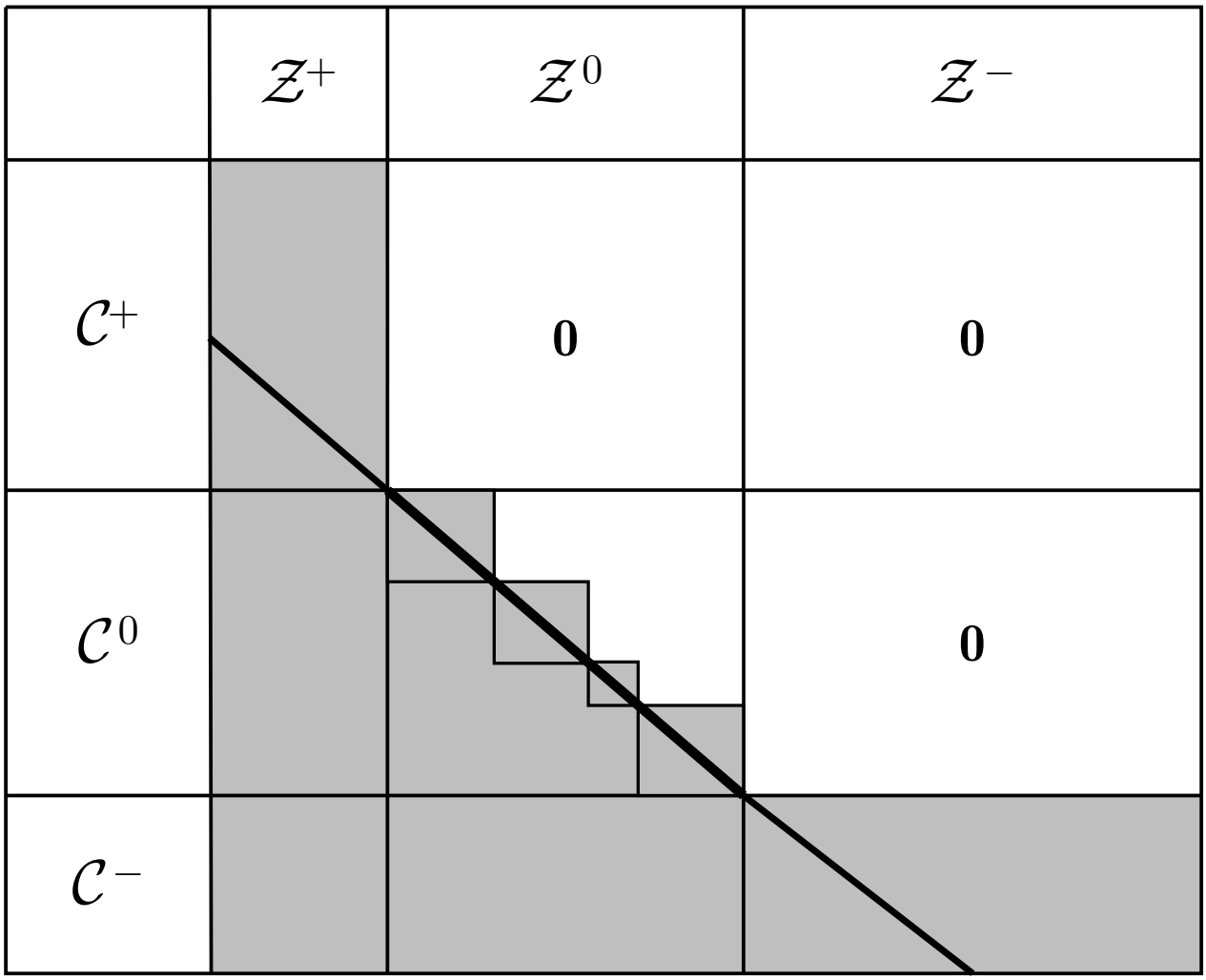

Fig. 5.19. Incidence matrix after the detailed decomposition of the just-constrained subgraph

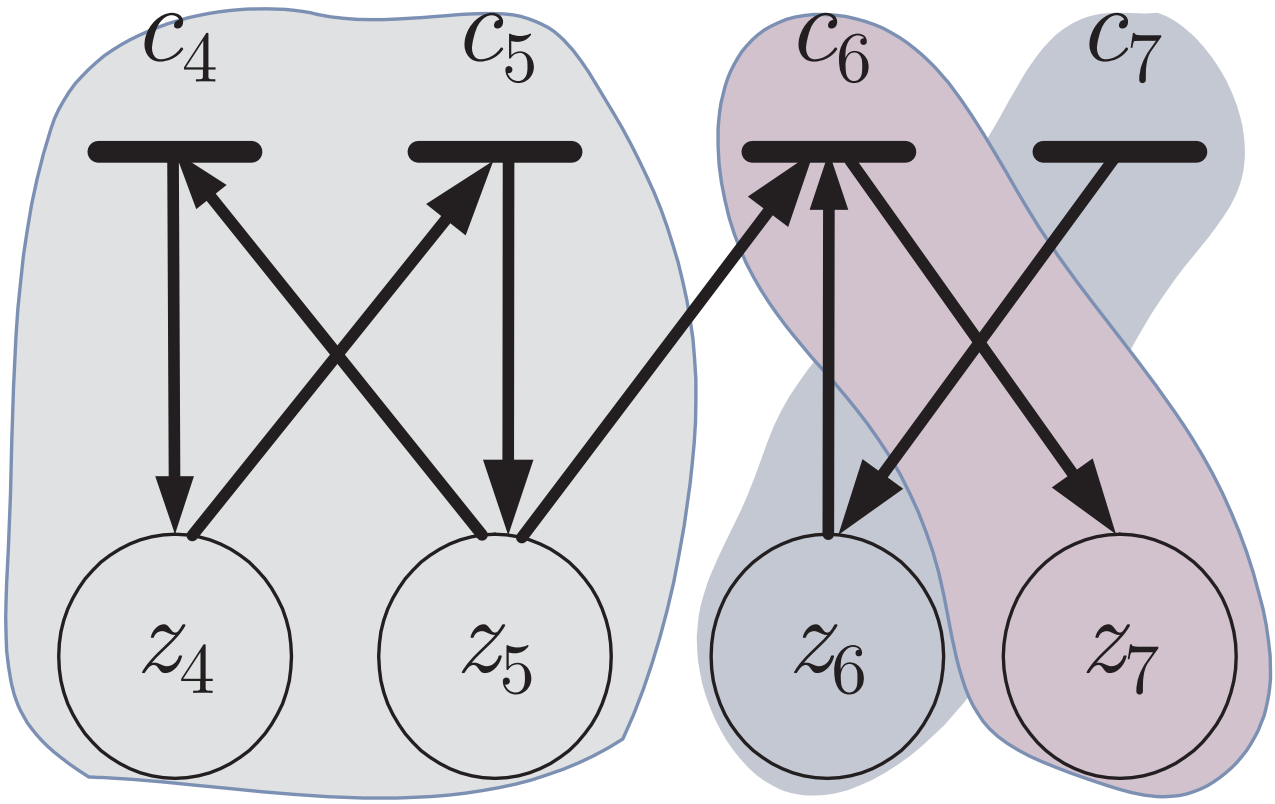

Fig. 5.20. Decomposition of the just-constrained subgraph $\mathcal{G}^0$ into strongly connected components

Blanke/Kinnaert/Lunze/Staroswiecki:
Diagnosis and Fault-Tolerant Control, (3rd edition), Springer-Verlag 2015

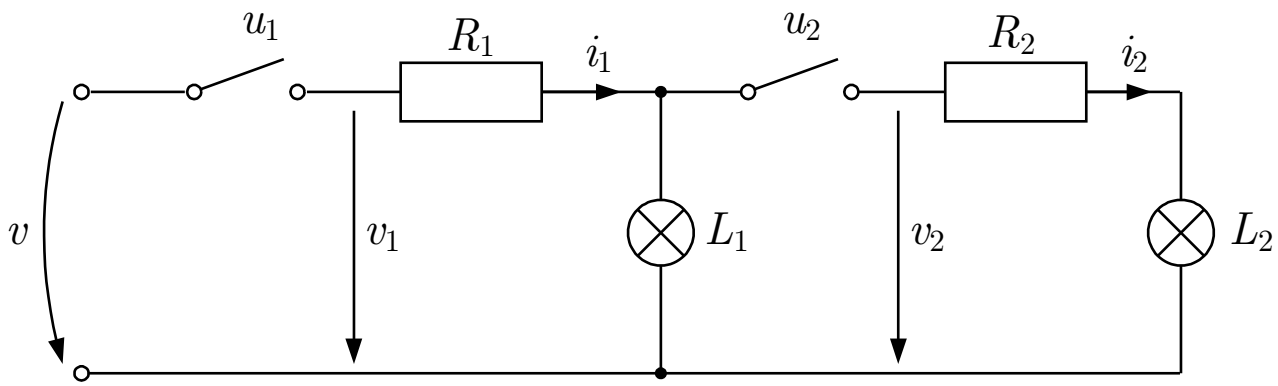

Fig. 5.21. Circuit of a tail lamp

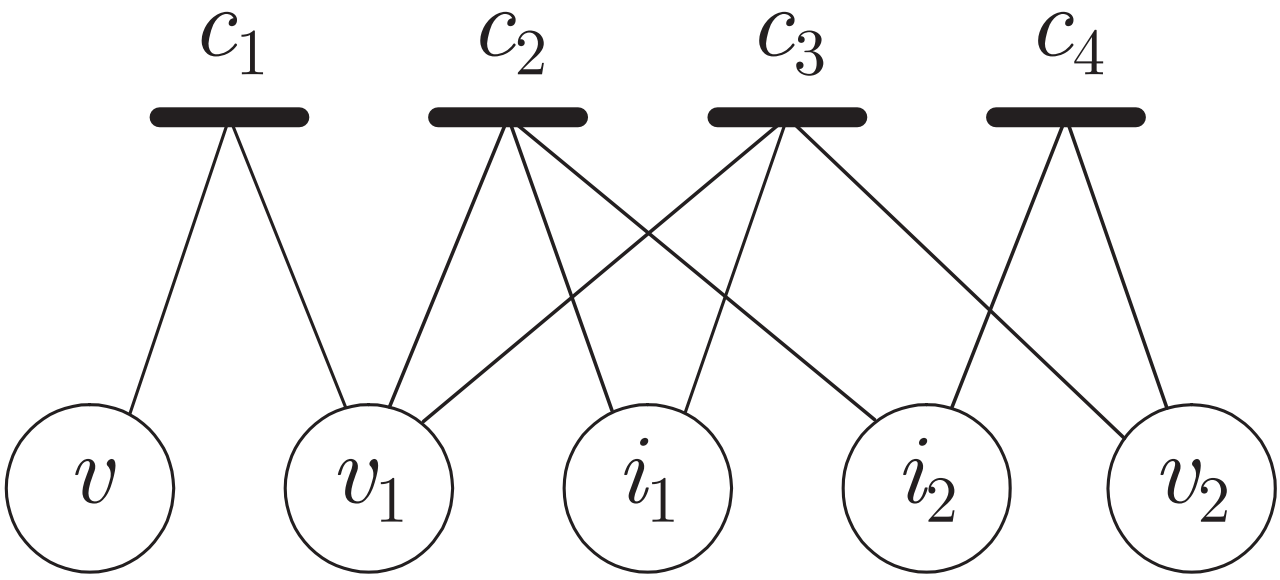

Fig. 5.22. Structure graph of the circuit (a) and DM decomposition of the reduced structure graph (b) (Part 1)

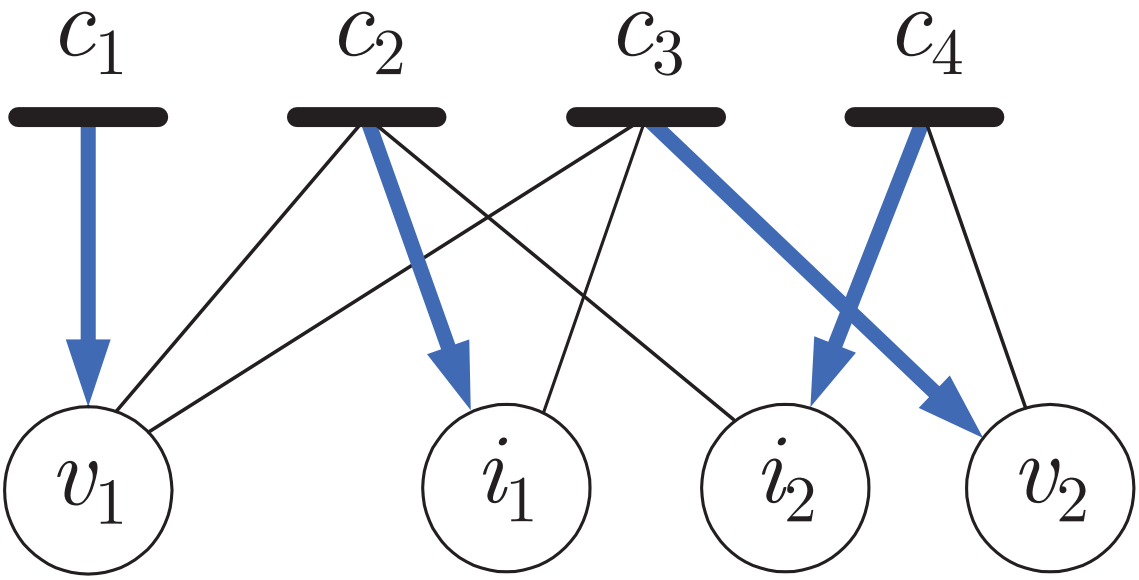

Fig. 5.22. Structure graph of the circuit (a) and DM decomposition of the reduced structure graph (b) (Part 2)

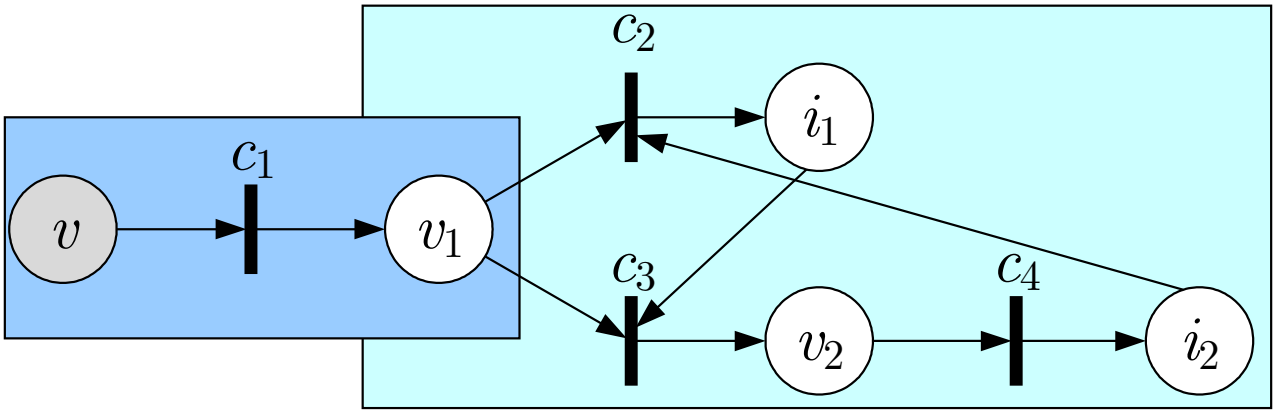

Fig. 5.23. Scheme for determining the unknown variables of the tail lamp for given input voltage v

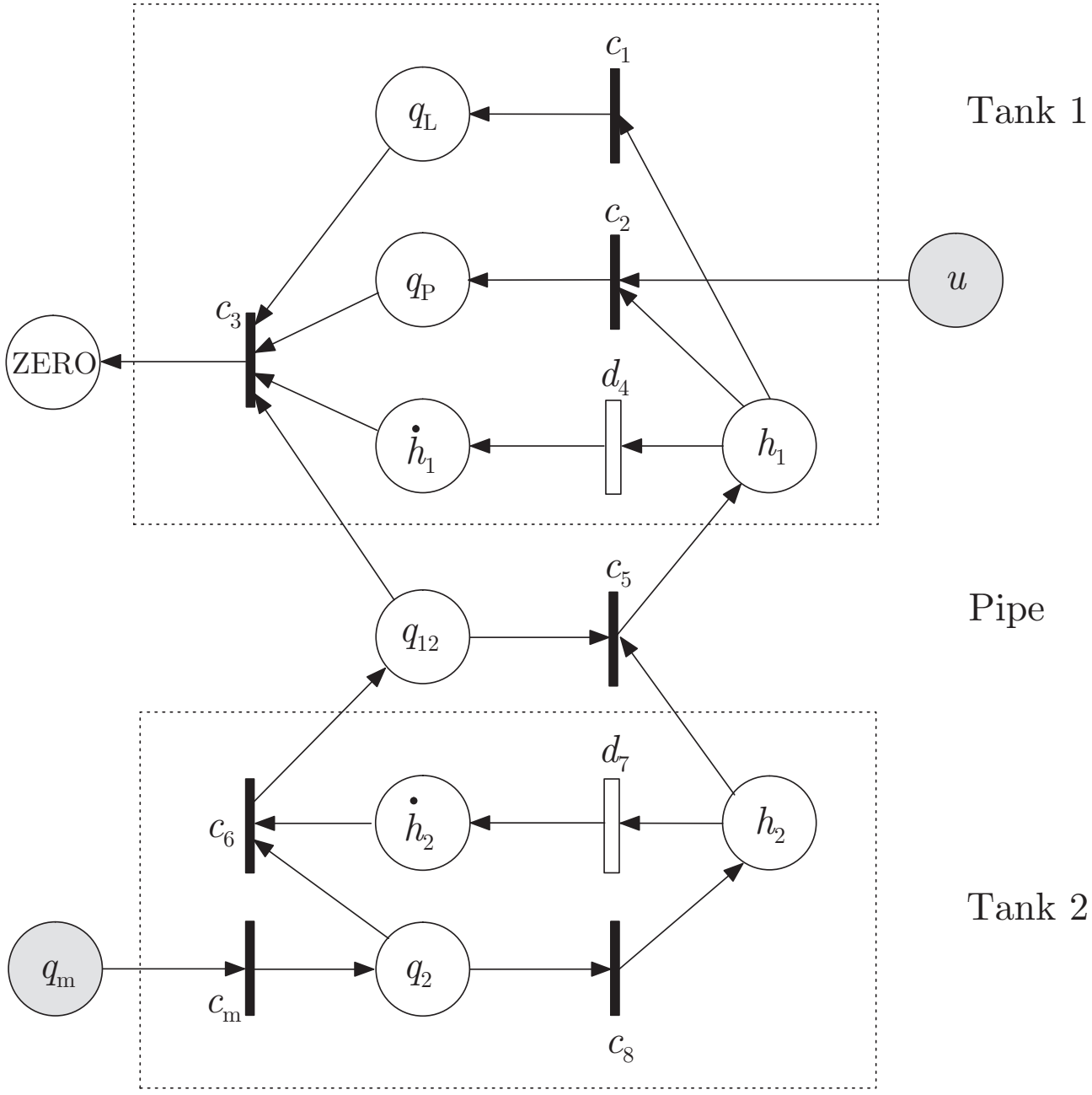

Fig. 5.24. Structure graph of the two-tank system

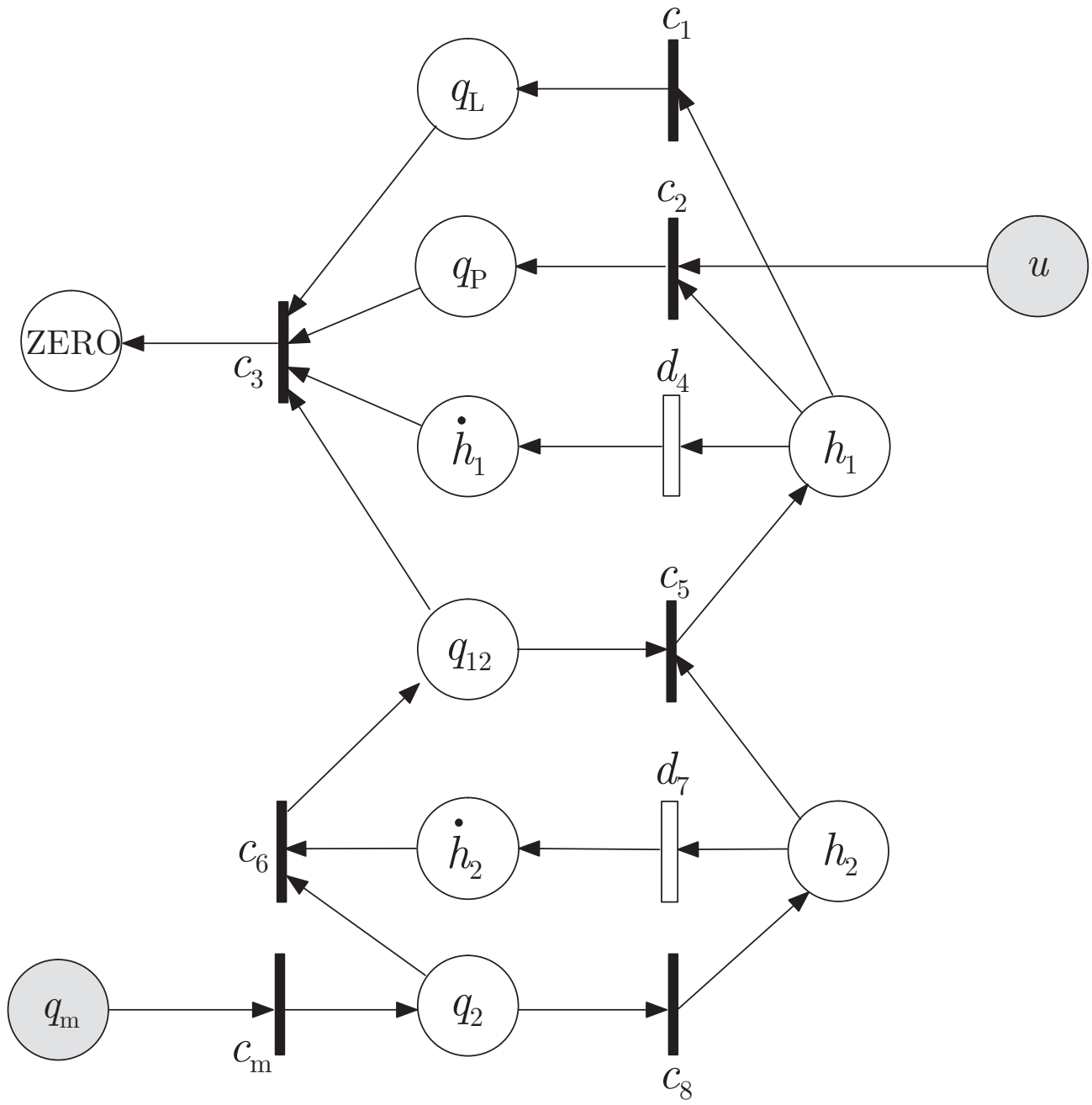

Fig. 5.25. Oriented graph of the two-tank system

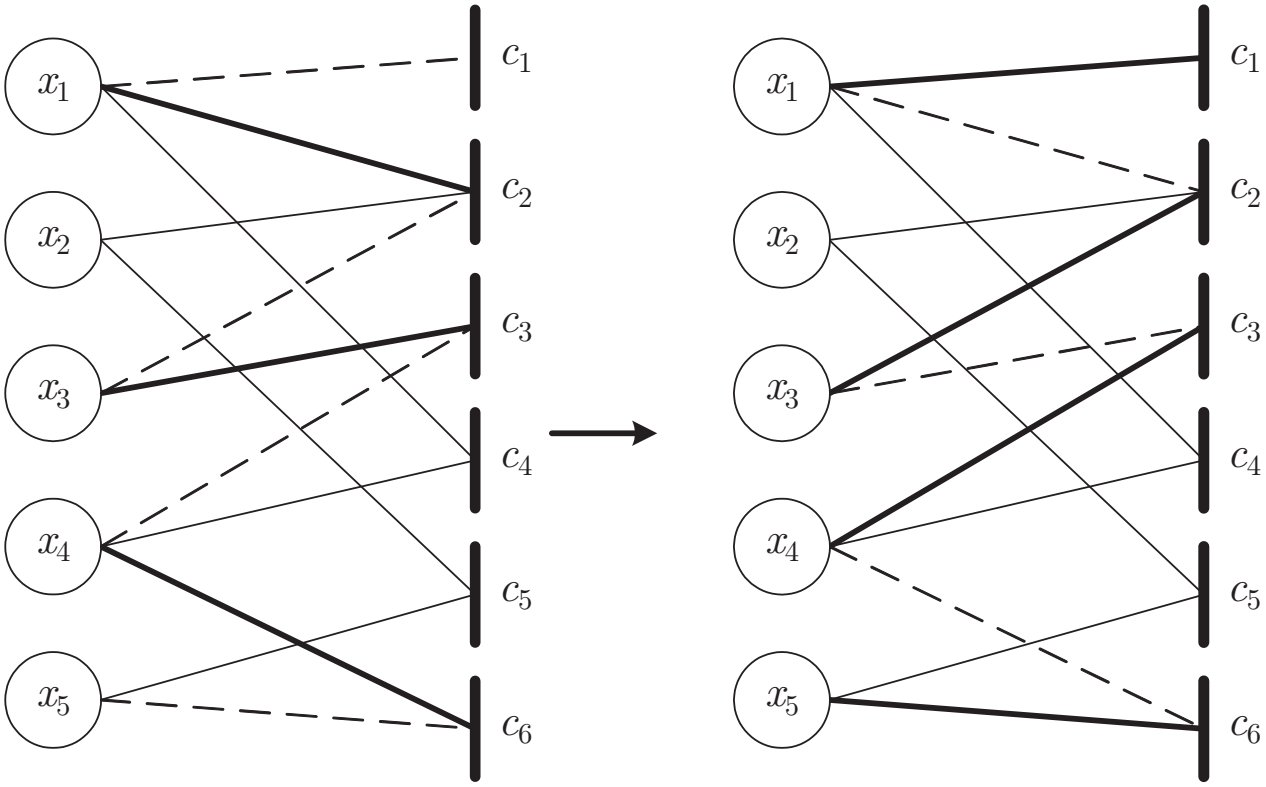

Fig. 5.26. Finding a new matching by using an augmenting path

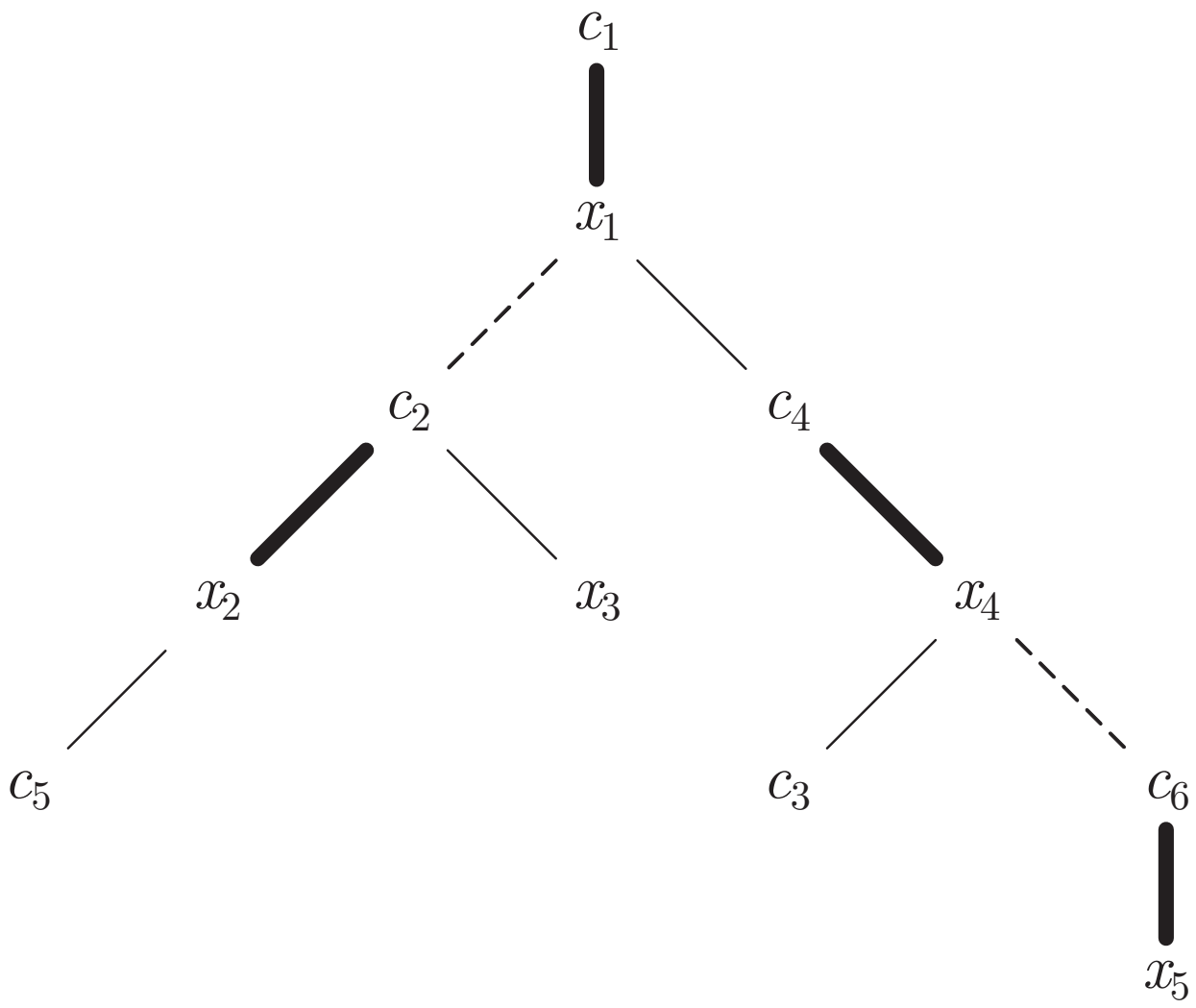

Fig. 5.27. Alternating tree with root c_1 (a) and with root c_3 (b) (Part 1)

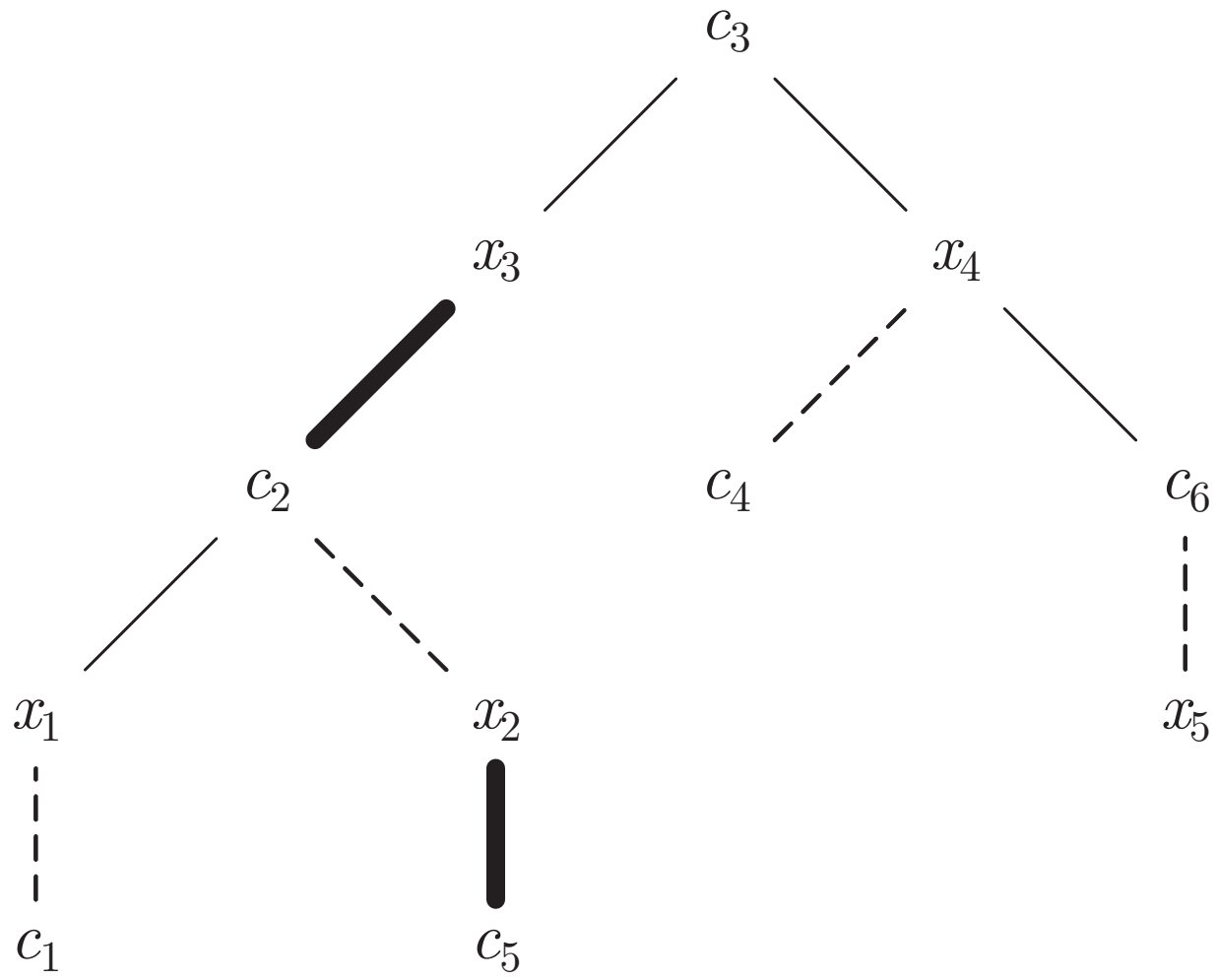

Fig. 5.27. Alternating tree with root c_1 (a) and with root c_3 (b) (Part 2)

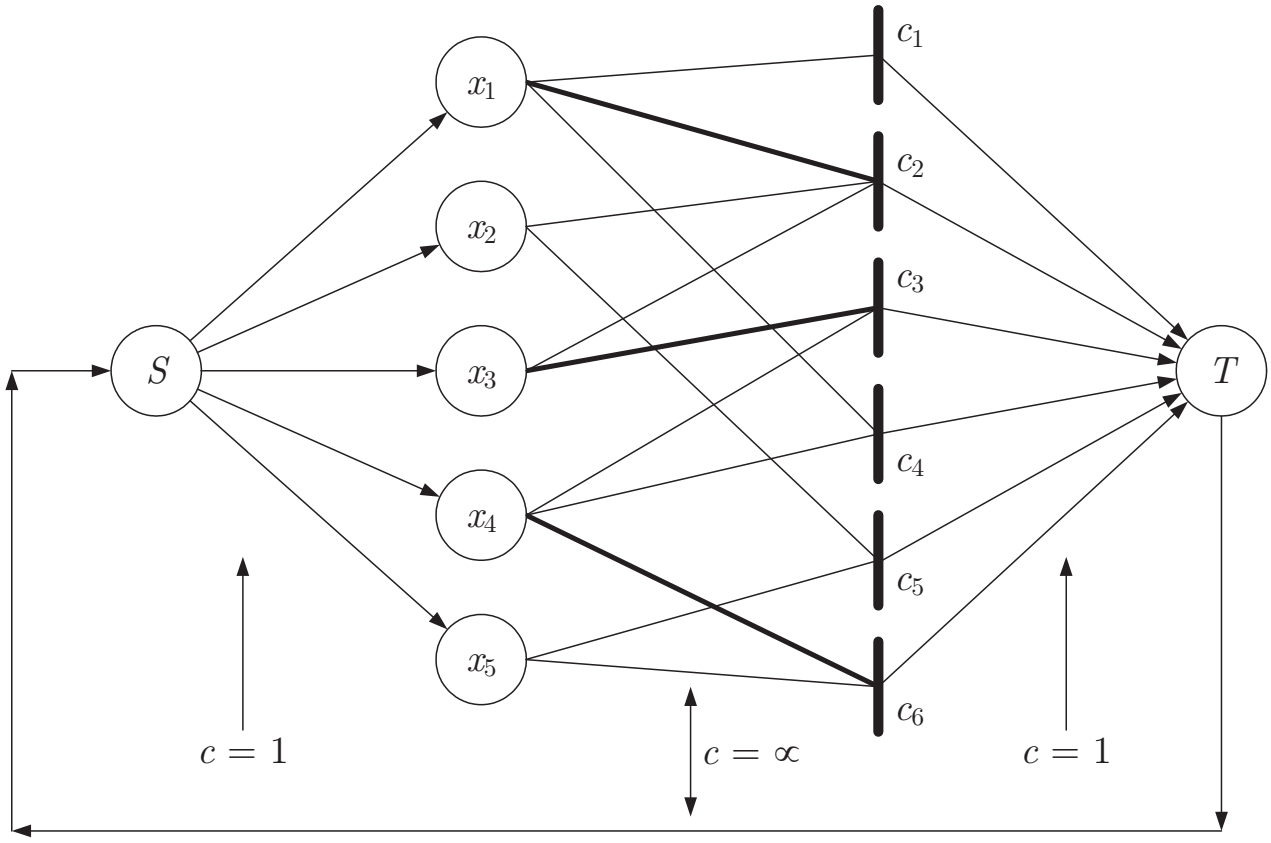

Fig. 5.28. Setting the maximum matching problem as a maximum flow problem.

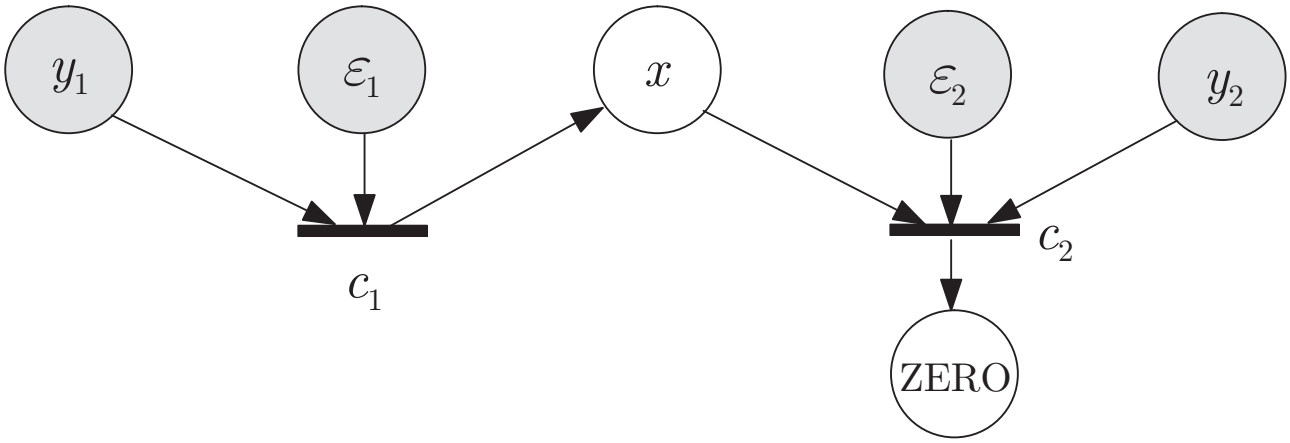

Fig. 5.29. Oriented structure graph for sensor monitoring

Blanke/Kinnaert/Lunze/Staroswiecki:
Diagnosis and Fault-Tolerant Control, (3rd edition), Springer-Verlag 2015

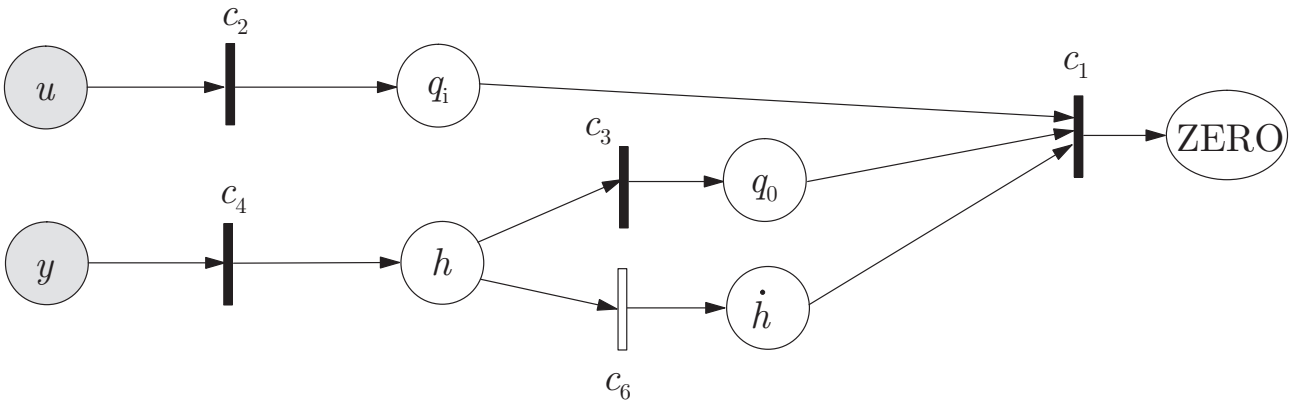

Fig. 5.30. Ranking for the single tank system

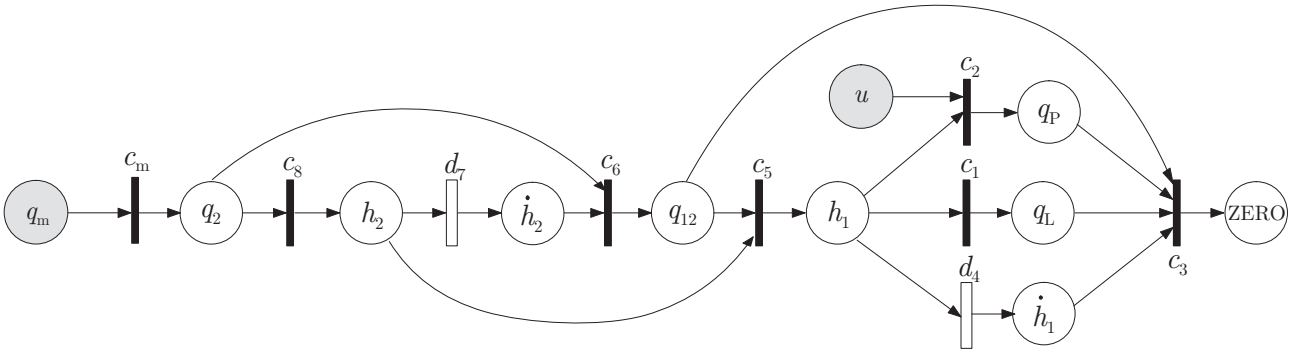

Fig. 5.31. Graph showing the order in which the unknown variables can be determined for given q_{m}

Blanke/Kinnaert/Lunze/Staroswiecki:
Diagnosis and Fault-Tolerant Control, (3rd edition), Springer-Verlag 2015

Page 188

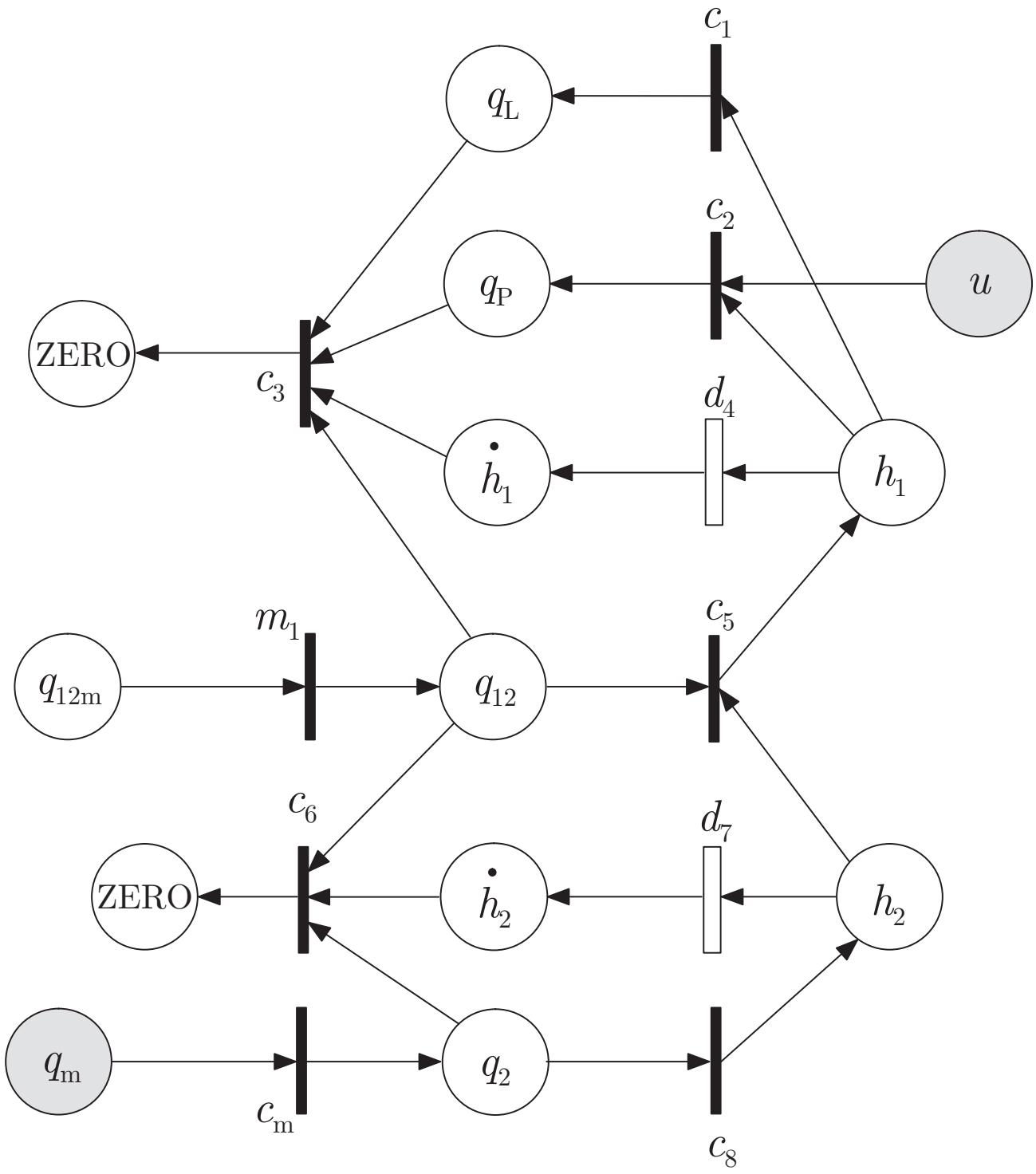

Fig. 5.32. Oriented graph, in which the arrows indicate the order of matching

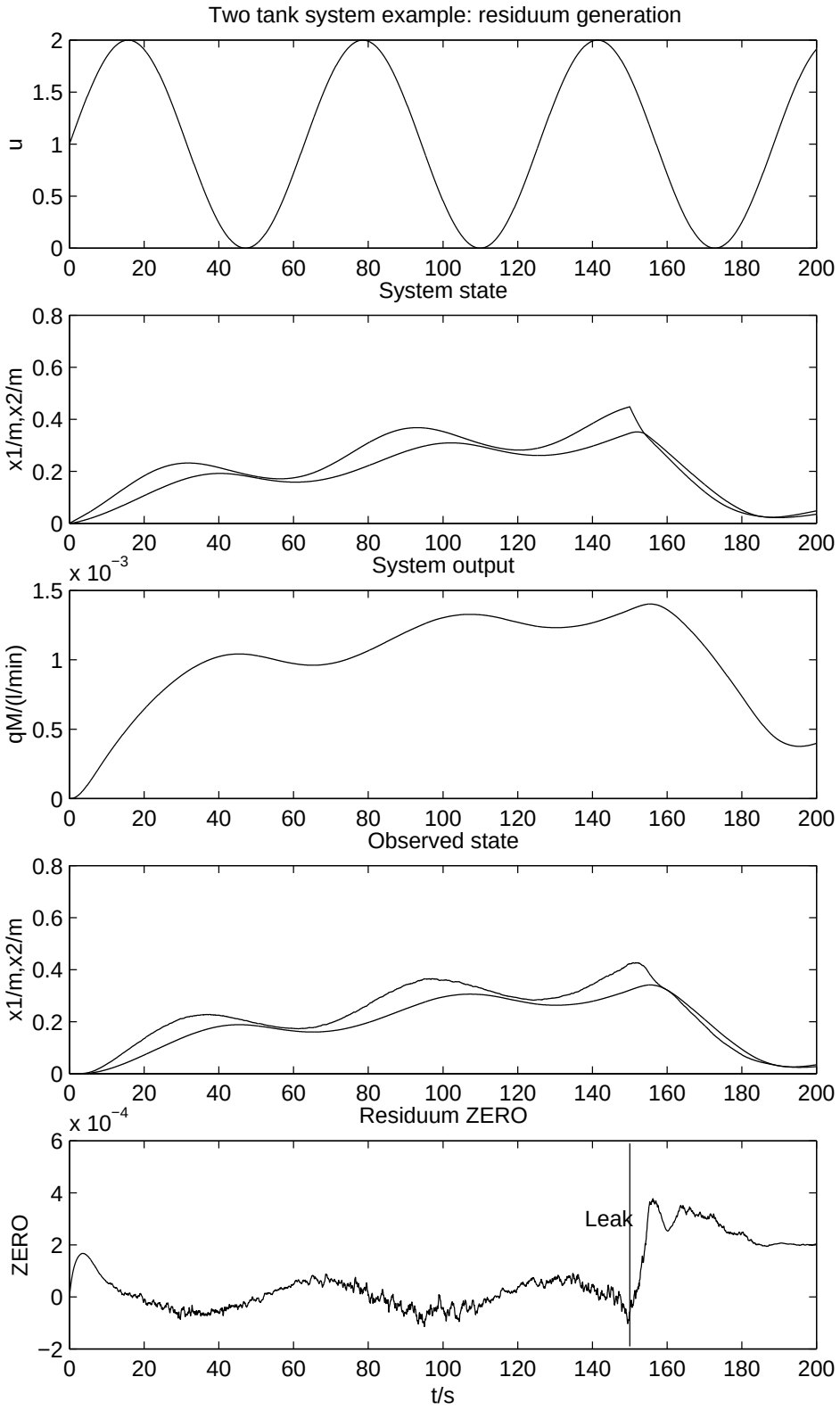

Fig. 5.33. Simulation results of the two-tank system

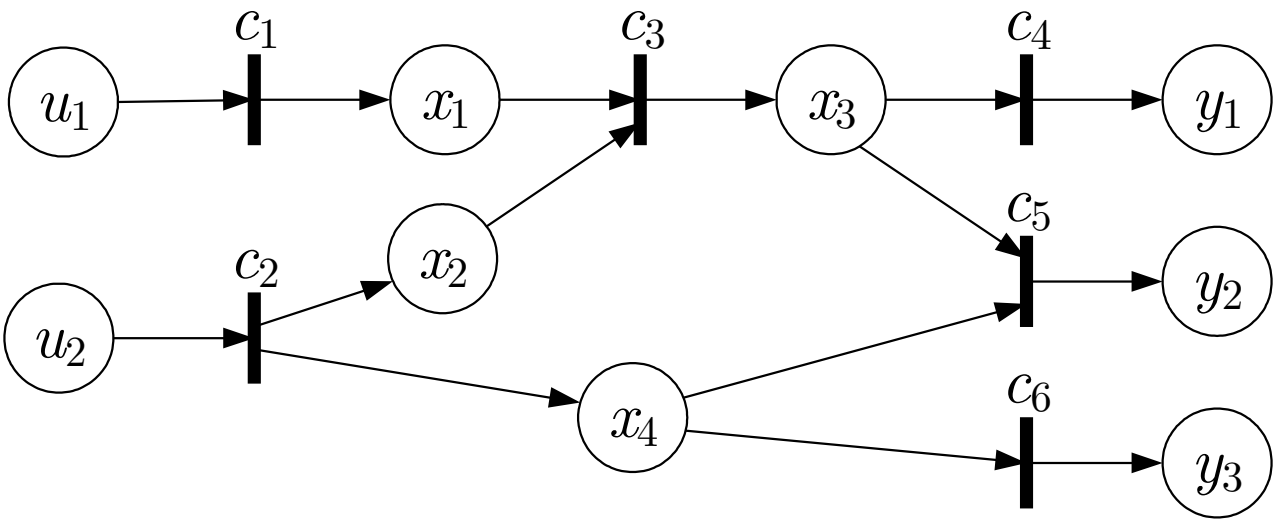

Fig. 5.34. Structure graph for the active diagnosis example

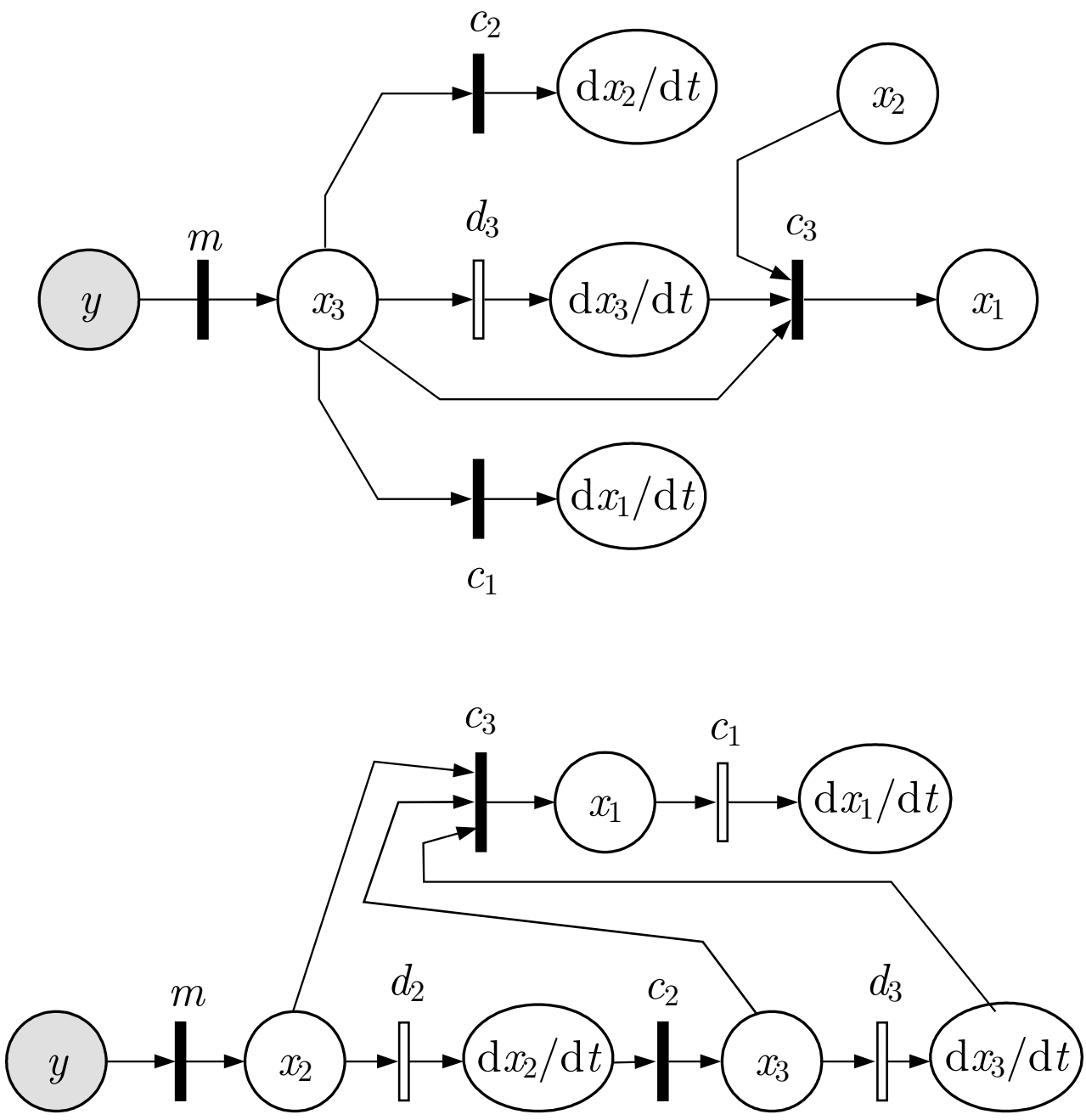

Fig. 5.35. Graph-based interpretation of the observability property

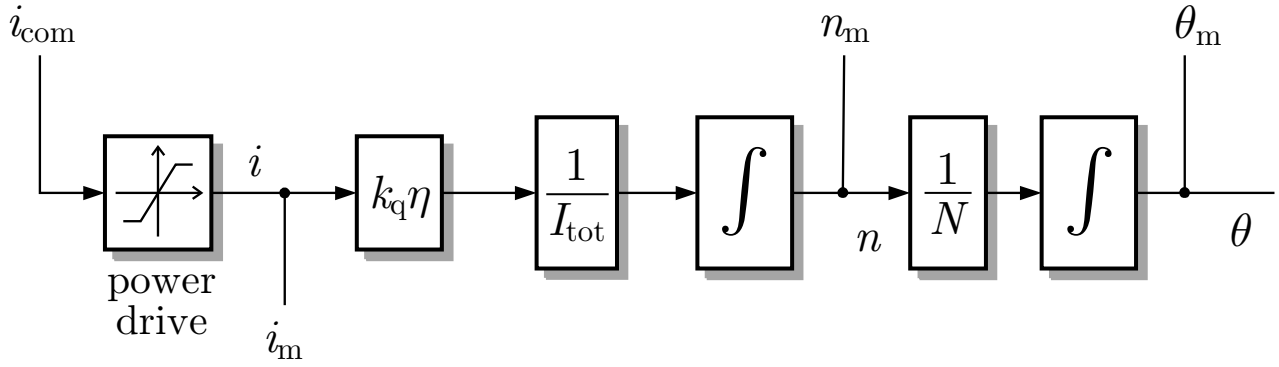

Fig. 5.36. Position actuator open loop

Blanke/Kinnaert/Lunze/Staroswiecki:
Diagnosis and Fault-Tolerant Control, (3rd edition), Springer-Verlag 2015

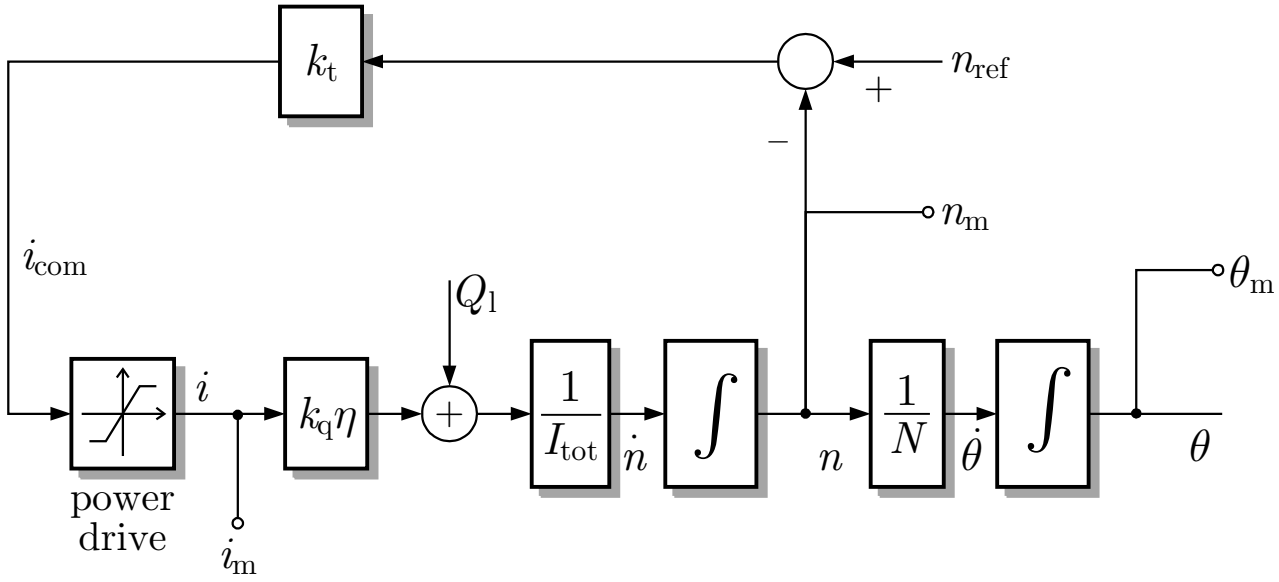

Fig. 5.37. Block diagram of DC motor with load torque and closed speed loop

Blanke/Kinnaert/Lunze/Staroswiecki:
Diagnosis and Fault-Tolerant Control, (3rd edition), Springer-Verlag 2015

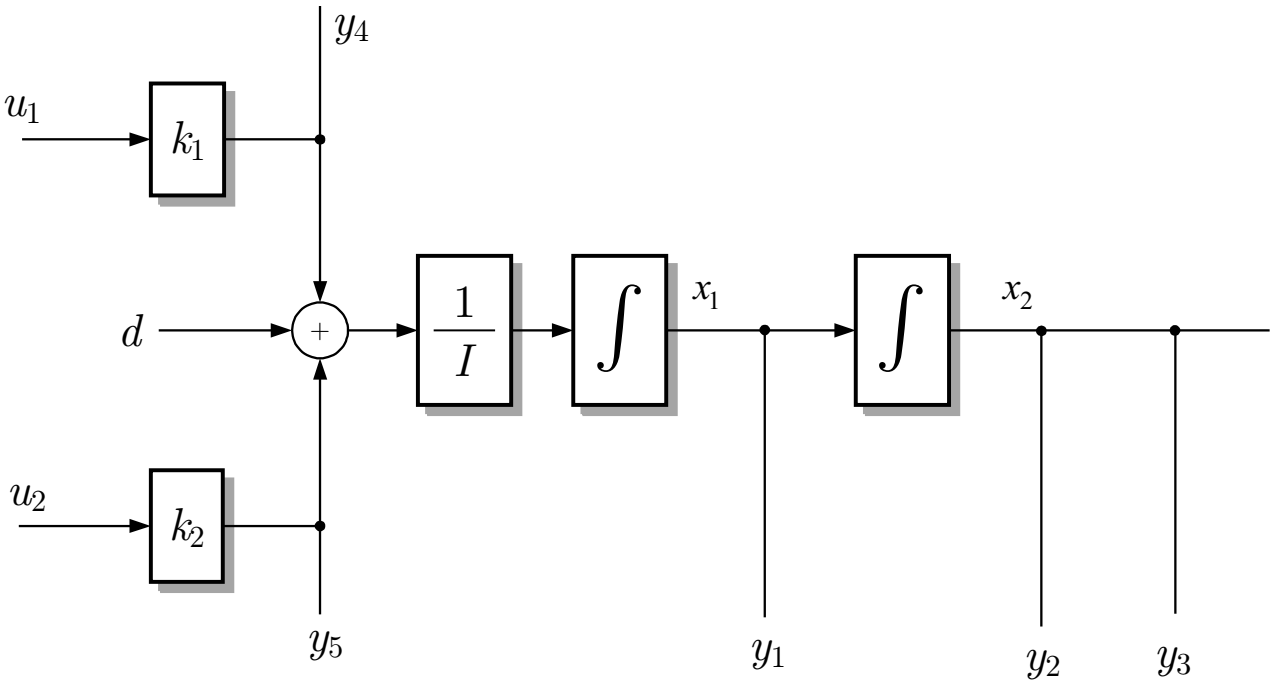

Fig. 5.38. Block diagram of single axis satellite with input from two redundant actuators, redundant measurements of attitude (angle), measurement of angular rate and measurement of delivered actuator torques

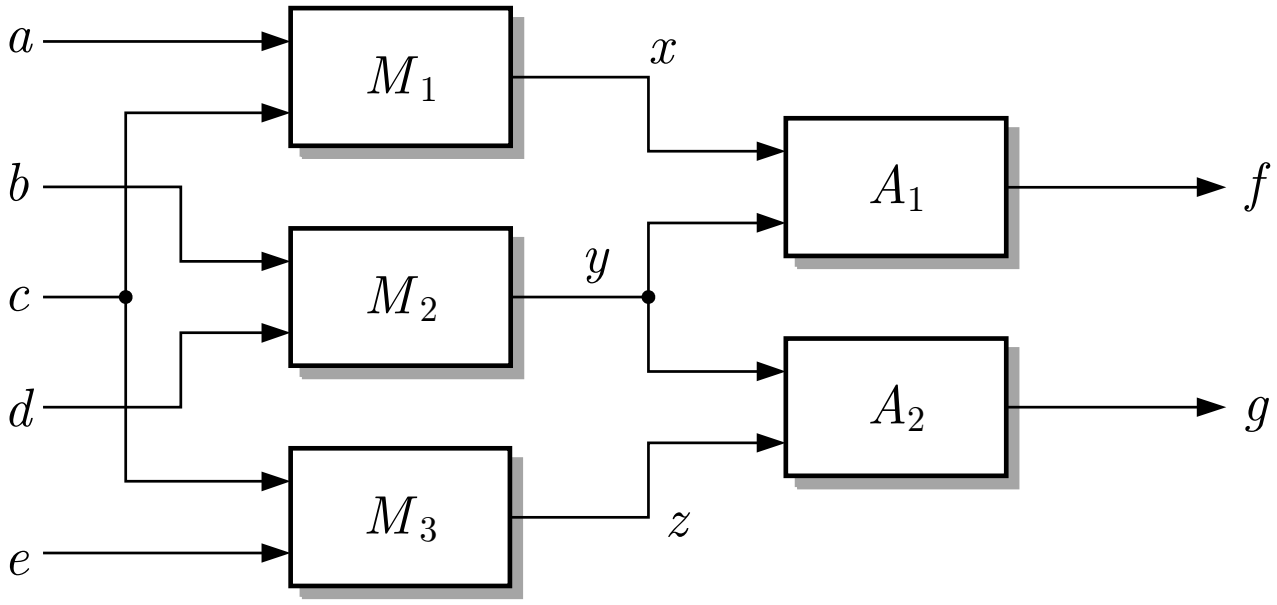

Fig. 5.39. Specialised computation circuit

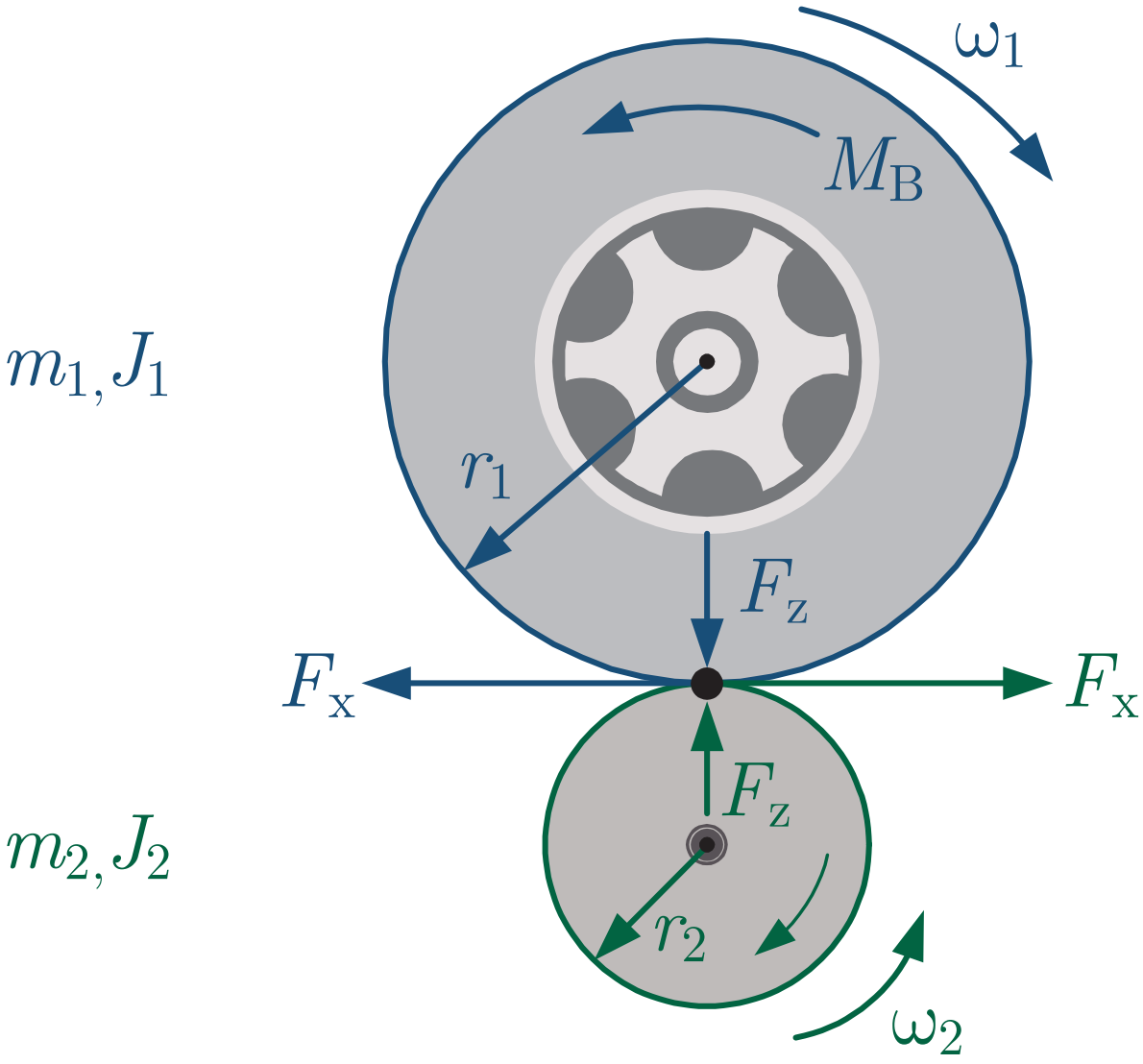

Fig. 5.40. Schematic representation of an ABS test bed

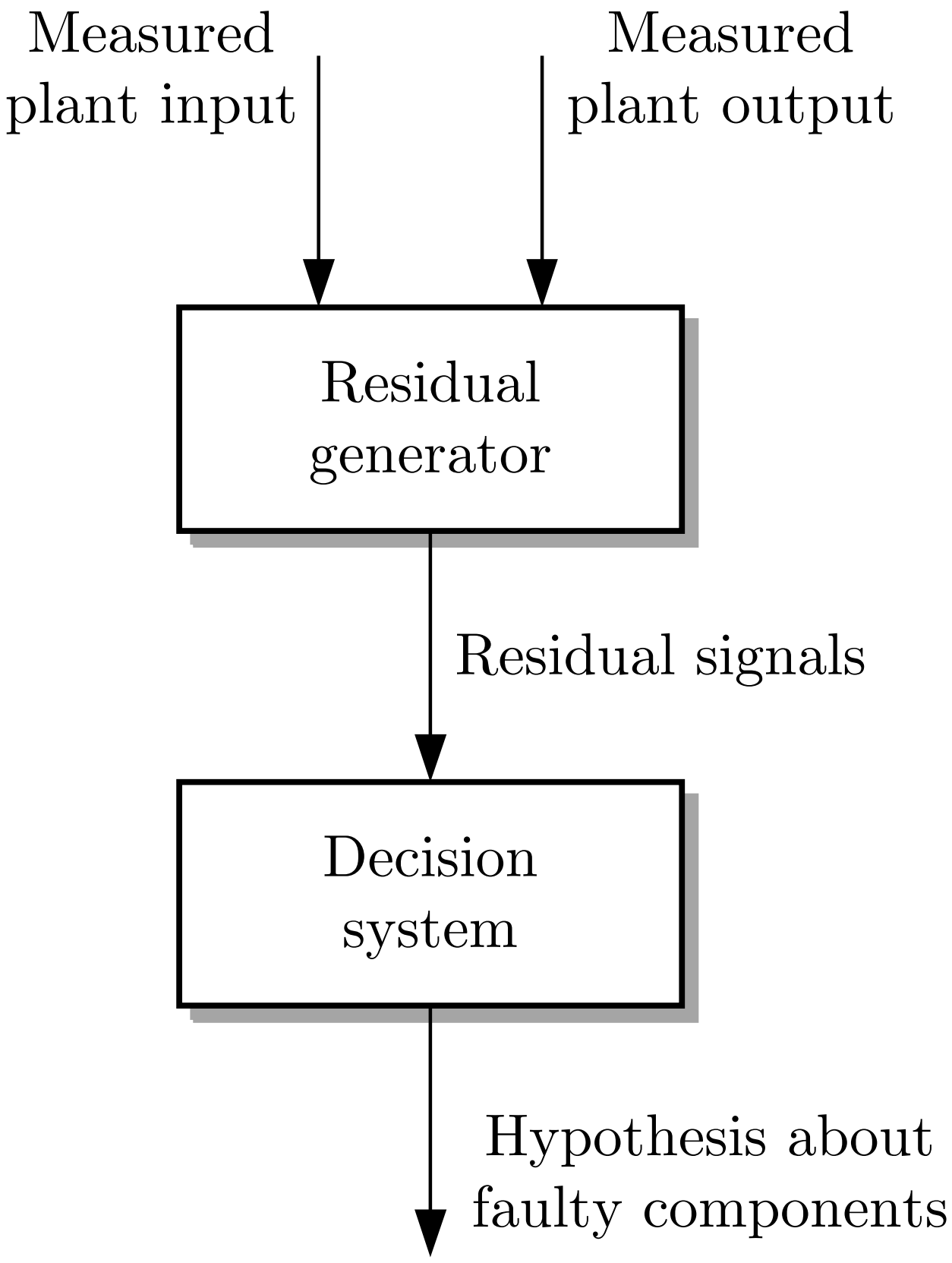

Fig. 6.1. Structure of a fault diagnosis system

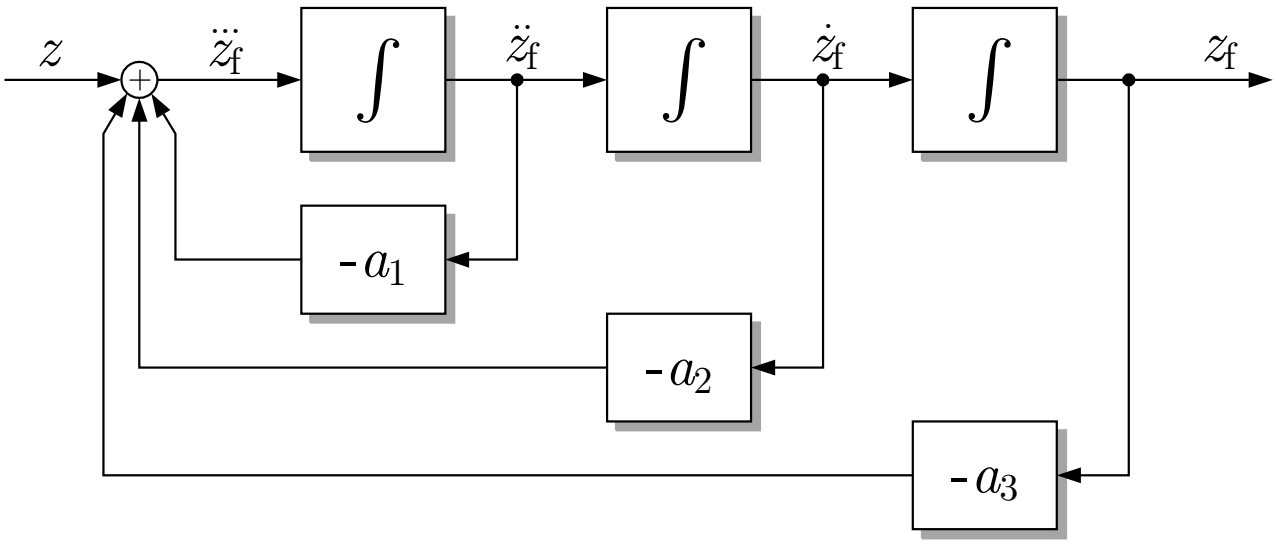

Fig. 6.2. Block diagram of a third-order state variable filter

Blanke/Kinnaert/Lunze/Staroswiecki:
Diagnosis and Fault-Tolerant Control, (3rd edition), Springer-Verlag 2015

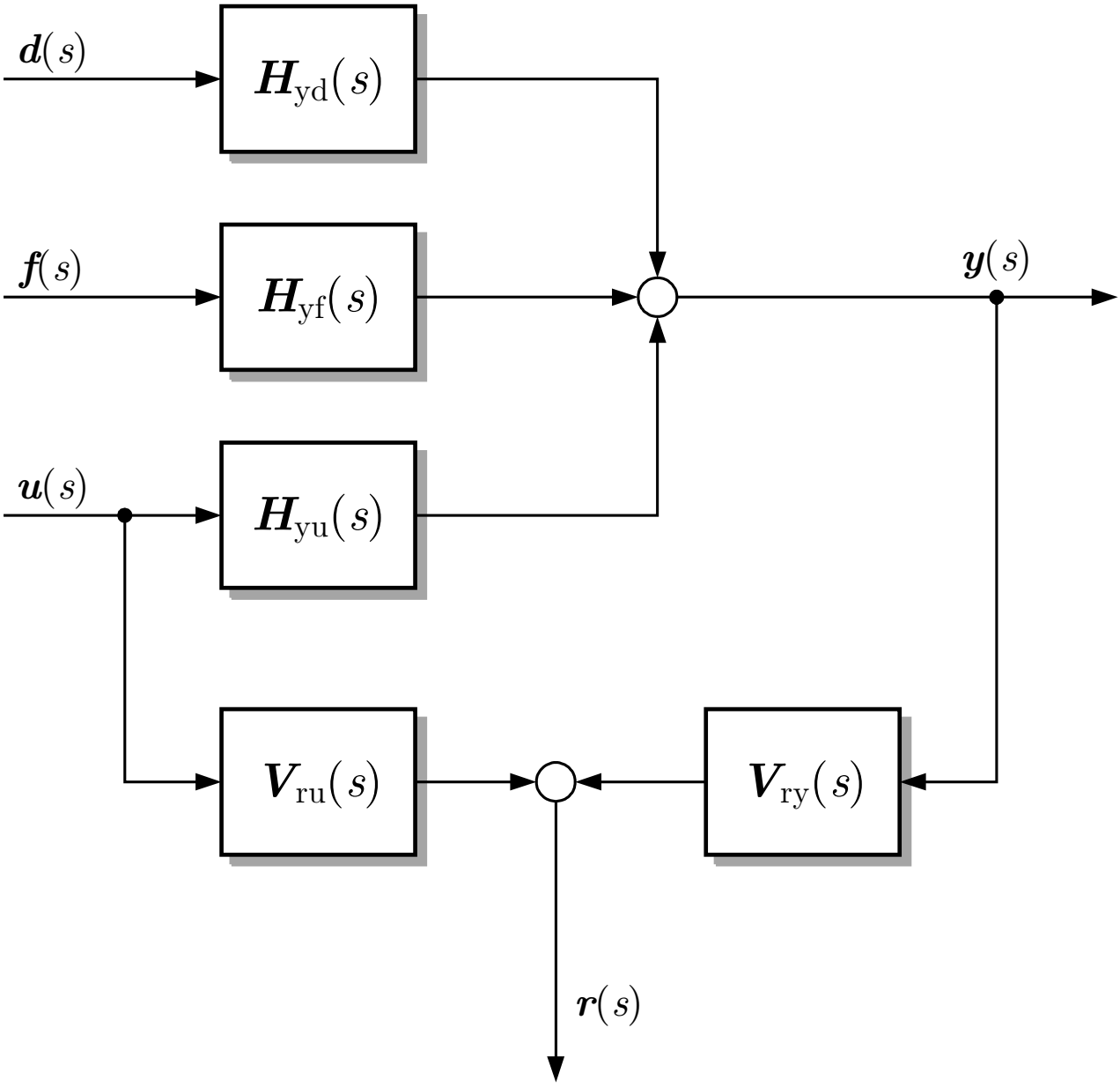

Fig. 6.3. Structure of residual generator in the parity space formulation

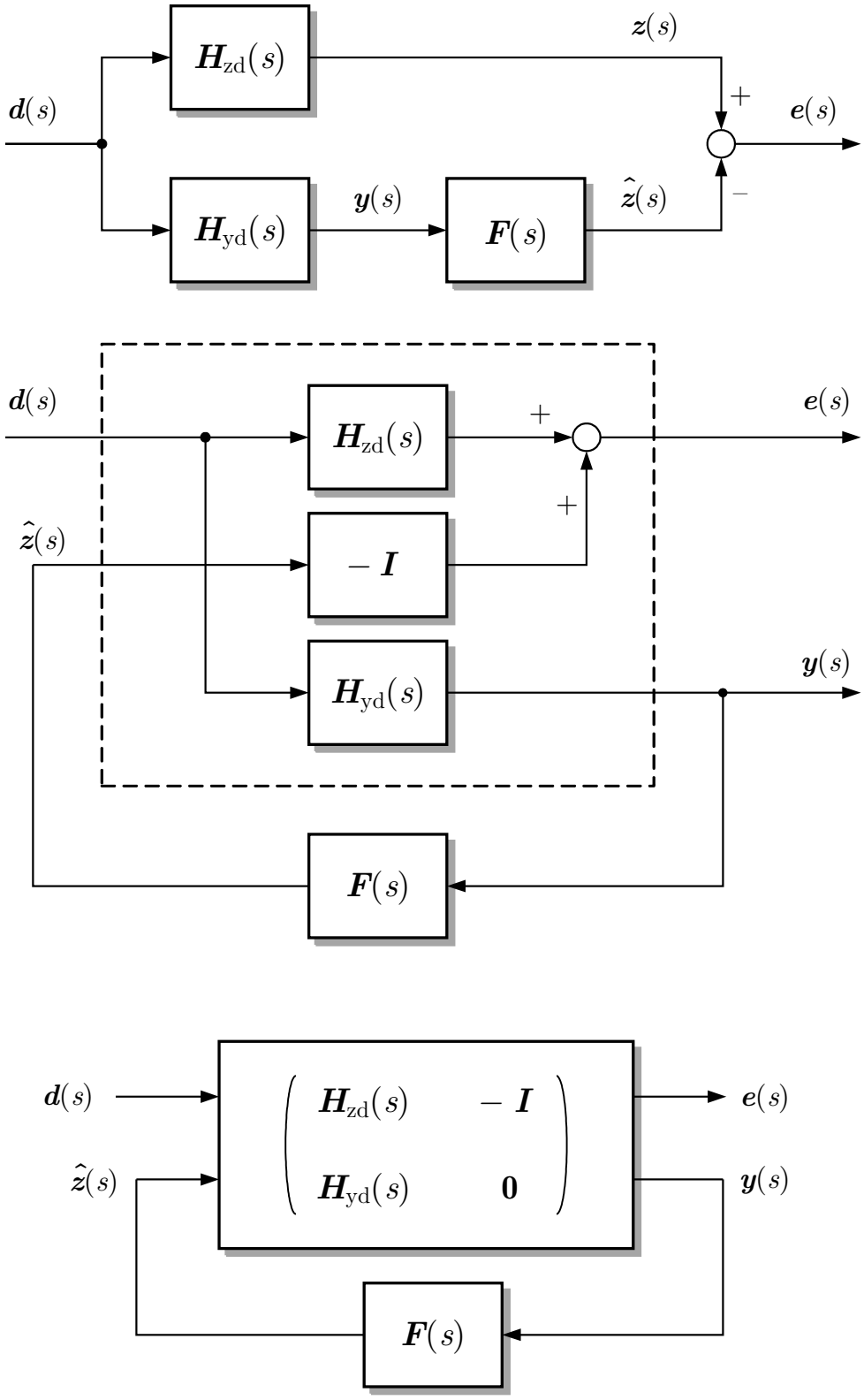

Fig. 6.4. Manipulation of the block diagram to arrive at a standard problem formulation

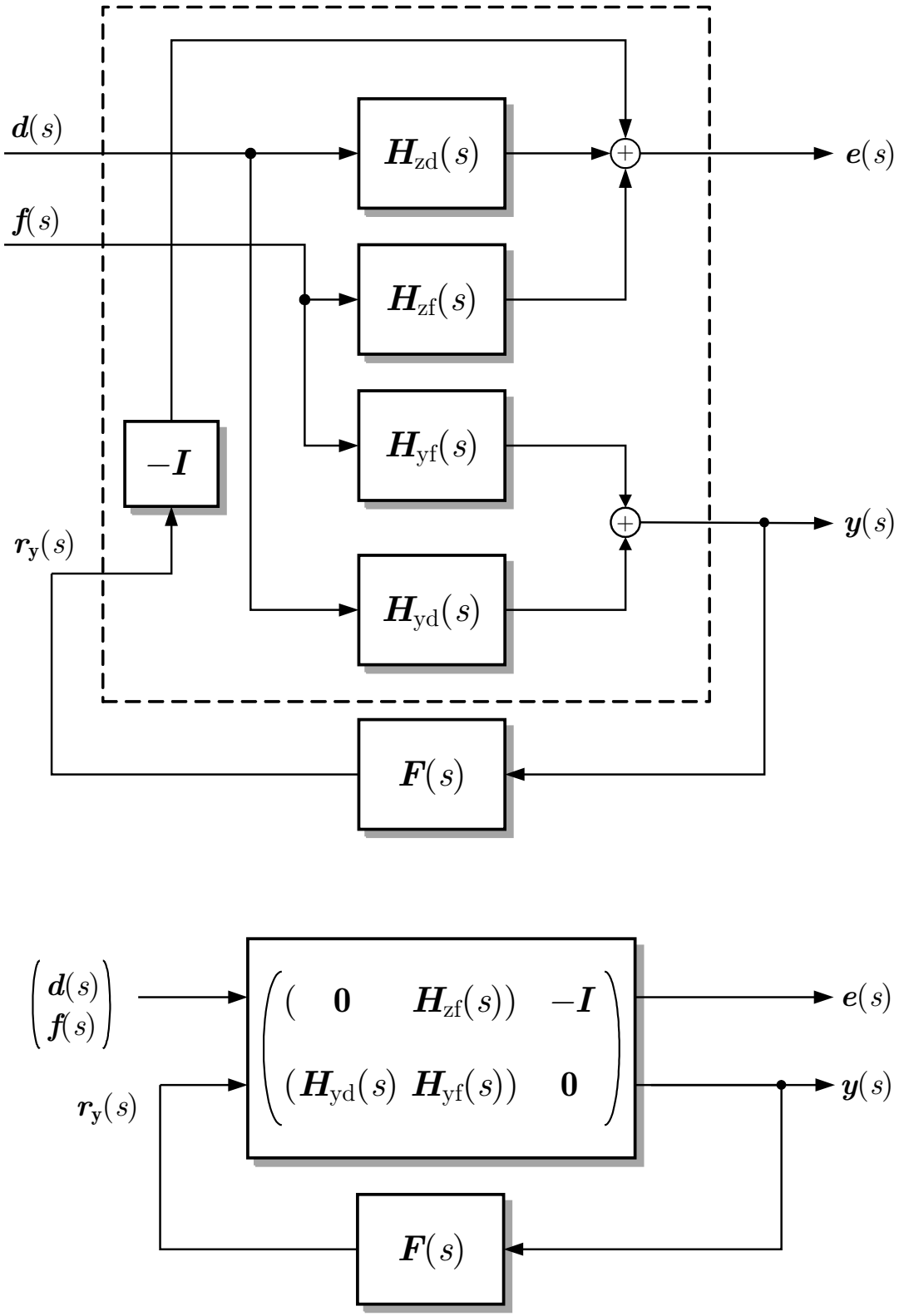

Fig. 6.5. Residual generator depicted in a standard setup formulation

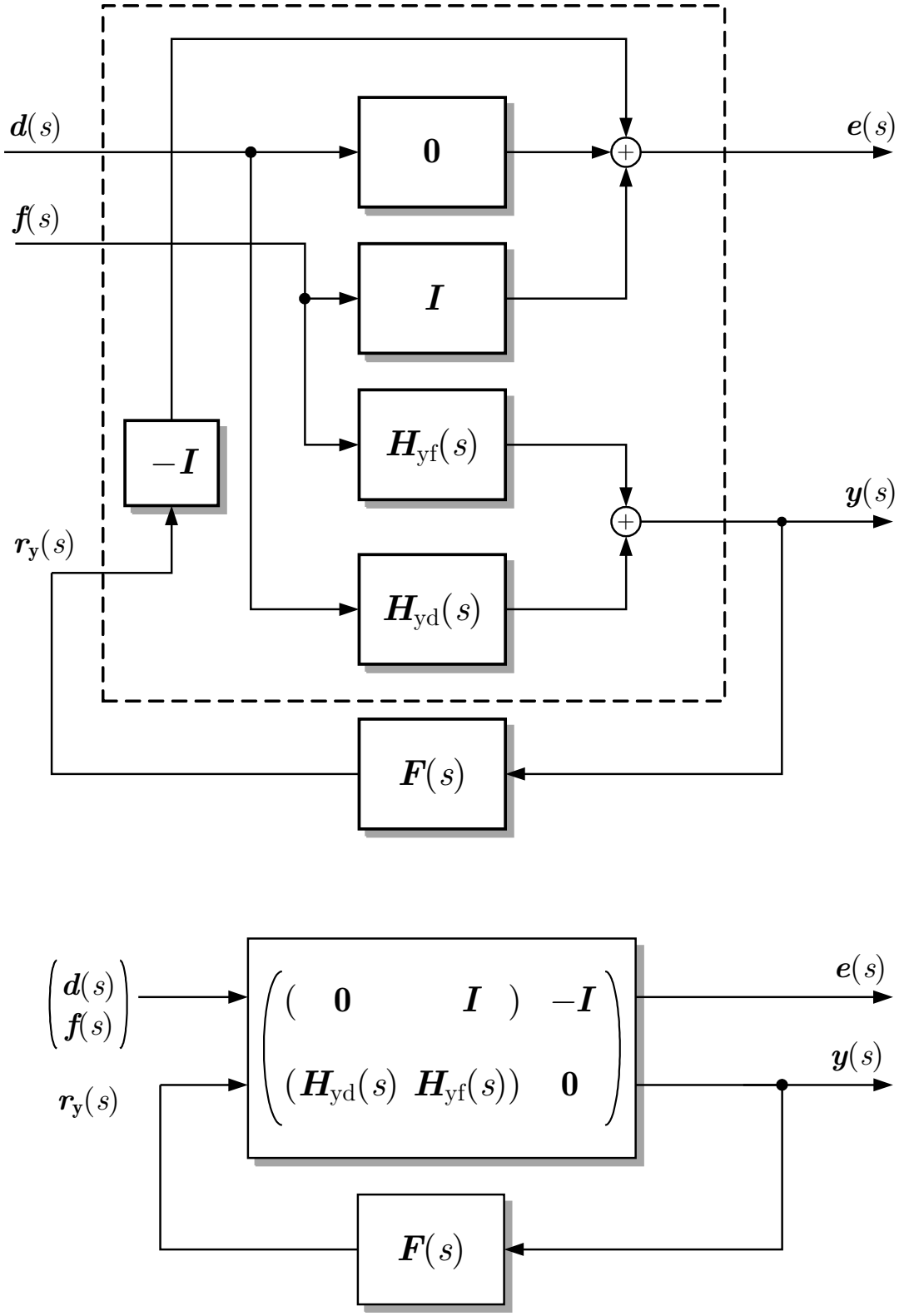

Fig. 6.6. If a solution exists, fault estimation is obtained by solving the standard problem

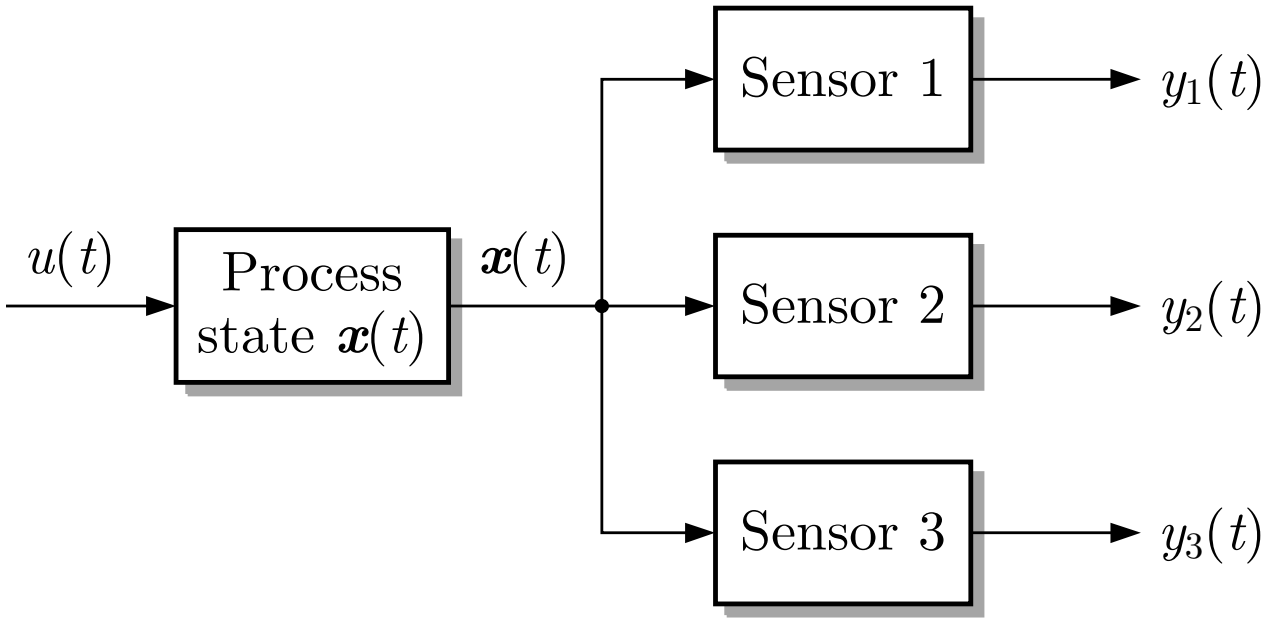

Fig. 6.7. System with three sensors

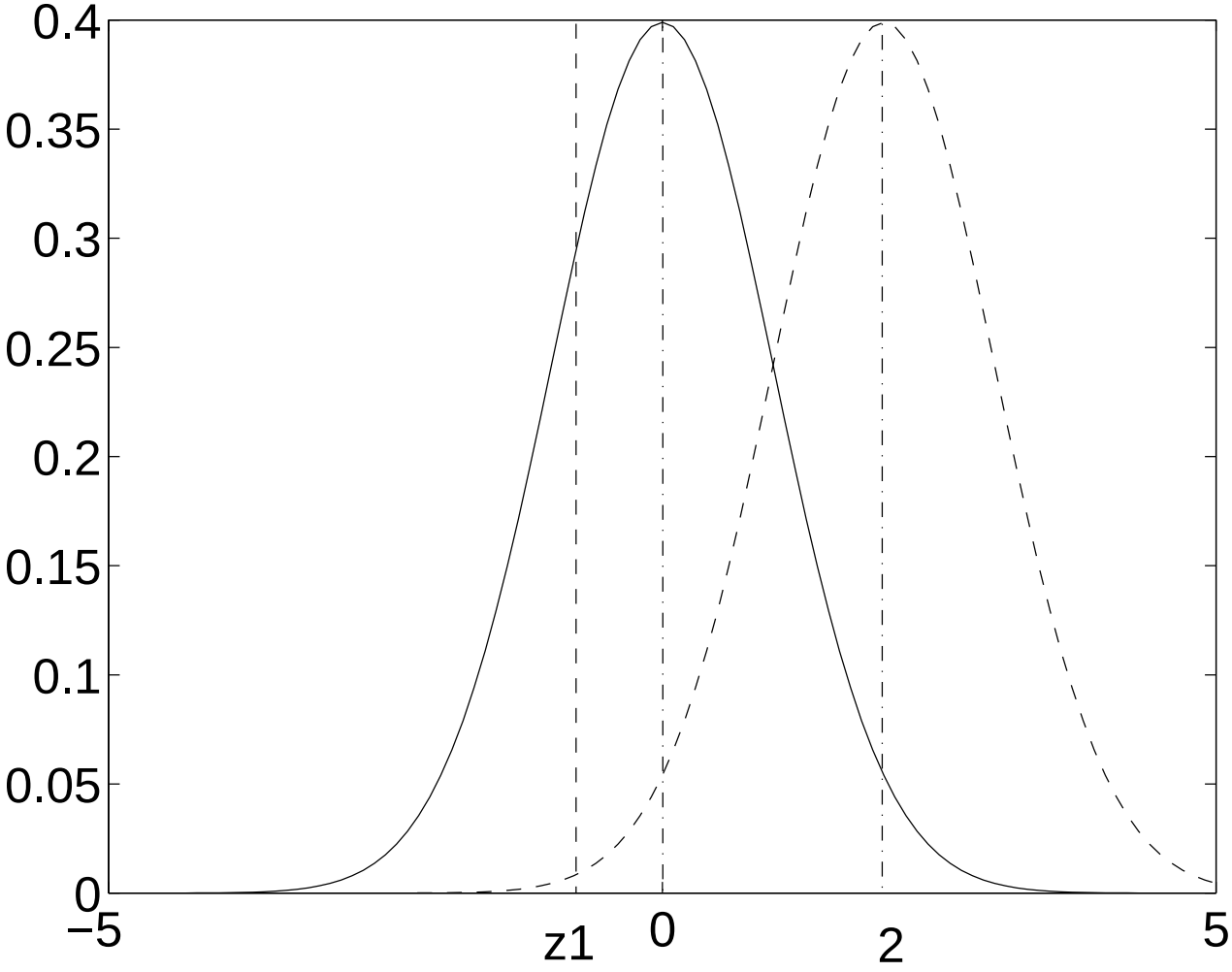

Fig. 7.1. Two Gaussian probability density functions with mean $\mu_0 = 0$ and $\mu_1 = 2$, and with the same variance $\sigma^2 = 1$

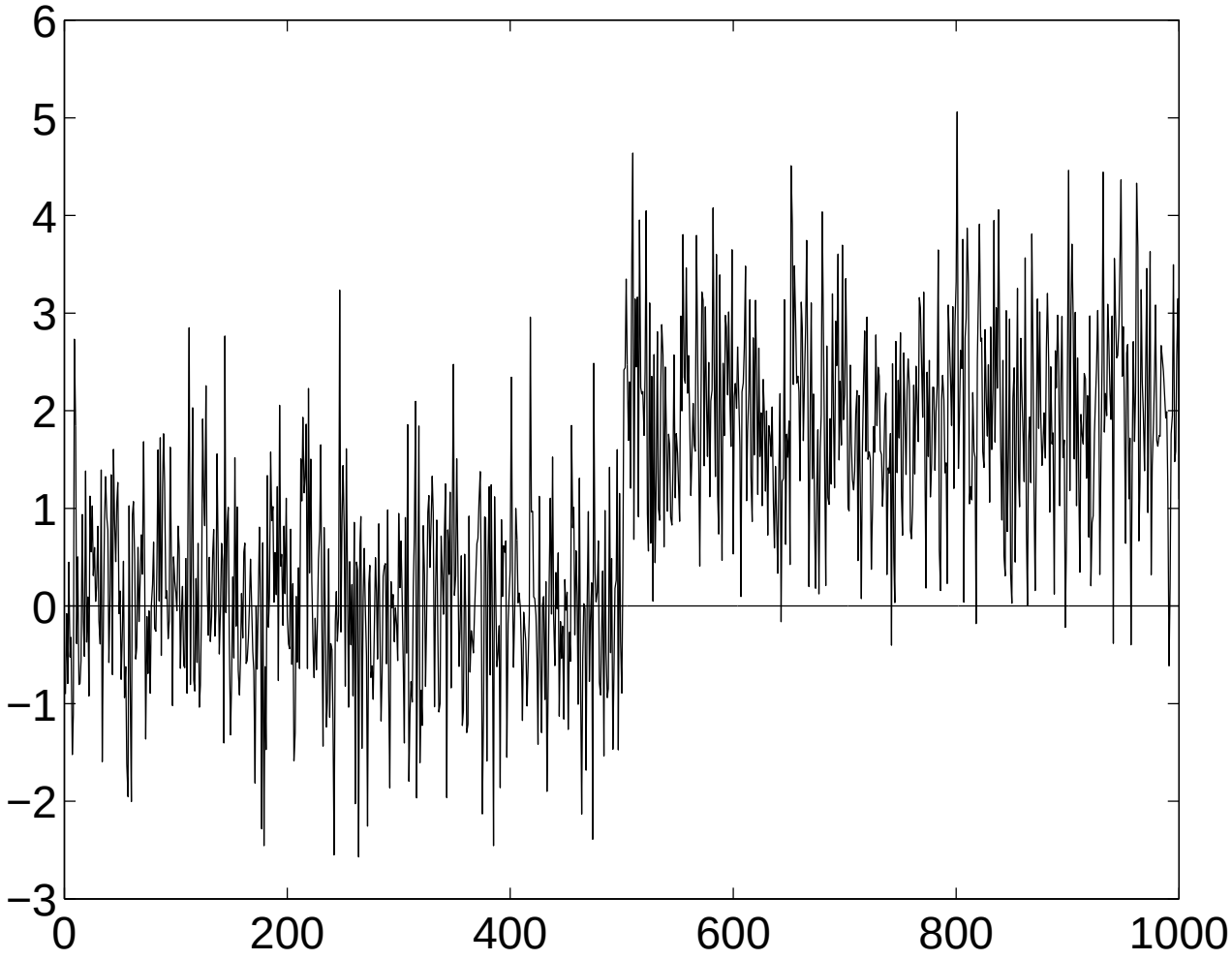

Fig. 7.2. Realisation of a sequence of independent random variables with distributions depicted in Fig. 7.1. Time on the x-axis is expressed in number of samples.

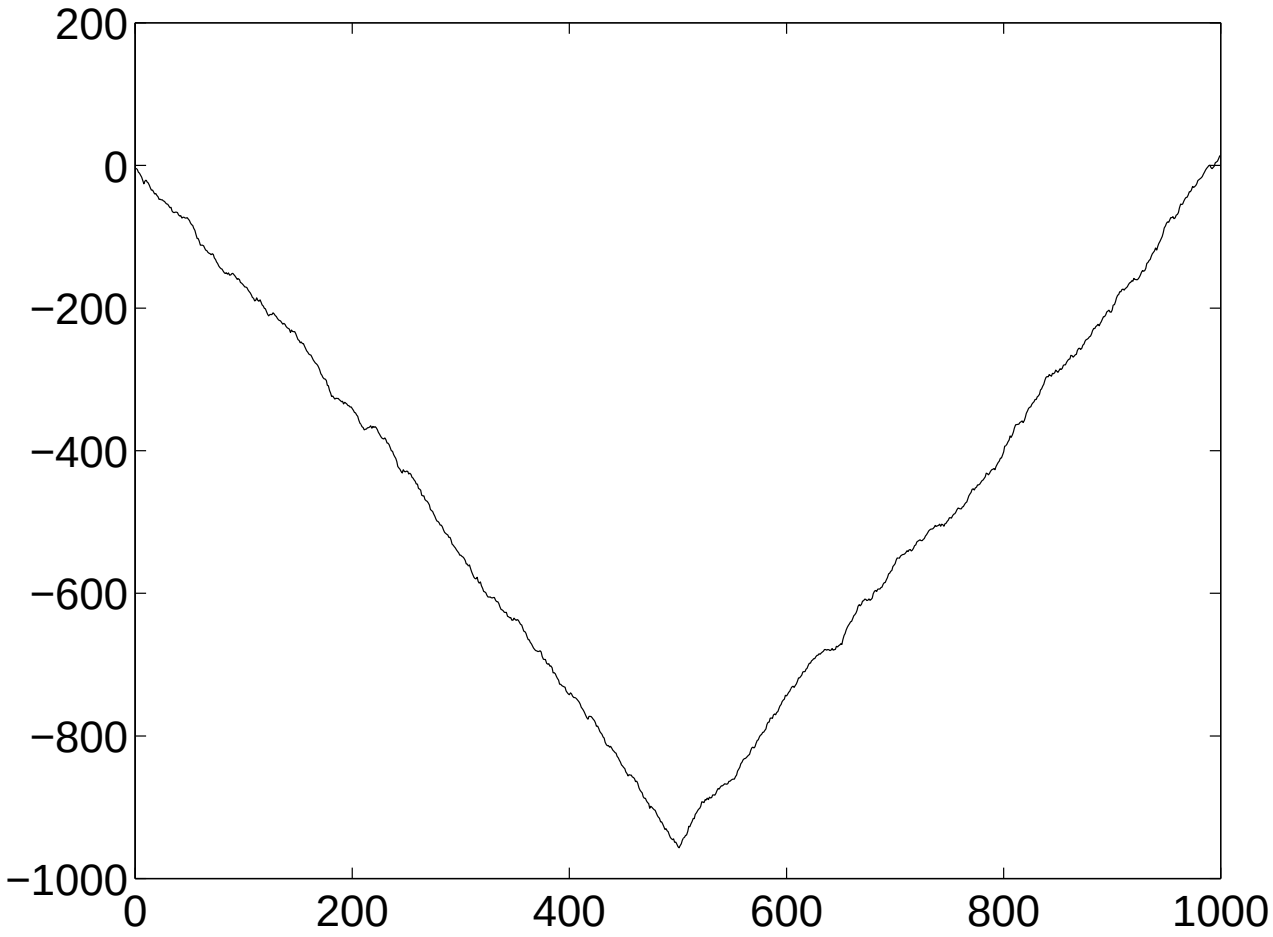

Fig. 7.3. Evolution of $S(k)$ for the sequence of Fig. 7.2, as a function of time in number of samples

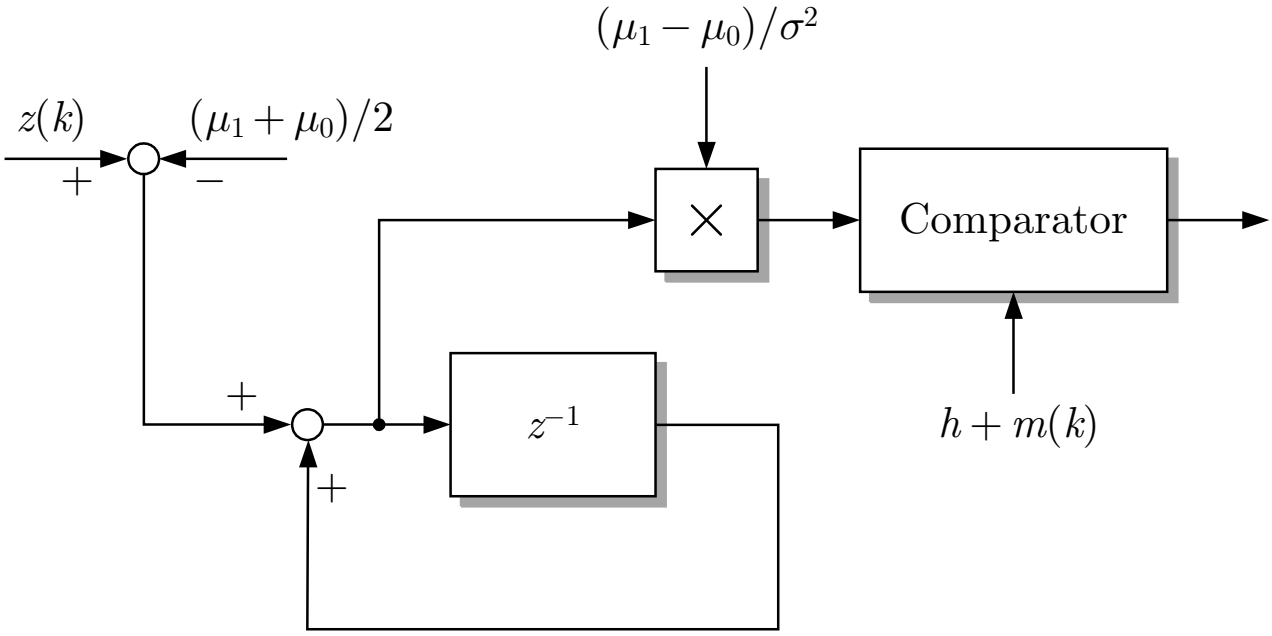

Fig. 7.4. Block diagram for the CUSUM test (7.4), (7.5), (7.7)

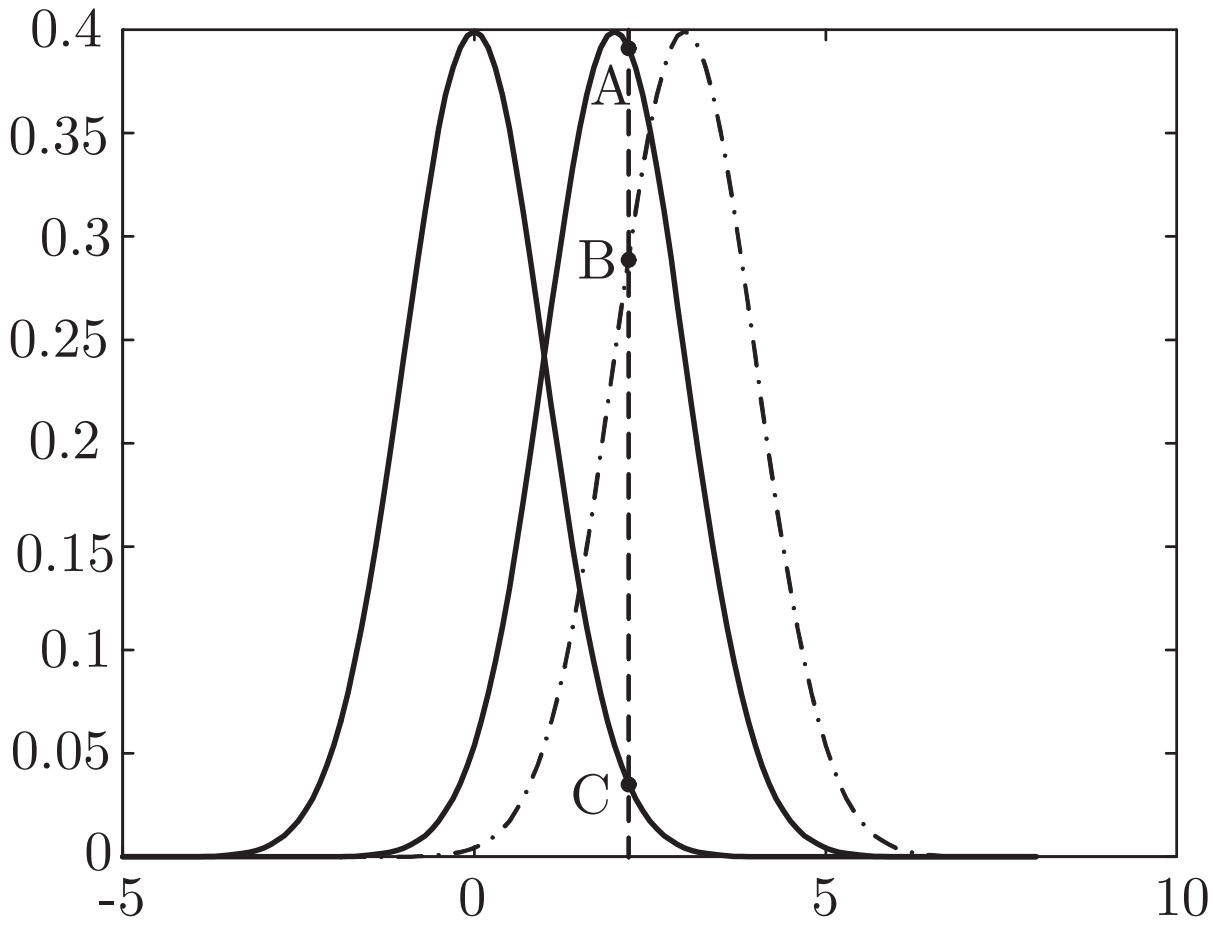

Fig. 7.5. Gaussian probability density functions with actual (continuous line) and overestimated means (dash-dotted line)

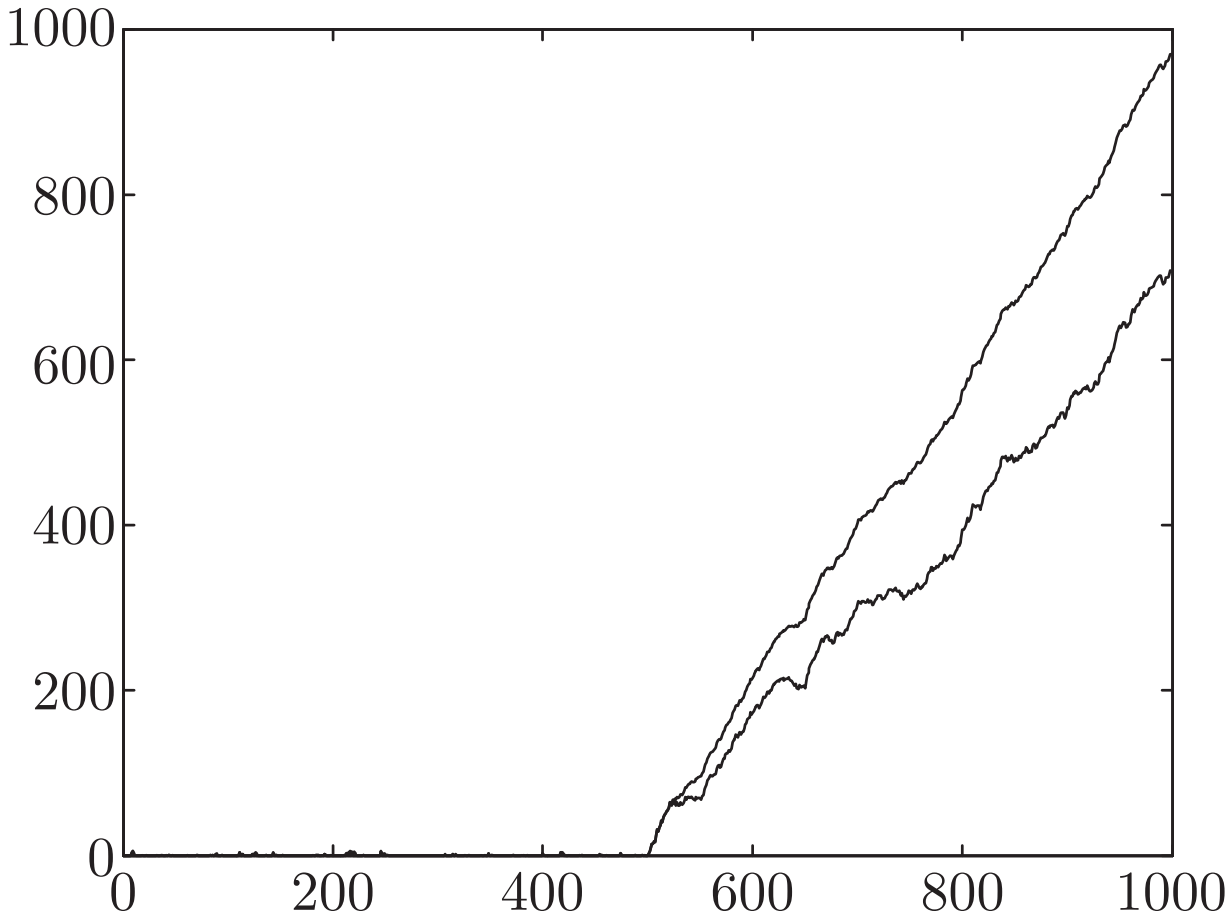

Fig. 7.5. Evolution of the recursive CUSUM decision functions computed with the exact (continuous line) and approximated likelihood ratios (dash-dotted line) for the data sequence of Fig. 7.2

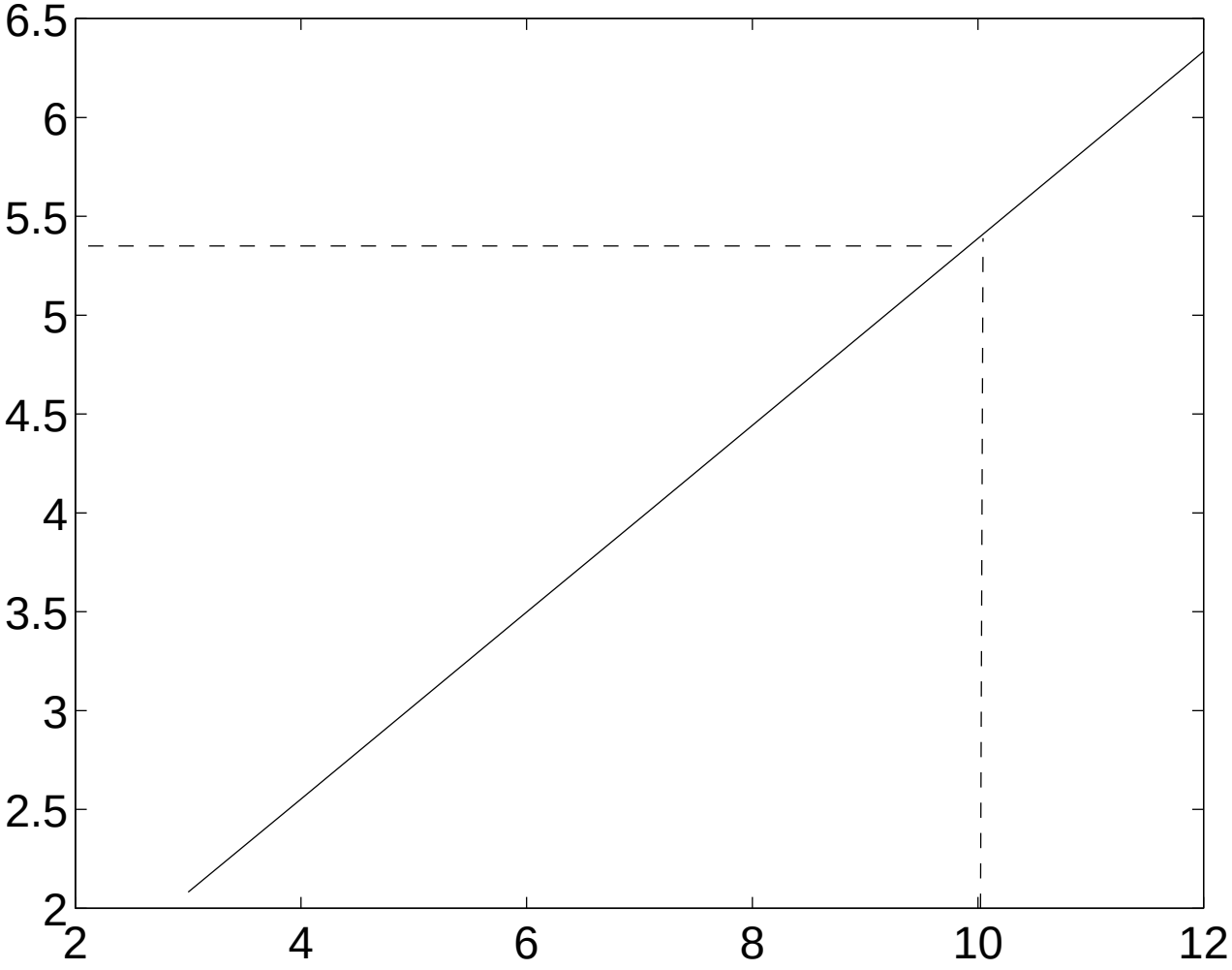

Fig. 7.6. Estimated mean detection delay in number of samples, as a function of h

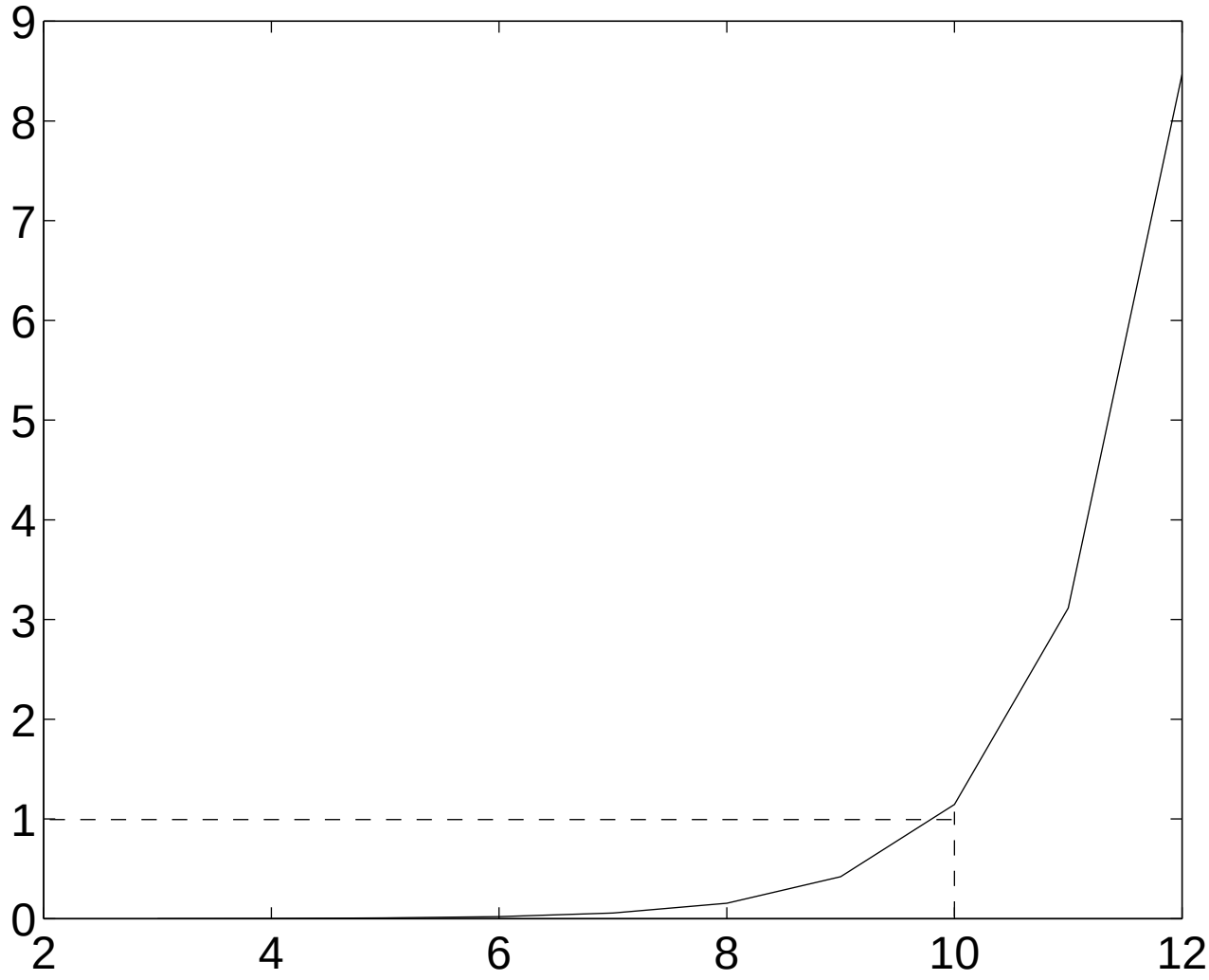

Fig. 7.6. Mean time between false alarms expressed in multiples of 10^5 samples as a function of h

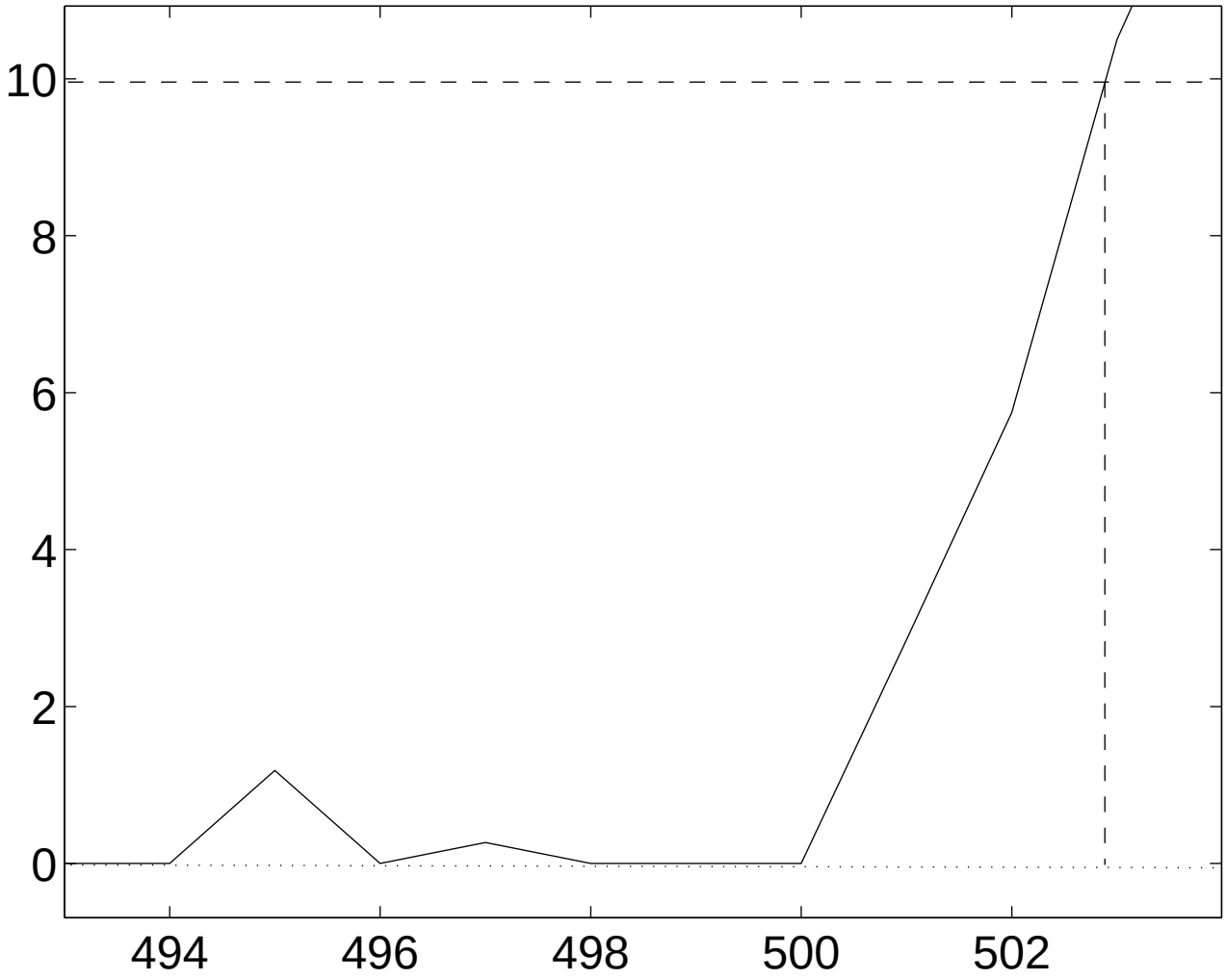

Fig. 7.7. Zoom on the decision function resulting from the recursive algorithm for the data of Fig. 7.2

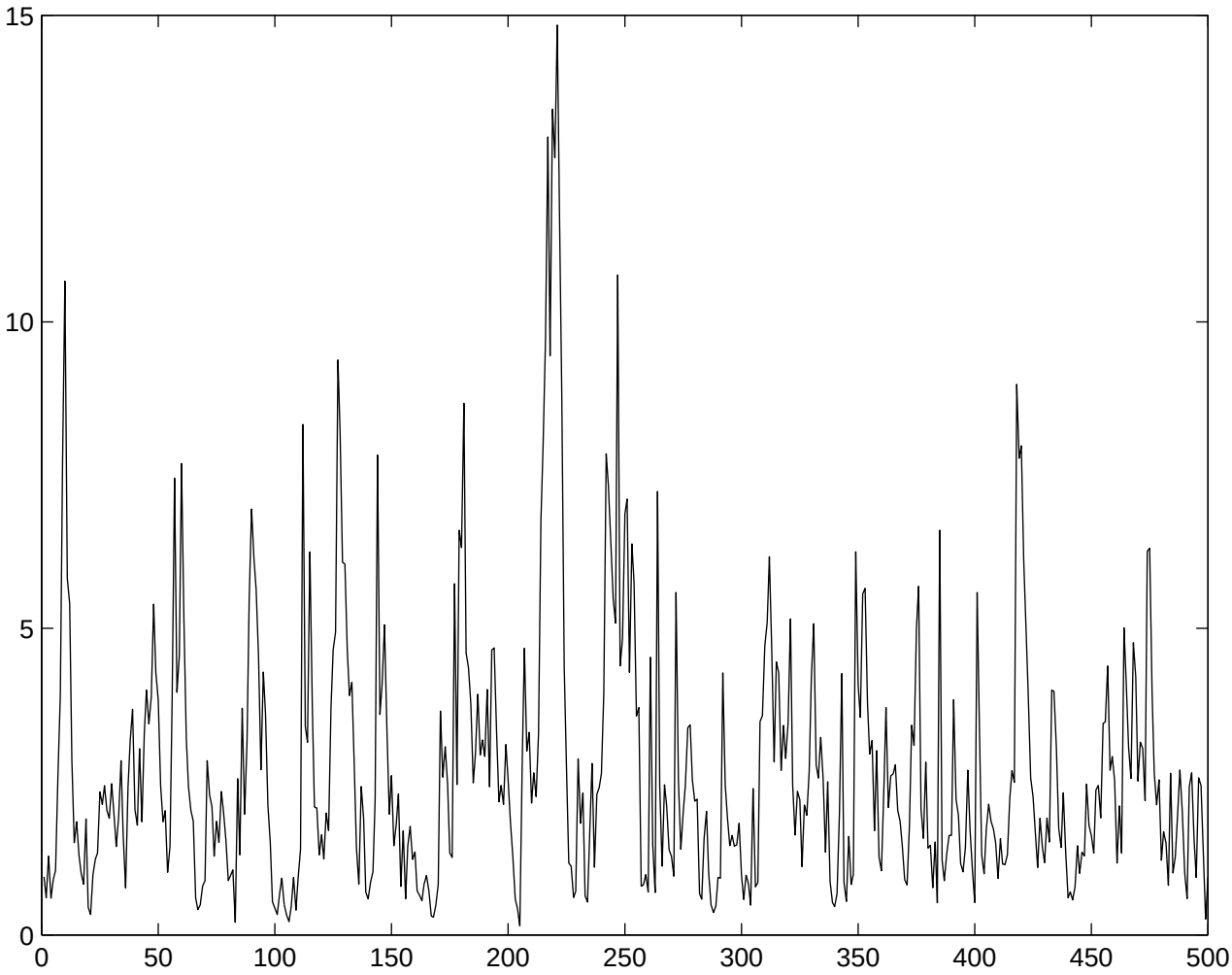

Fig. 7.8. Two GLR decision functions (Part 1)

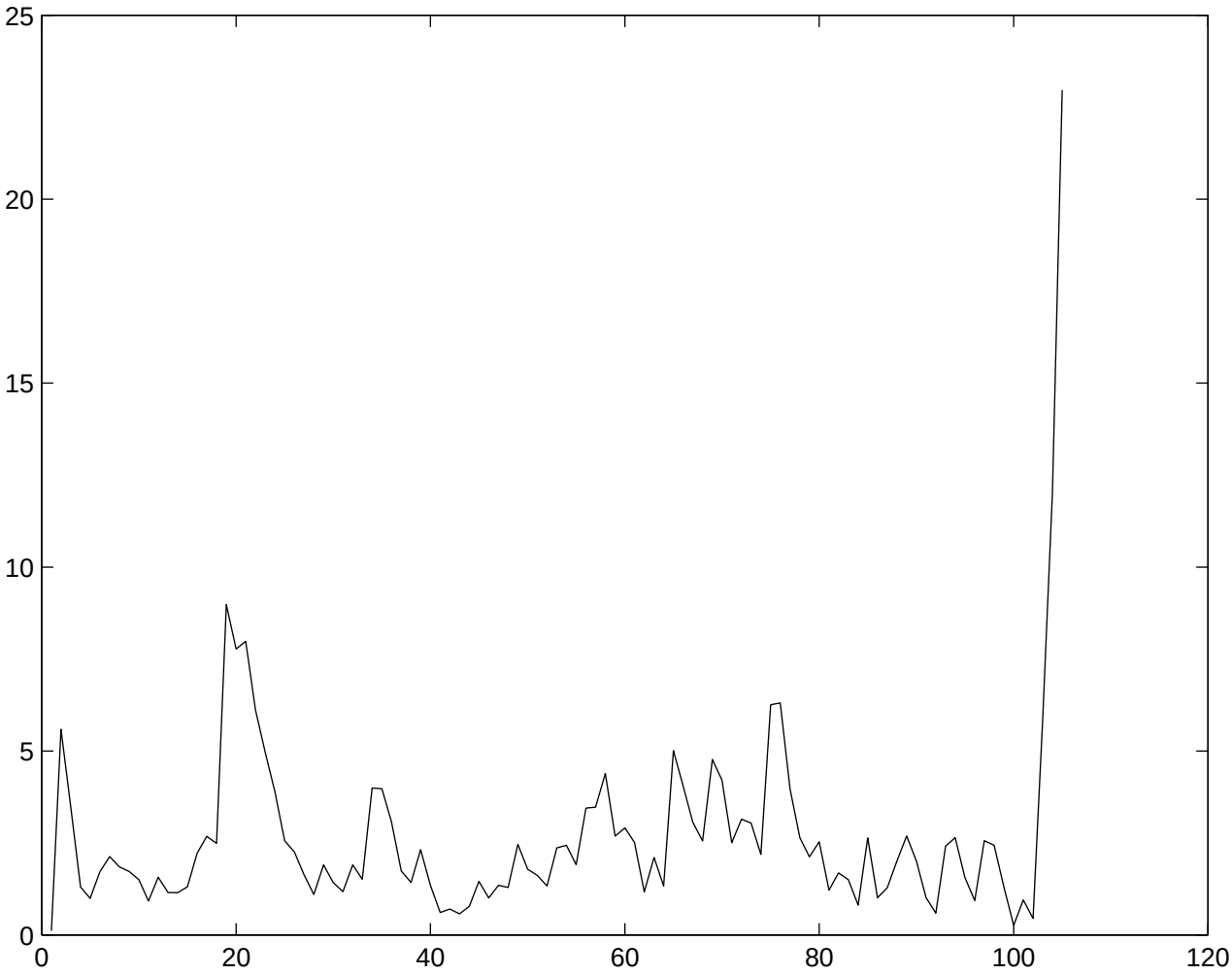

Fig. 7.8. Two GLR decision functions (Part 2)

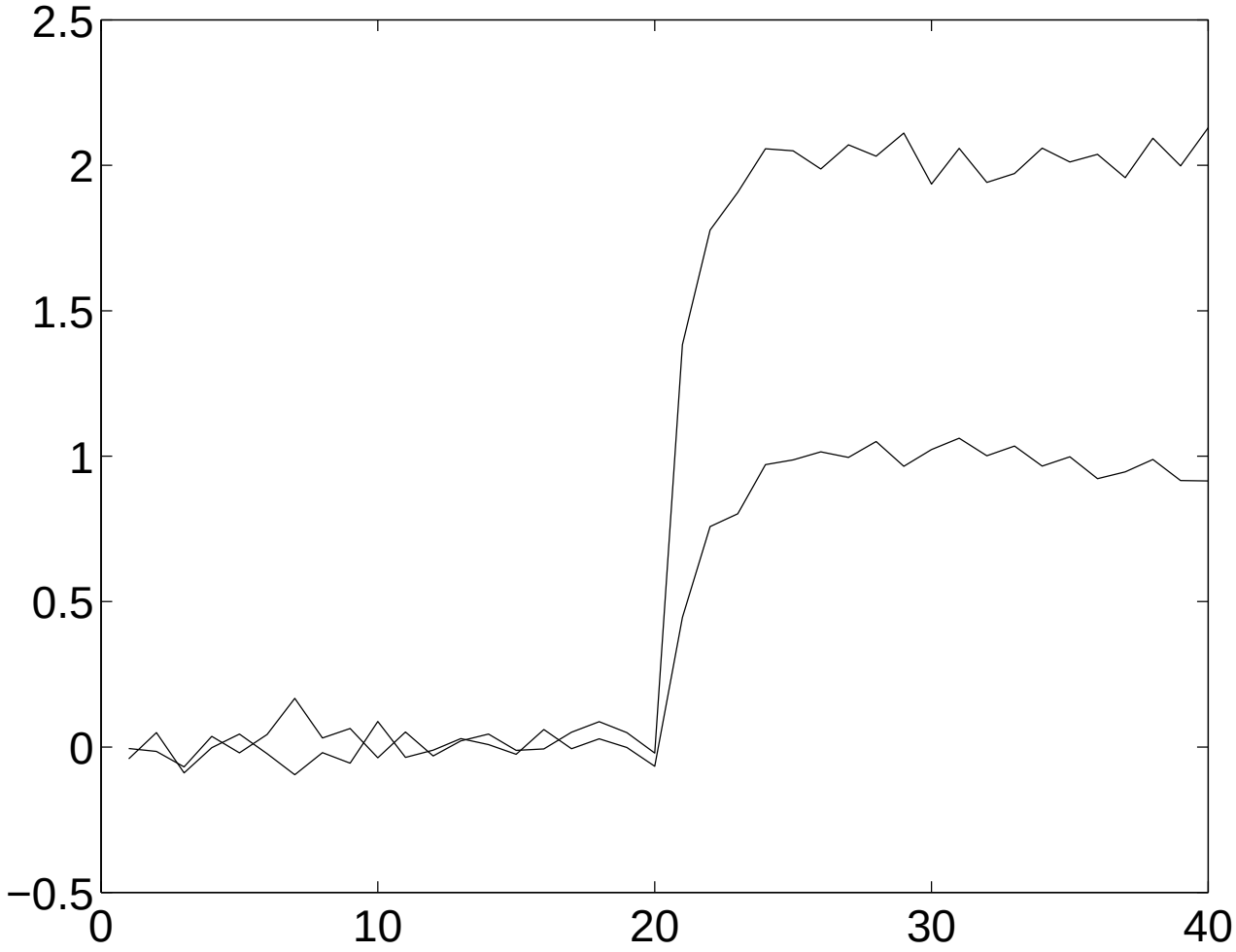

Fig. 7.9. Realisation of the vector sequence (7.62)

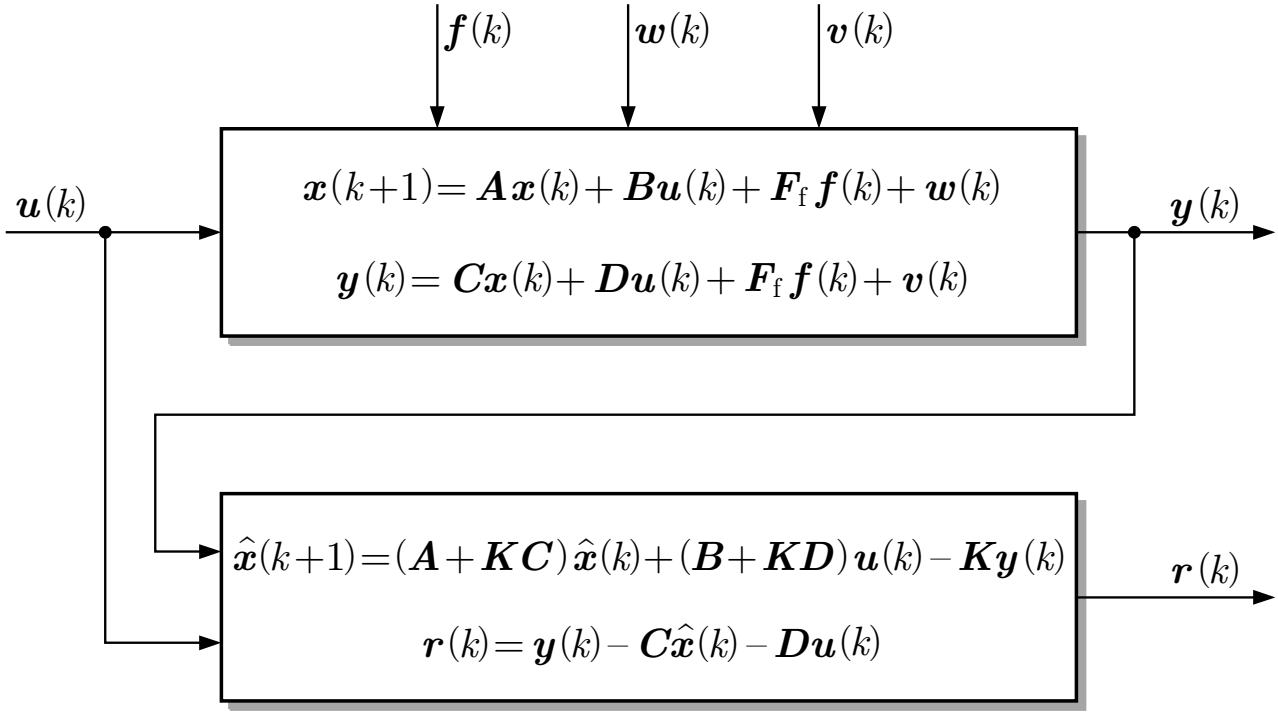

Fig. 7.10. Block diagram of the supervised system together with the innovation filter

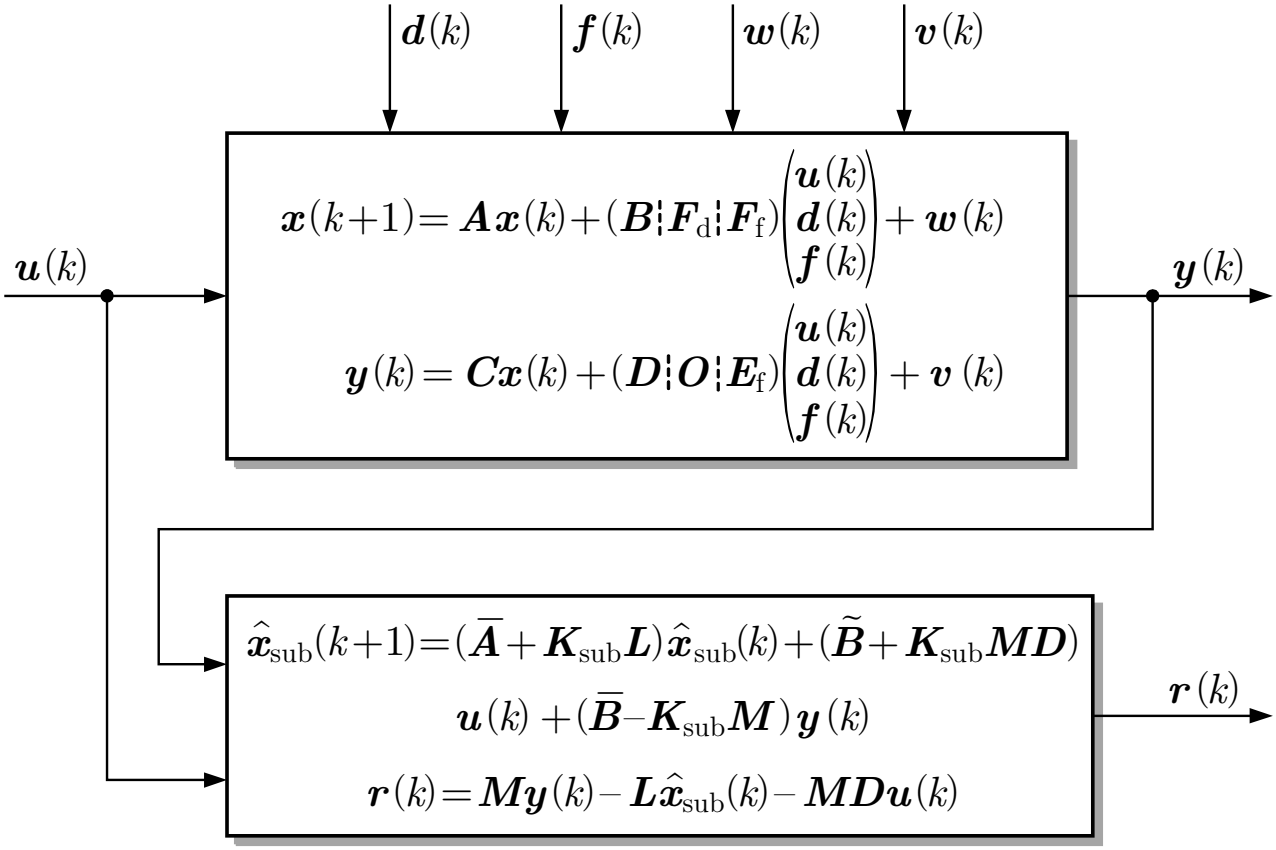

Fig. 7.11. Block diagram of the supervised system together with the innovation filter in the presence of unknown inputs

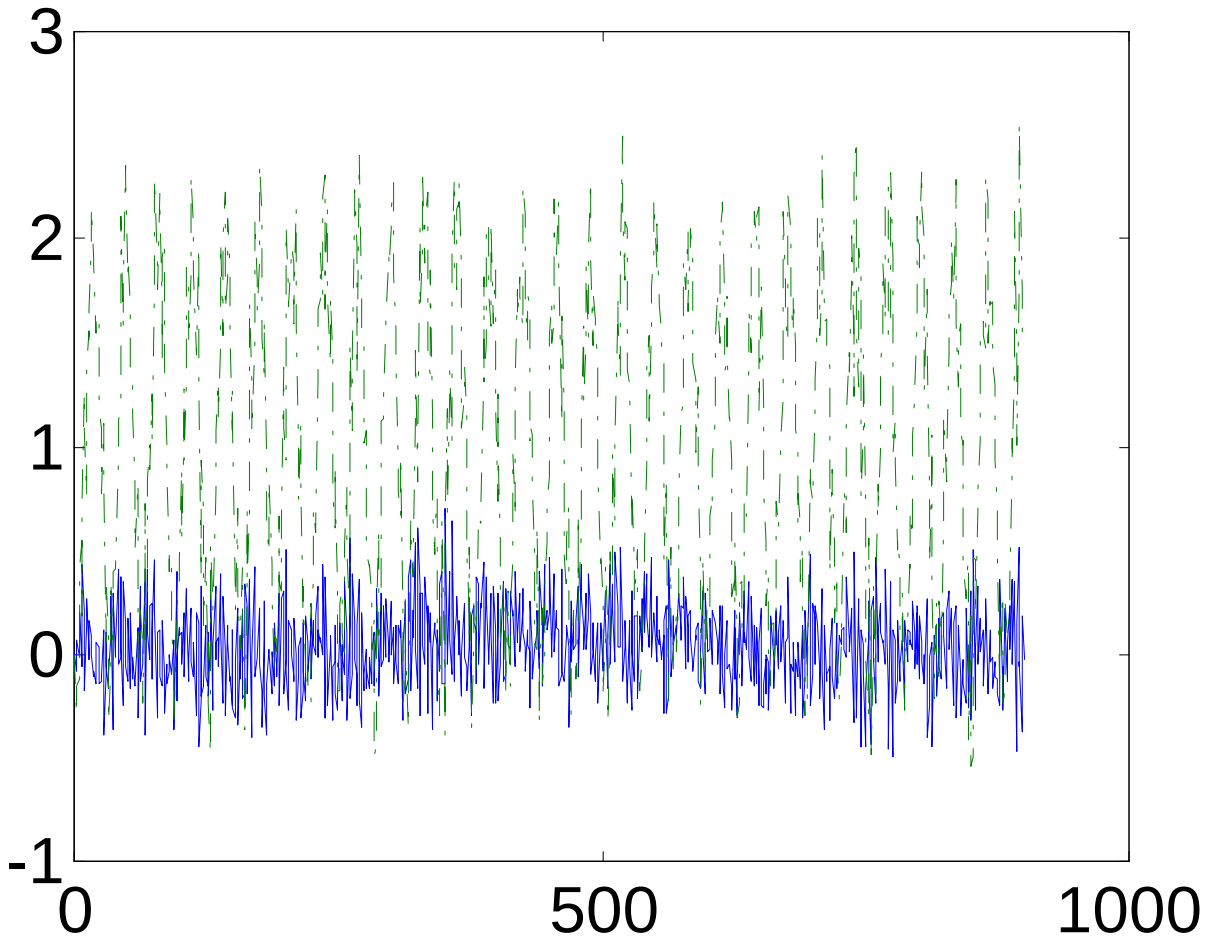

Fig. 7.12. Sampled output sequence of ship model in healthy and faulty working modes; ω_{3m} as a function of sample number (continuous line), ψ_m as a function of sample number (dash-dotted line)

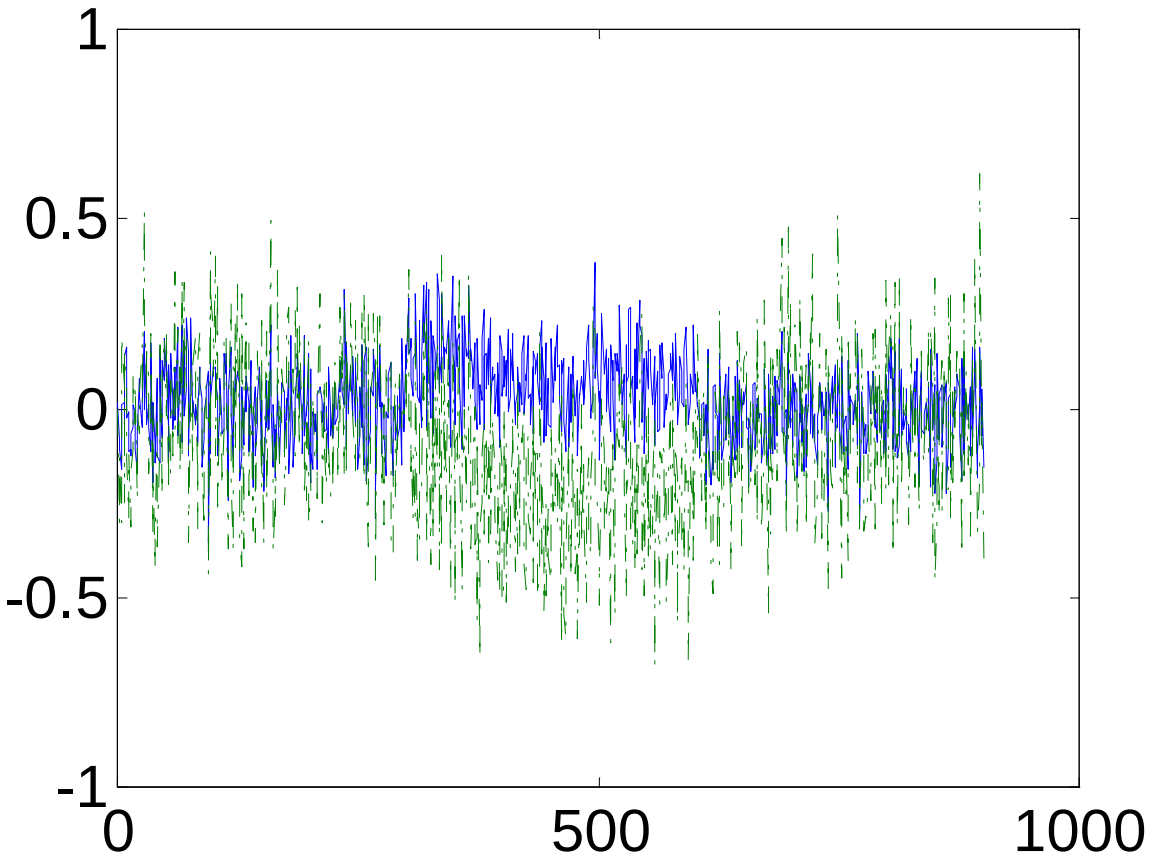

Fig. 7.13. Innovation sequences computed by (7.117), (7.118) from the data of Fig. 7.12; first component (continuous line); second component (dash-dotted line)

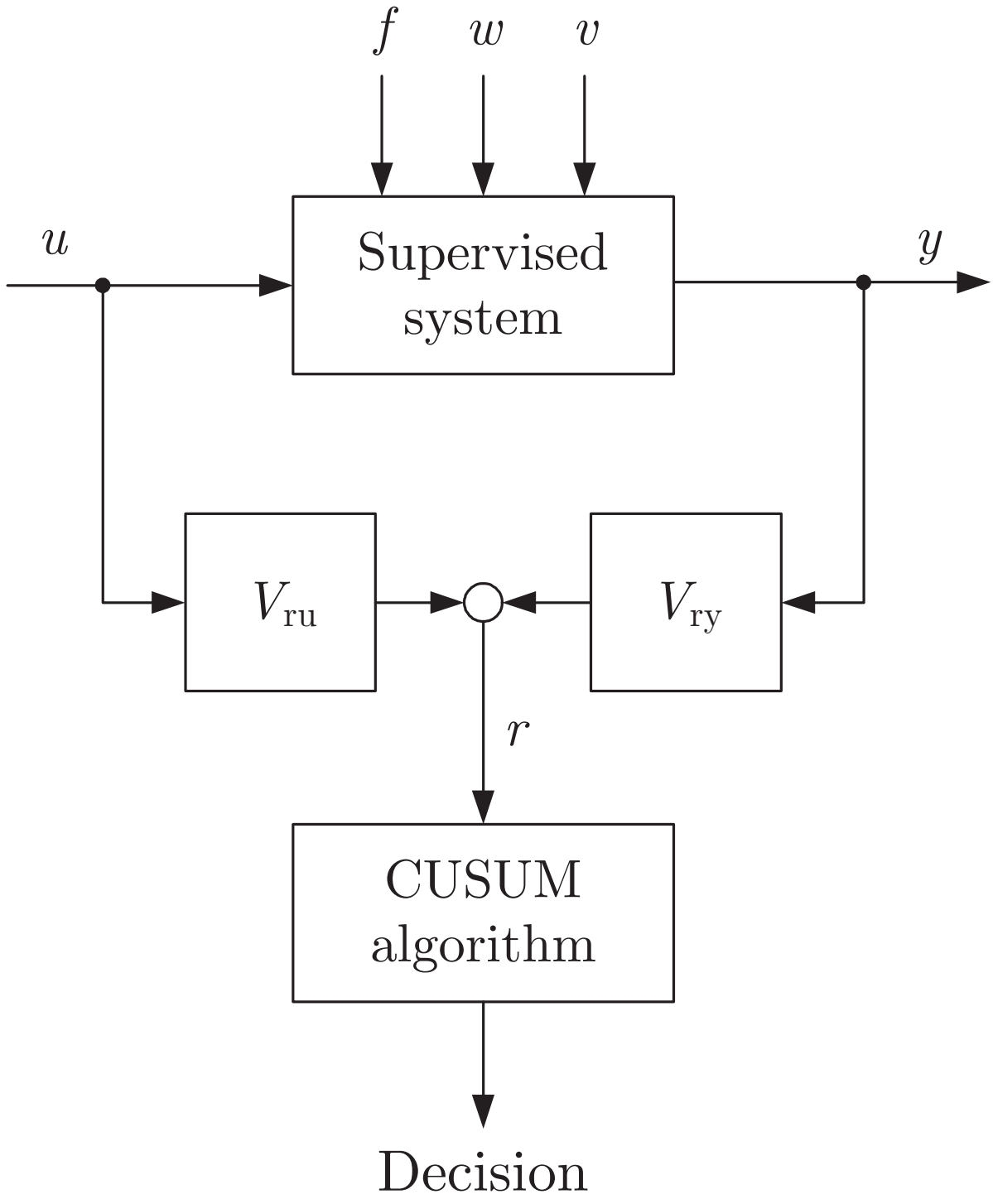

Fig. 7.14. Fault detection system

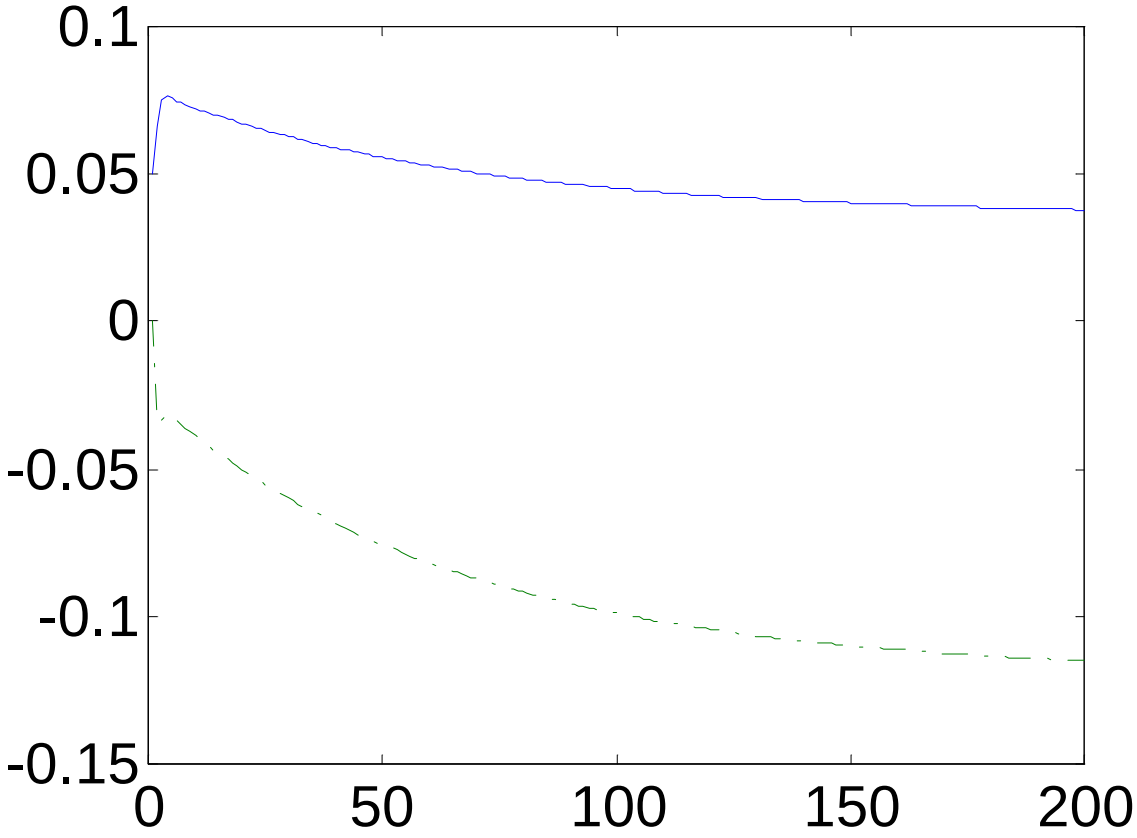

Fig. 7.15. Dynamic profile of change for fault f_ω; first component of $0.05\,\tilde{\rho}_\omega$ (continuous line); second component (dash-dotted line)

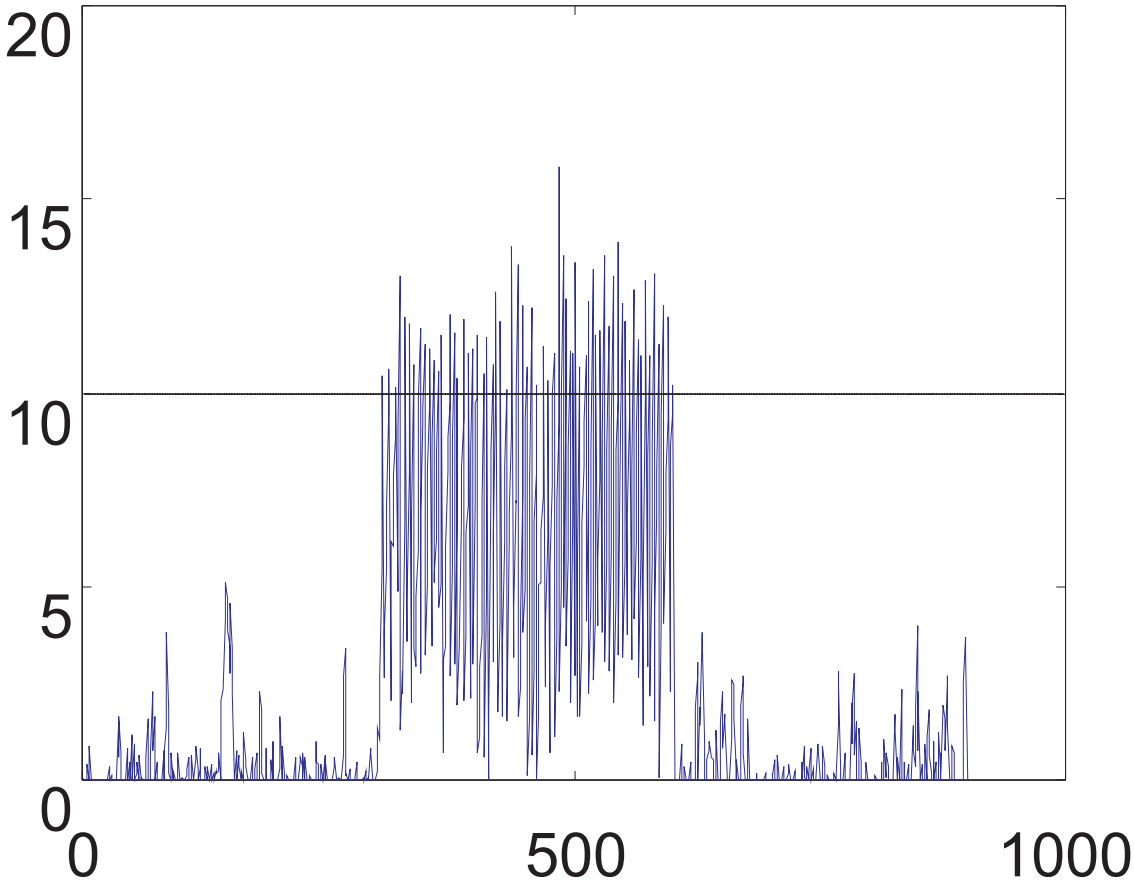

Fig. 7.16. CUSUM decision function resulting from application to the innovation sequence of Fig. 7.13 of the CUSUM algorithm based on the known dynamical profile of change (Fig. 7.15)

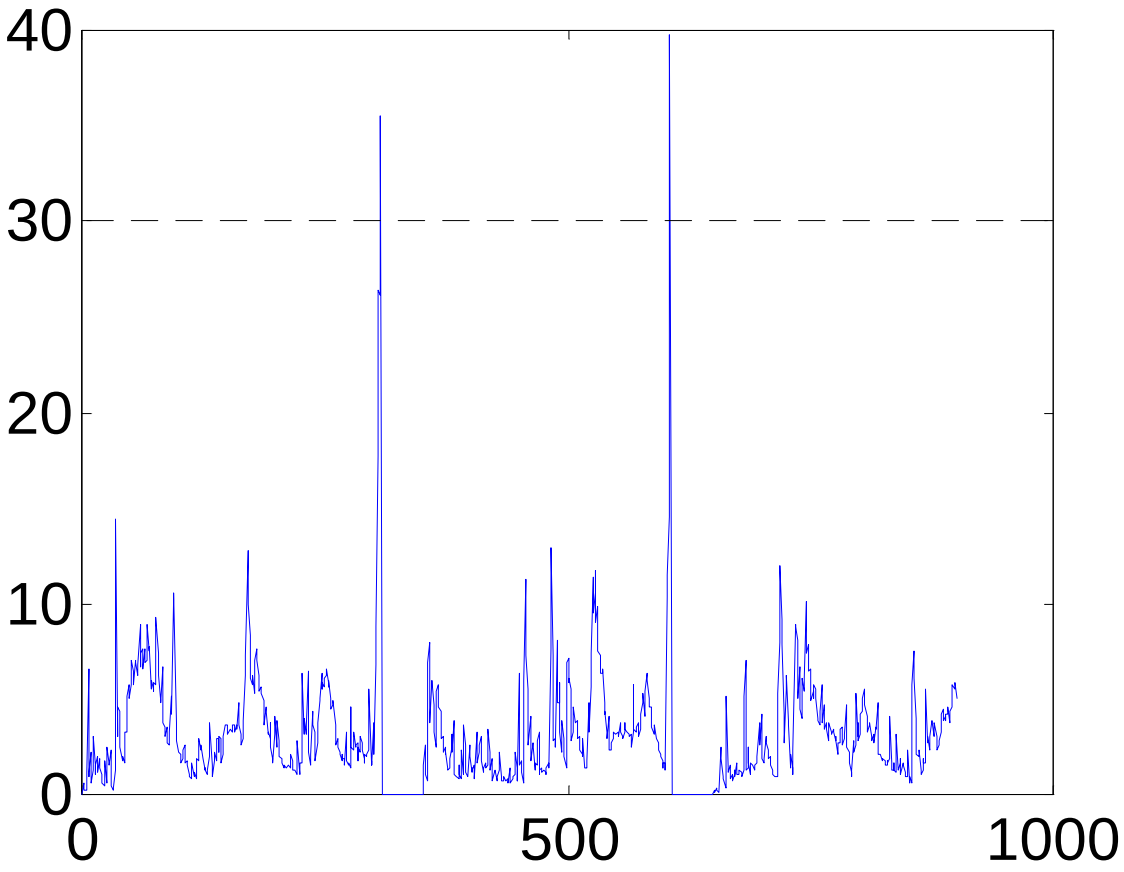

Fig. 7.17. GLR decision function resulting from application to the innovation sequence of Fig. 7.13 of the algorithm with known dynamical profile of change

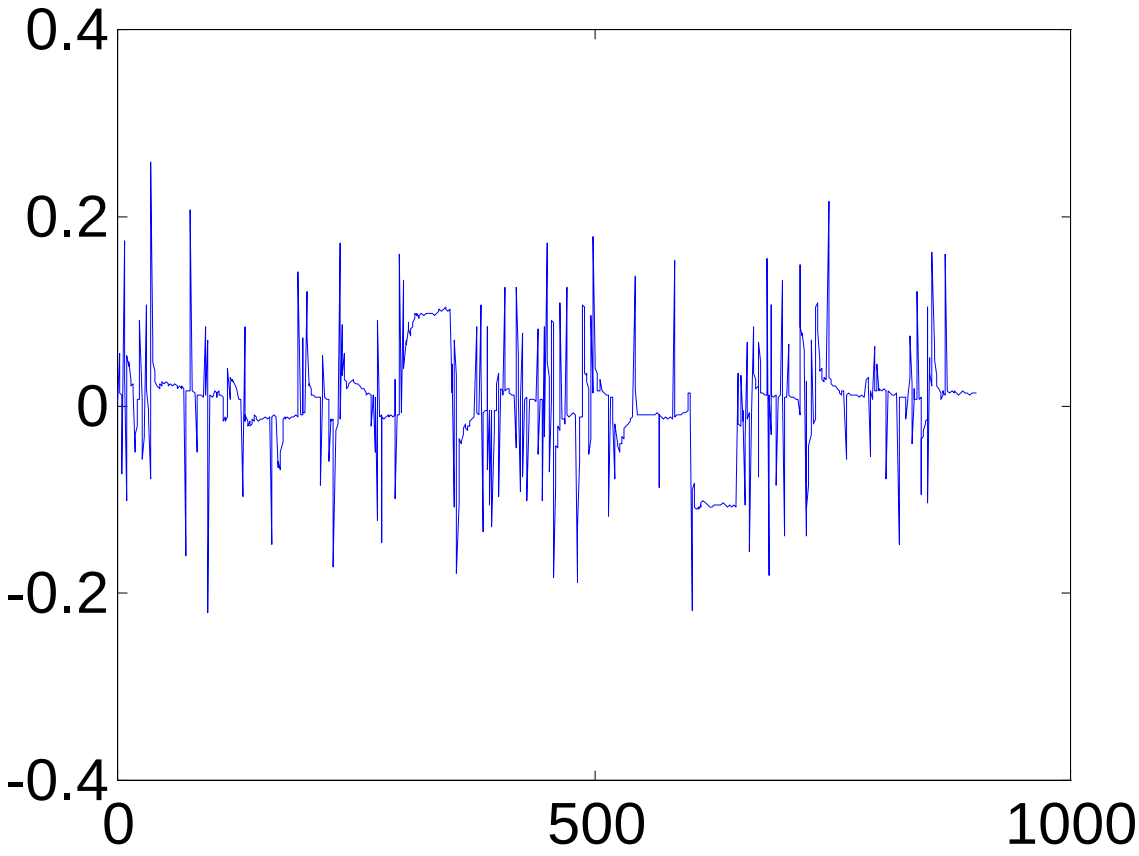

Fig. 7.18. Estimate of the change magnitude resulting from application to the innovation sequence of Fig. 7.13 of the GLR algorithm with known dynamical profile of change

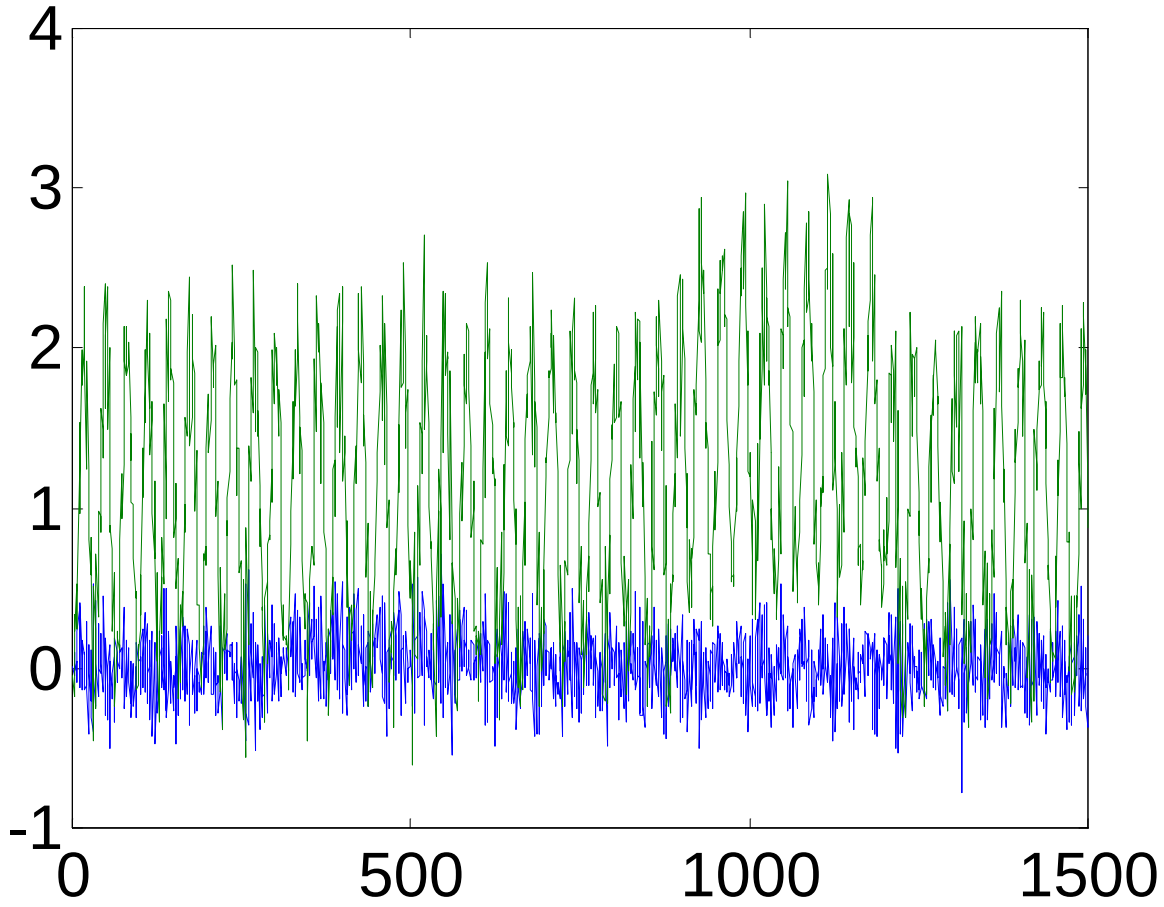

Fig. 7.19. Angular rate and heading measurements

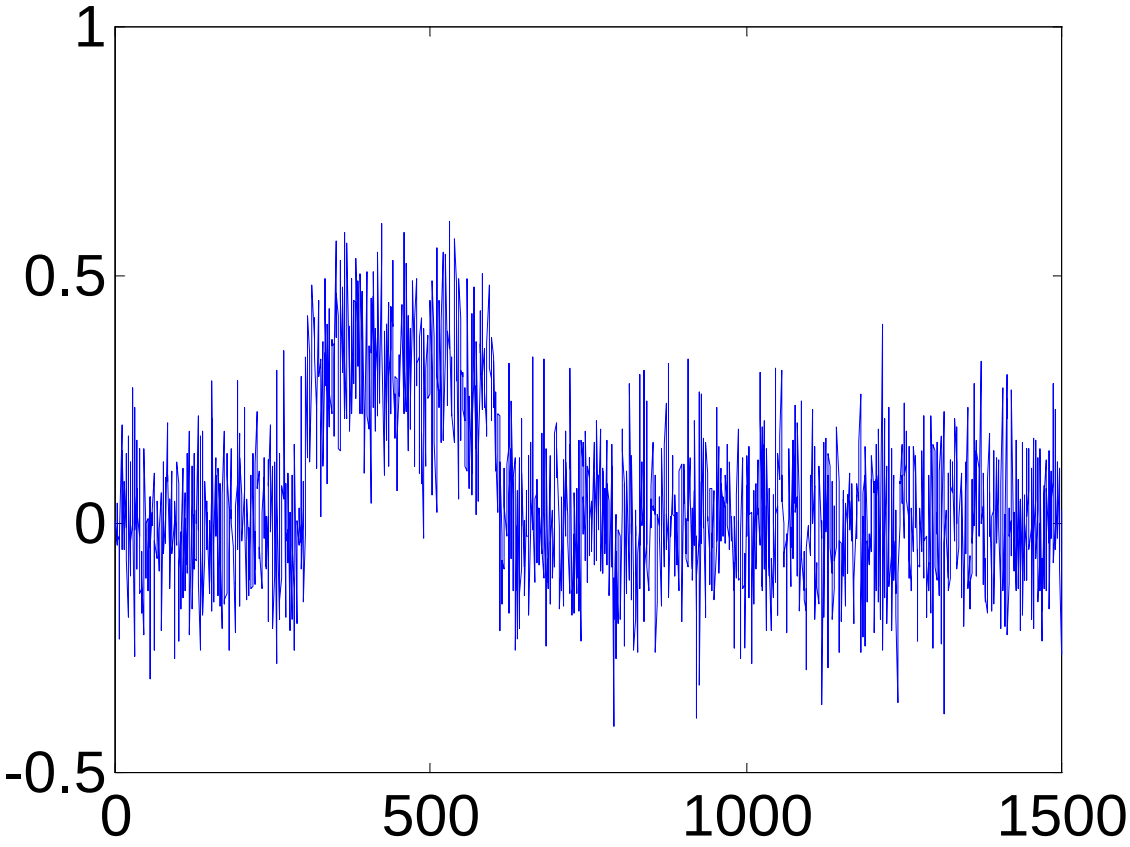

Fig. 7.20. Residual affected by f_ω

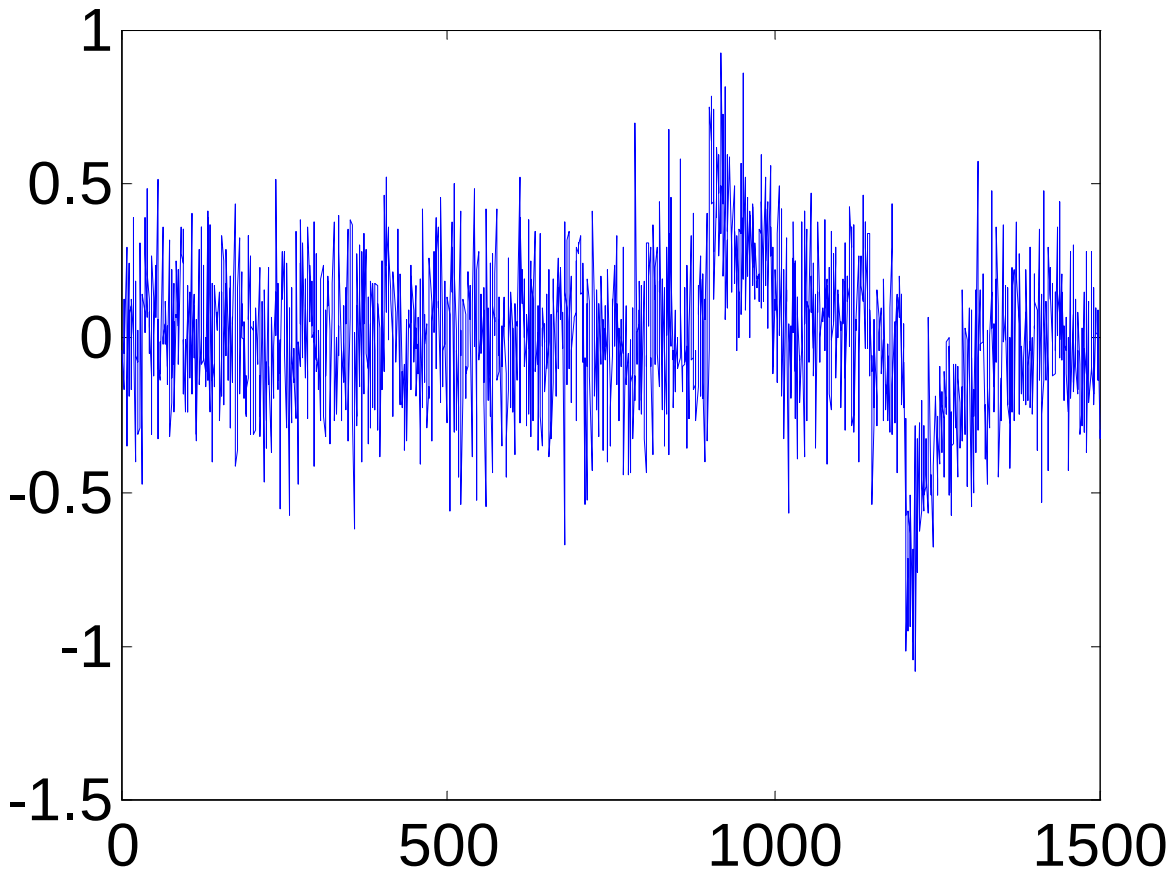

Fig. 7.20. Residual affected by f_ψ

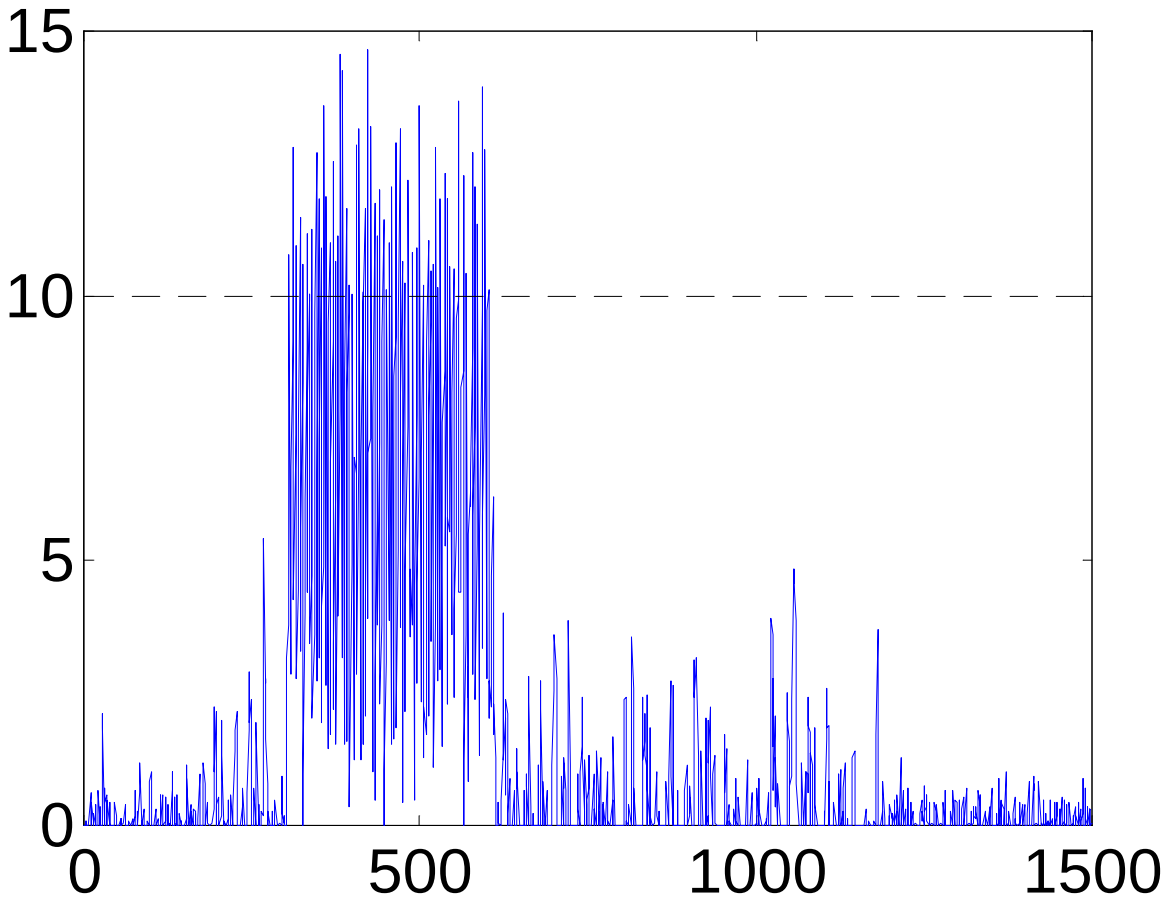

Fig. 7.21. CUSUM decision function and GLR decision function resulting from evaluation of r_ψ

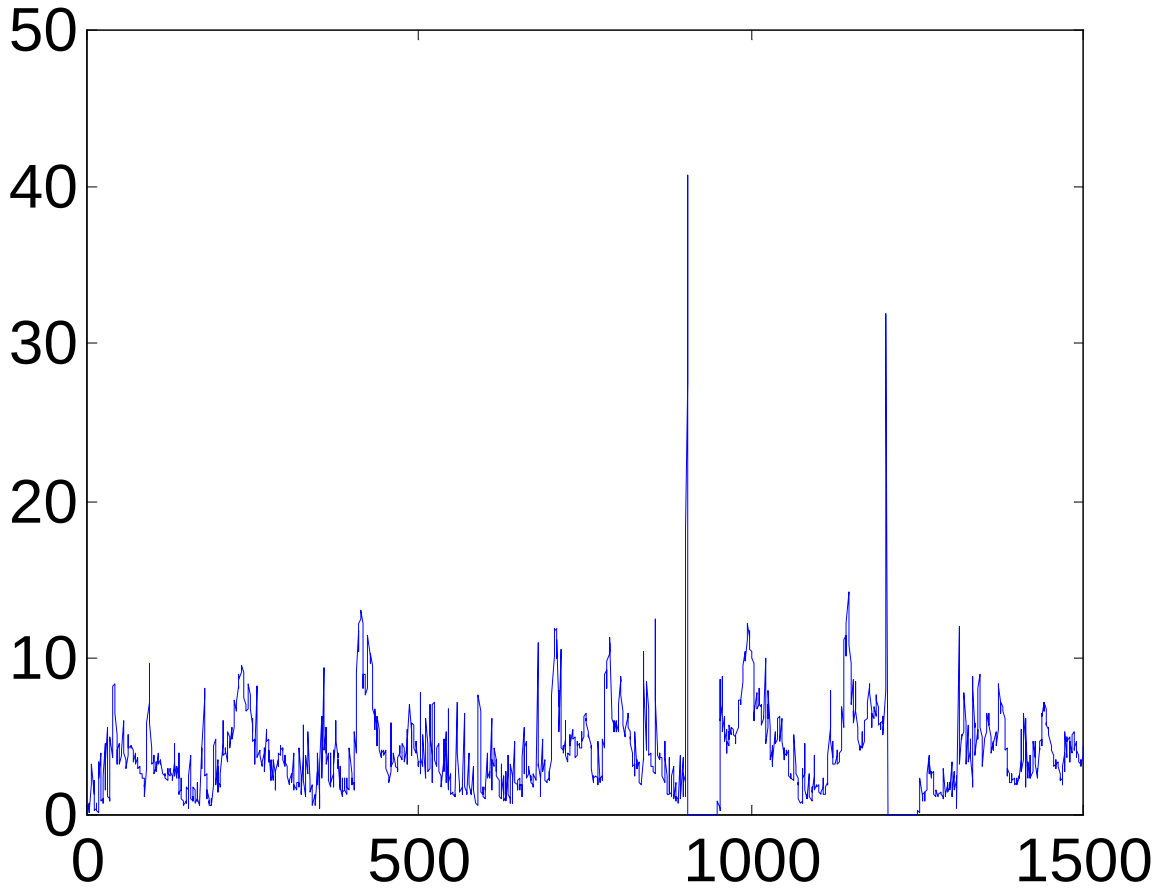

Fig. 7.21. CUSUM decision function and GLR decision function resulting from evaluation of r_{ω_3}

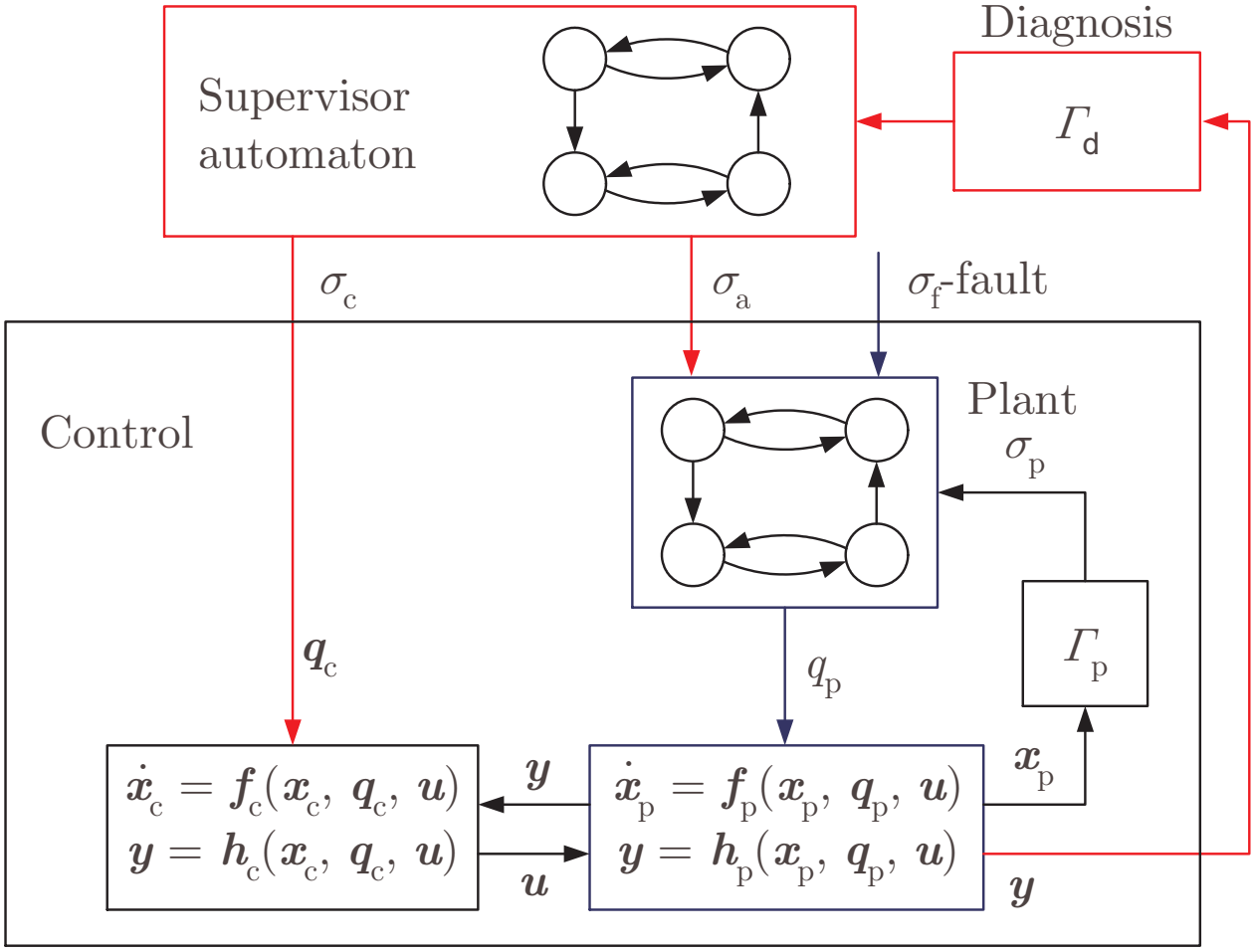

Fig. 8.1. The plant can change in a discrete way through change in states, a plant fault can cause a discrete event

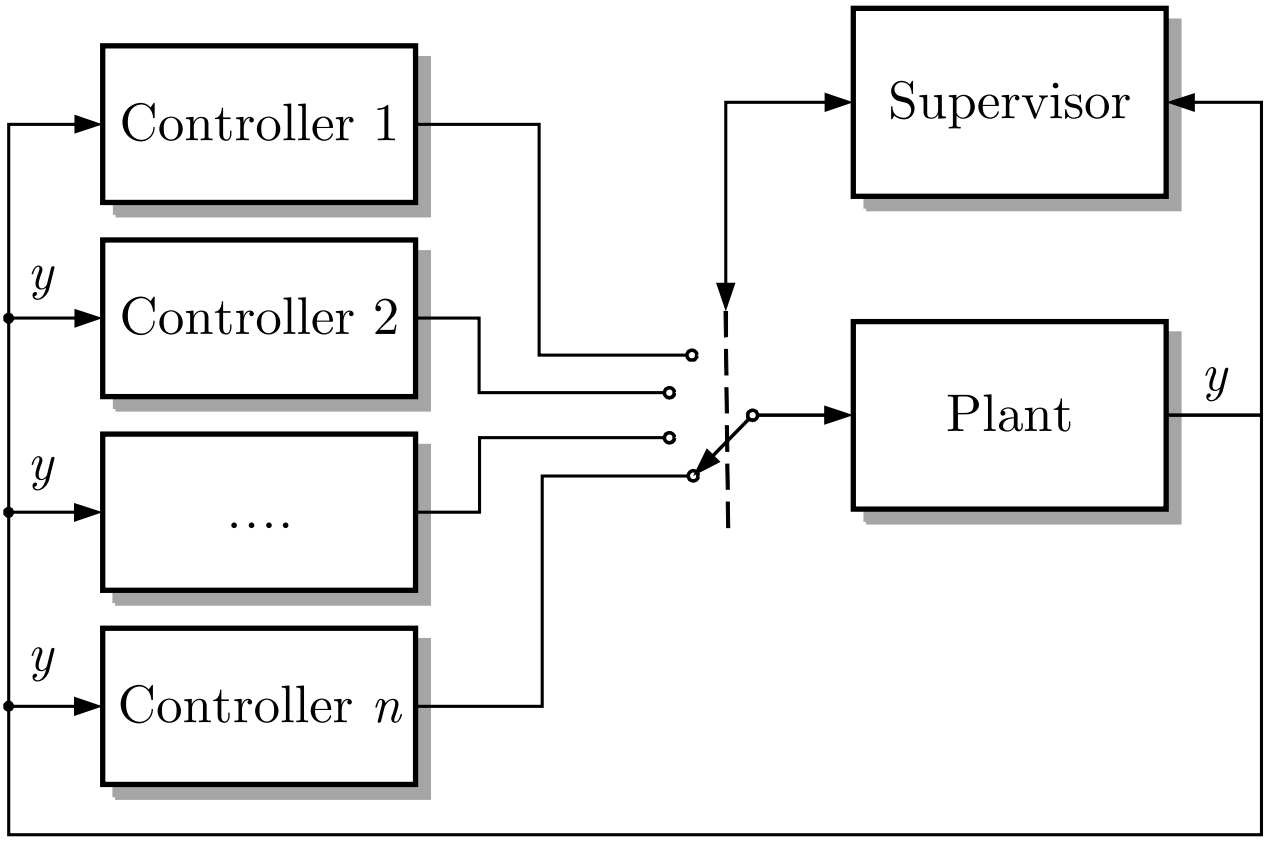

Fig. 8.2. Structure of logic-based switching controller

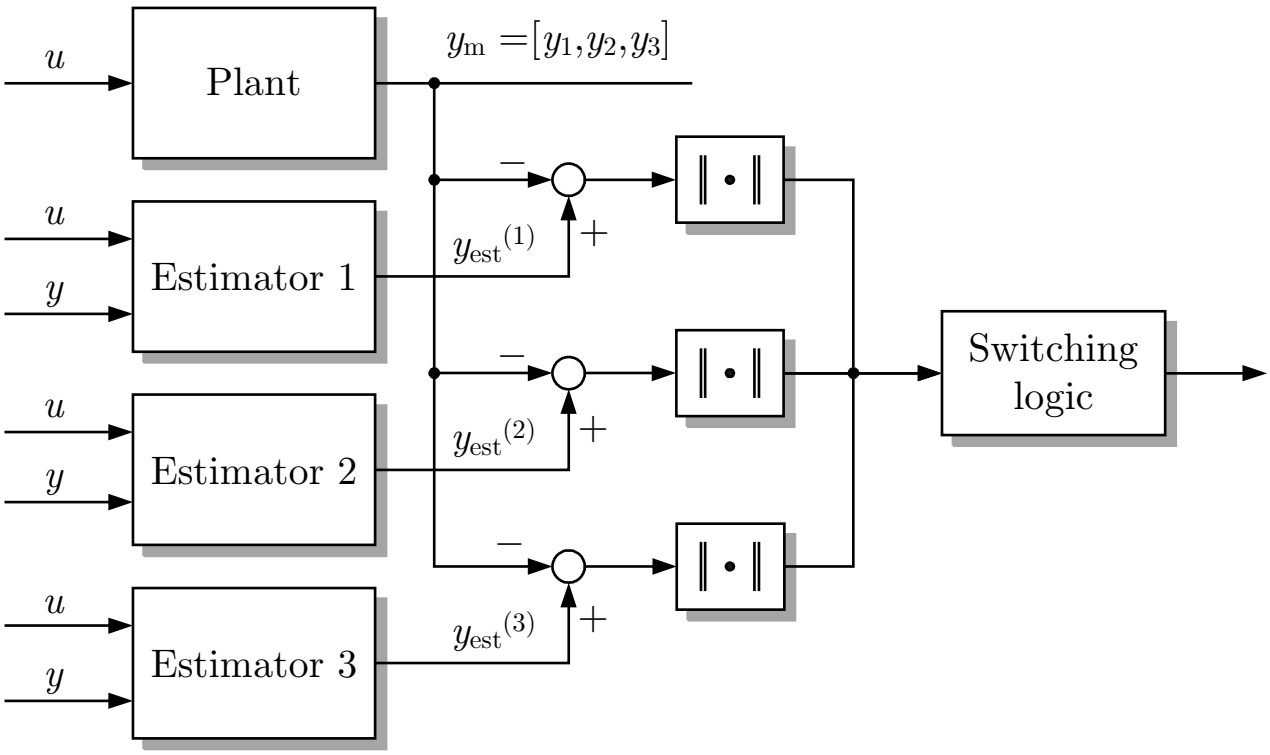

Fig. 8.3. Logic within a supervisor selects an output estimate from a bank of estimators

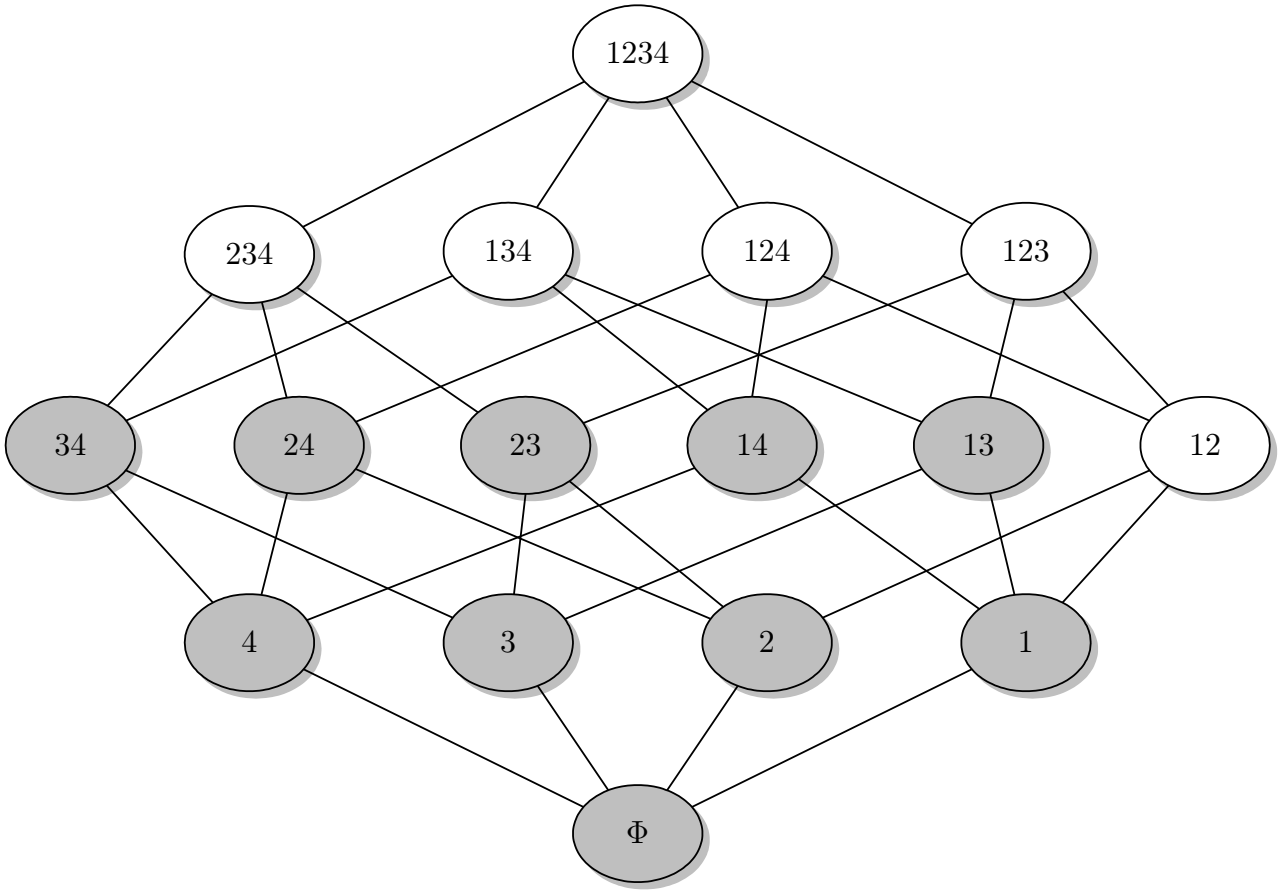

Fig. 8.4. The lattice of the actuators subsets in the example

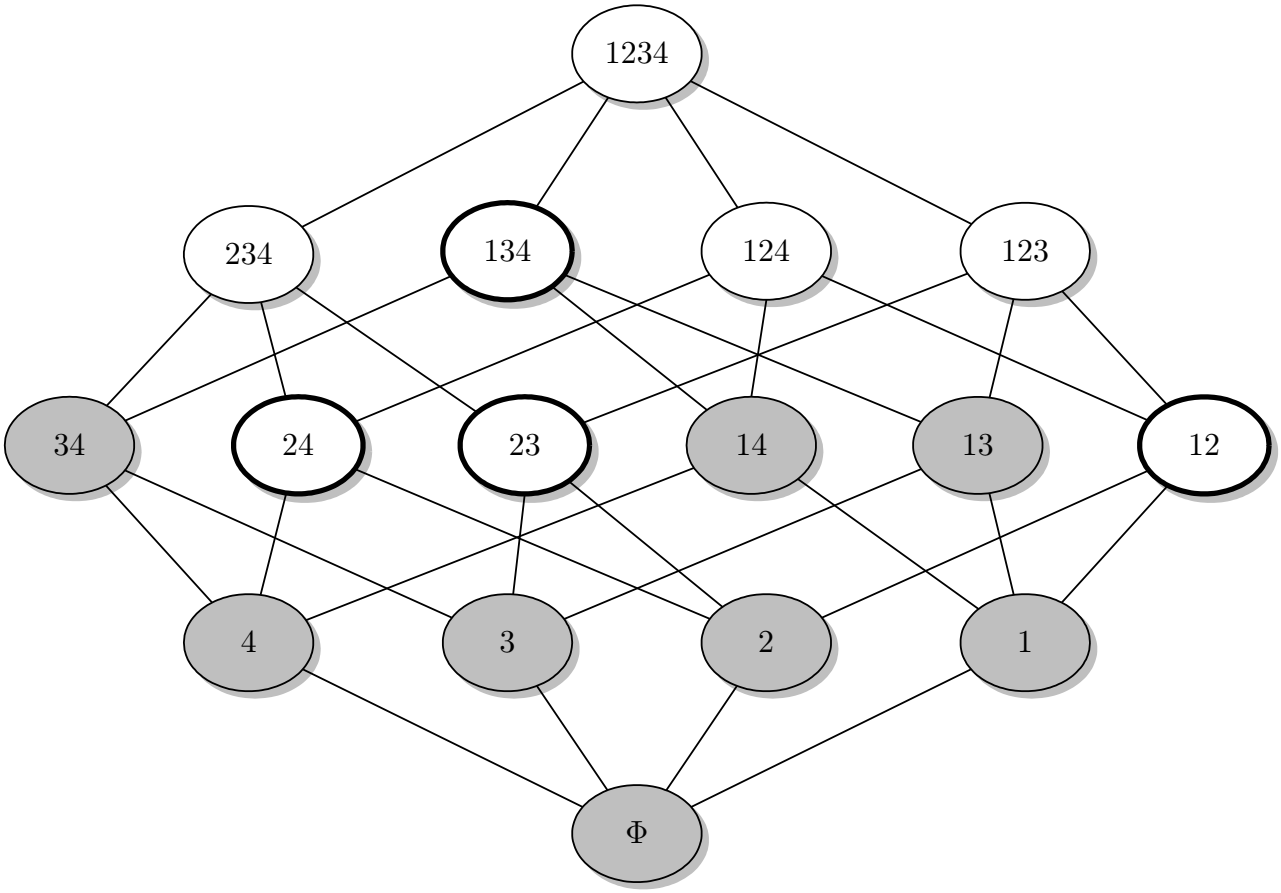

Fig. 8.5. The lattice of actuator configurations

Blanke/Kinnaert/Lunze/Staroswiecki:
Diagnosis and Fault-Tolerant Control, (3rd edition), Springer-Verlag 2015

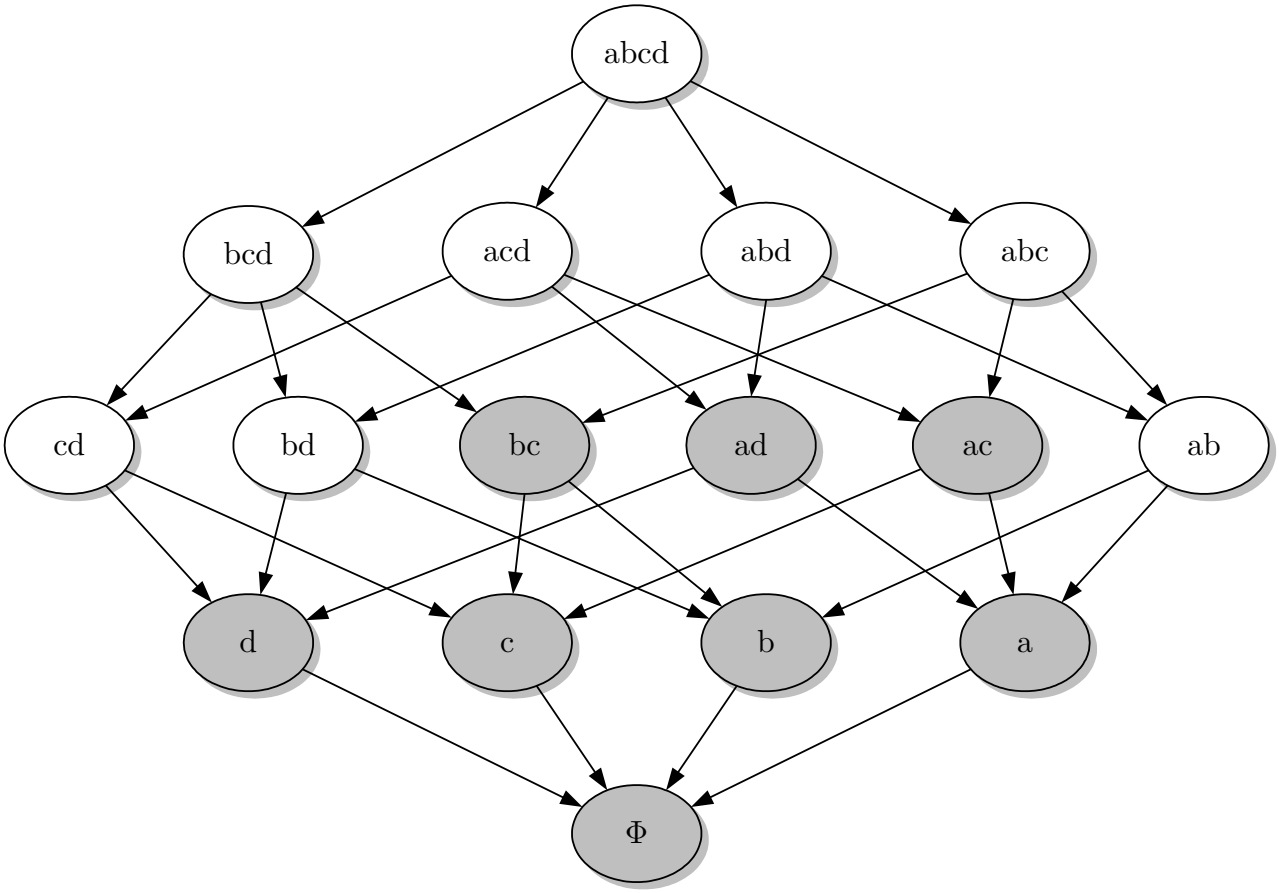

Fig. 8.6. Recoverable configurations

Blanke/Kinnaert/Lunze/Staroswiecki:
Diagnosis and Fault-Tolerant Control, (3rd edition), Springer-Verlag 2015

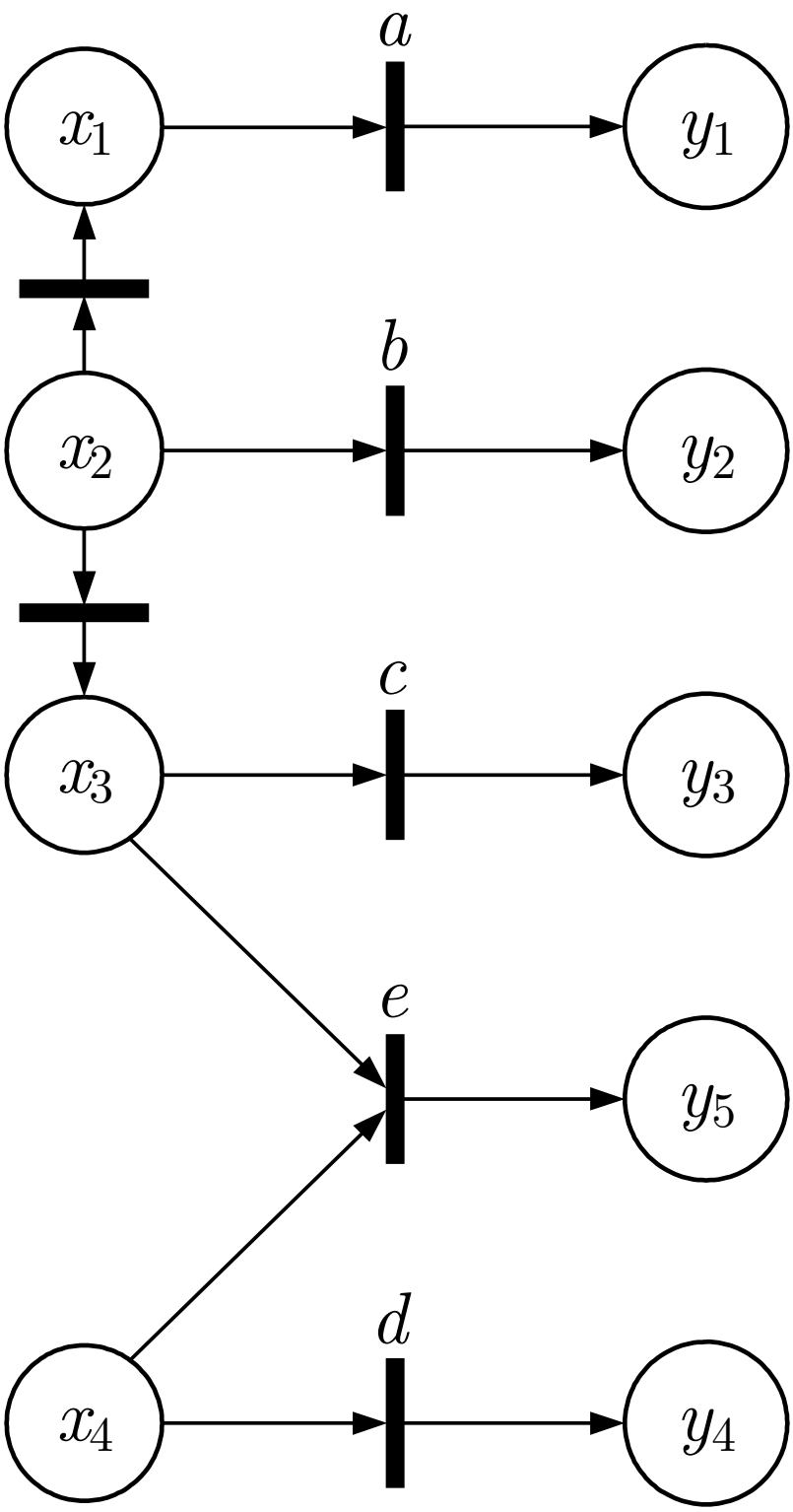

Fig. 8.7. Structural graph of the measurement system

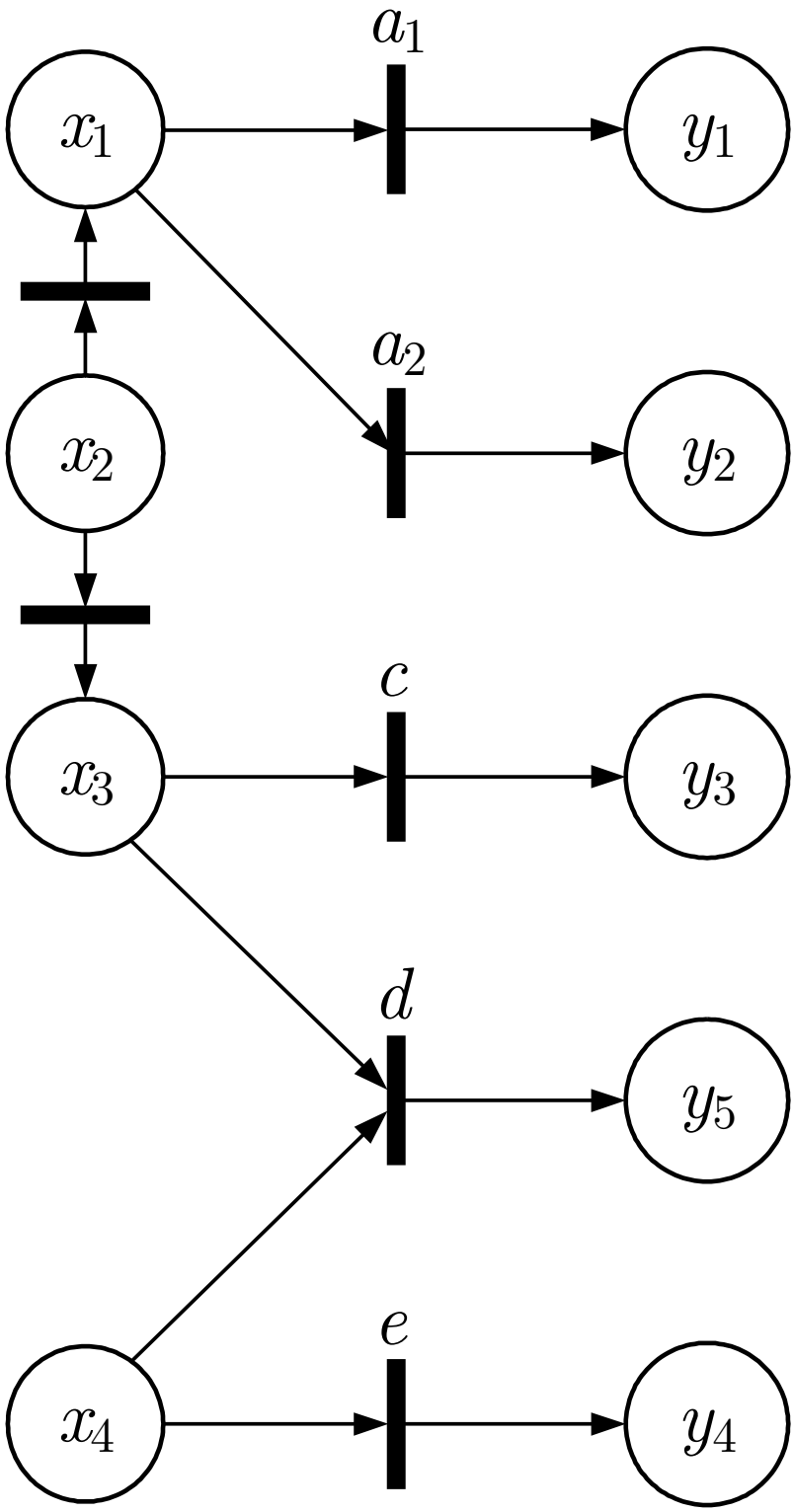

Fig. 8.8. The new system with b removed and a duplicated

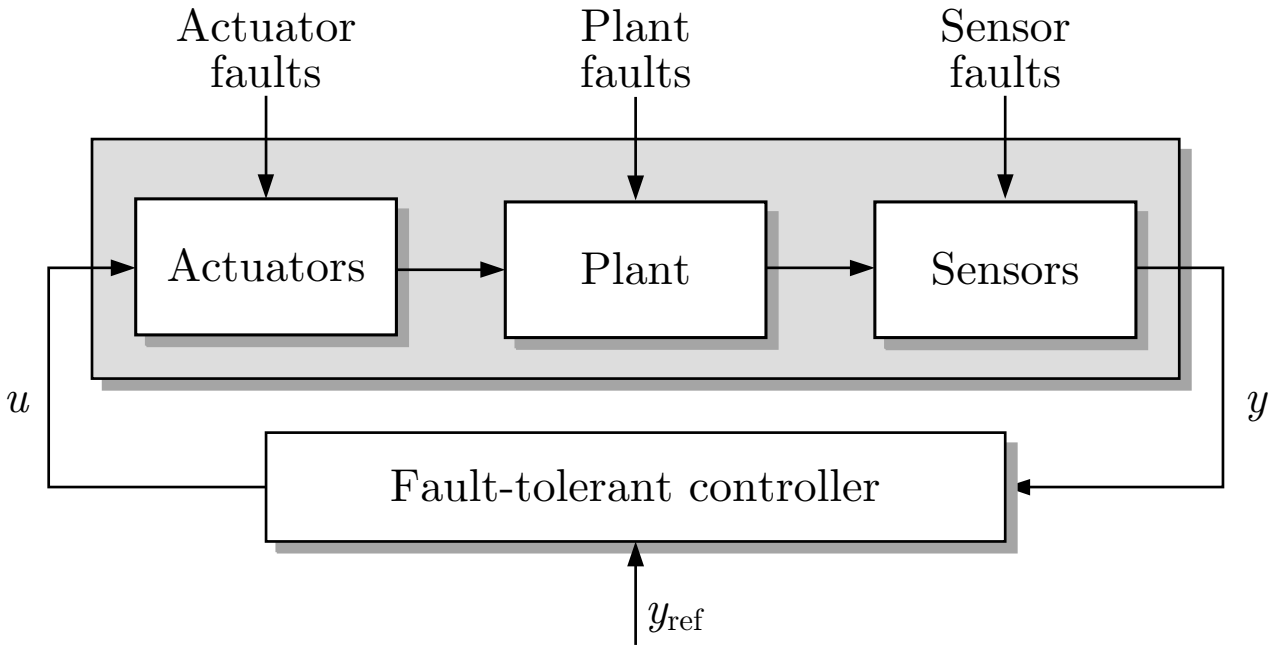

Fig. 9.1. Fault-tolerant controller

Blanke/Kinnaert/Lunze/Staroswiecki:
Diagnosis and Fault-Tolerant Control, (3rd edition), Springer-Verlag 2015

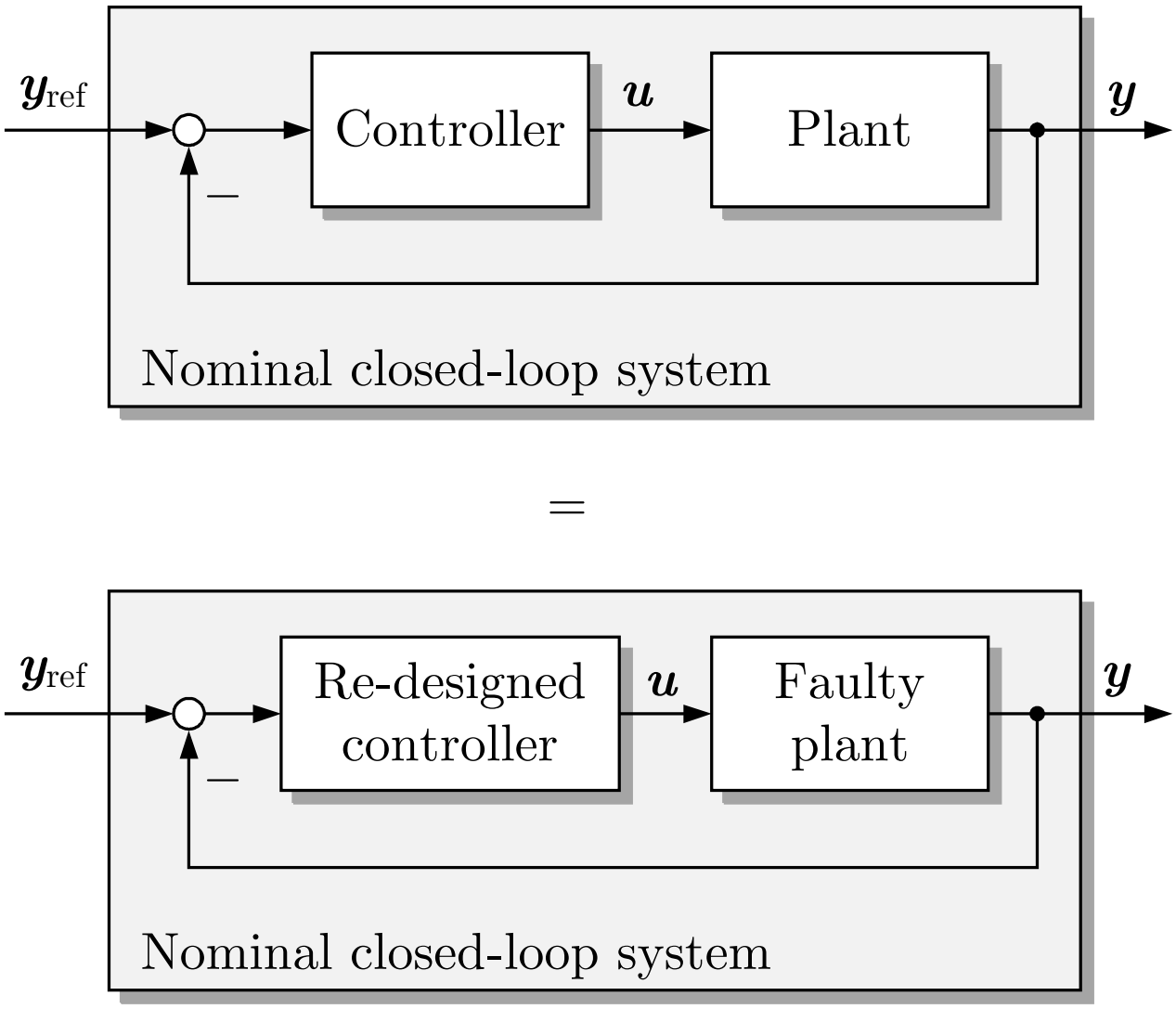

Fig. 9.2. Idea of the model-matching approach to control reconfiguration

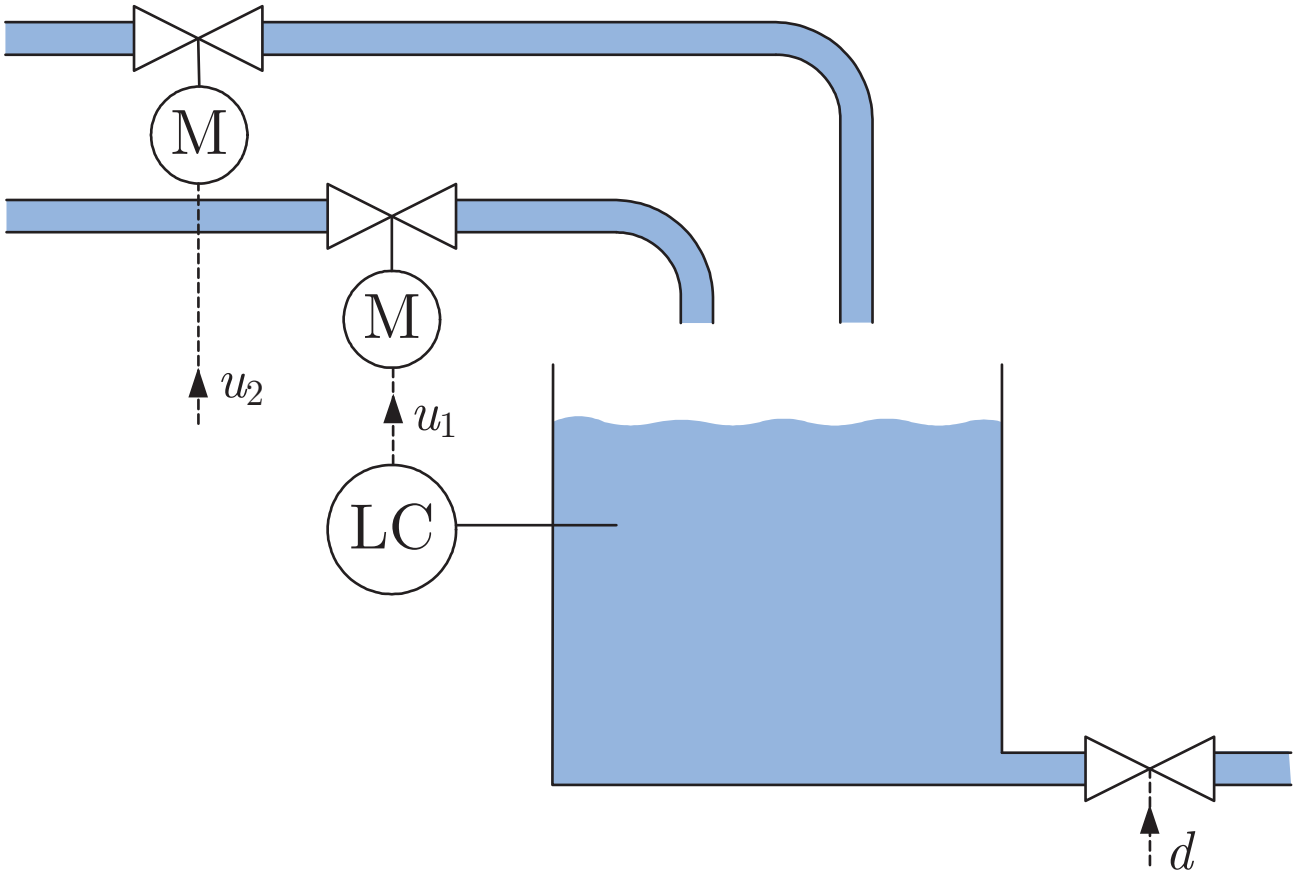

Fig. 9.3. Example demonstrating the model-matching reconfiguration strategy

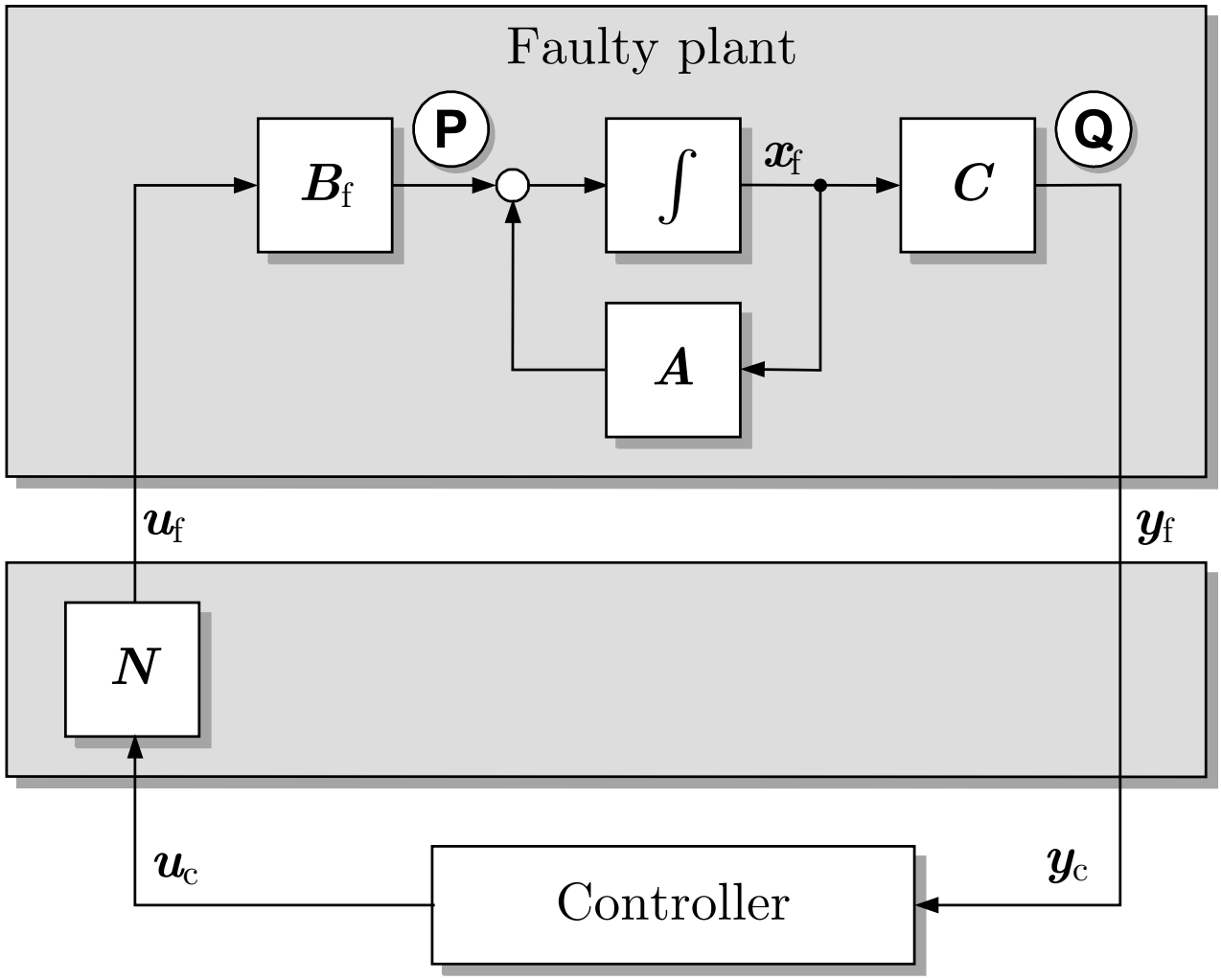

Fig. 9.4. Input/output-based reconfiguration after actuator failures

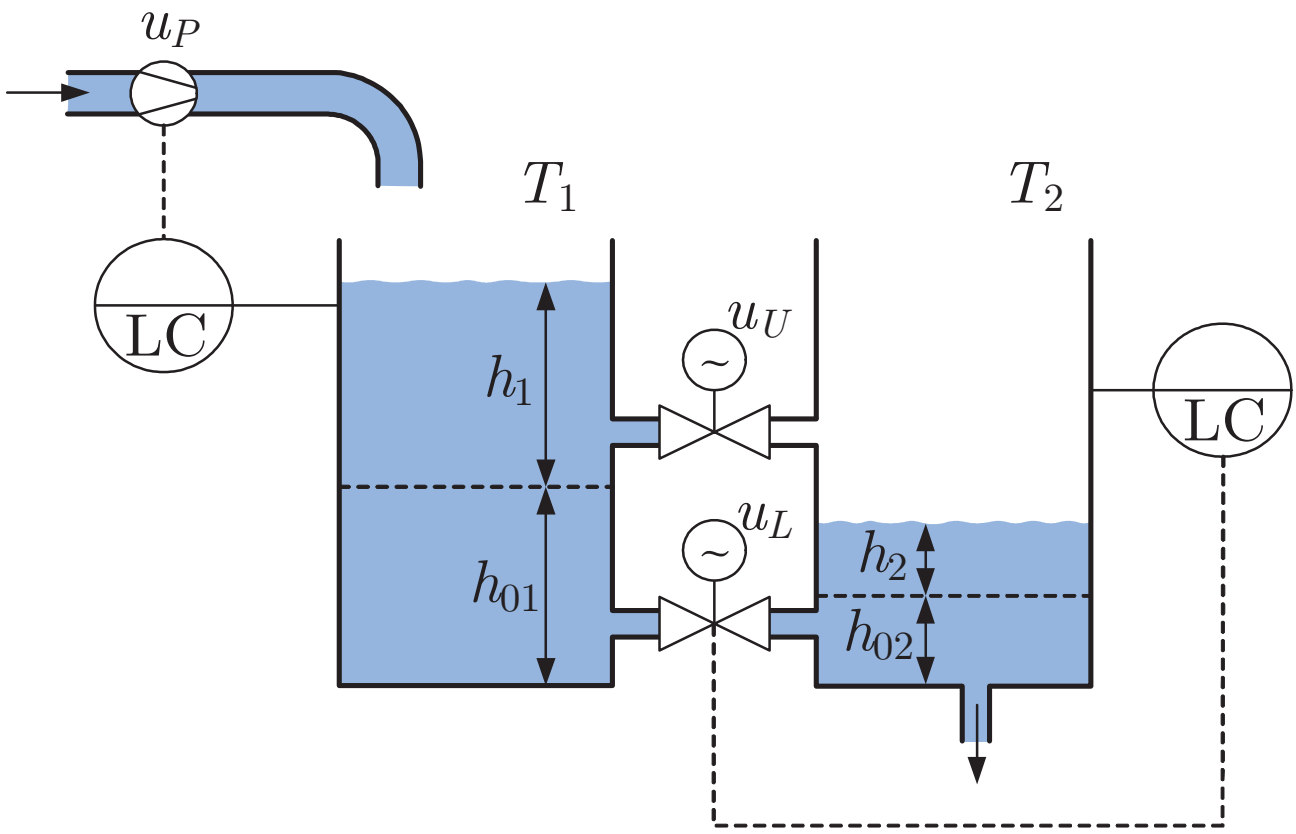

Fig. 9.5. Reconfiguration of a two-tank system

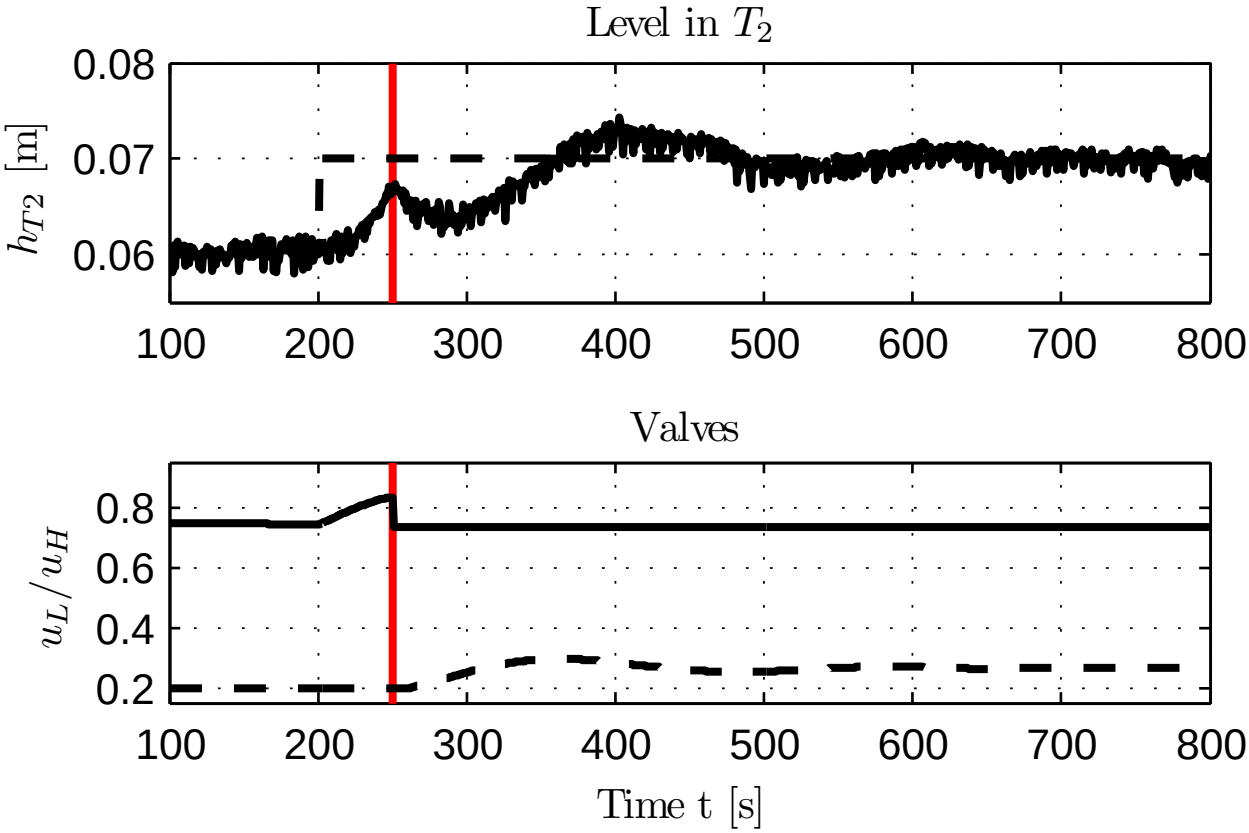

Fig. 9.6. Experimental results with the reconfigured tank system: After the failure of the lower valve (u_L, solid line) the controller acts at the upper valve (u_H, dashed line)

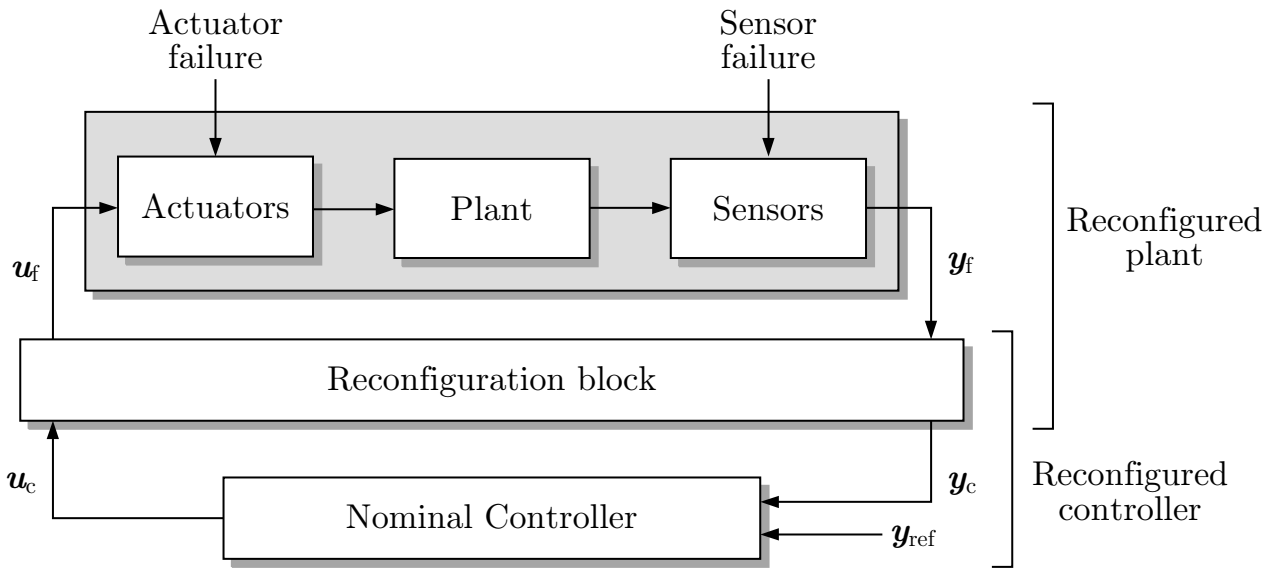

Fig. 9.7. Principle of control reconfiguration for actuator or sensor failures

Blanke/Kinnaert/Lunze/Staroswiecki:
Diagnosis and Fault-Tolerant Control, (3rd edition), Springer-Verlag 2015

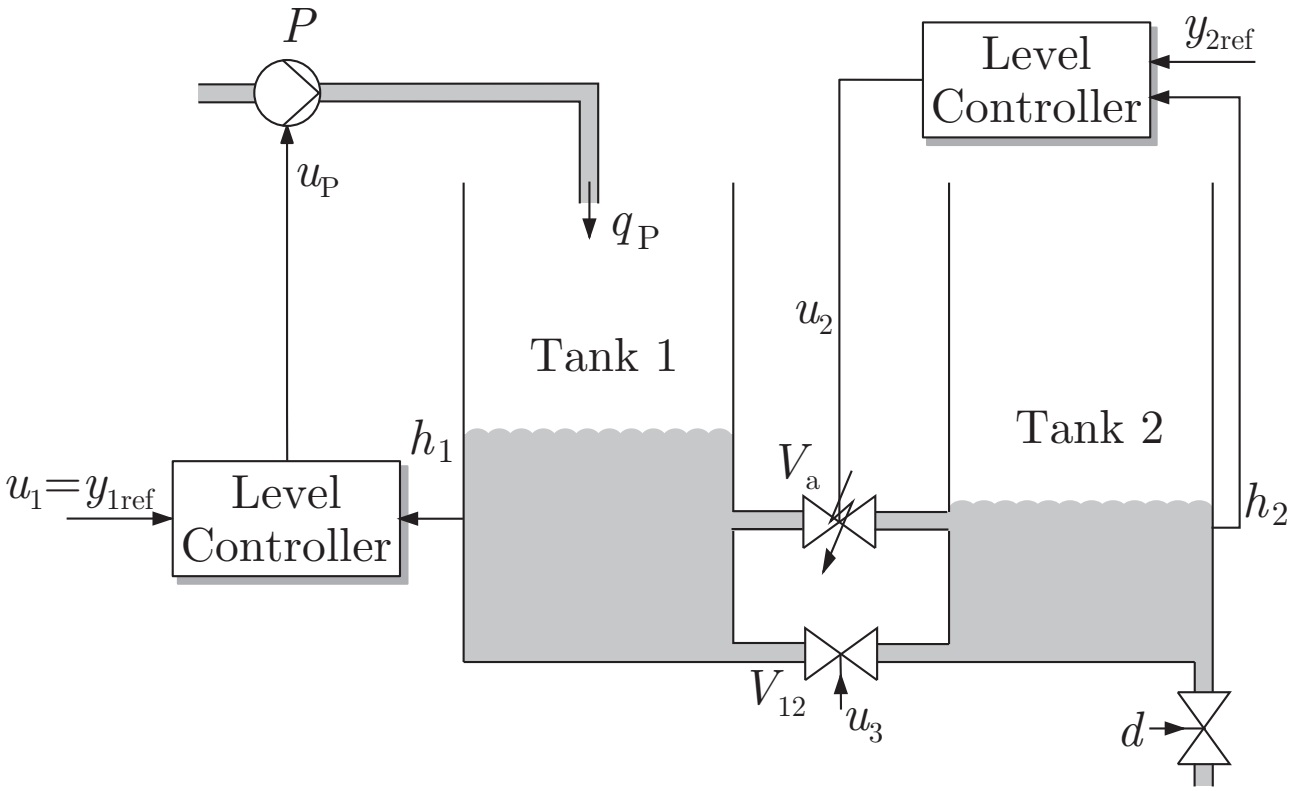

Fig. 9.8. Reconfiguration problem for the tank example

Blanke/Kinnaert/Lunze/Staroswiecki:
Diagnosis and Fault-Tolerant Control, (3rd edition), Springer-Verlag 2015

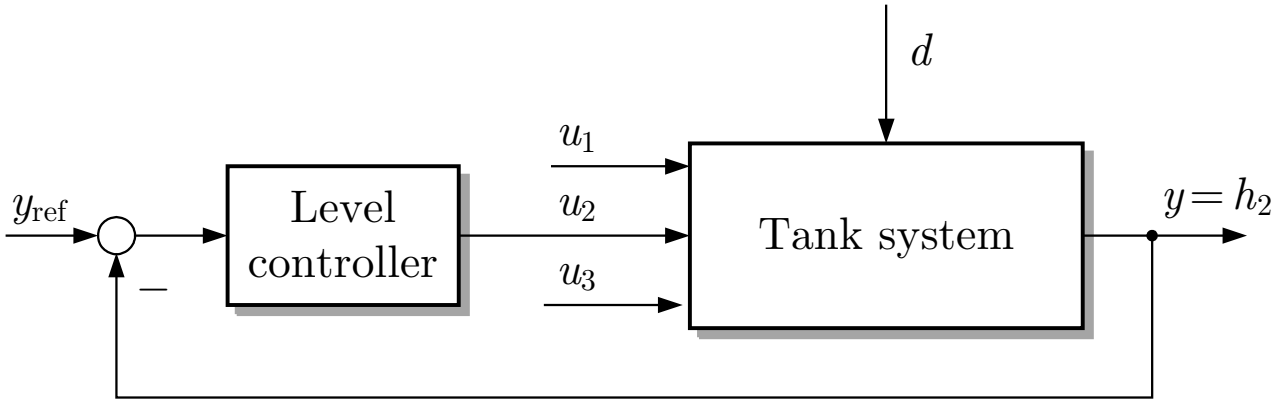

Fig. 9.9. Block diagram of the reconfiguration problem

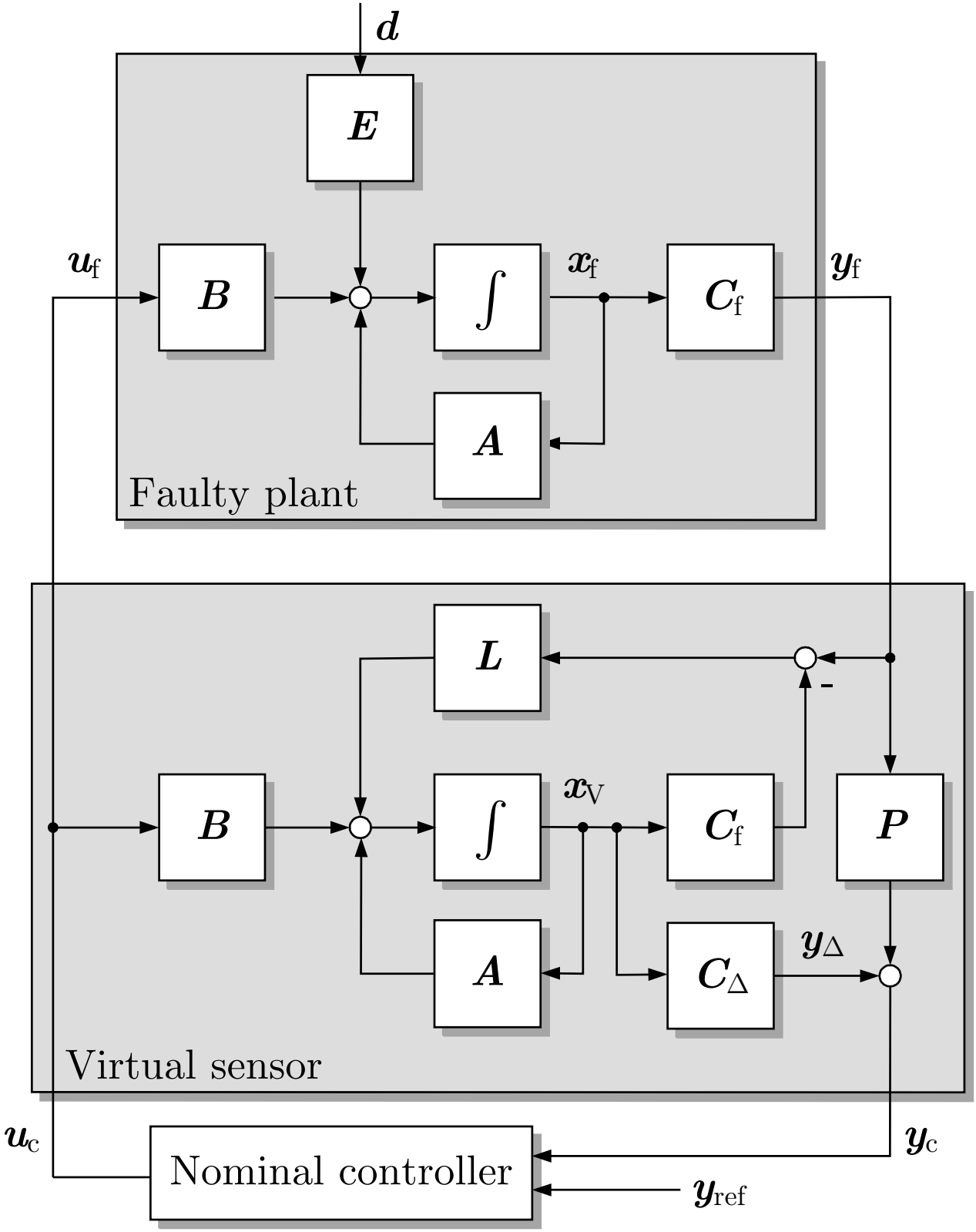

Fig. 9.10. Reconfiguration by using a virtual sensor

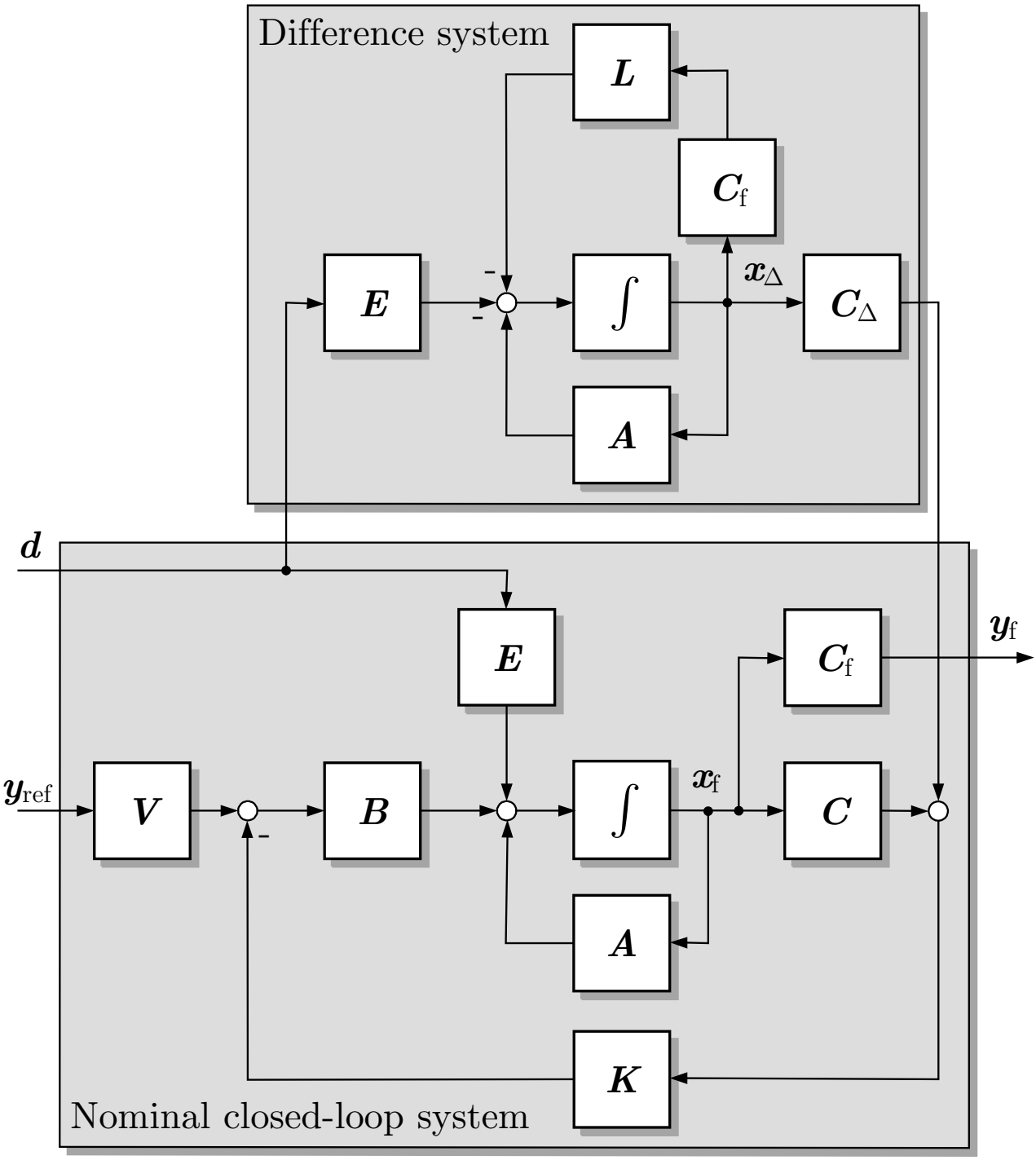

Fig. 9.11. Analysis of the closed-loop system with virtual sensor

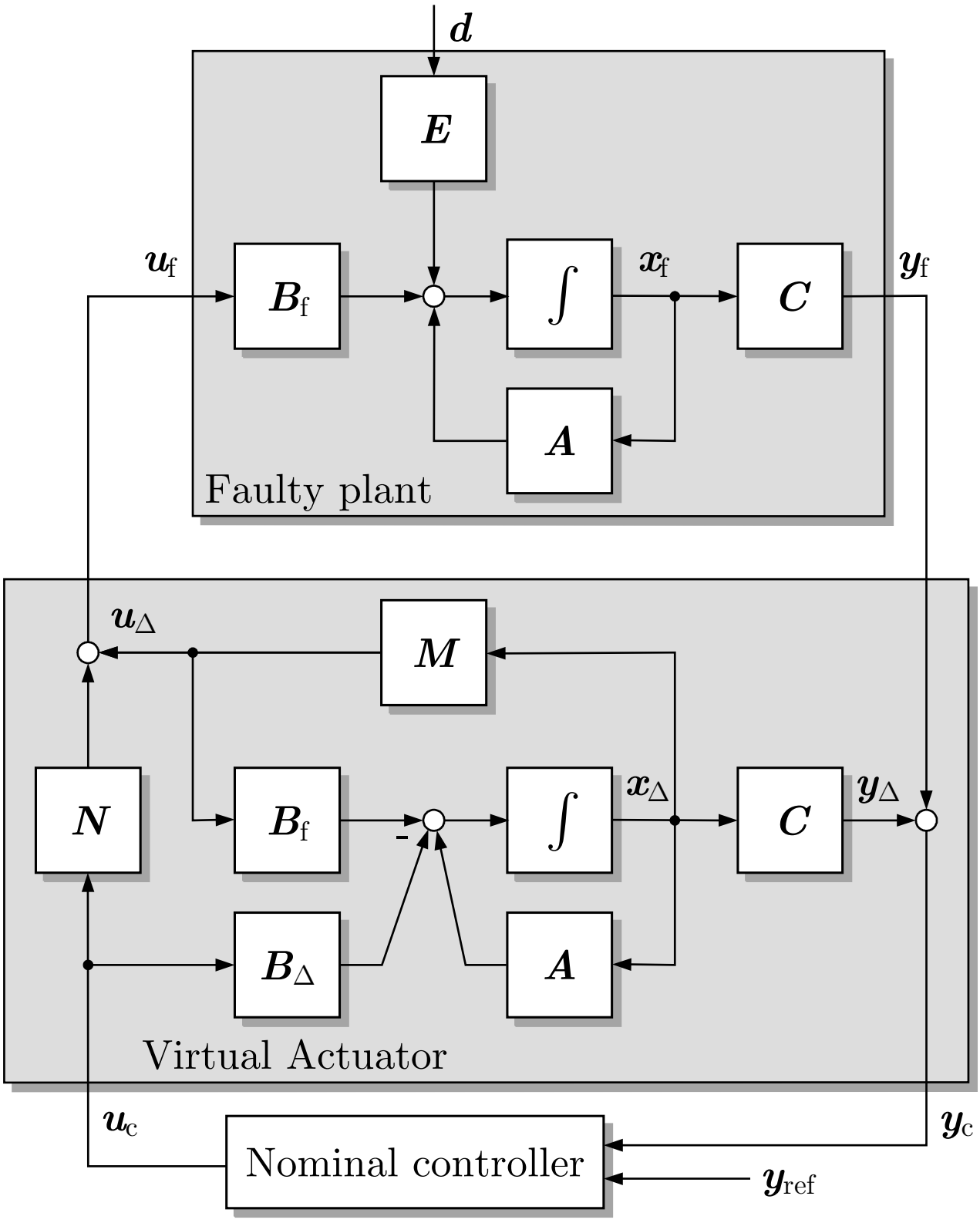

Fig. 9.12. Reconfiguration by means of a virtual actuator

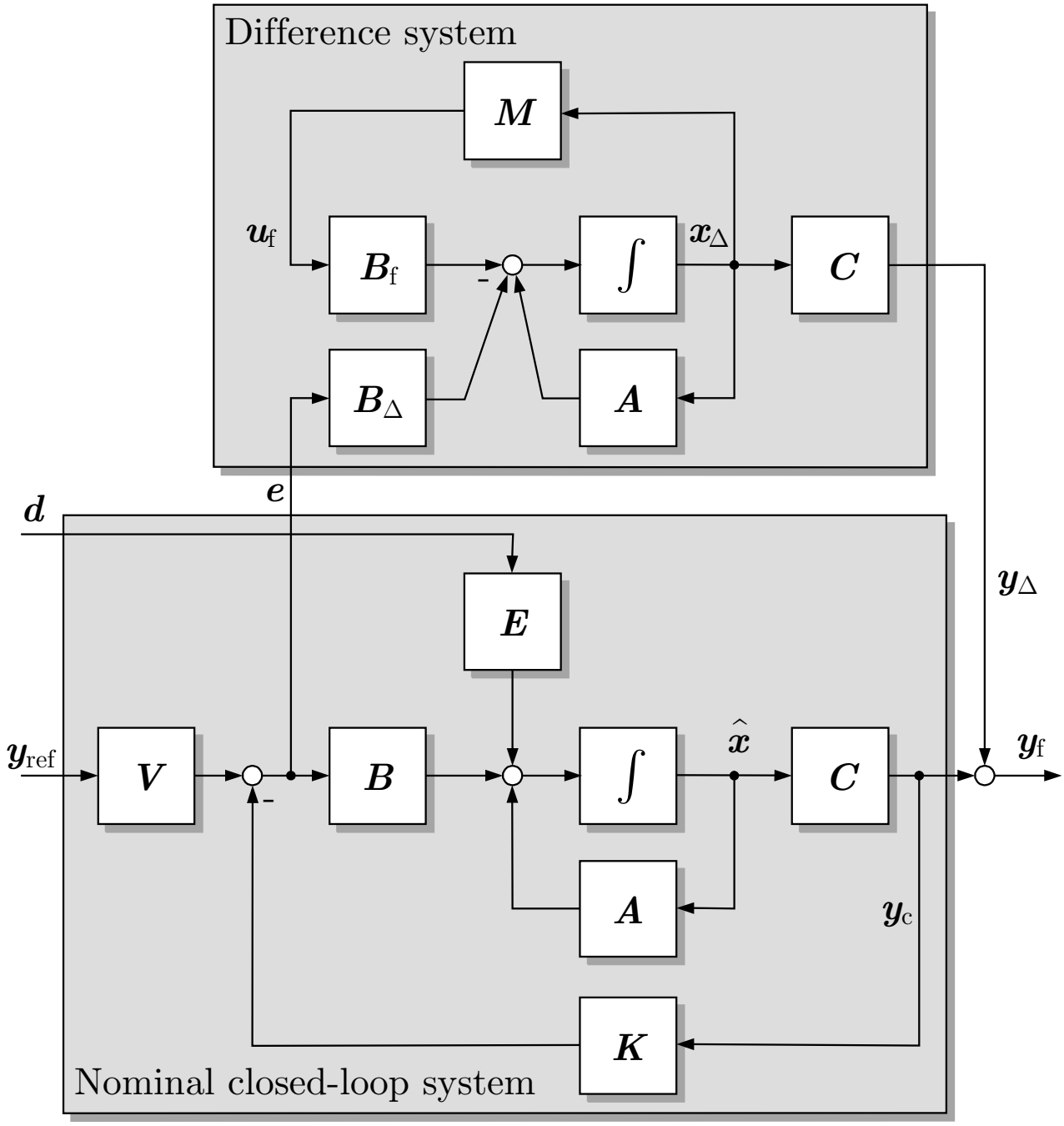

Fig. 9.13. Transformed closed-loop system showing the separation principle

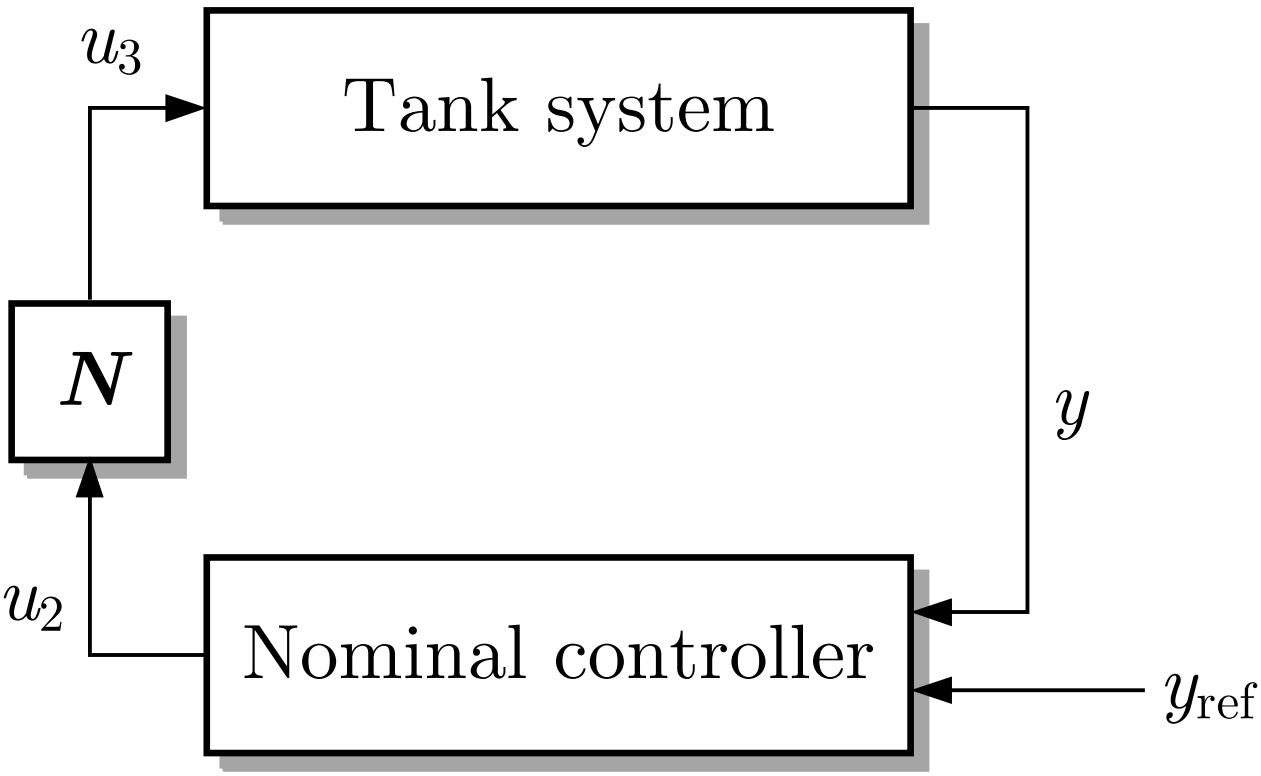

Fig. 9.14. Static reconfiguration of the tank system

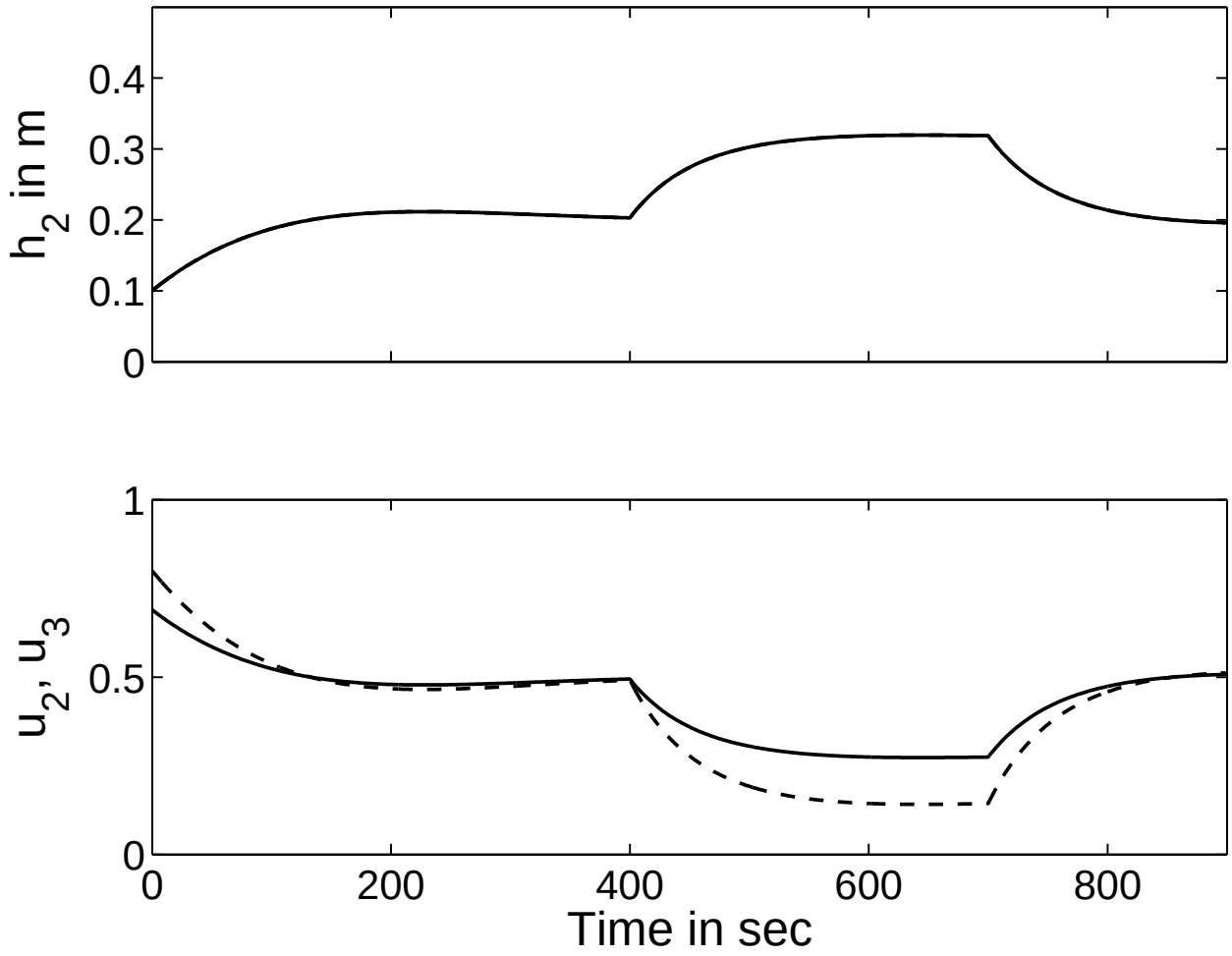

Fig. 9.15. Behaviour of the reconfigured closed-loop system where the reconfigured controller uses the input u_3

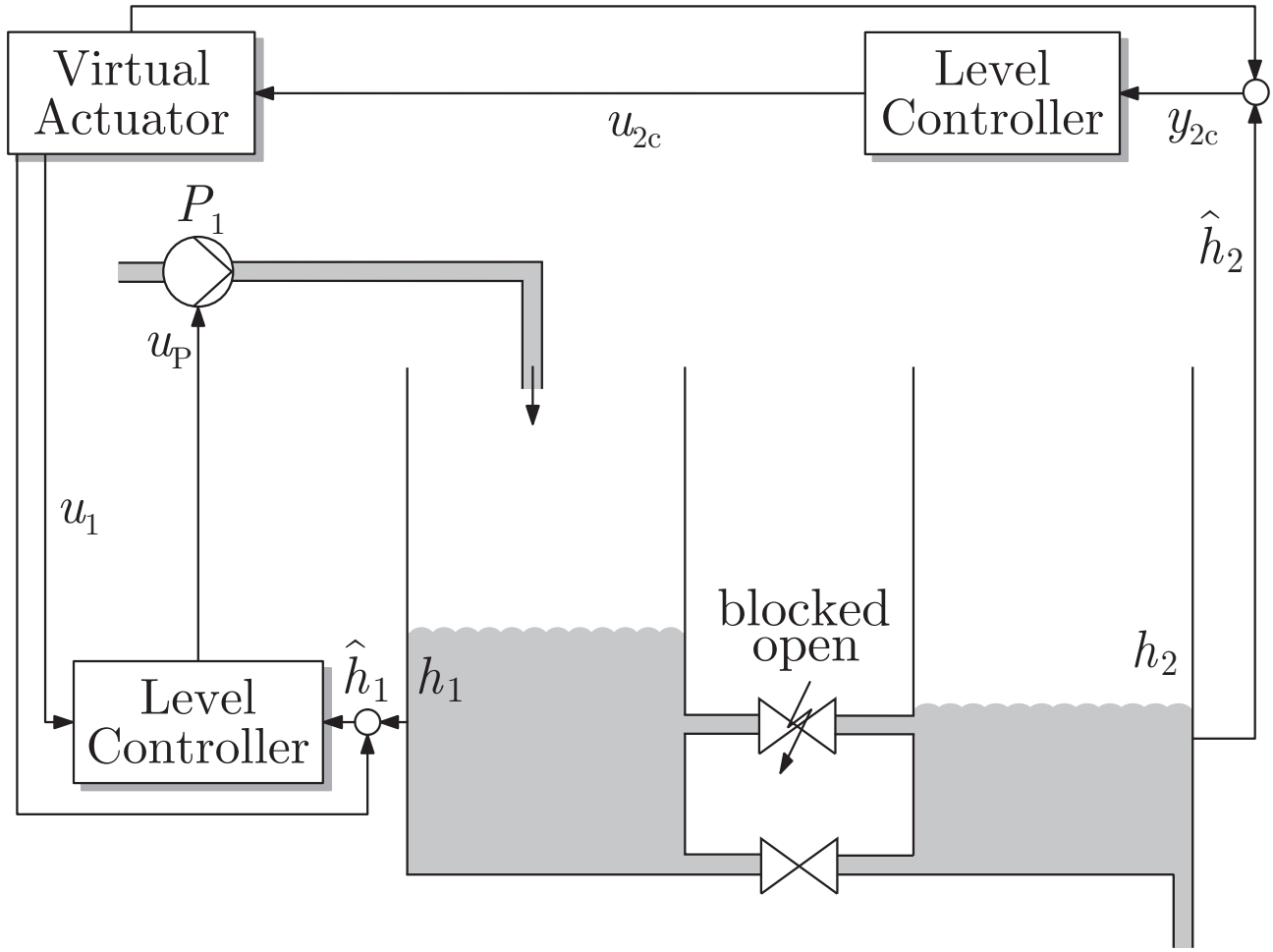

Fig. 9.16. Reconfigured system with virtual actuator

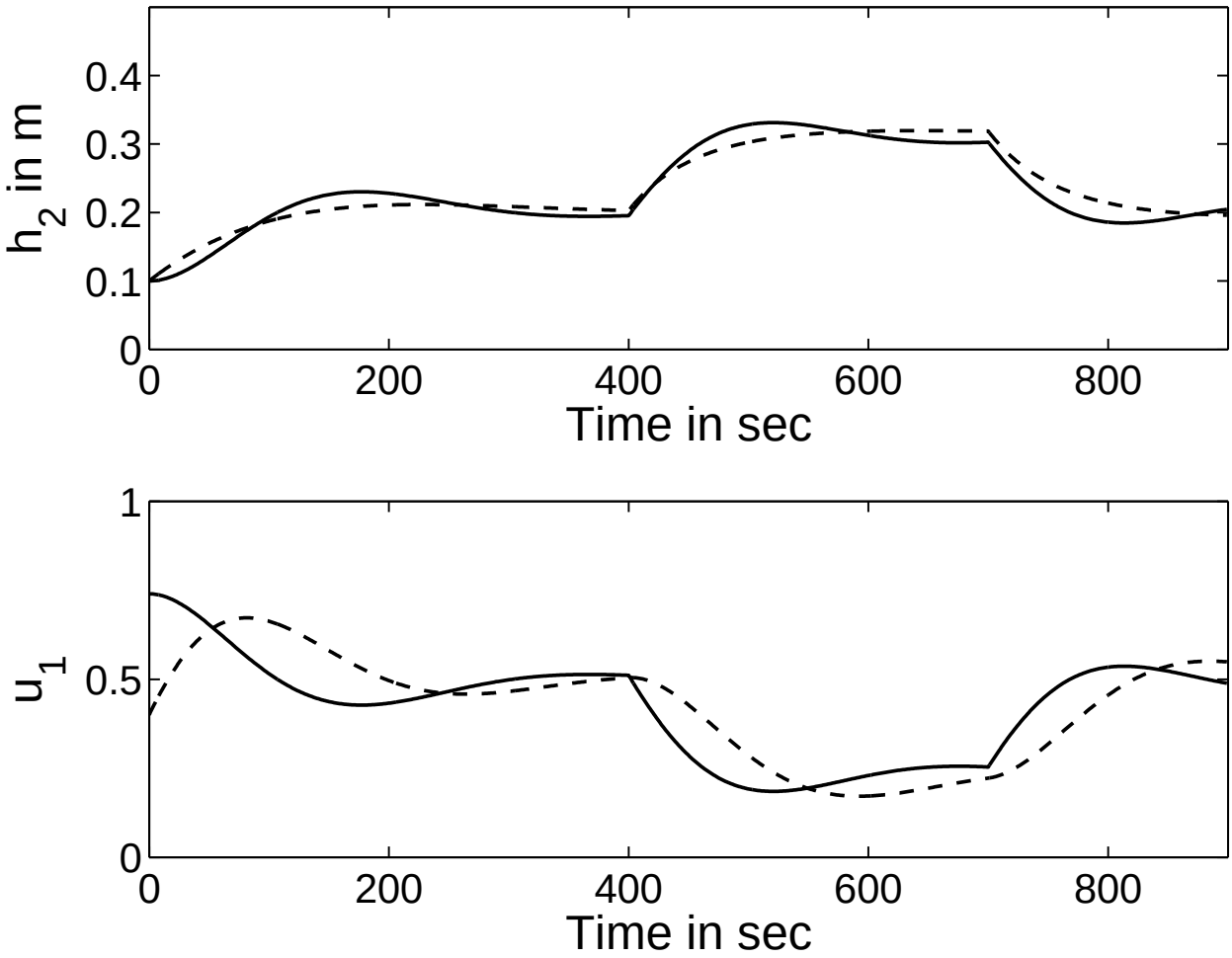

Fig. 9.17. Behaviour of the reconfigured closed-loop system where the reconfigured controller uses the input u_1

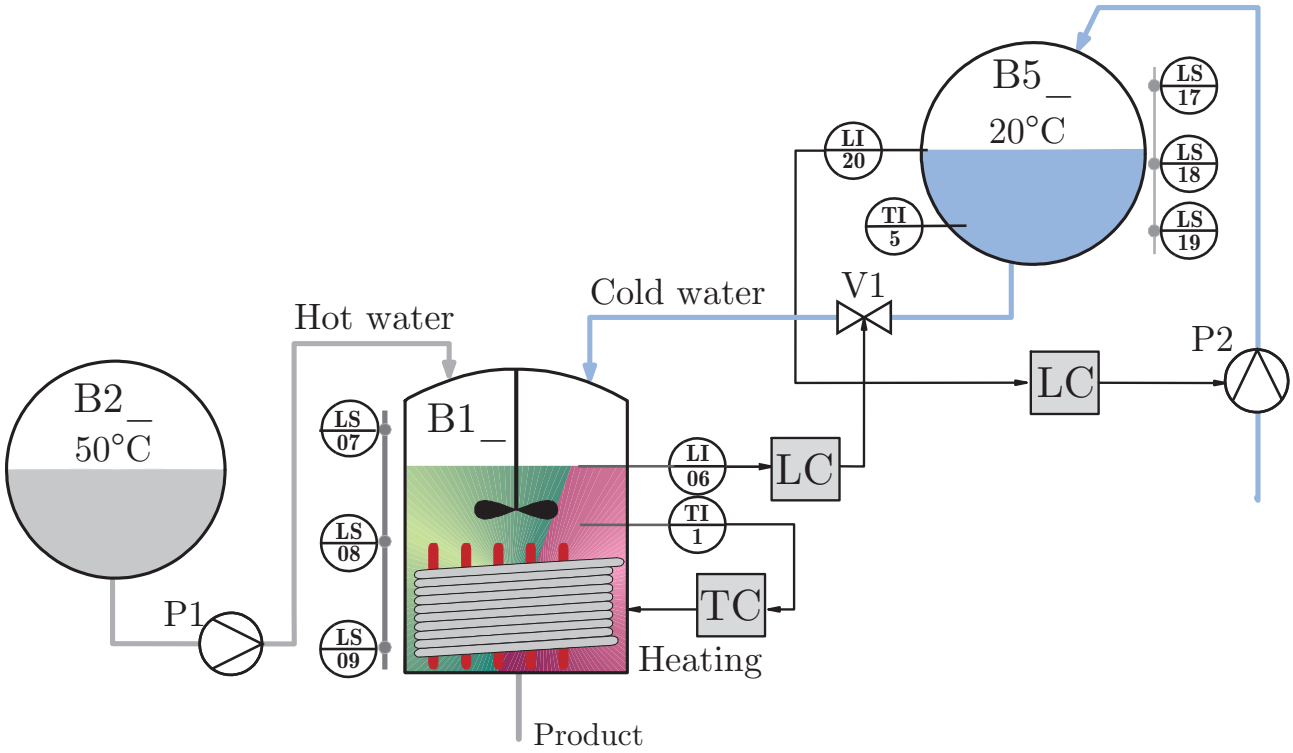

Fig. 9.18. Plant used for control reconfiguration (LC - level control, TC - temperature control)

Blanke/Kinnaert/Lunze/Staroswiecki:
Diagnosis and Fault-Tolerant Control, (3rd edition), Springer-Verlag 2015

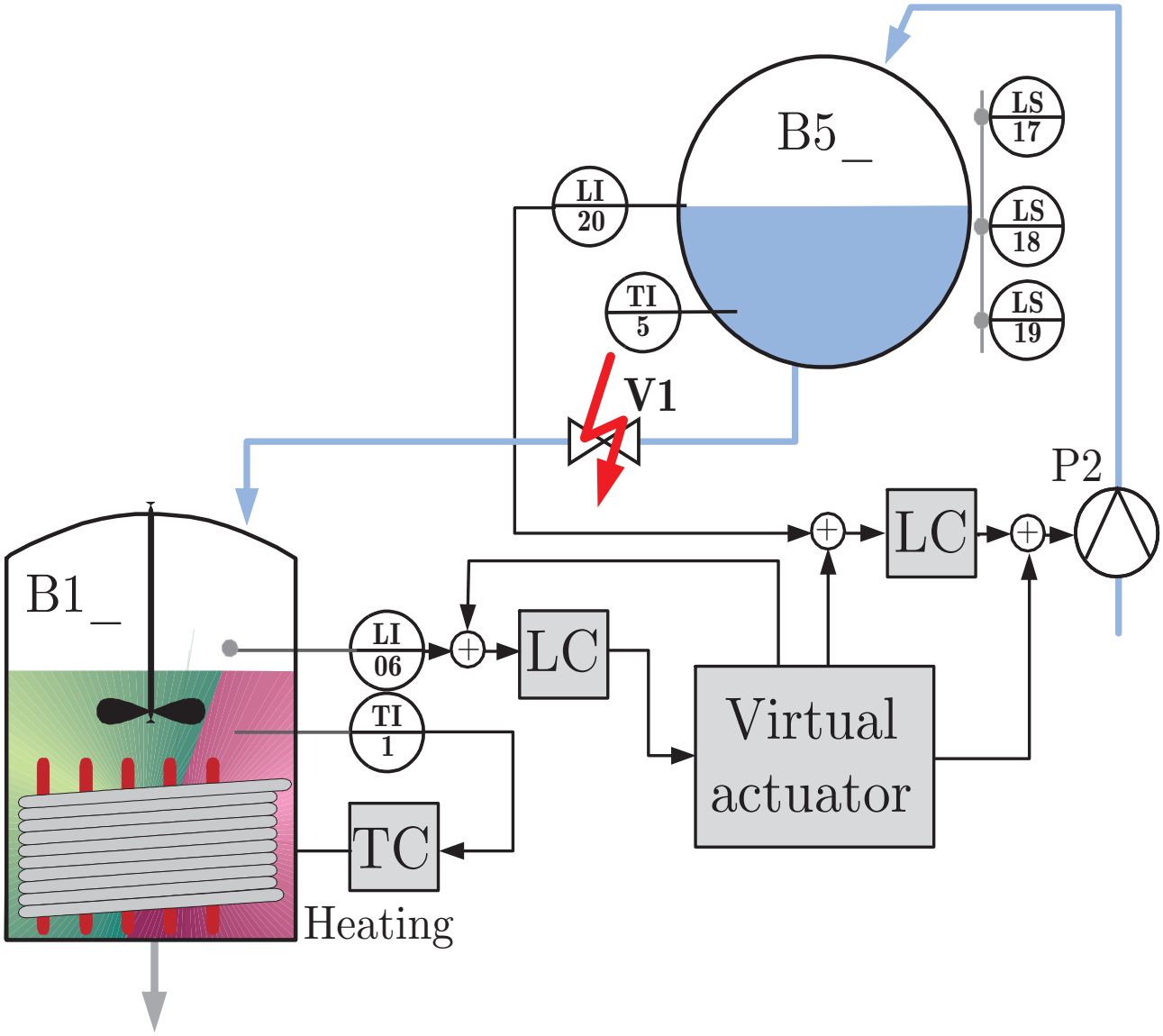

Fig. 9.19. Reconfigured controller including a virtual actuator

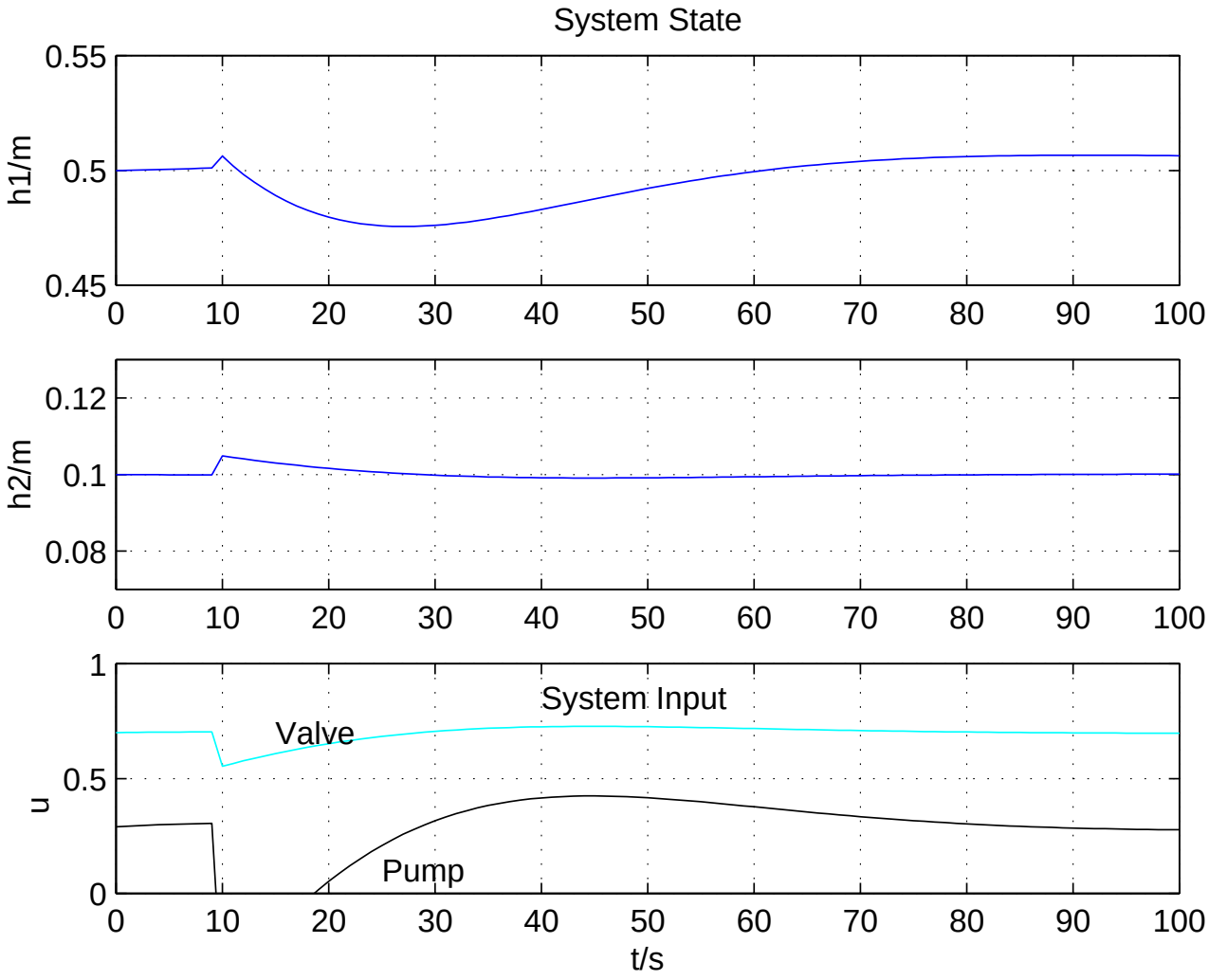

Fig. 9.20. Results of the reconfiguration experiment (Reactor temperature $\vartheta_{\mathrm{B1}}(t)$ (top), reactor content $V_{\mathrm{B1}}(t)$ (middle) and reactor content $V_{\mathrm{B5}}(t)$

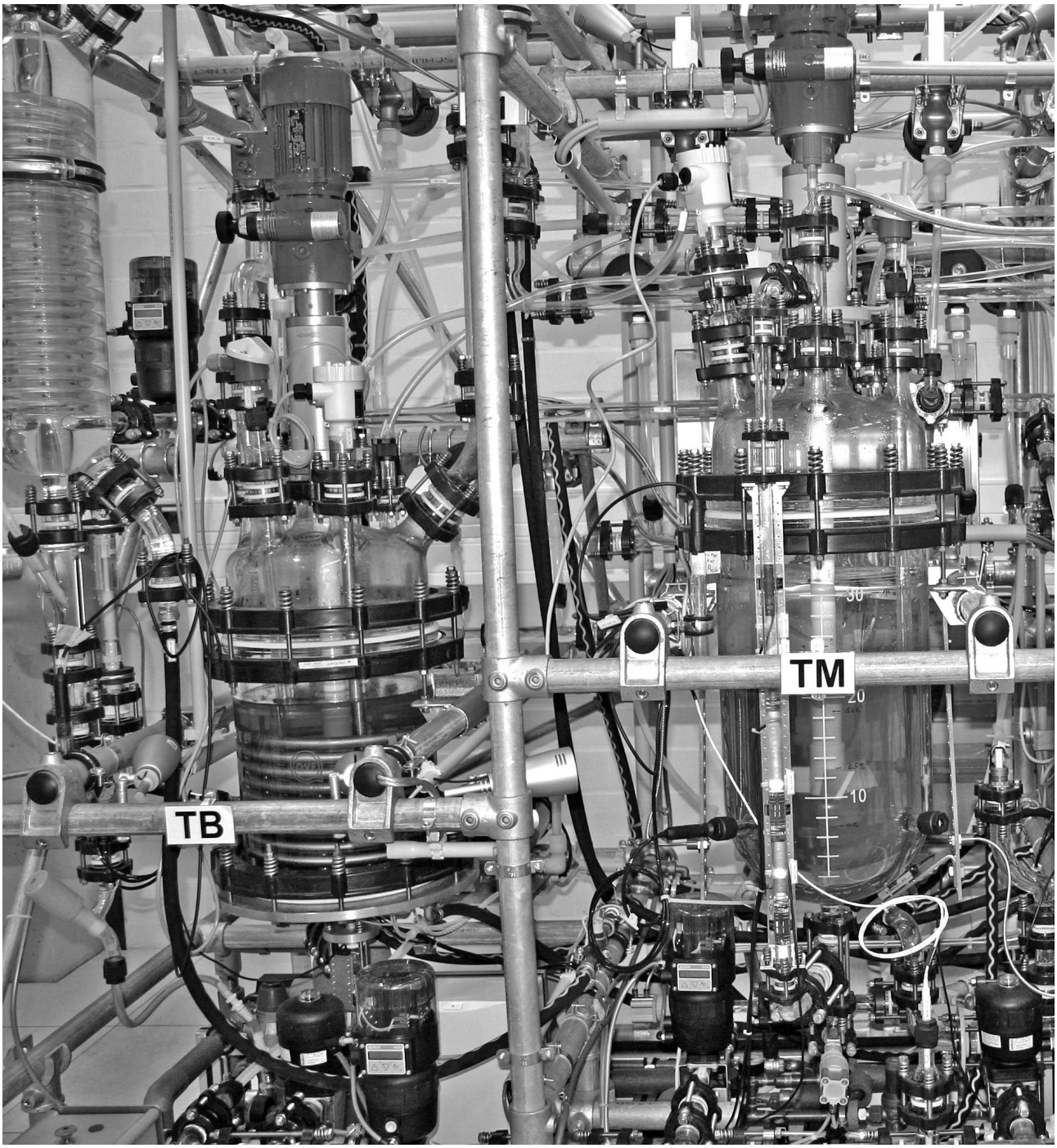

Fig. 9.21. Part of the chemical plant VERA used in the experiment

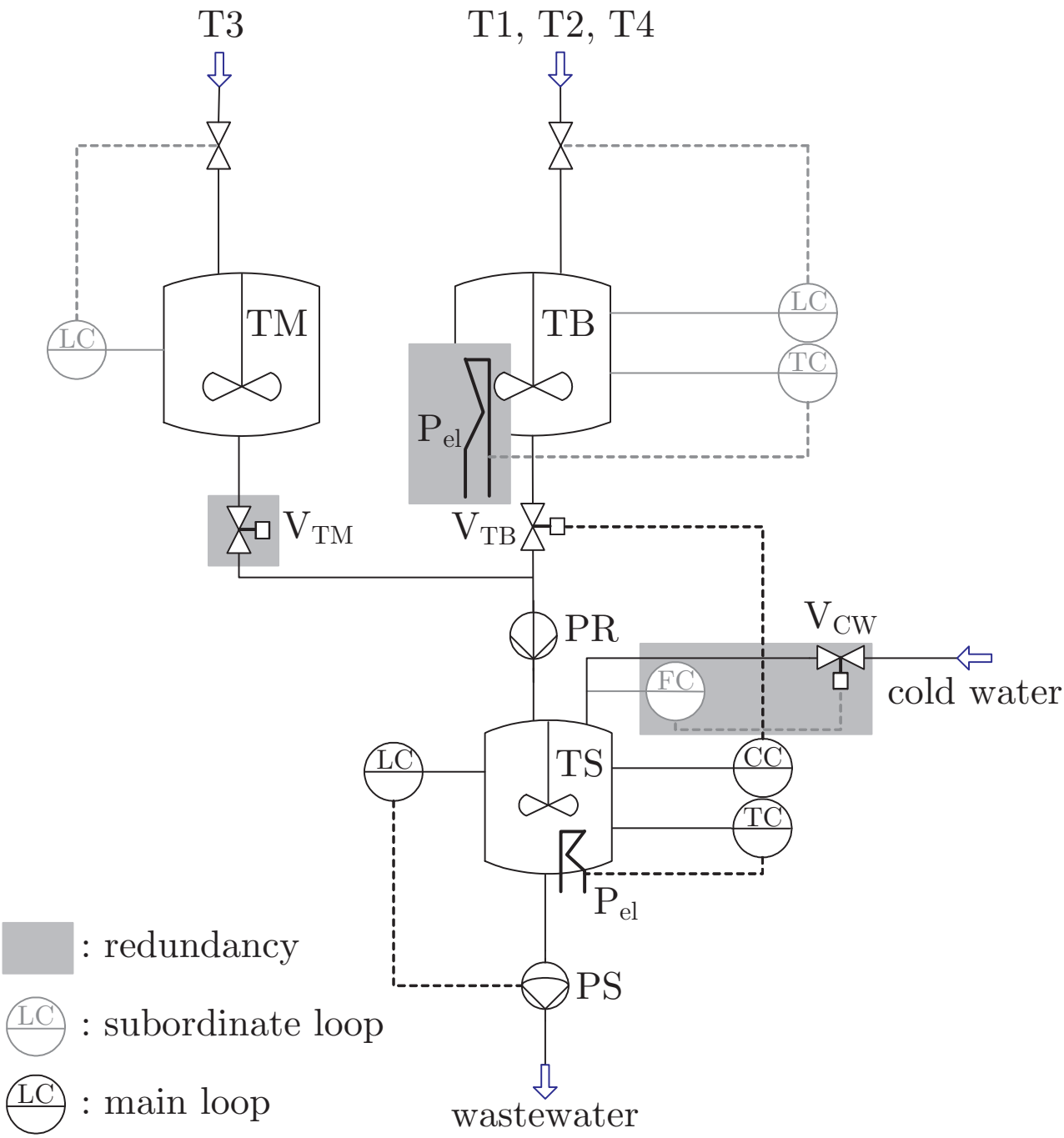

Fig. 9.22. Schematic diagram of the process

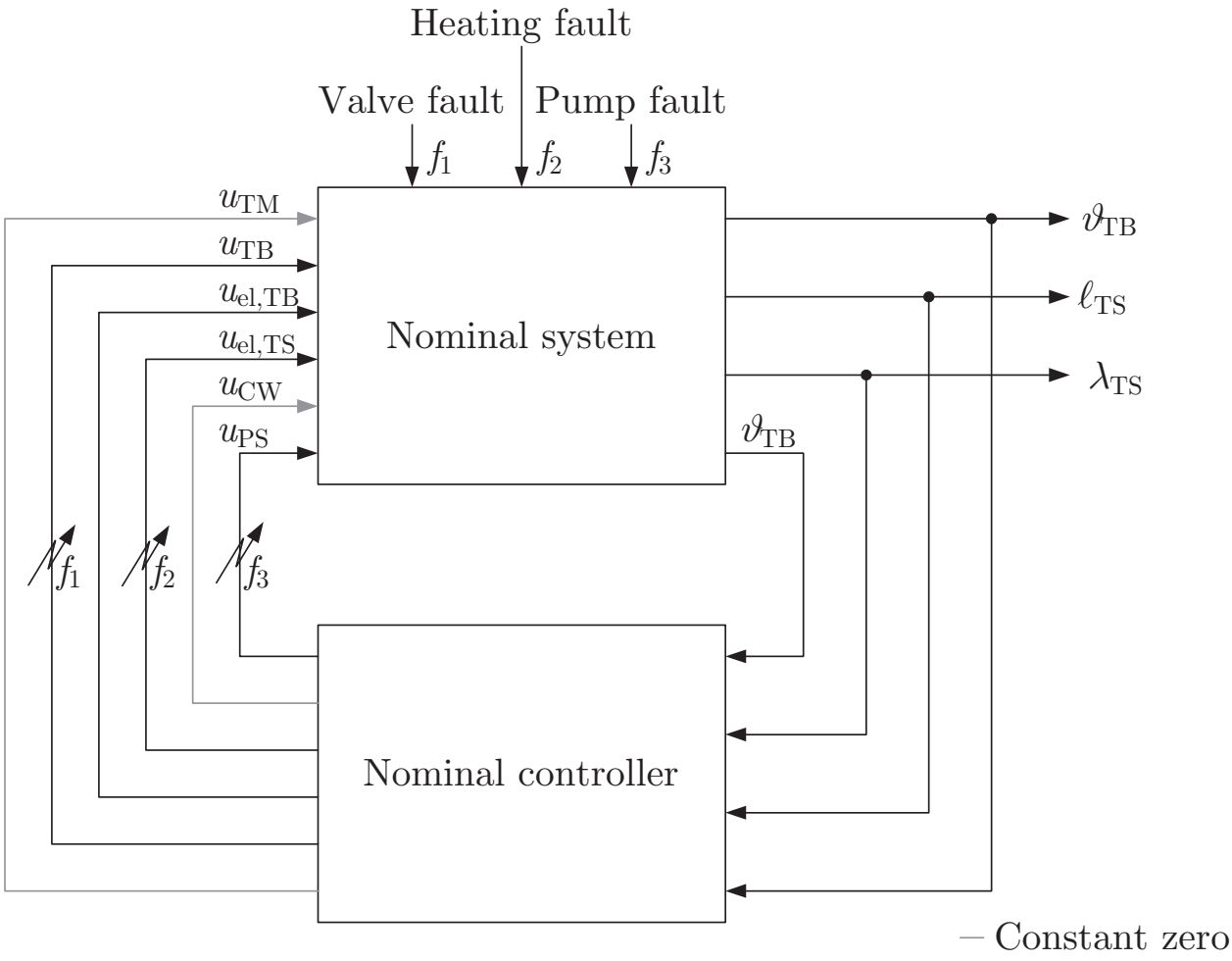

Fig. 9.23. Schematic diagram of the process

Blanke/Kinnaert/Lunze/Staroswiecki:
Diagnosis and Fault-Tolerant Control, (3rd edition), Springer-Verlag 2015

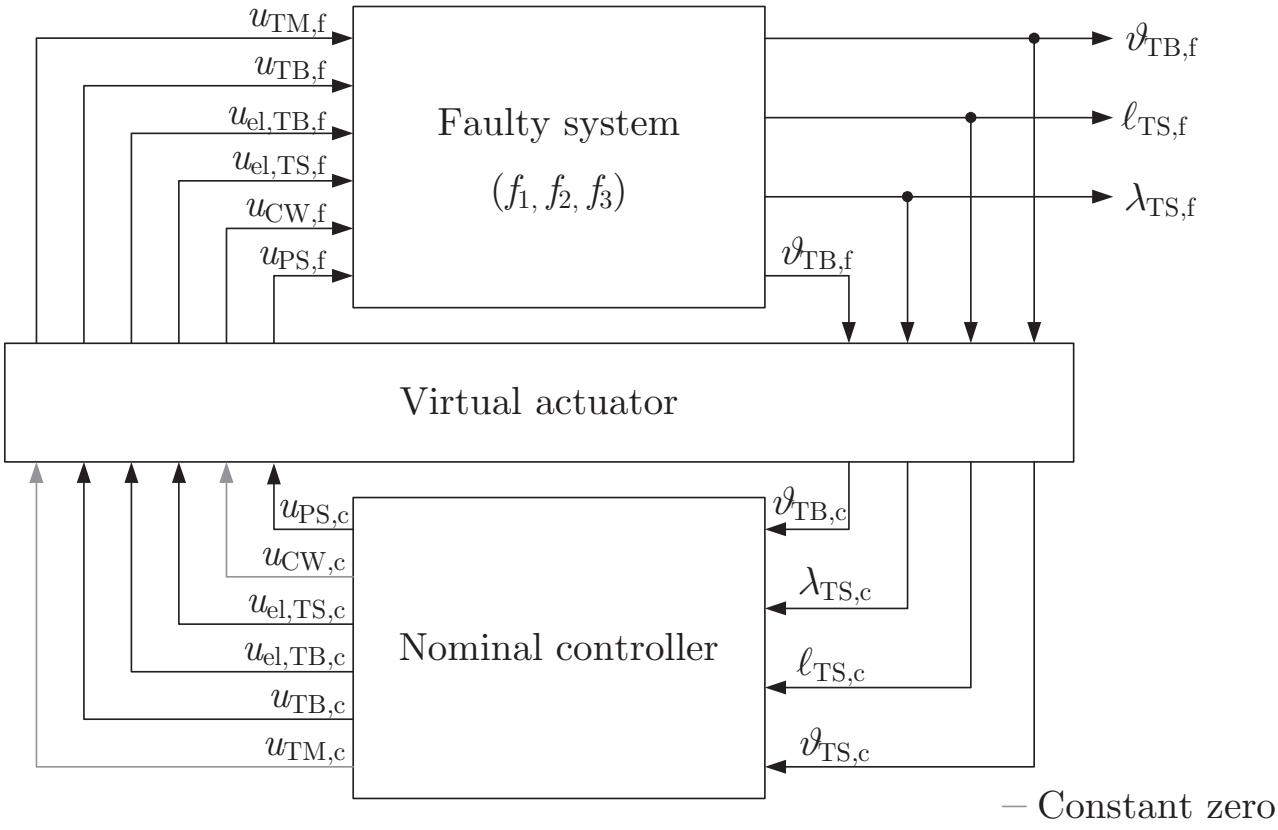

Fig. 9.24. Reconfiguration by means of a virtual actuator

Blanke/Kinnaert/Lunze/Staroswiecki:
Diagnosis and Fault-Tolerant Control, (3rd edition), Springer-Verlag 2015

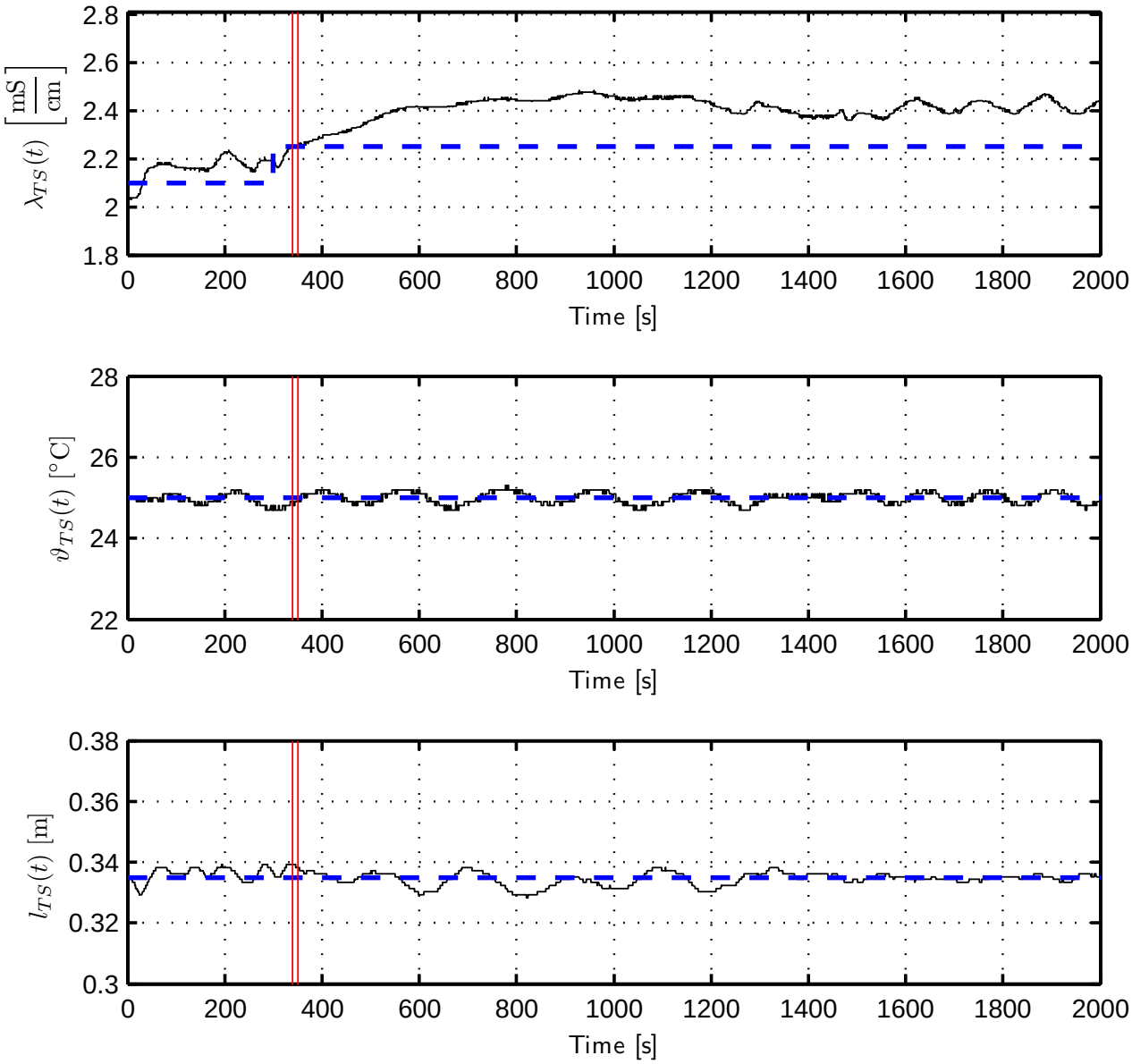

Fig. 9.25. Reconfiguration in case of the valve failure

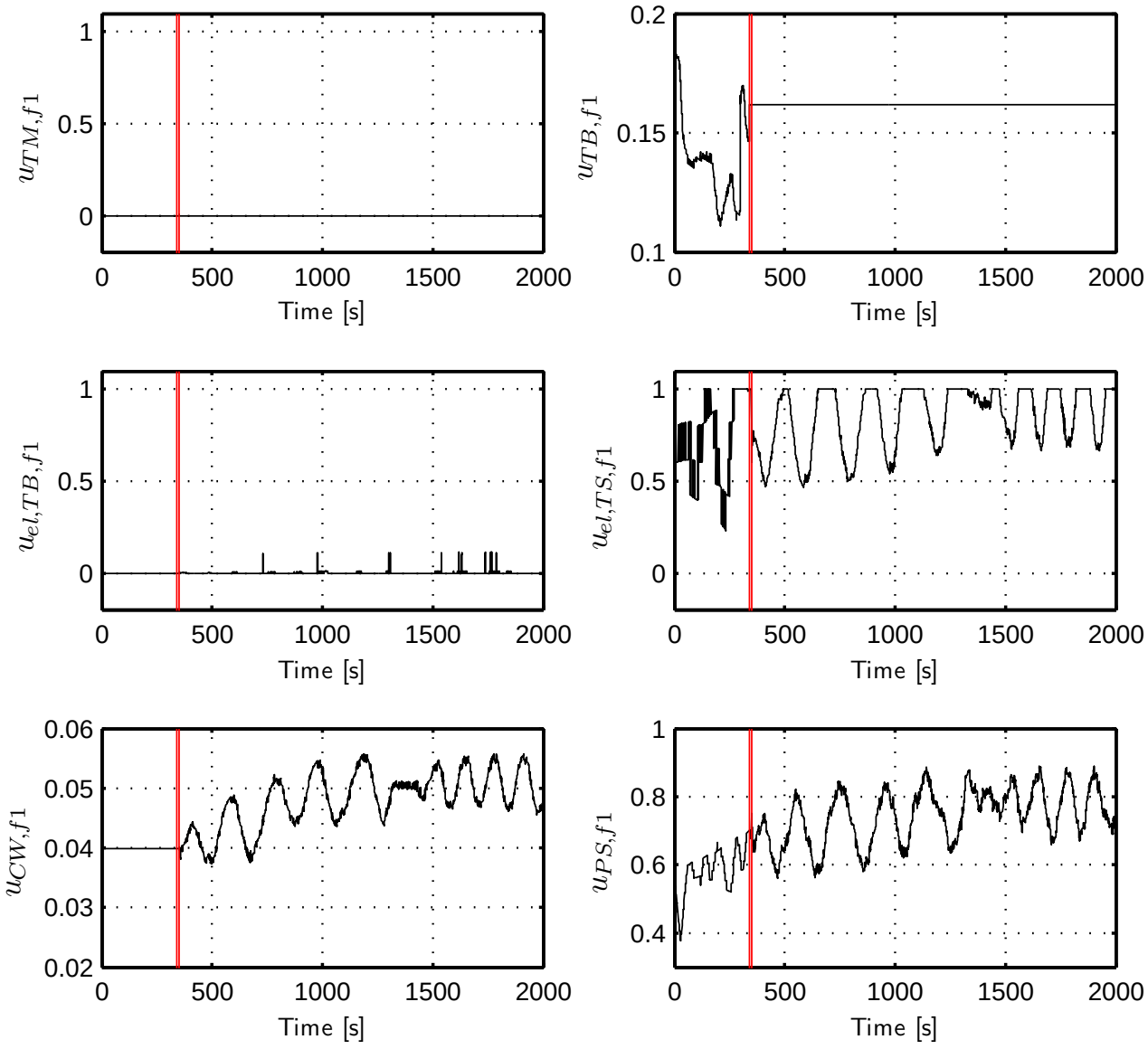

Fig. 9.26. Absolute values of the control inputs after the reconfiguration in case of the valve V_{TB}-failure

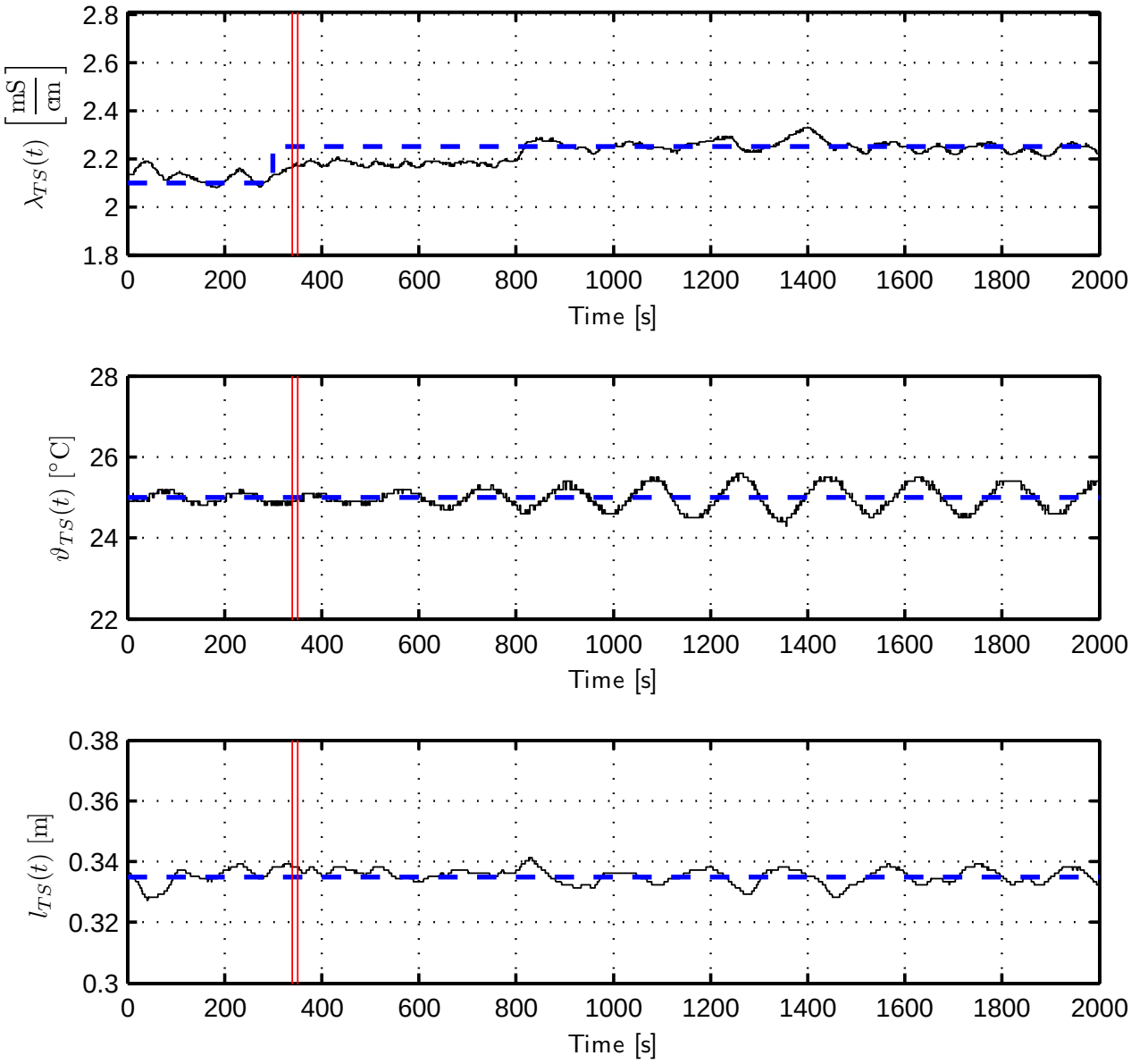

Fig. 9.27. Reconfiguration after valve V_{TB}-failure

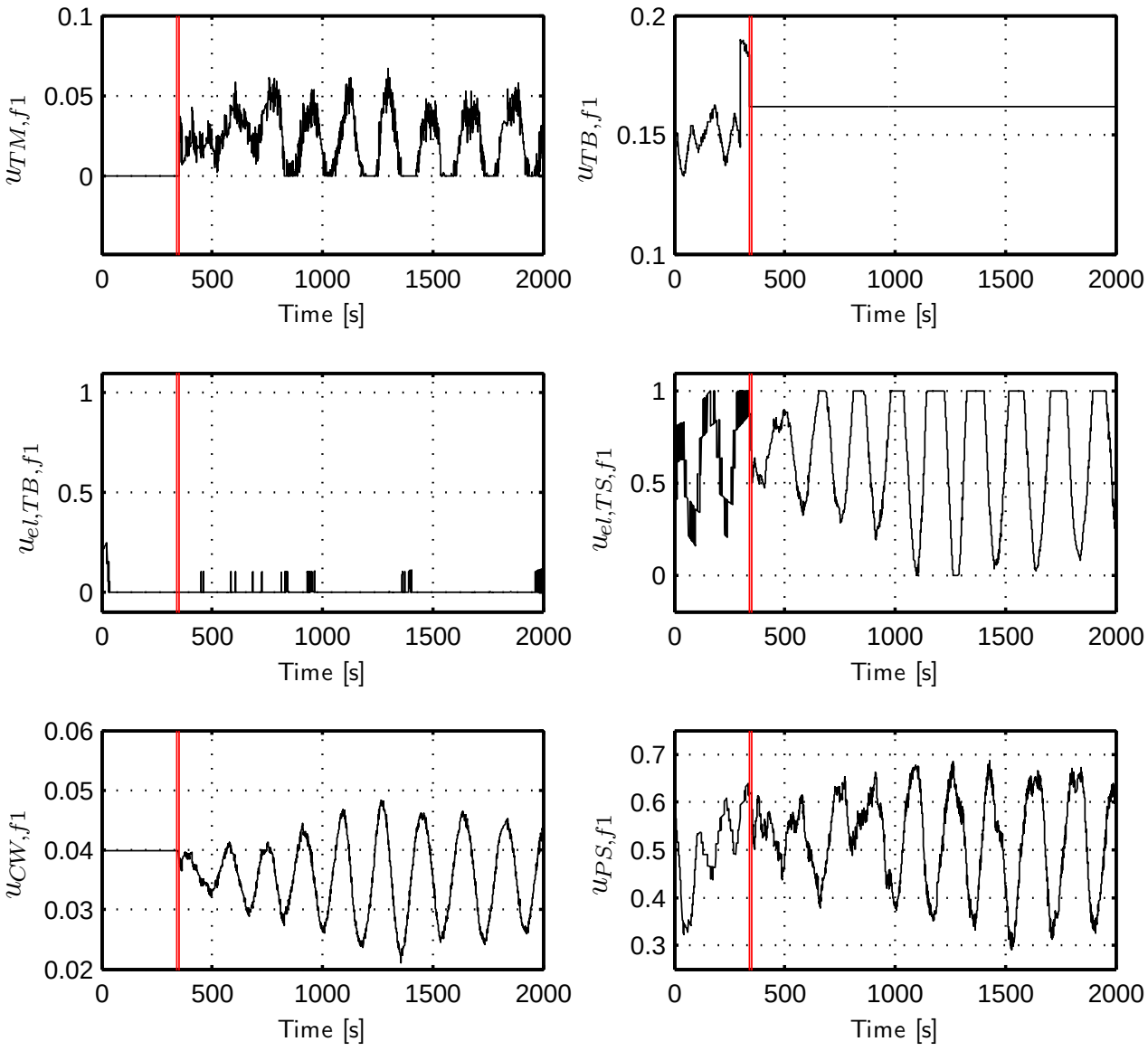

Fig. 9.28. Control input after the reconfiguration for valve V_{TM}-failure

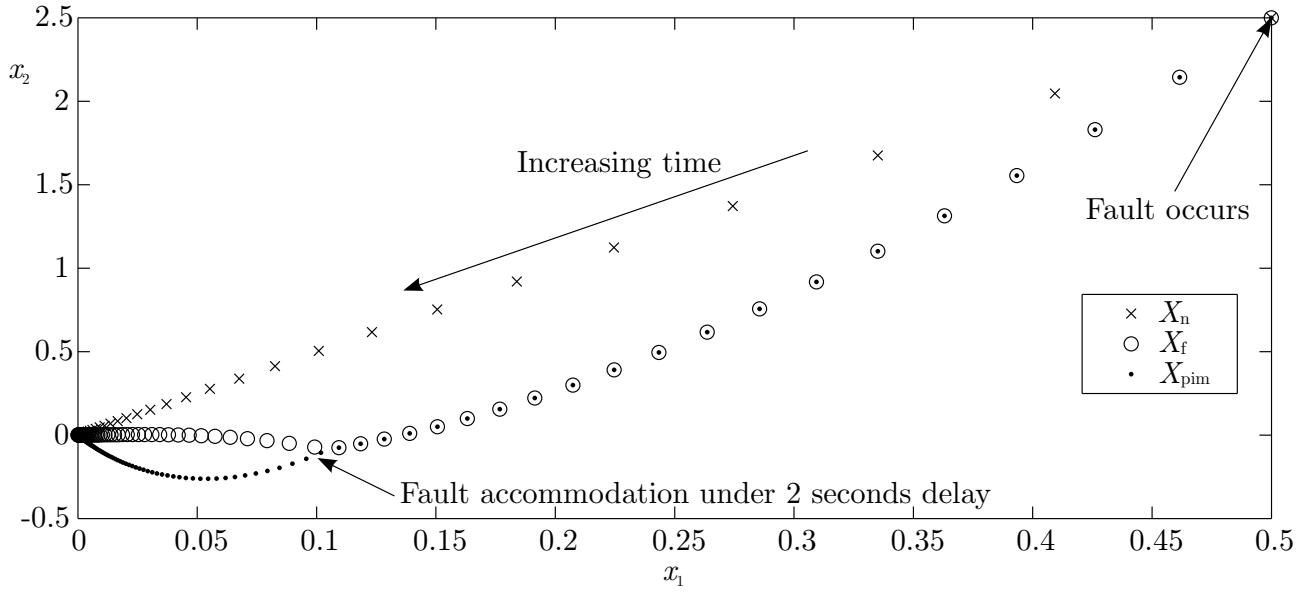

Fig. 9.29. Nominal, PIM and NTT state trajectories

Blanke/Kinnaert/Lunze/Staroswiecki:
Diagnosis and Fault-Tolerant Control, (3rd edition), Springer-Verlag 2015

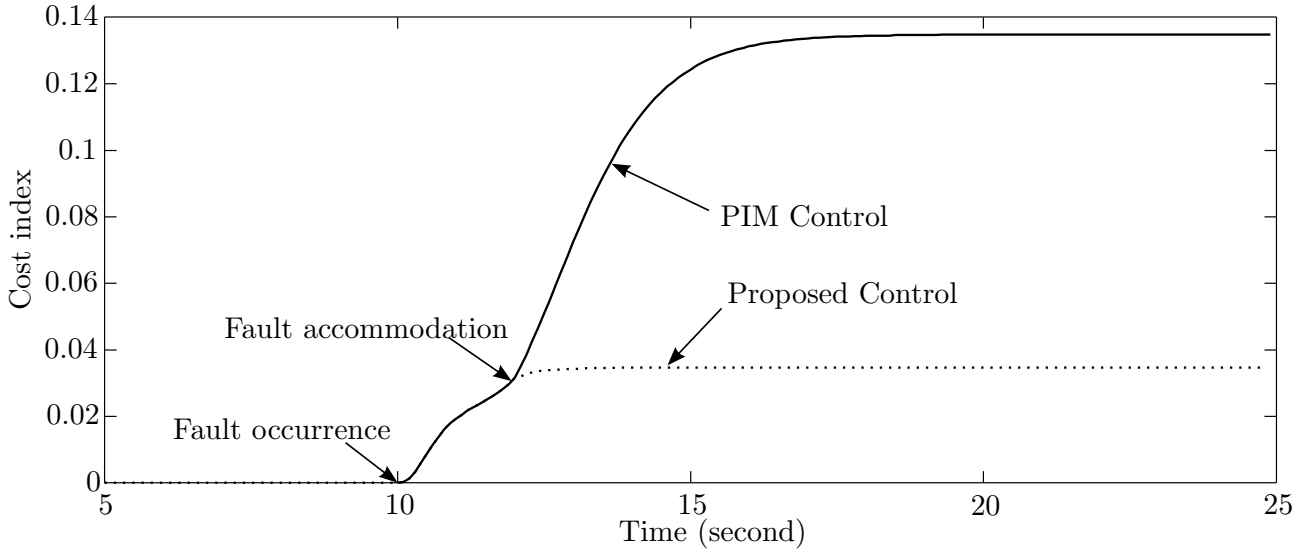

Fig. 9.30. PIM versus NTT costs

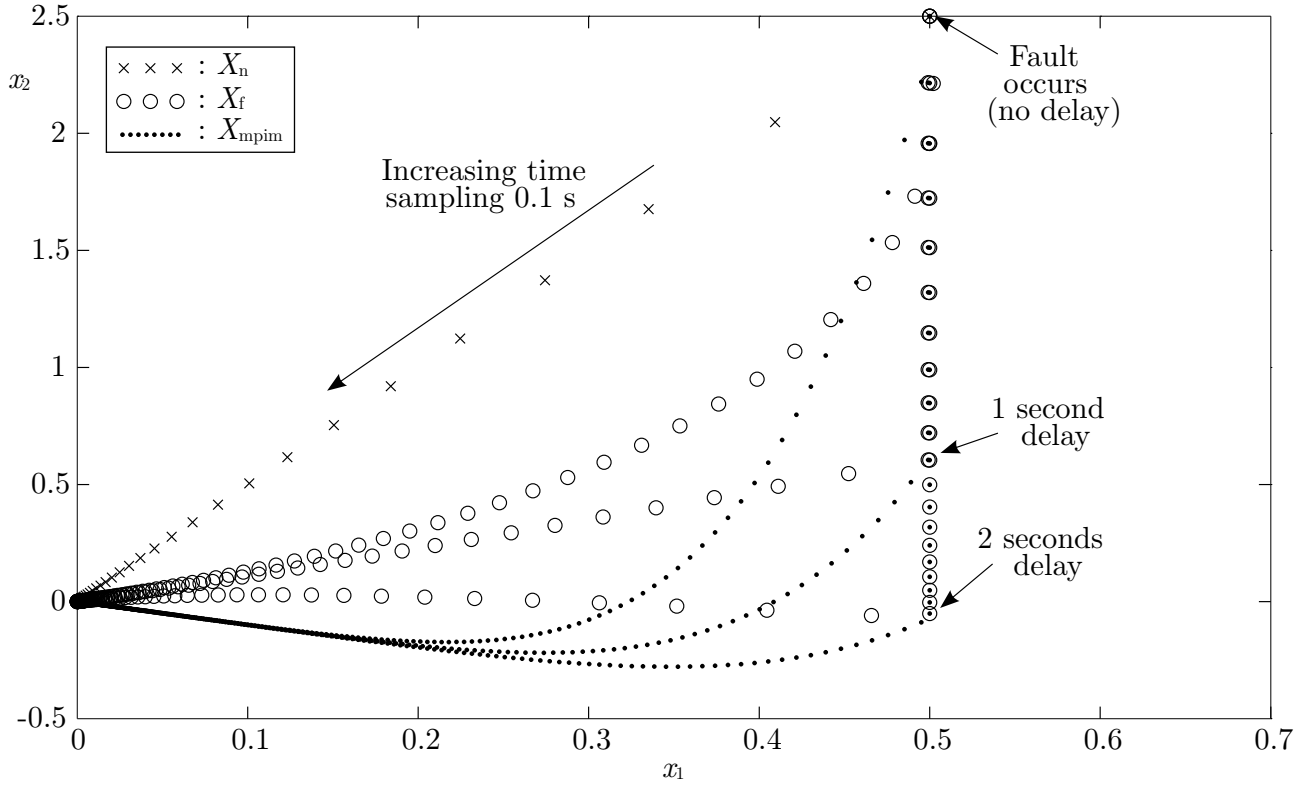

Fig. 9.31. Nominal, MPIM and NTT state trajectories

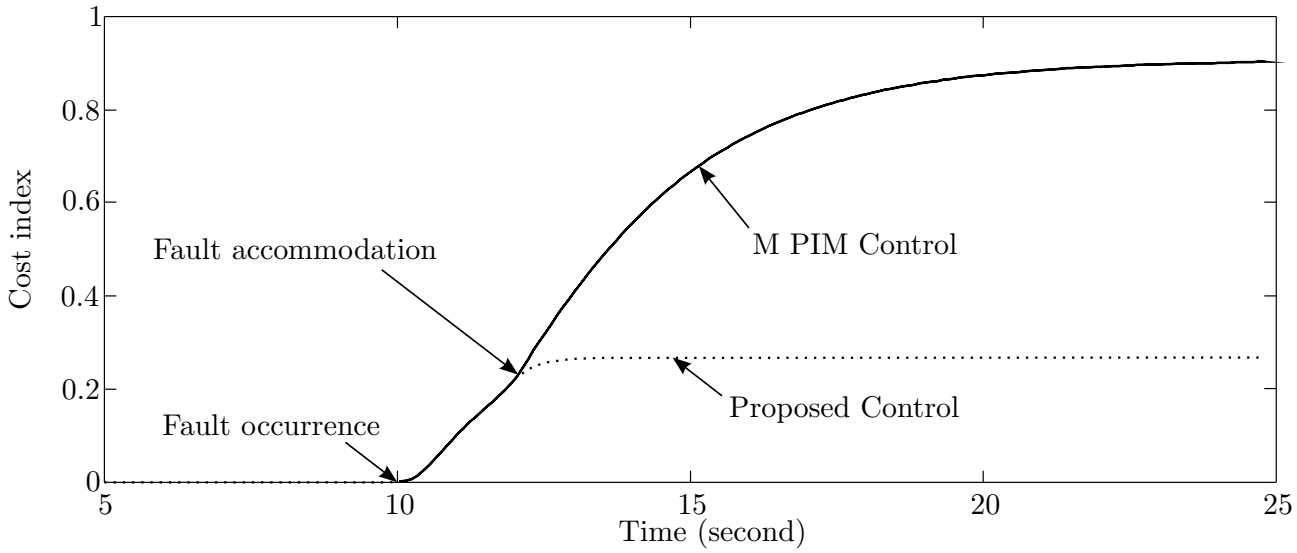

Fig. 9.32. MPIM vs NTT costs

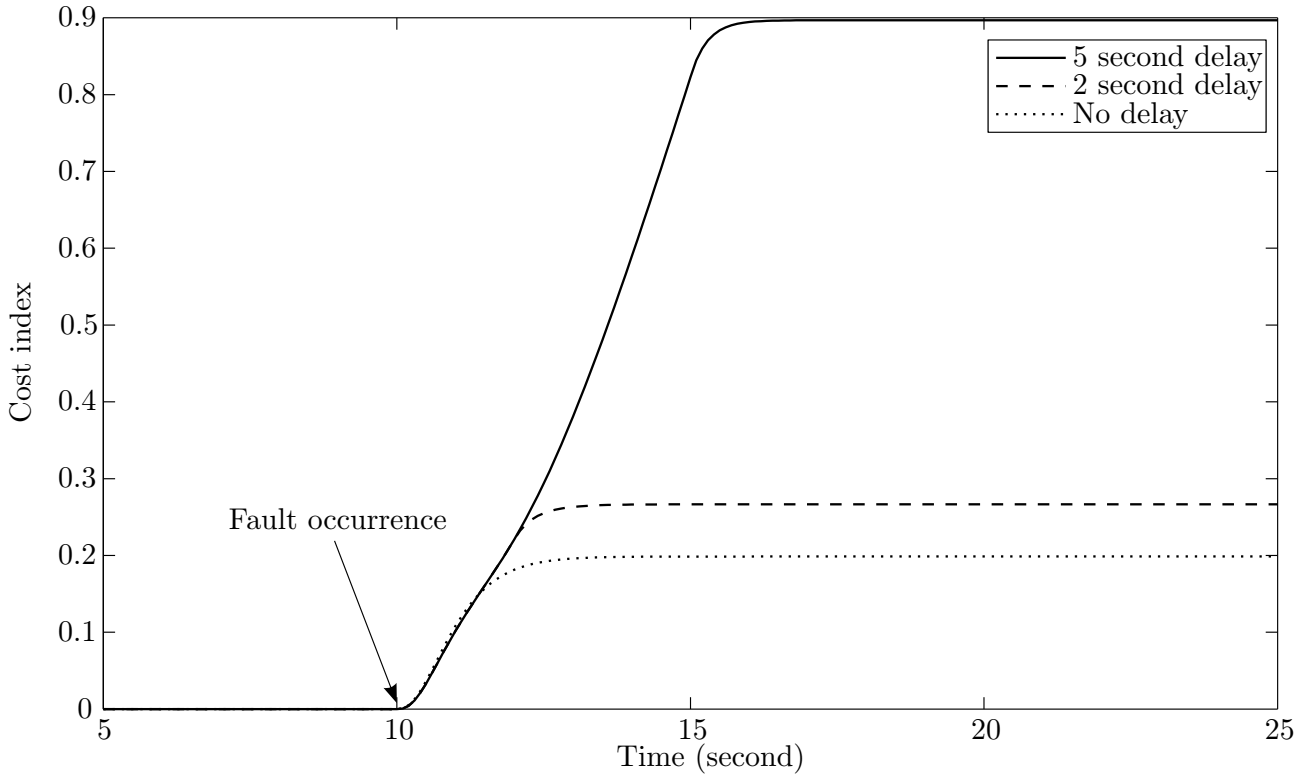

Fig. 9.33. Trajectory tracking cost vs fault accommodation delay

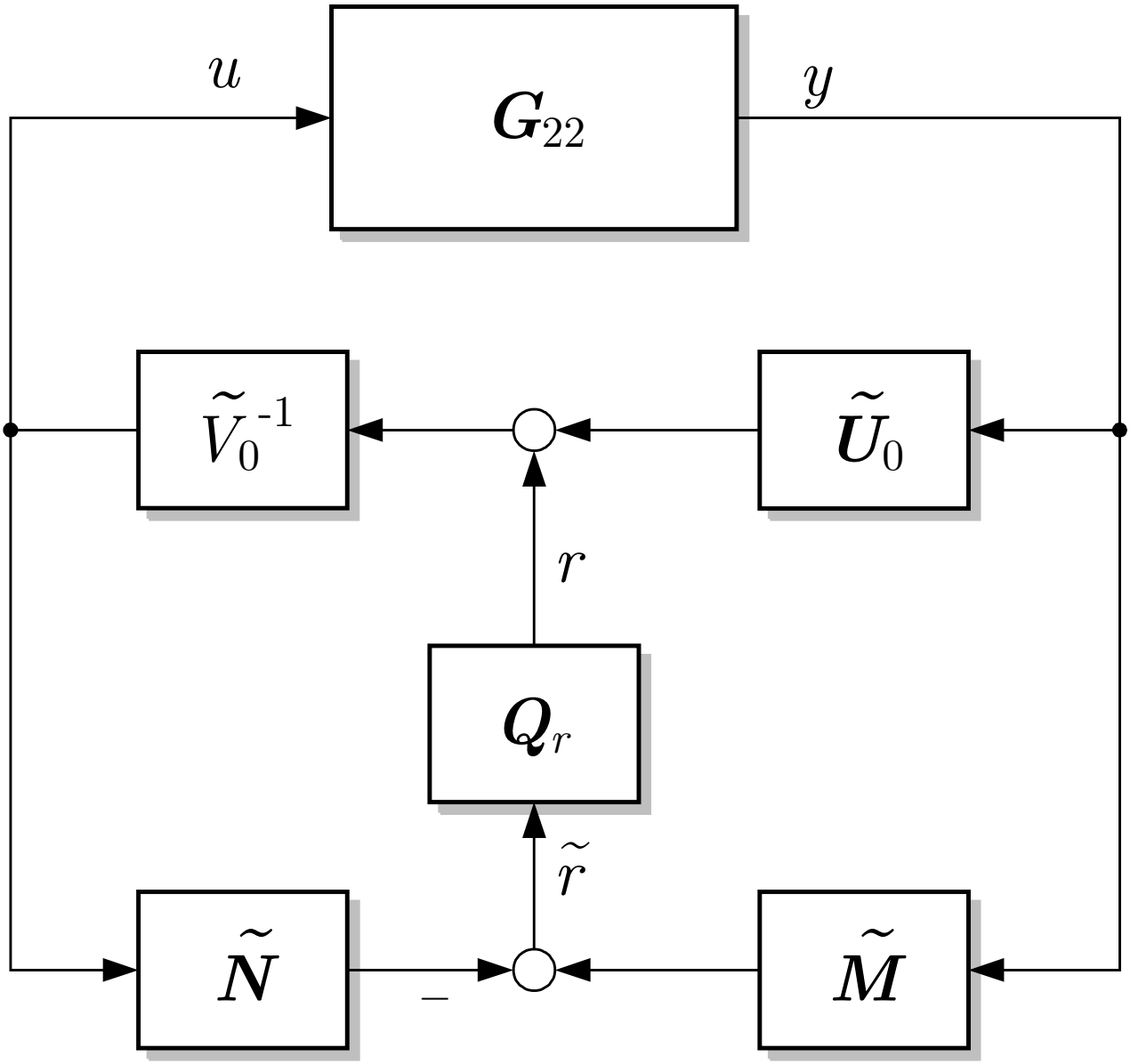

Fig. 9.34. Controller structure for the Youla-Kucera parametrisation

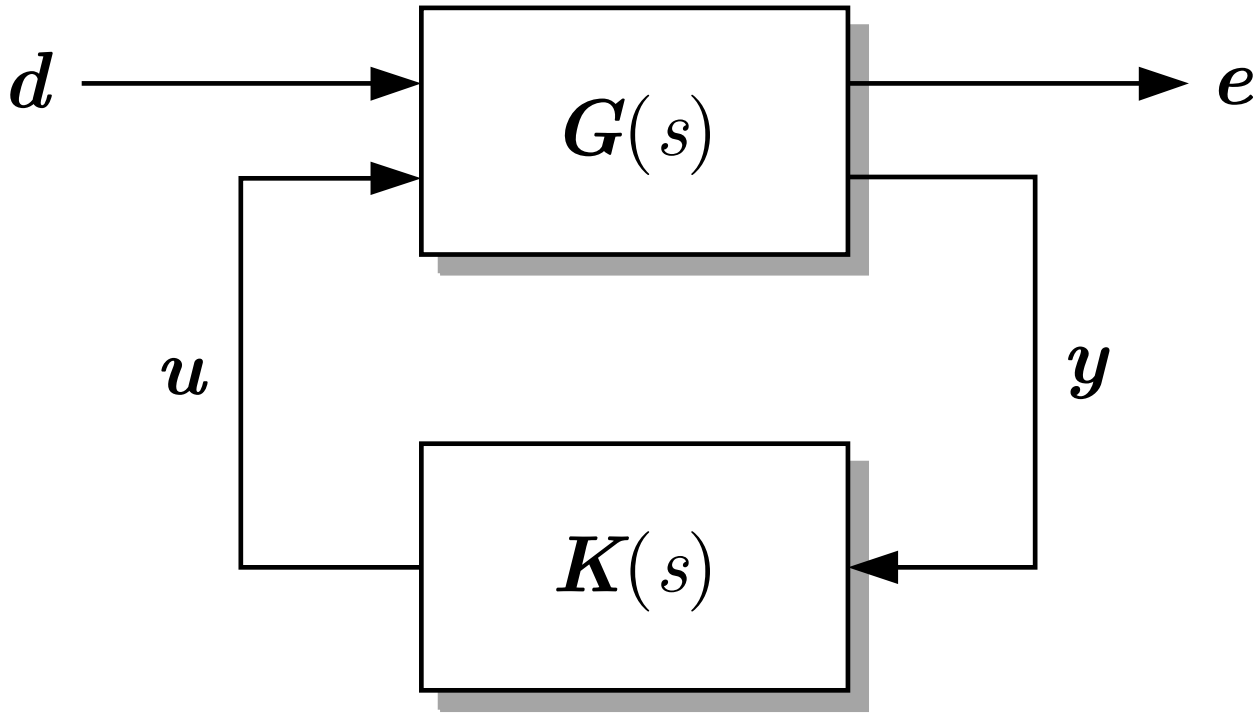

Fig. 9.35. Control system in standard configuration

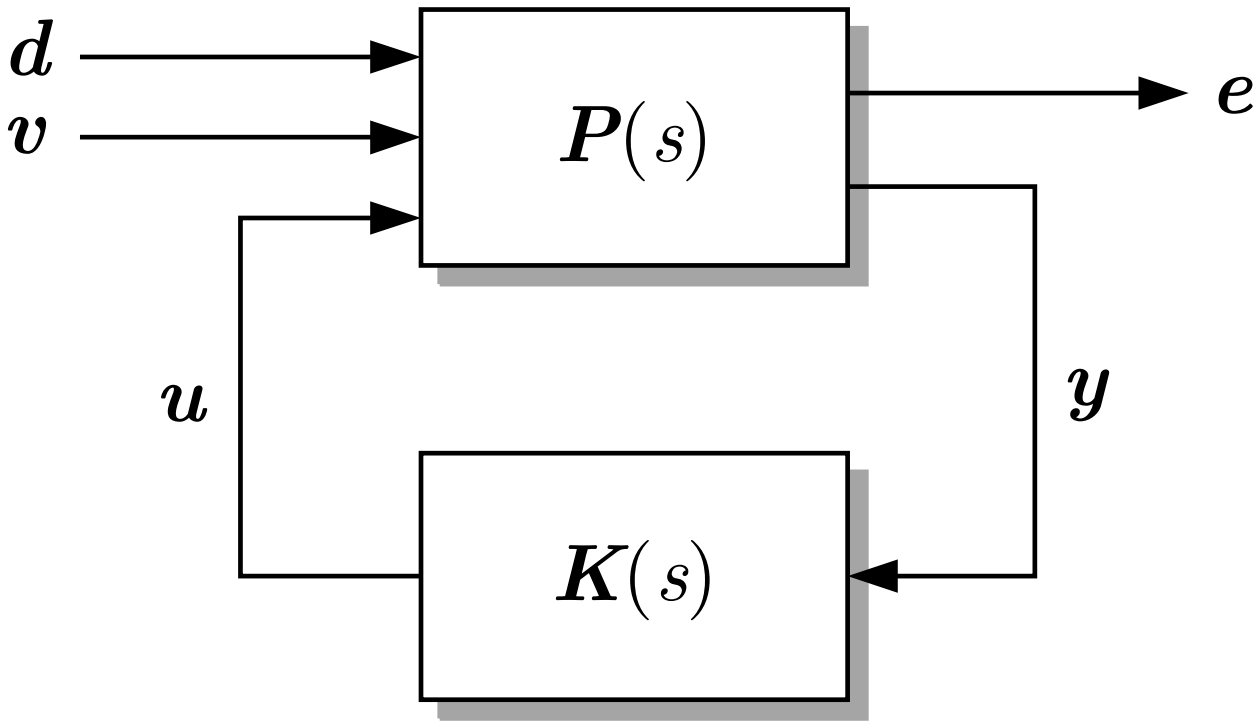

Fig. 9.35. Control system in generalised setup for fault-tolerant control

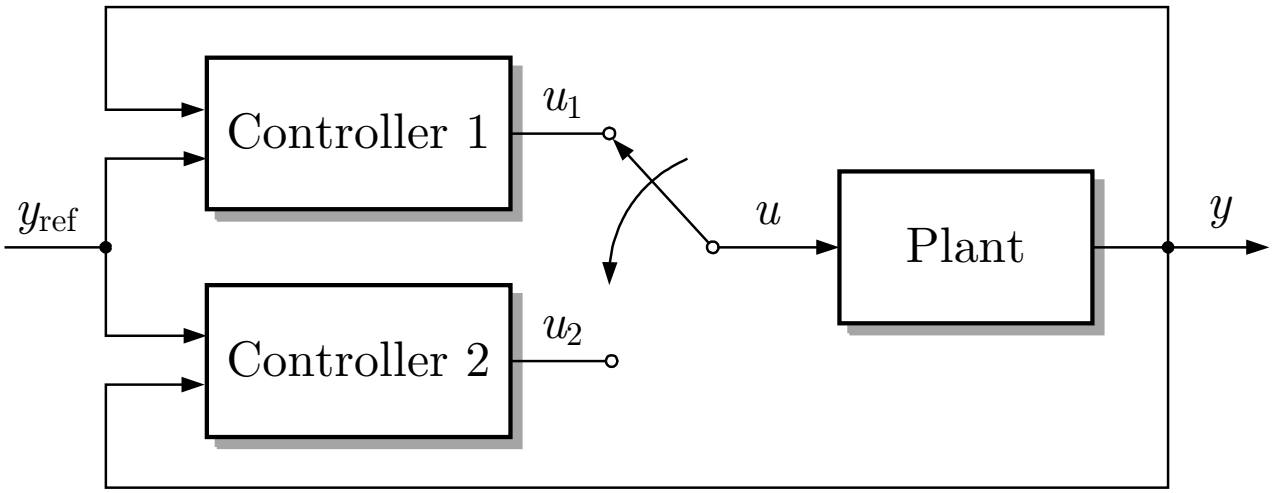

Fig. 9.36. Two-controller scheme

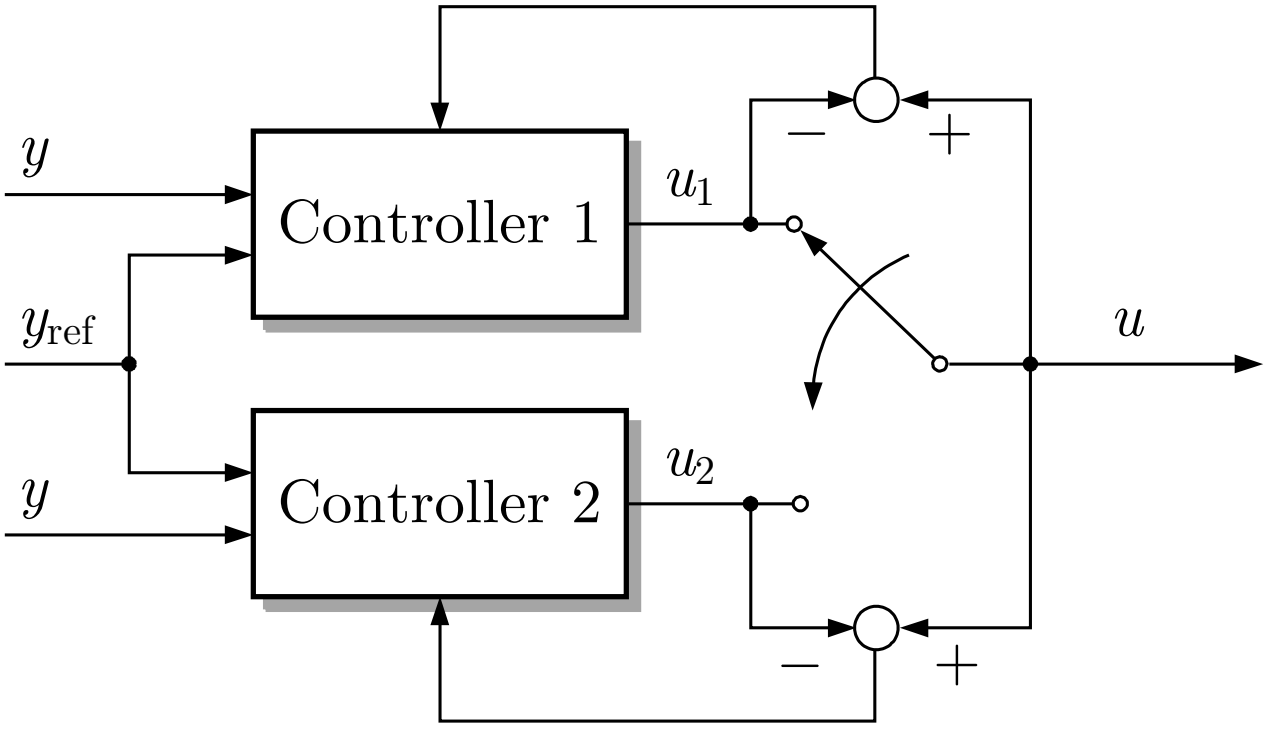

Fig. 9.37. Two-controller scheme with anti-windup mechanism

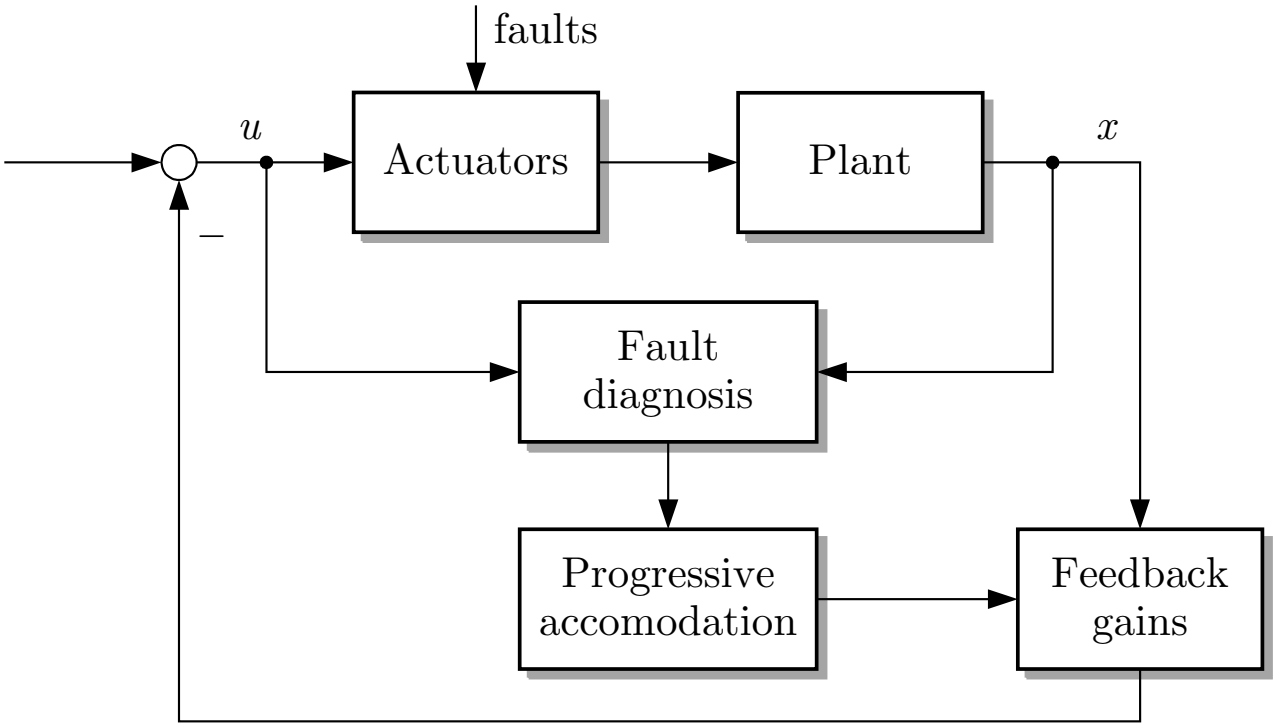

Fig. 9.38. Progressive Accommodation scheme

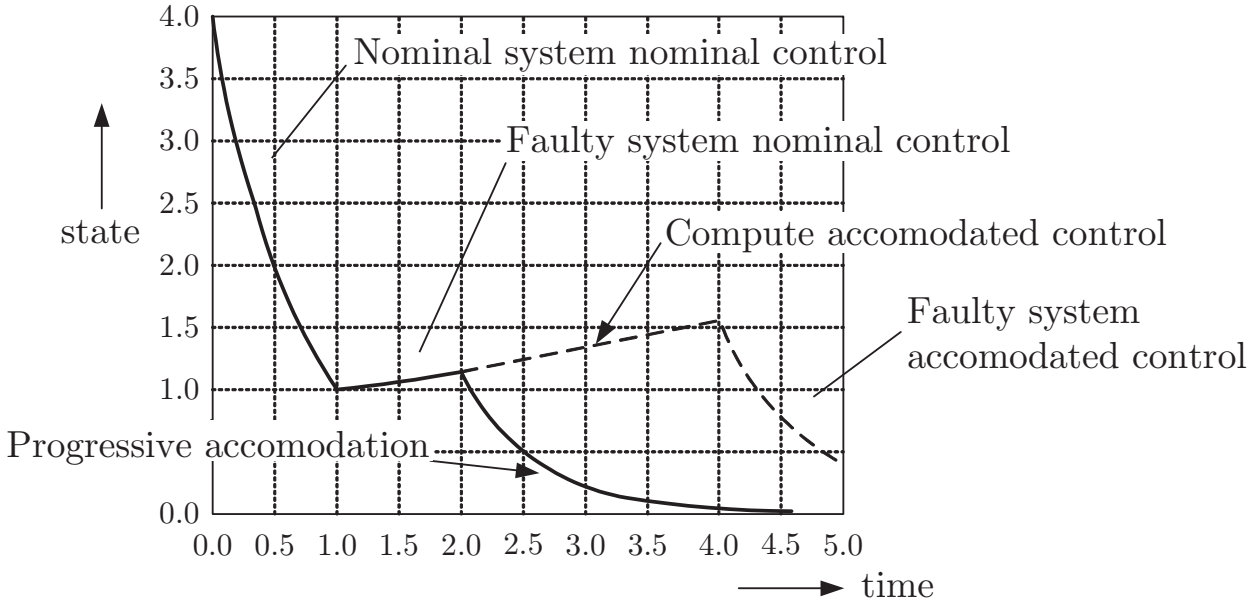

Fig. 9.39. Comparison of the classical and the progressive accommodation schemes

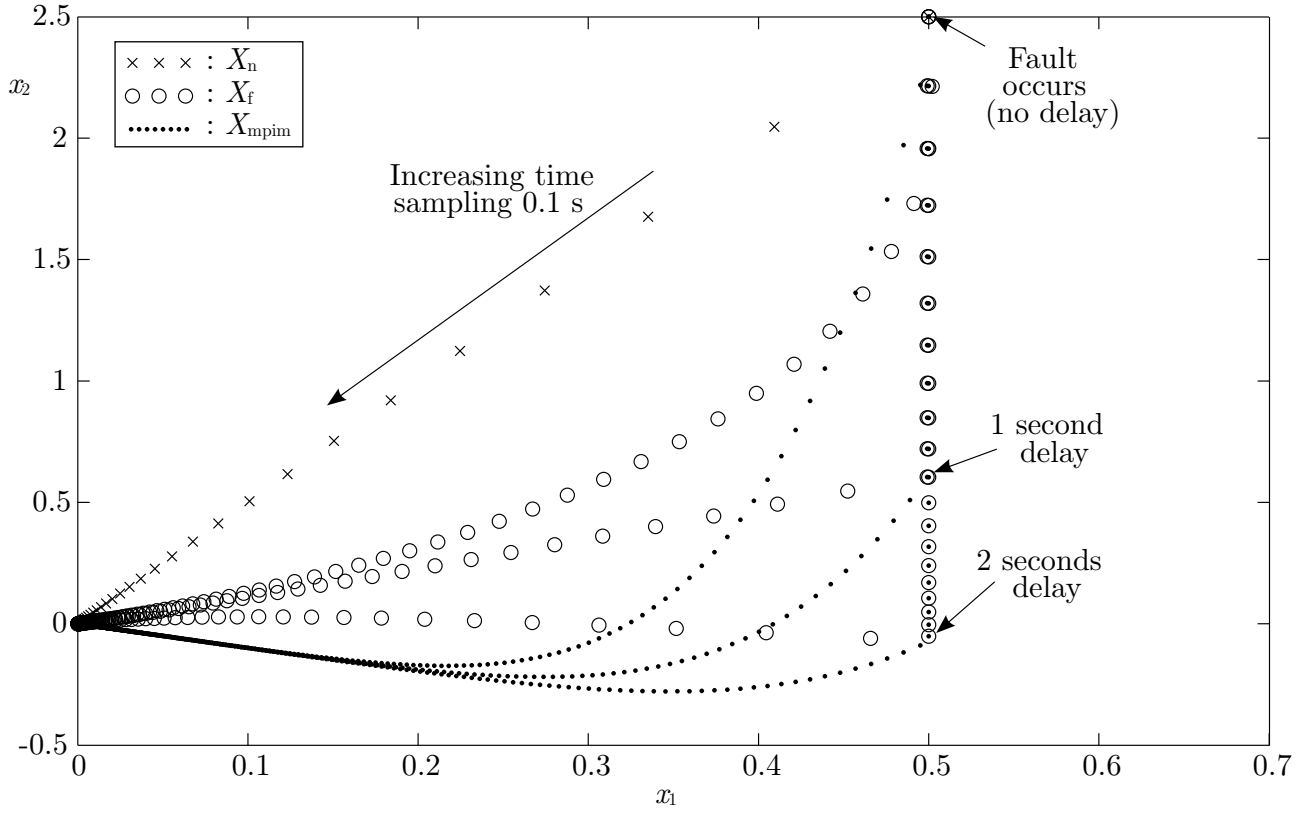

Fig. 9.40. Nominal, MPIM and NTT state trajectories

Blanke/Kinnaert/Lunze/Staroswiecki:
Diagnosis and Fault-Tolerant Control, (3rd edition), Springer-Verlag 2015

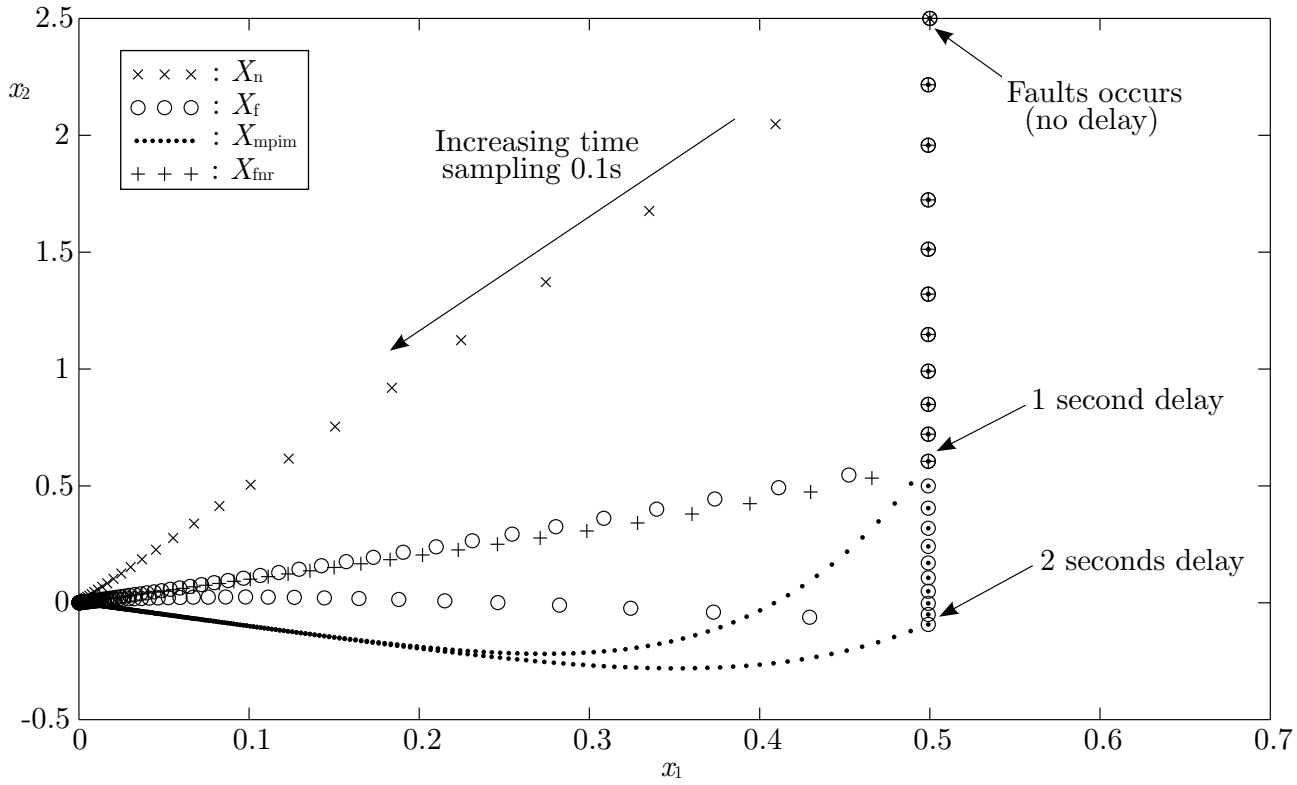

Fig. 9.41. Progressive Accommodation in the nominal trajectory tracking state trajectories

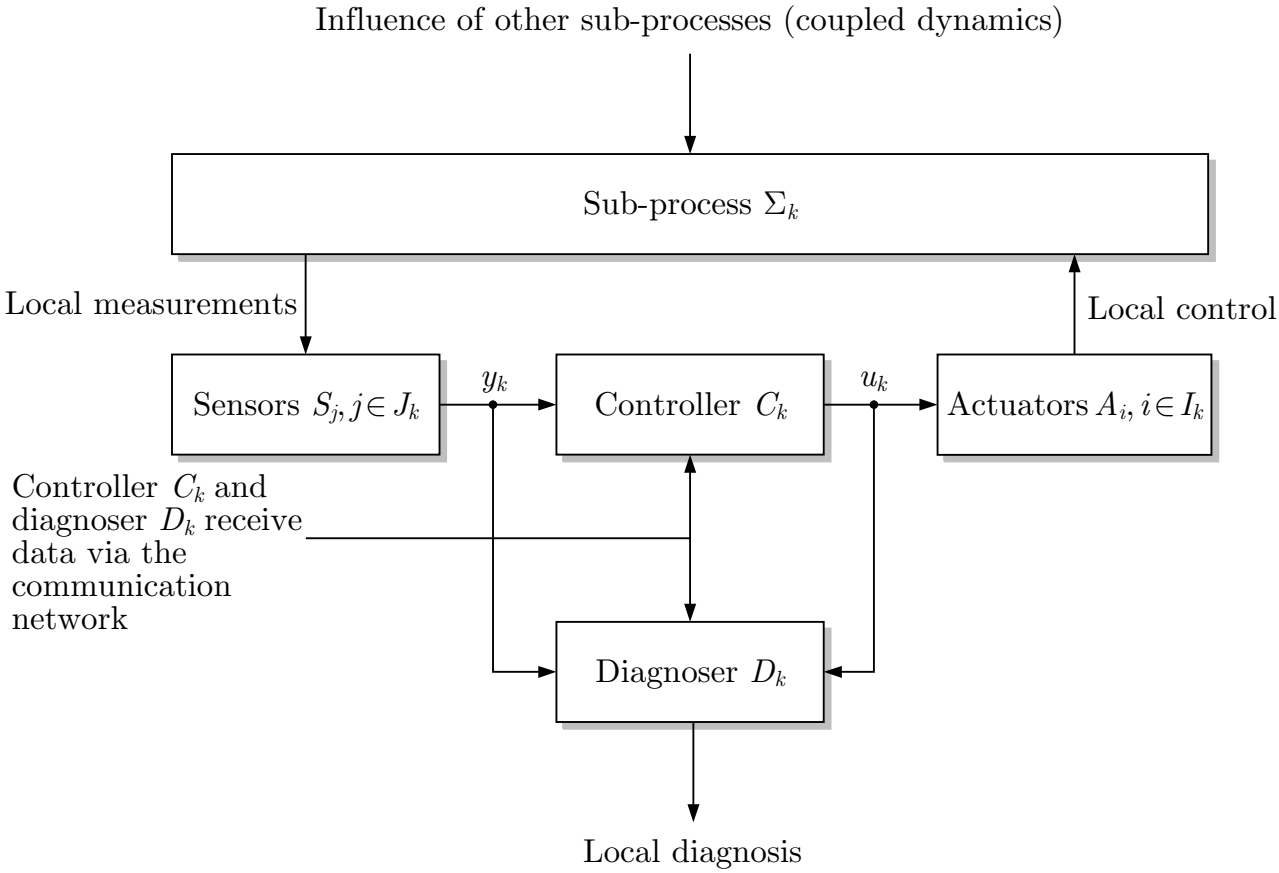

Fig. 10.1. Local controller and diagnoser

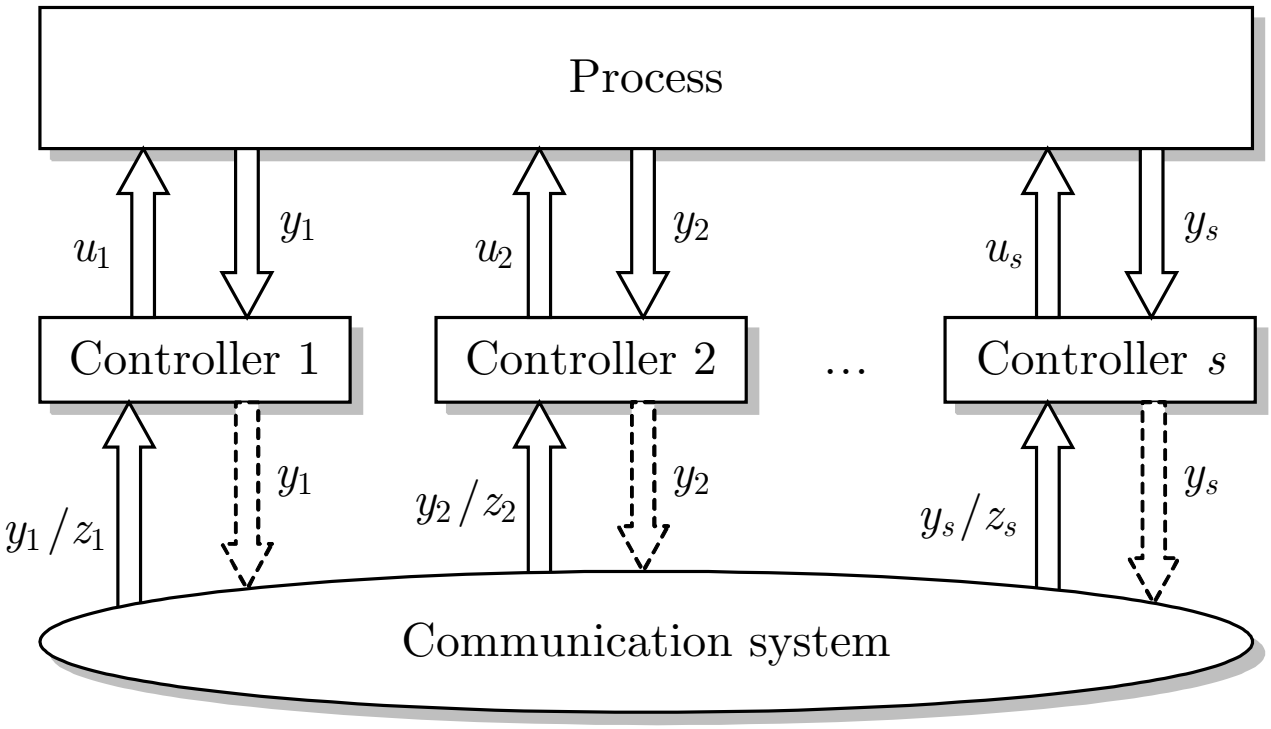

Fig. 10.2. Distributed system architecture

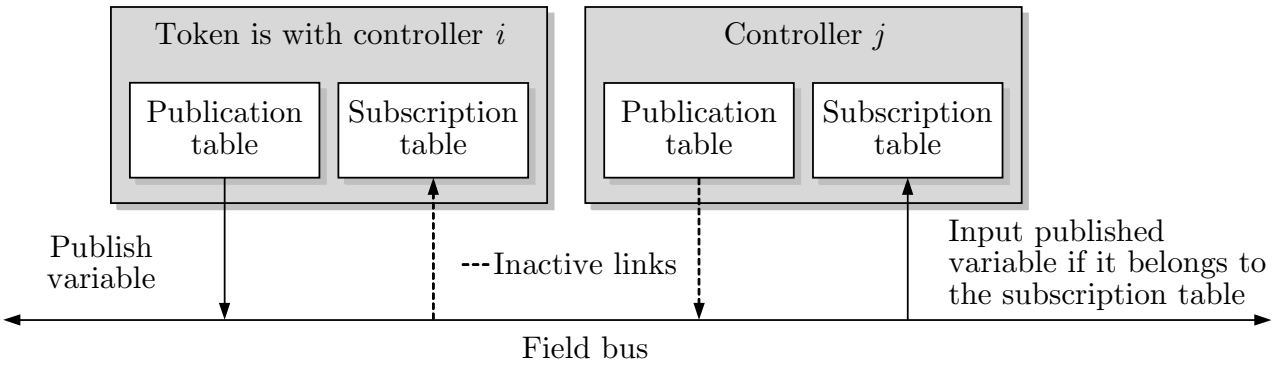

Fig. 10.3. The publisher/subscriber scheme

Blanke/Kinnaert/Lunze/Staroswiecki:
Diagnosis and Fault-Tolerant Control, (3rd edition), Springer-Verlag 2015

Page 471

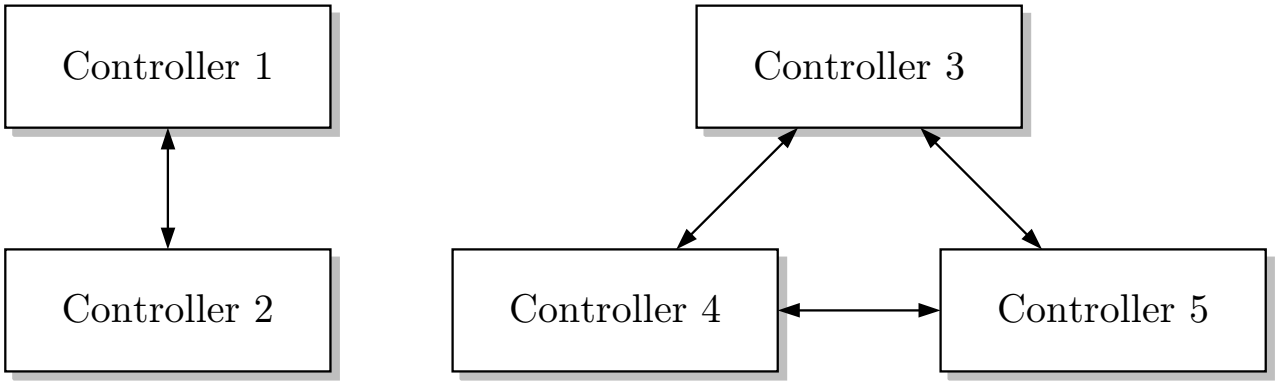

Fig. 10.4. Two agreement classes between 5 controllers

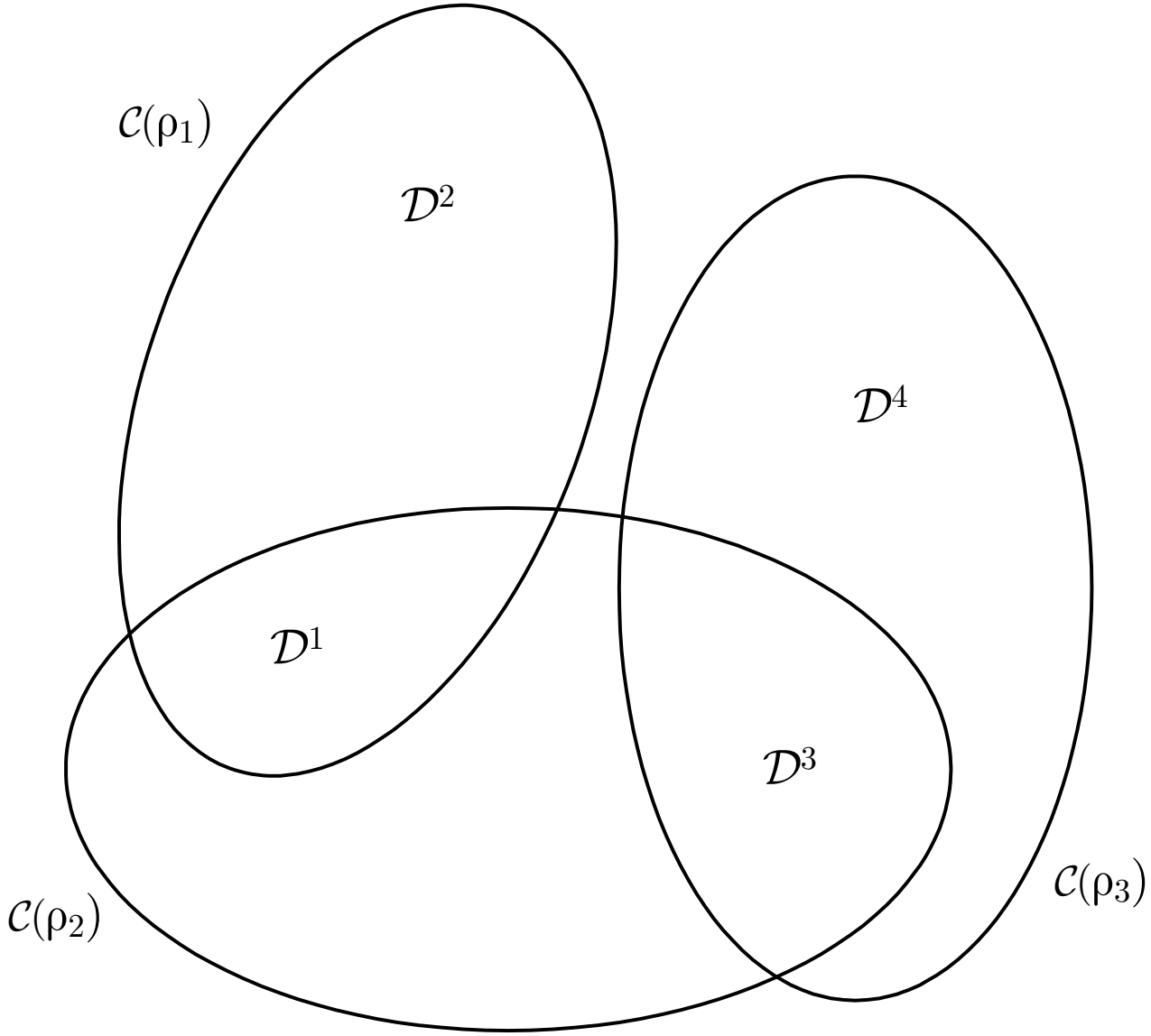

Fig. 10.5. The three conflicts associated with the signature 111

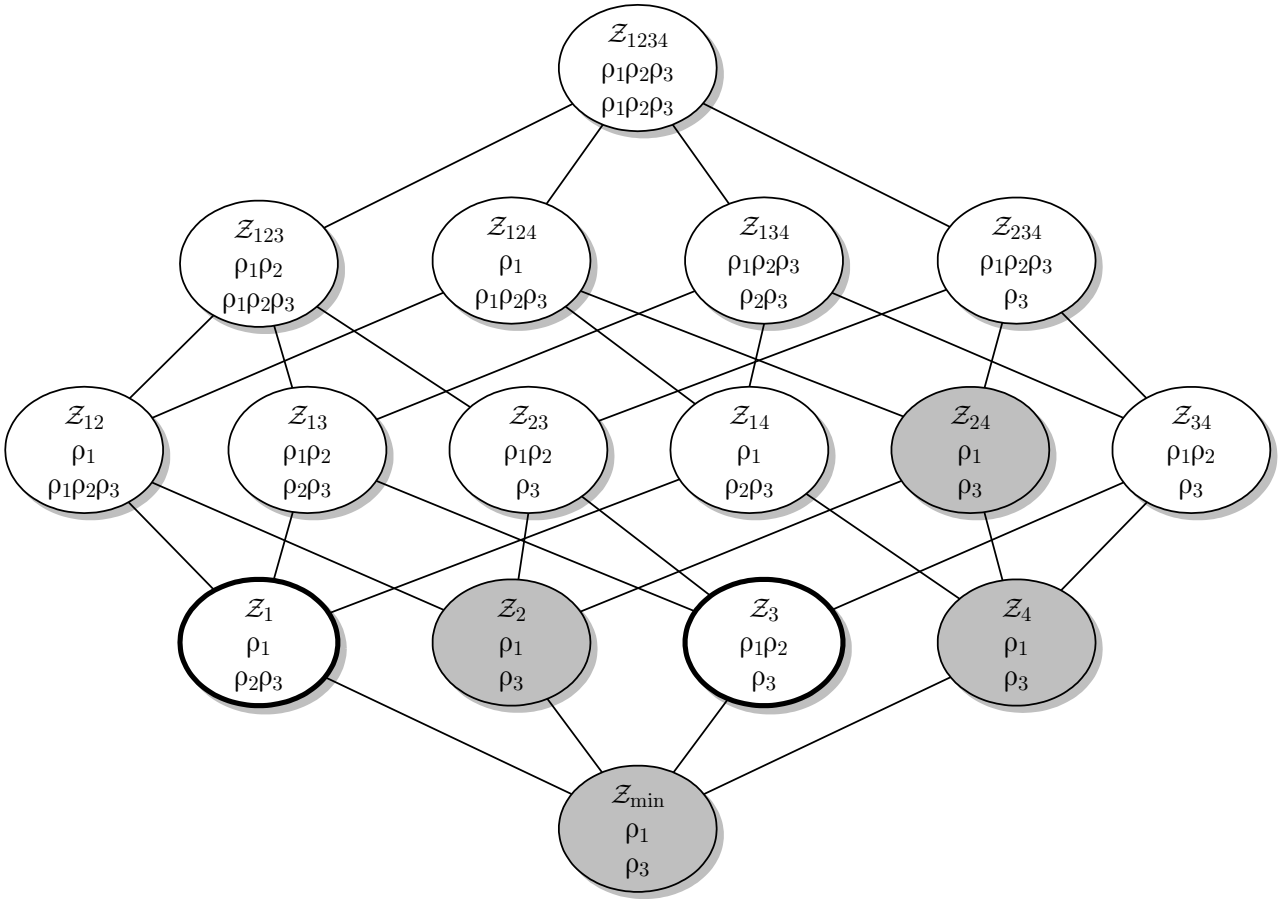

Fig. 10.6. Information patterns and diagnosis distribution in the ship example

Blanke/Kinnaert/Lunze/Staroswiecki:
Diagnosis and Fault-Tolerant Control, (3rd edition), Springer-Verlag 2015

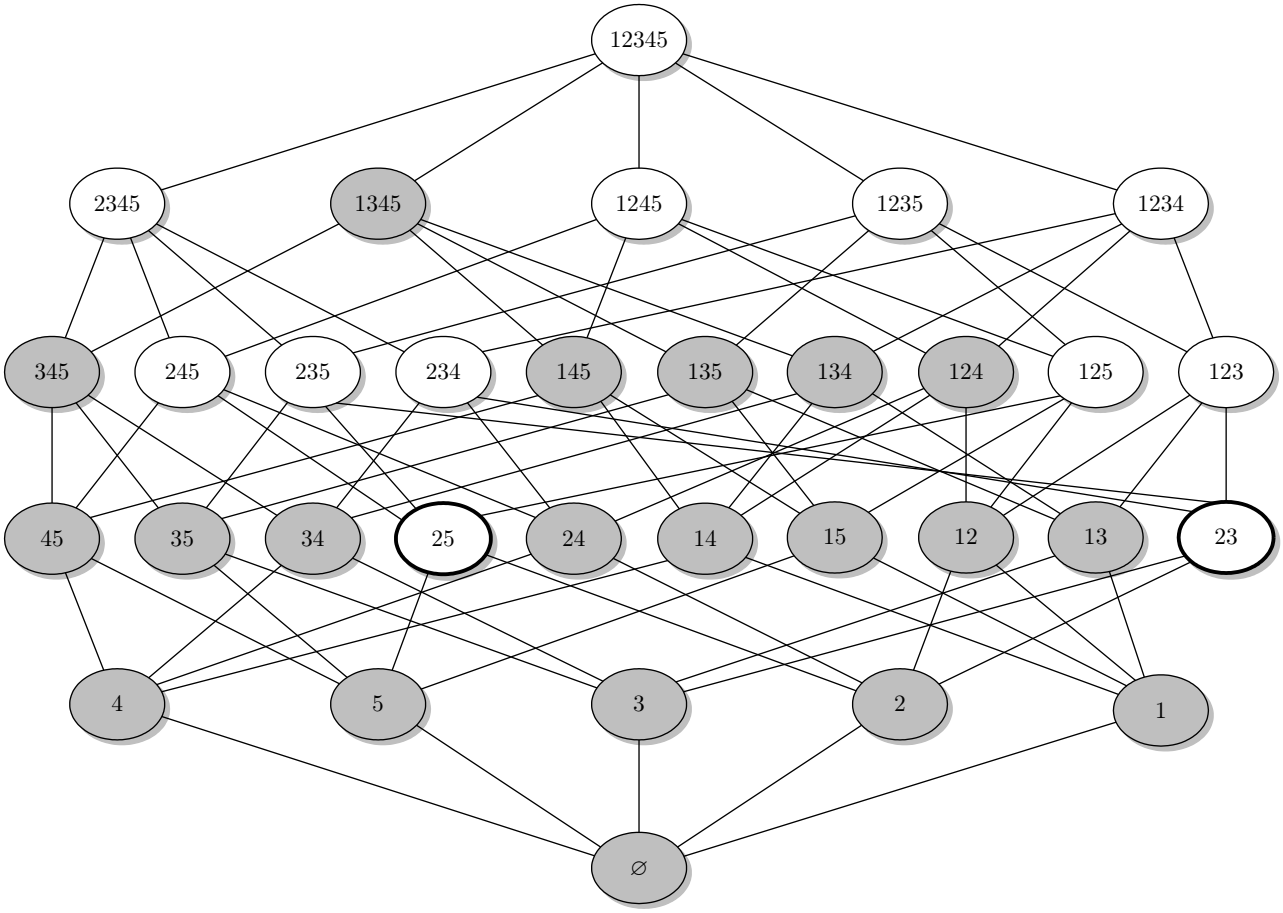

Fig. 10.7. Recoverability span under $\mathcal{Z}_{\min}$

Blanke/Kinnaert/Lunze/Staroswiecki:
Diagnosis and Fault-Tolerant Control, (3rd edition), Springer-Verlag 2015

Page 501

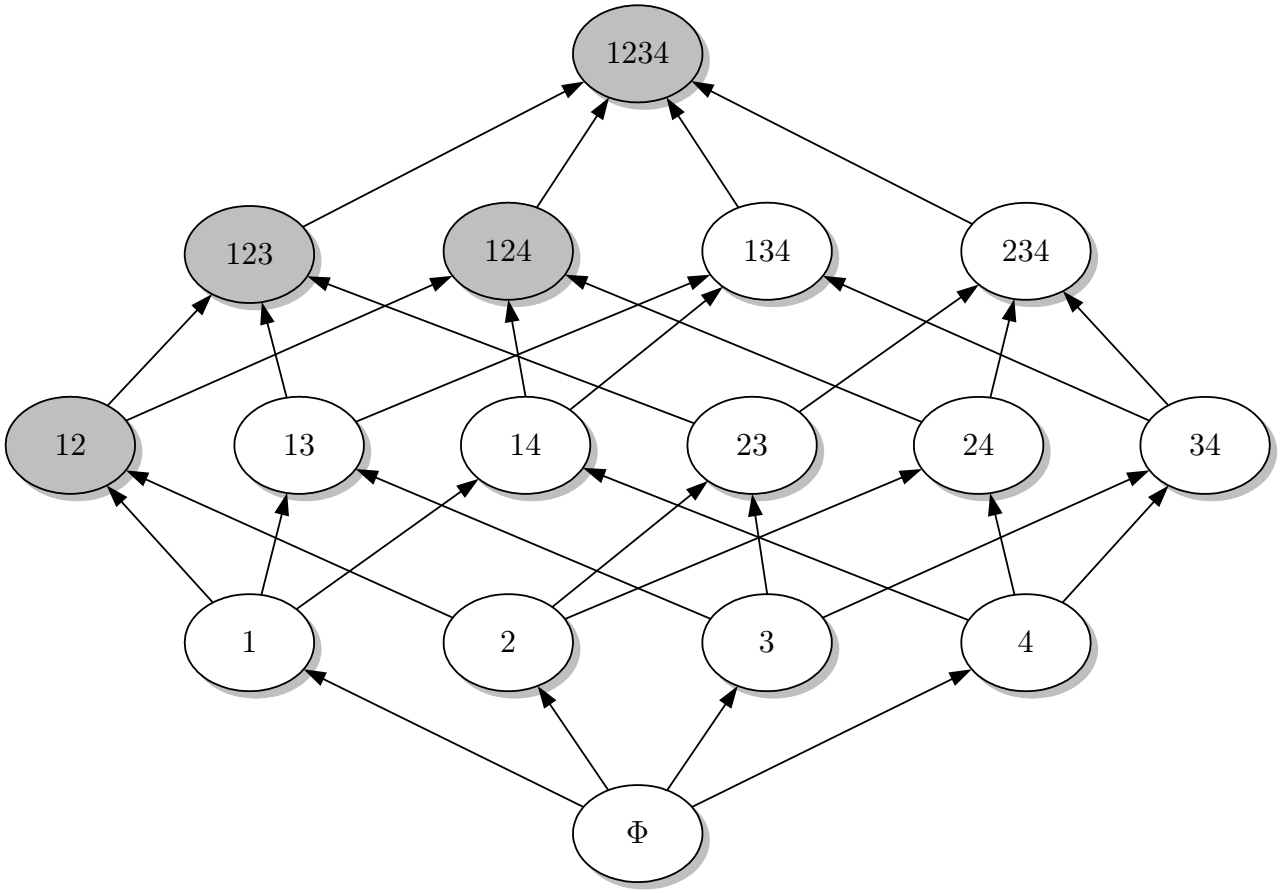

Fig. 10.8. Publishable sets of data

Blanke/Kinnaert/Lunze/Staroswiecki:
Diagnosis and Fault-Tolerant Control, (3rd edition), Springer-Verlag 2015

Page 505

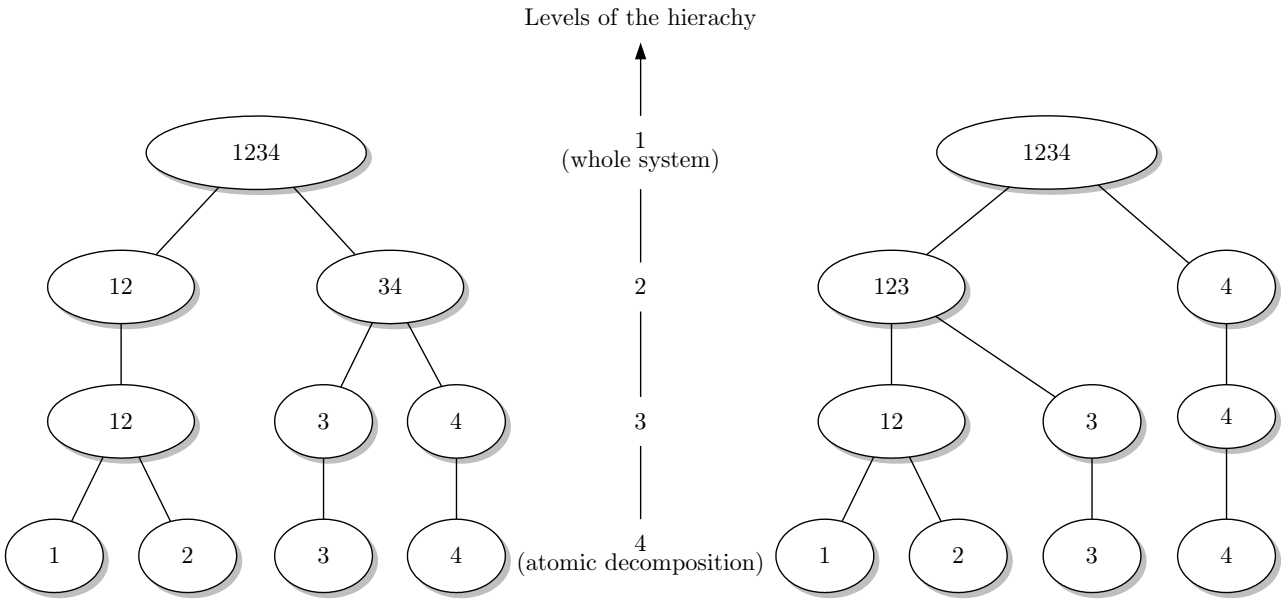

Fig. 10.9. Two possible decomposition hierarchies

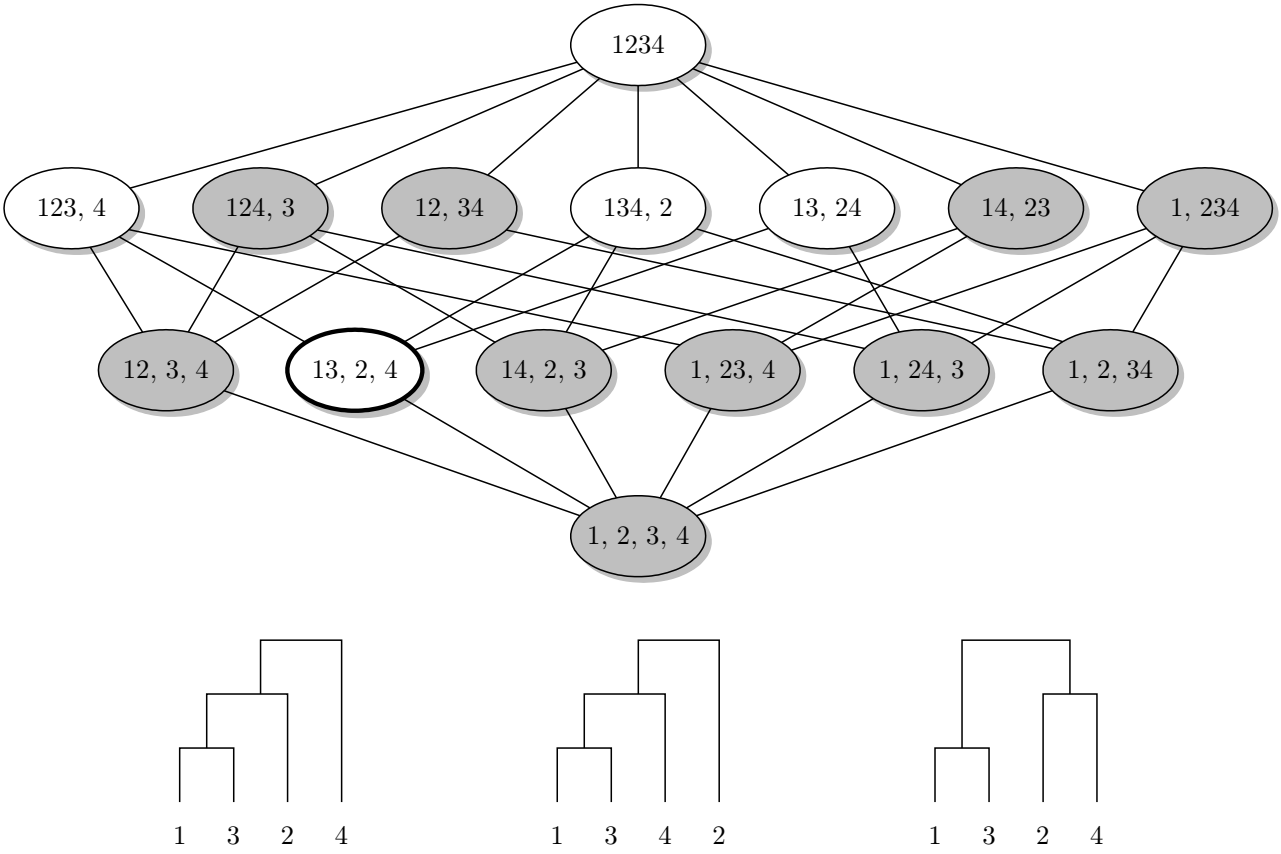

Fig. 10.10. Information patterns under bilateral agreements for 4 subsystems

Blanke/Kinnaert/Lunze/Staroswiecki:
Diagnosis and Fault-Tolerant Control, (3rd edition), Springer-Verlag 2015

Page 508

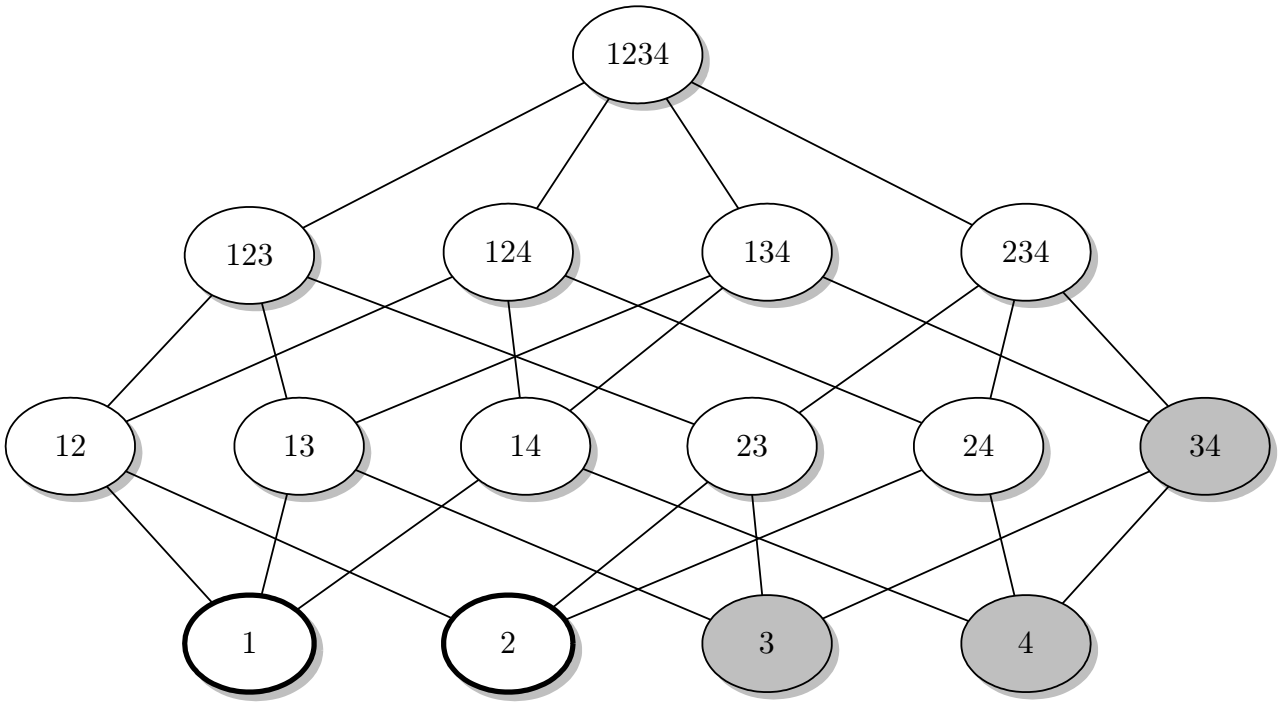

Fig. 10.11. Σ_{K}-recoverability of configuration 1345

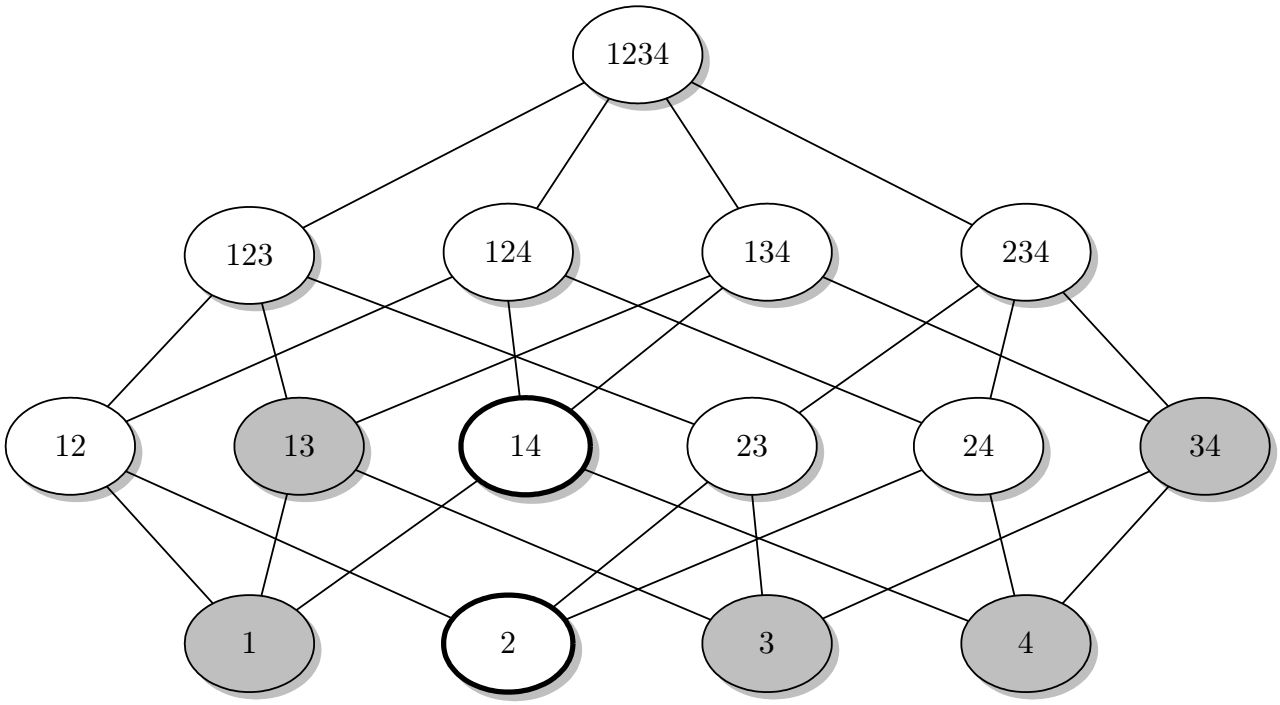

Fig. 10.12. Strong Σ_K-recoverability of configuration 1345

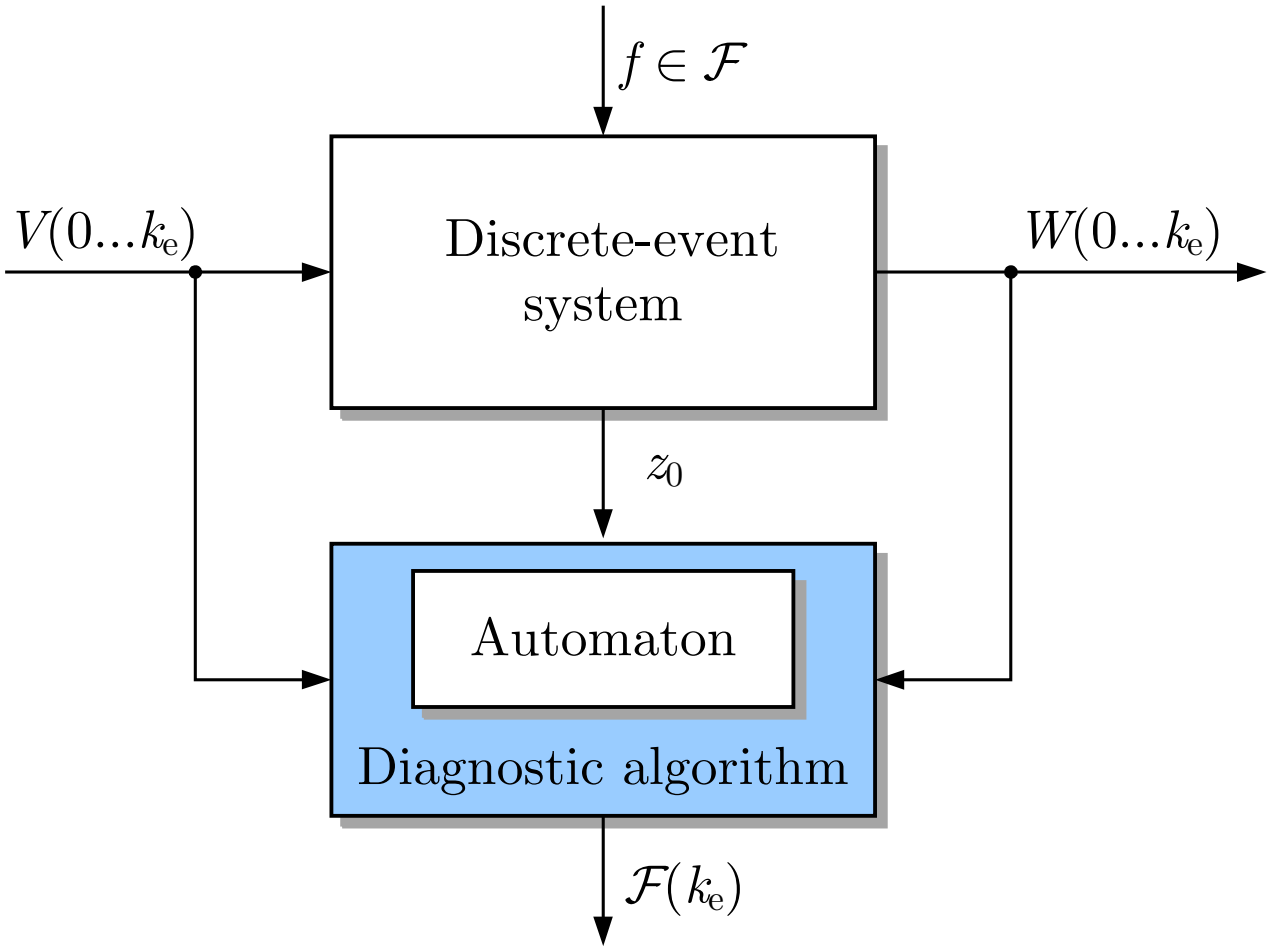

Fig. 11.1. Diagnostic problem

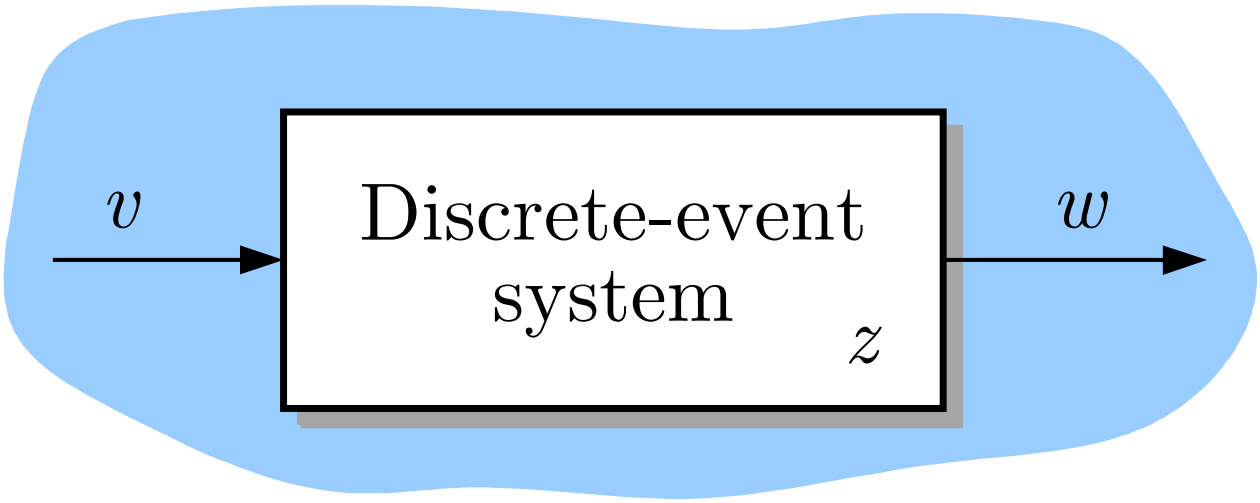

Fig. 11.2. Discrete-event system

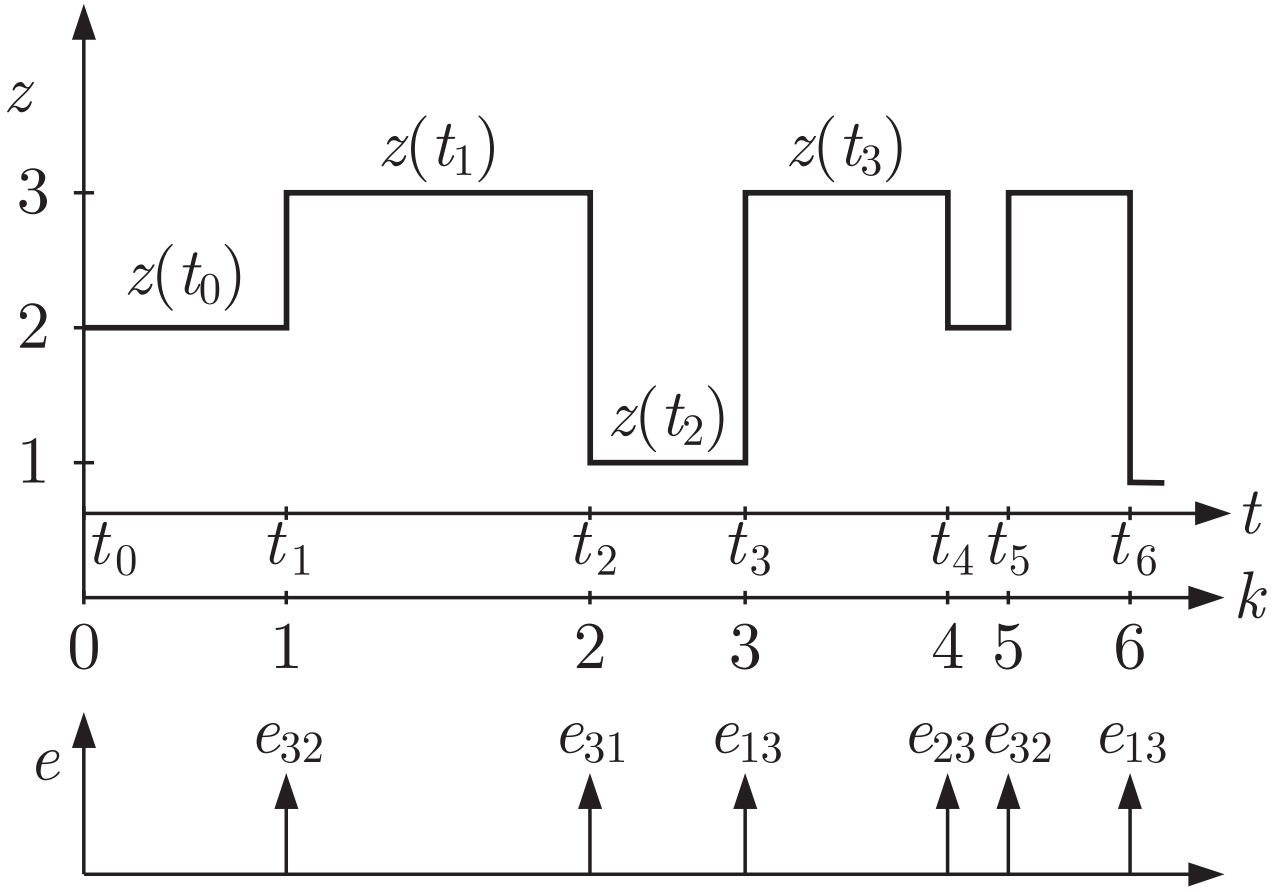

Fig. 11.3. Sequences of symbolic states and event sequences

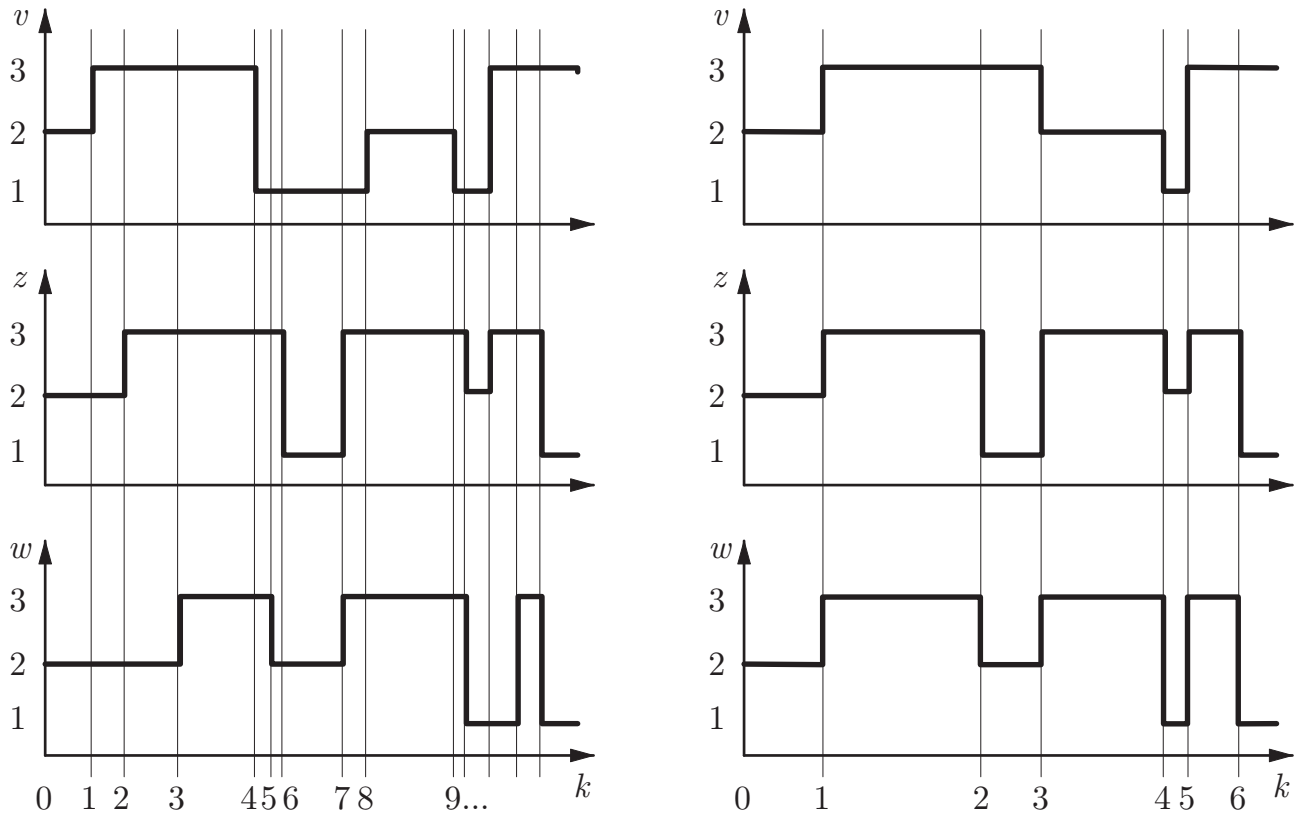

Fig. 11.4. Asynchronous (left) and synchronous (right) input, state and output sequences

Blanke/Kinnaert/Lunze/Staroswiecki:
Diagnosis and Fault-Tolerant Control, (3rd edition), Springer-Verlag 2015

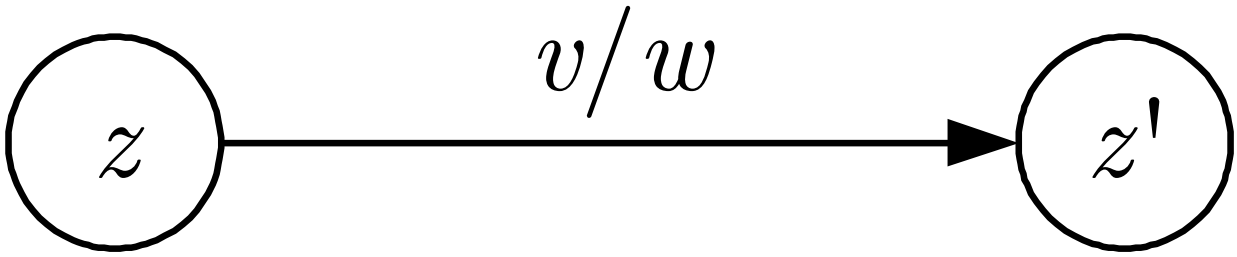

Fig. 11.5. Automaton graph of a deterministic automaton (Part 1)

Blanke/Kinnaert/Lunze/Staroswiecki:
Diagnosis and Fault-Tolerant Control, (3rd edition), Springer-Verlag 2015

Page 524

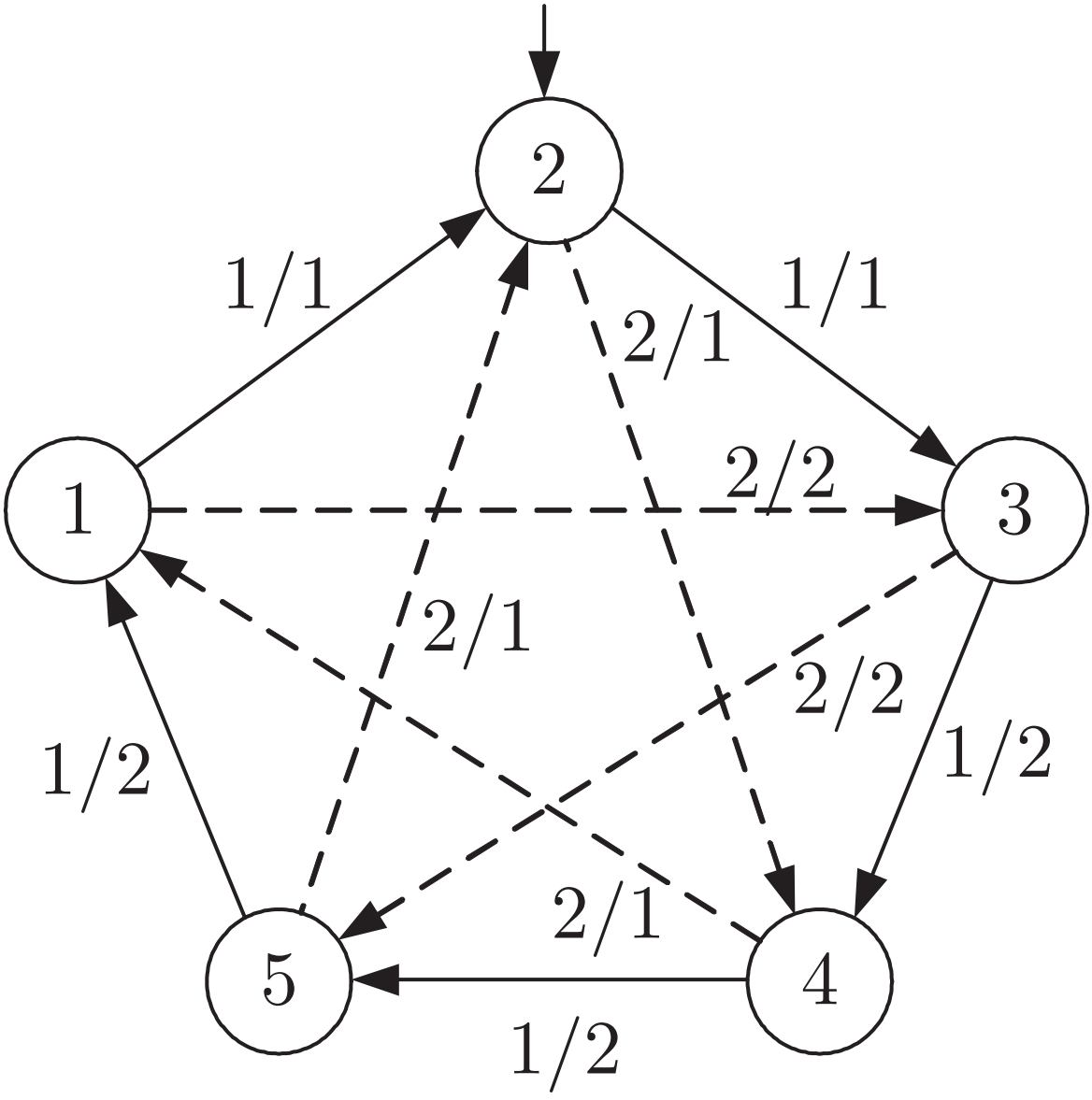

Fig. 11.5. Automaton graph of a deterministic automaton (Part 2)

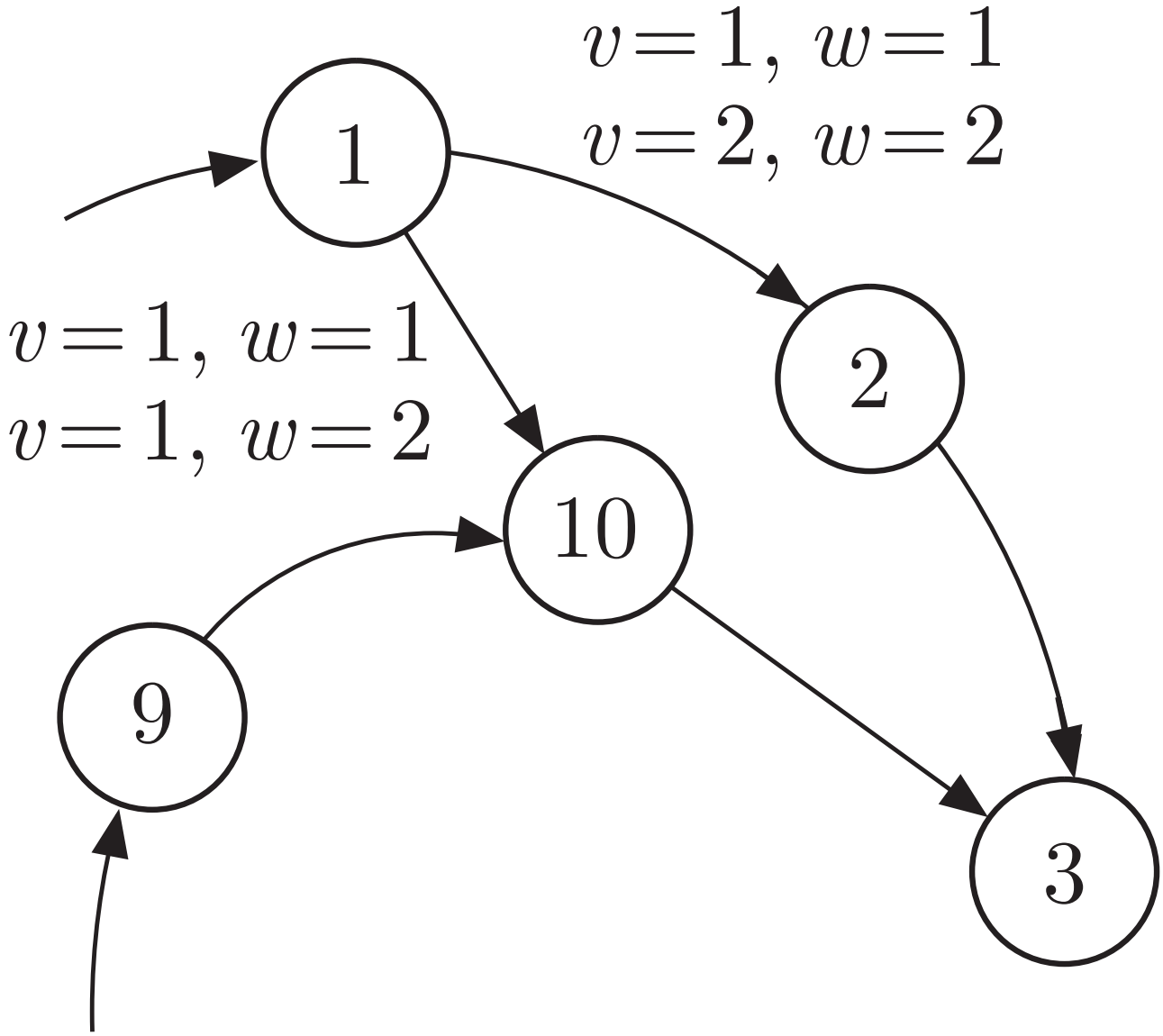

Fig. 11.6. Part of the automaton graph of a nondeterministic automaton

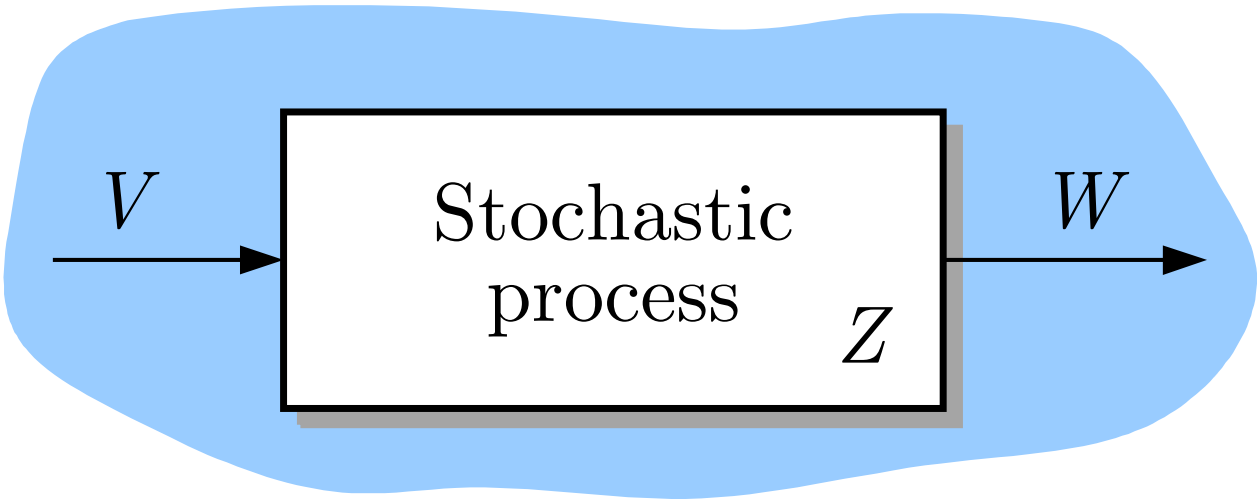

Fig. 11.7. Stochastic process

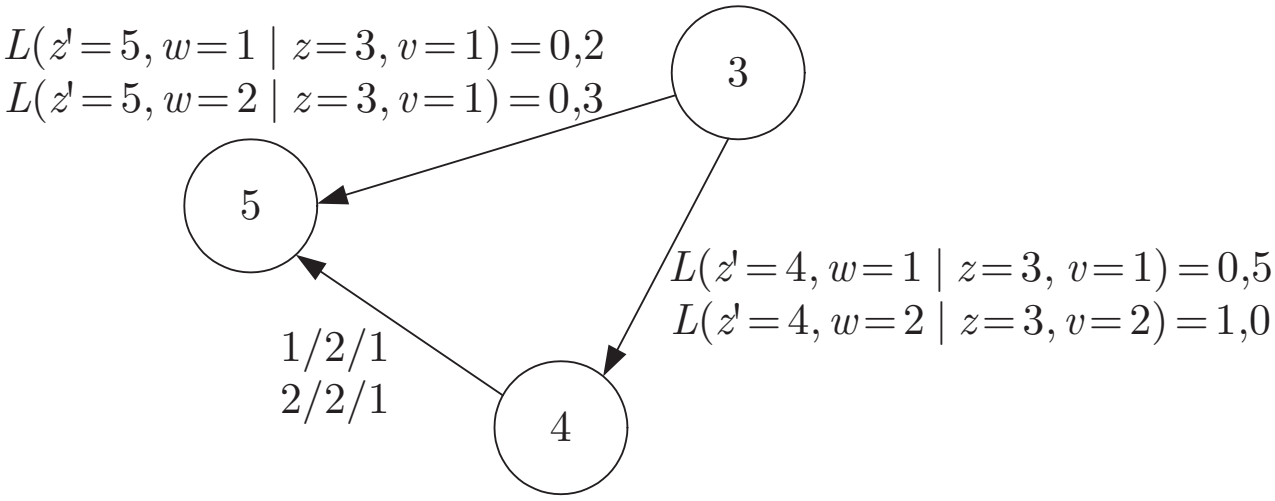

Fig. 11.8. Autonomous stochastic automaton

Blanke/Kinnaert/Lunze/Staroswiecki:
Diagnosis and Fault-Tolerant Control, (3rd edition), Springer-Verlag 2015

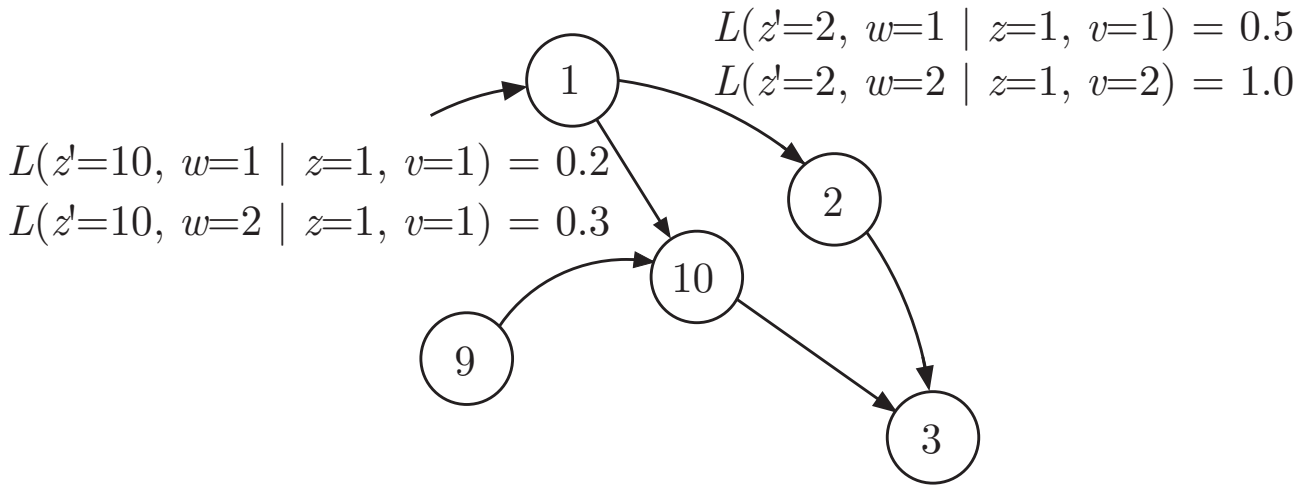

Fig. 11.9. Part of the automaton graph of a stochastic automaton with input and output

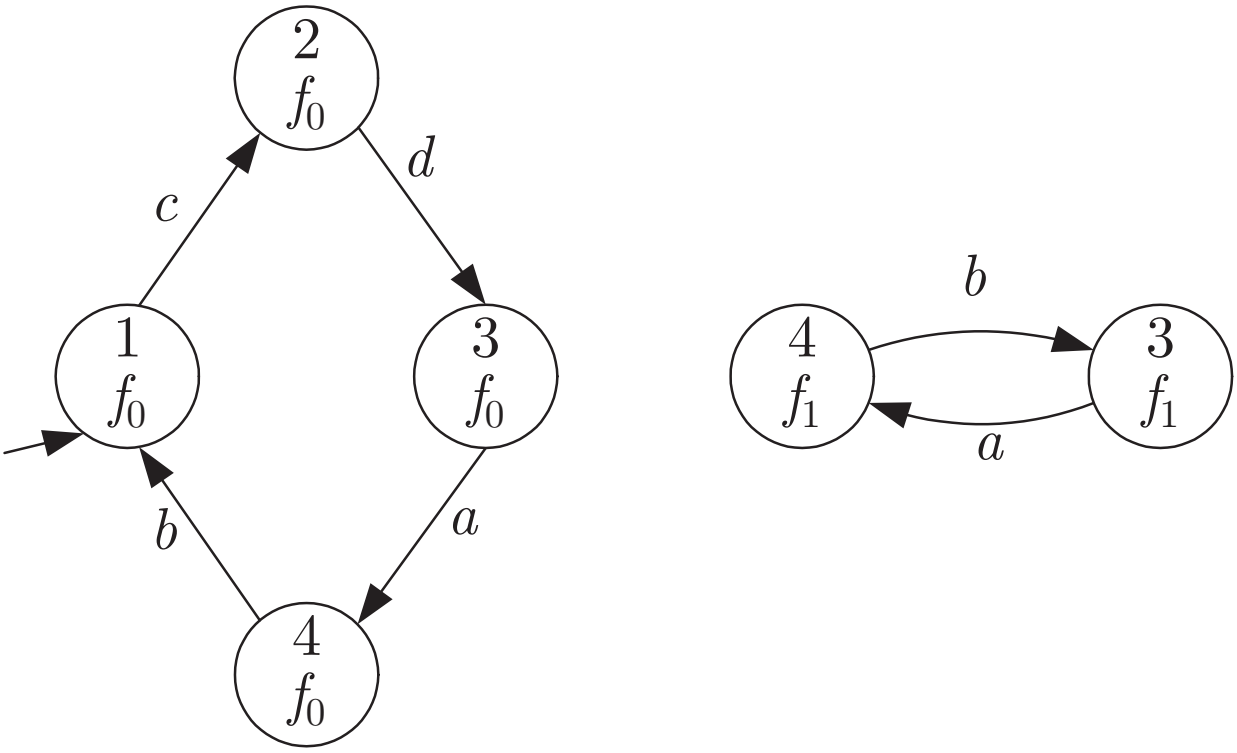

Fig. 11.10. Faults change the system properties (Part 1)

Blanke/Kinnaert/Lunze/Staroswiecki:
Diagnosis and Fault-Tolerant Control, (3rd edition), Springer-Verlag 2015

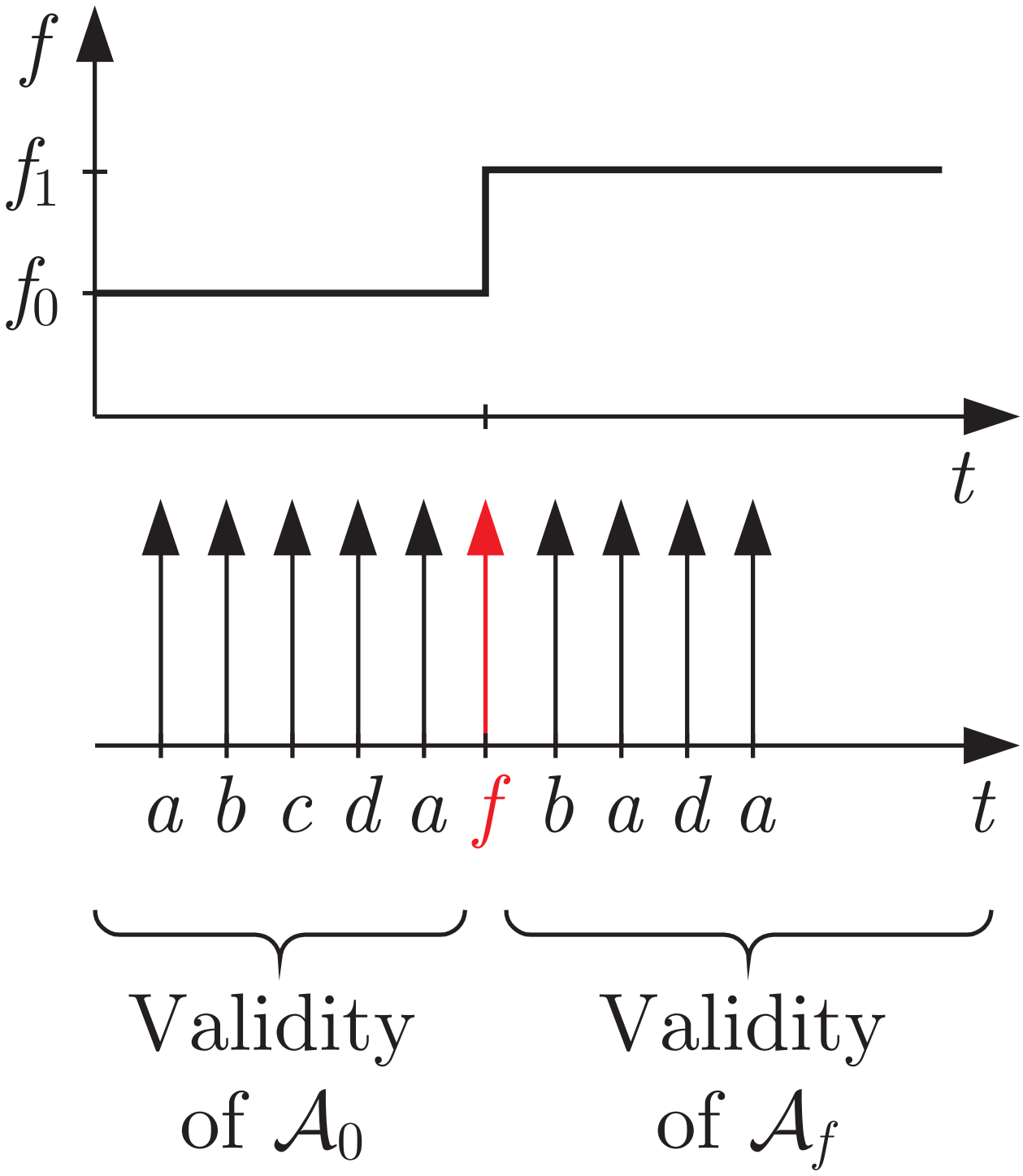

Fig. 11.10. Faults change the system properties (Part 2)

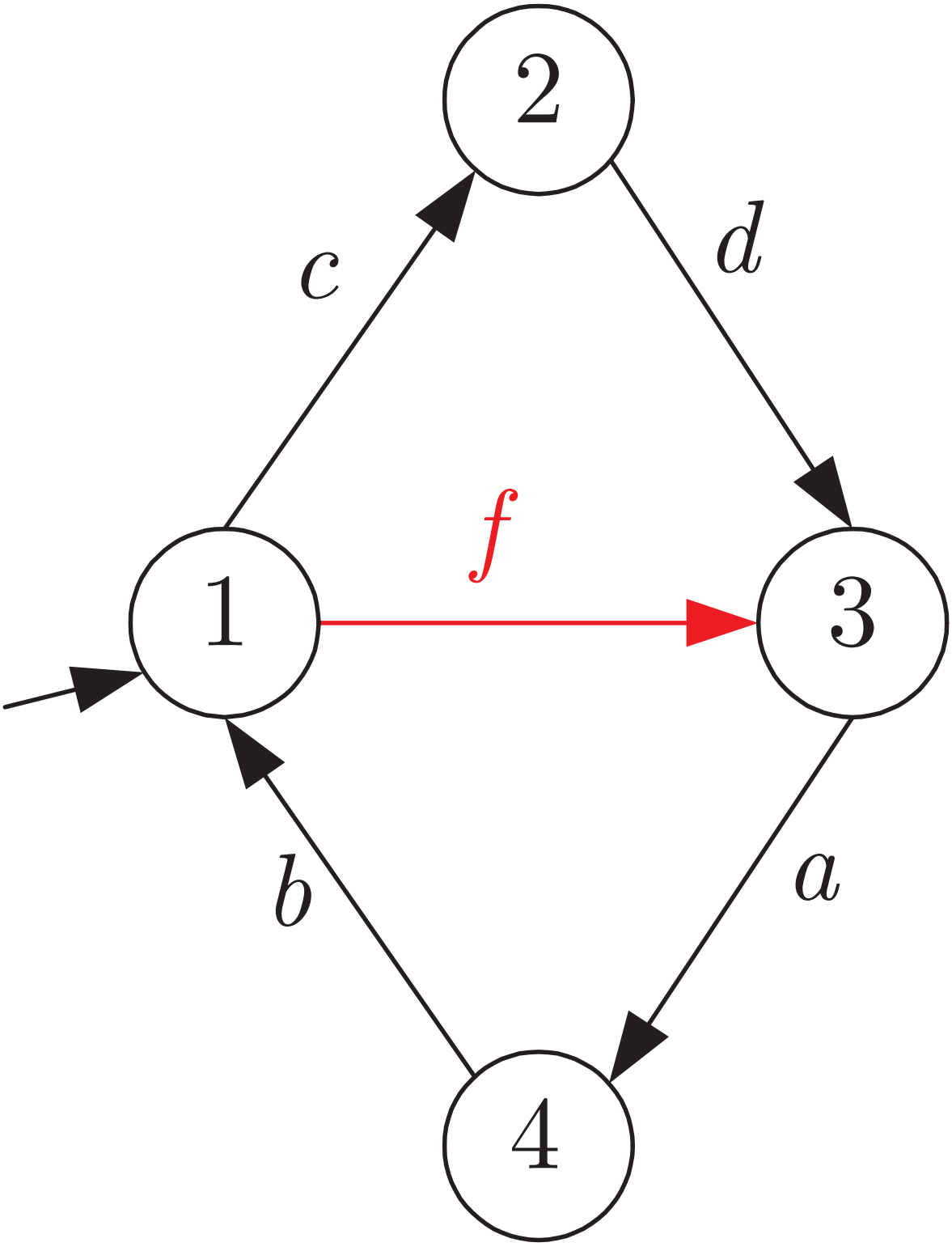

Fig. 11.11. Fault interpreted as an unobservable event (Part 1)

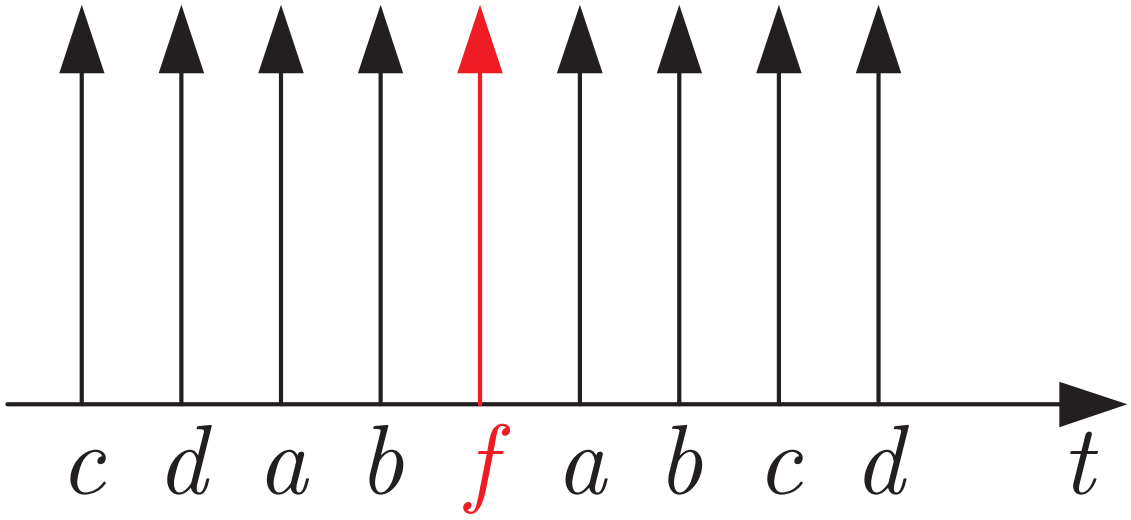

Fig. 11.11. Fault interpreted as an unobservable event (Part 2)

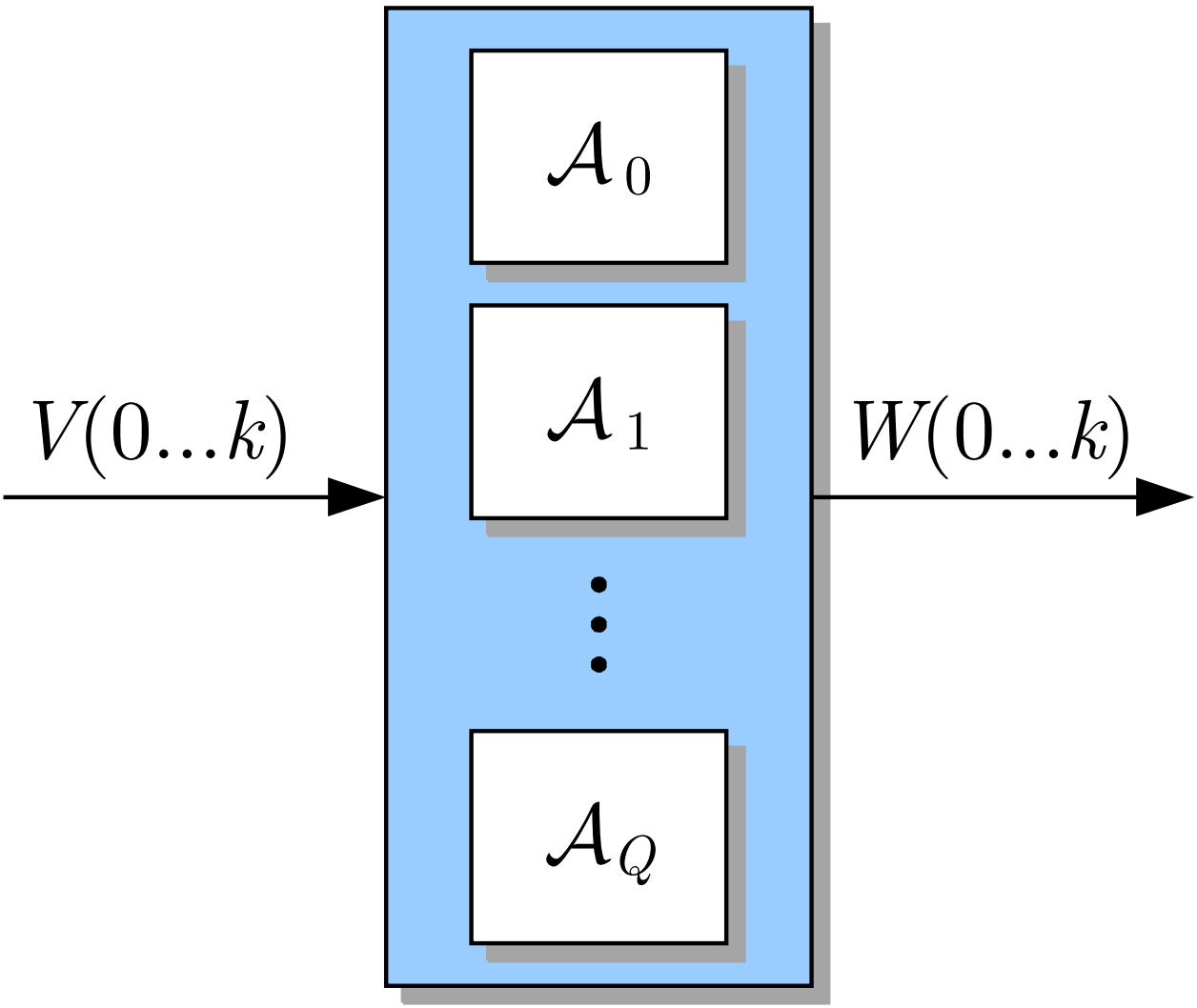

Fig. 11.12. Fault identification as model identification problem

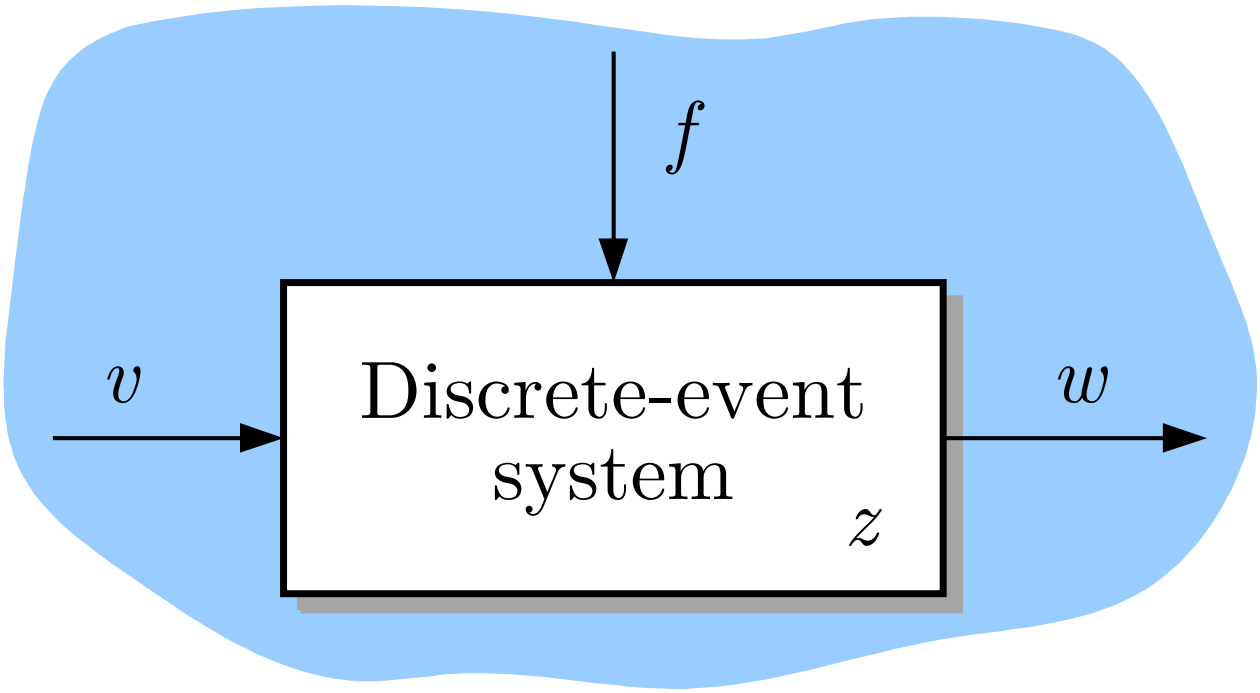

Fig. 11.13. Fault interpreted as an additional input

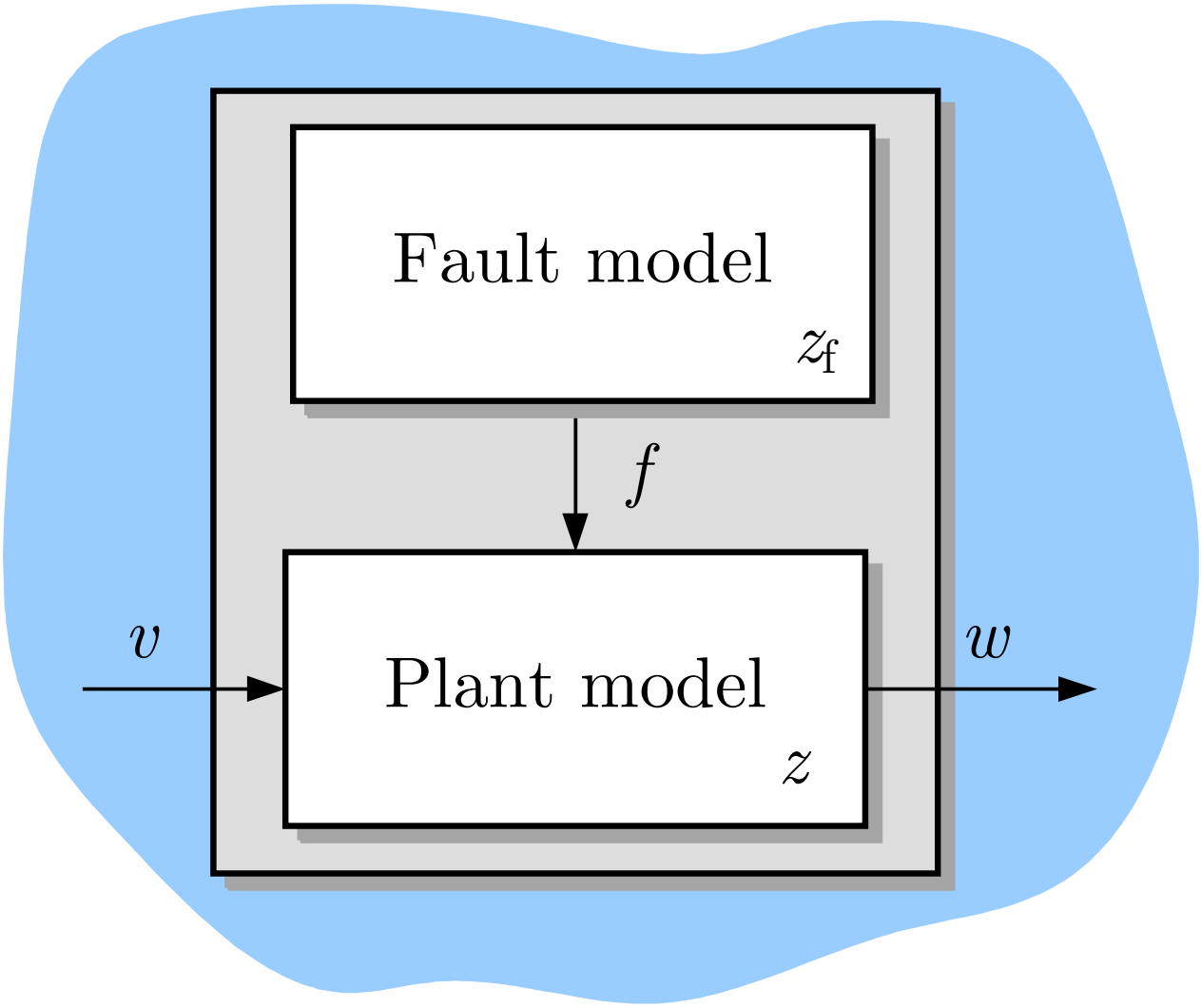

Fig. 11.14. Representation of a faulty system including a fault model

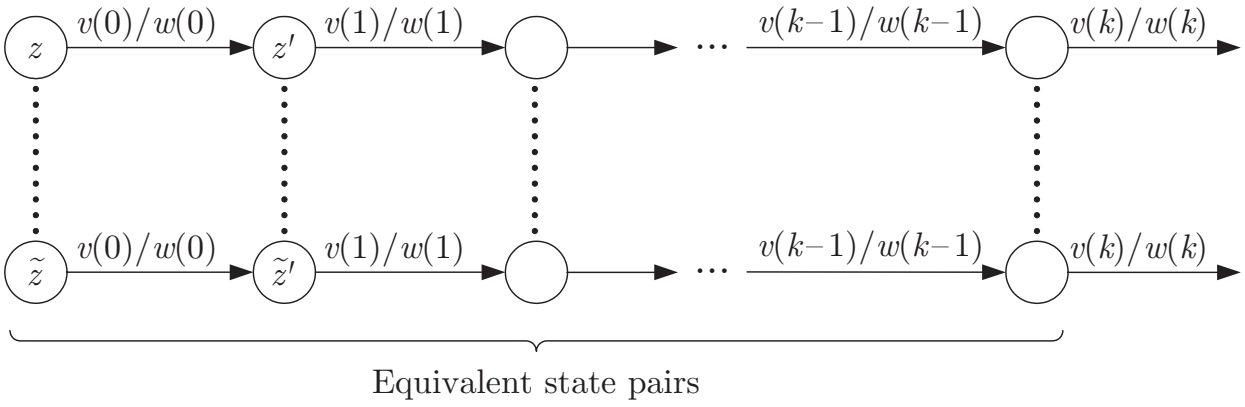

Fig. 11.15. State trajectories over equivalent state pairs

Blanke/Kinnaert/Lunze/Staroswiecki:
Diagnosis and Fault-Tolerant Control, (3rd edition), Springer-Verlag 2015

Page 548

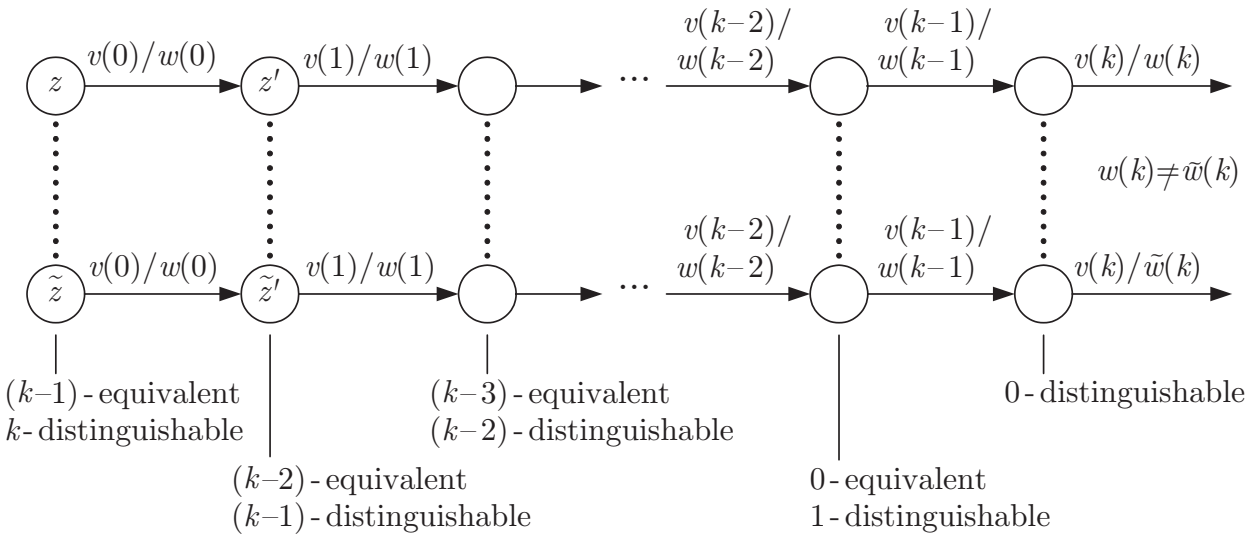

Fig. 11.16. State trajectories generated by a distinguishing input sequence $\bar{V}(0\,...\,k)$ that start in a k-distinguishable, $(k-1)$-equivalent state pair

Blanke/Kinnaert/Lunze/Staroswiecki:
Diagnosis and Fault-Tolerant Control, (3rd edition), Springer-Verlag 2015

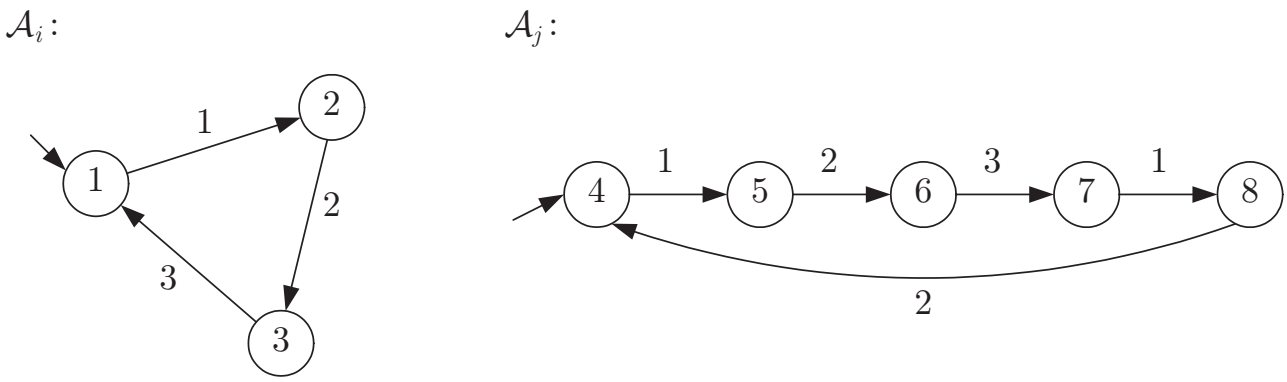

Fig. 11.17. Two automata

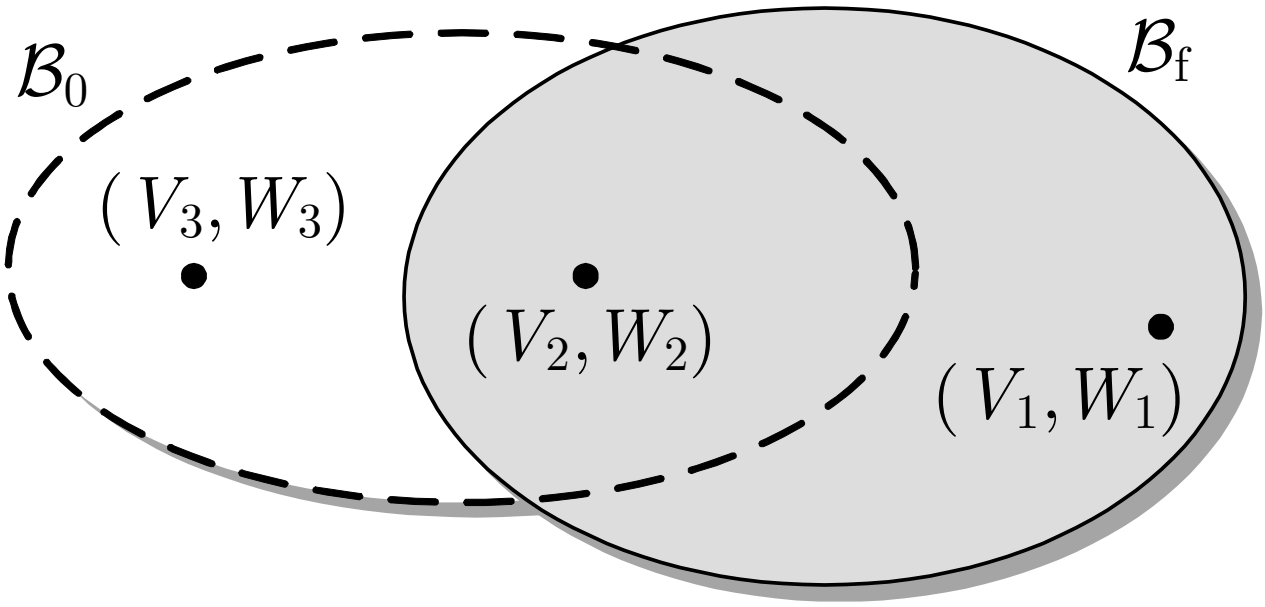

Fig. 11.18. Illustration of the detectability condition (11.60)

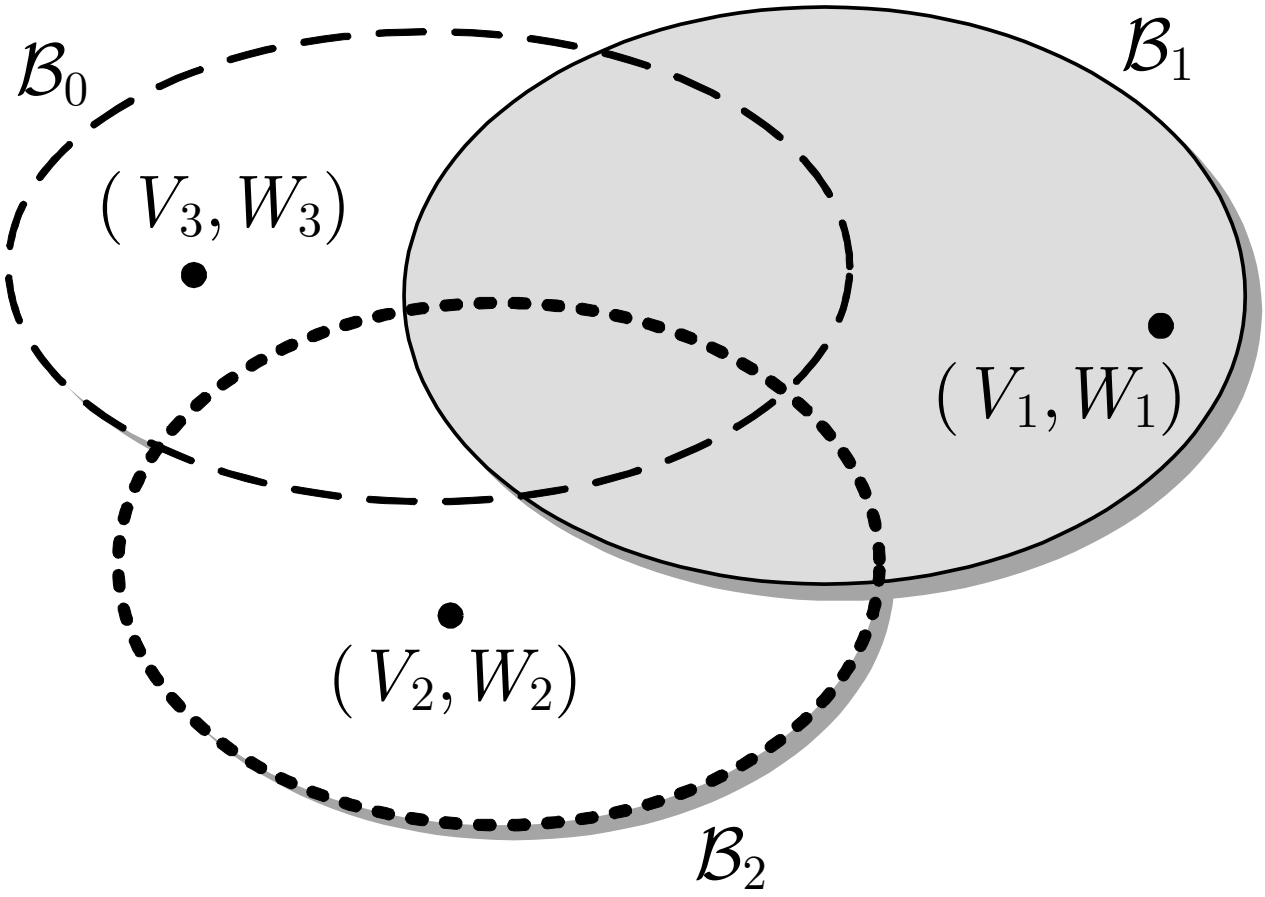

Fig. 11.19. Illustration of fault identification

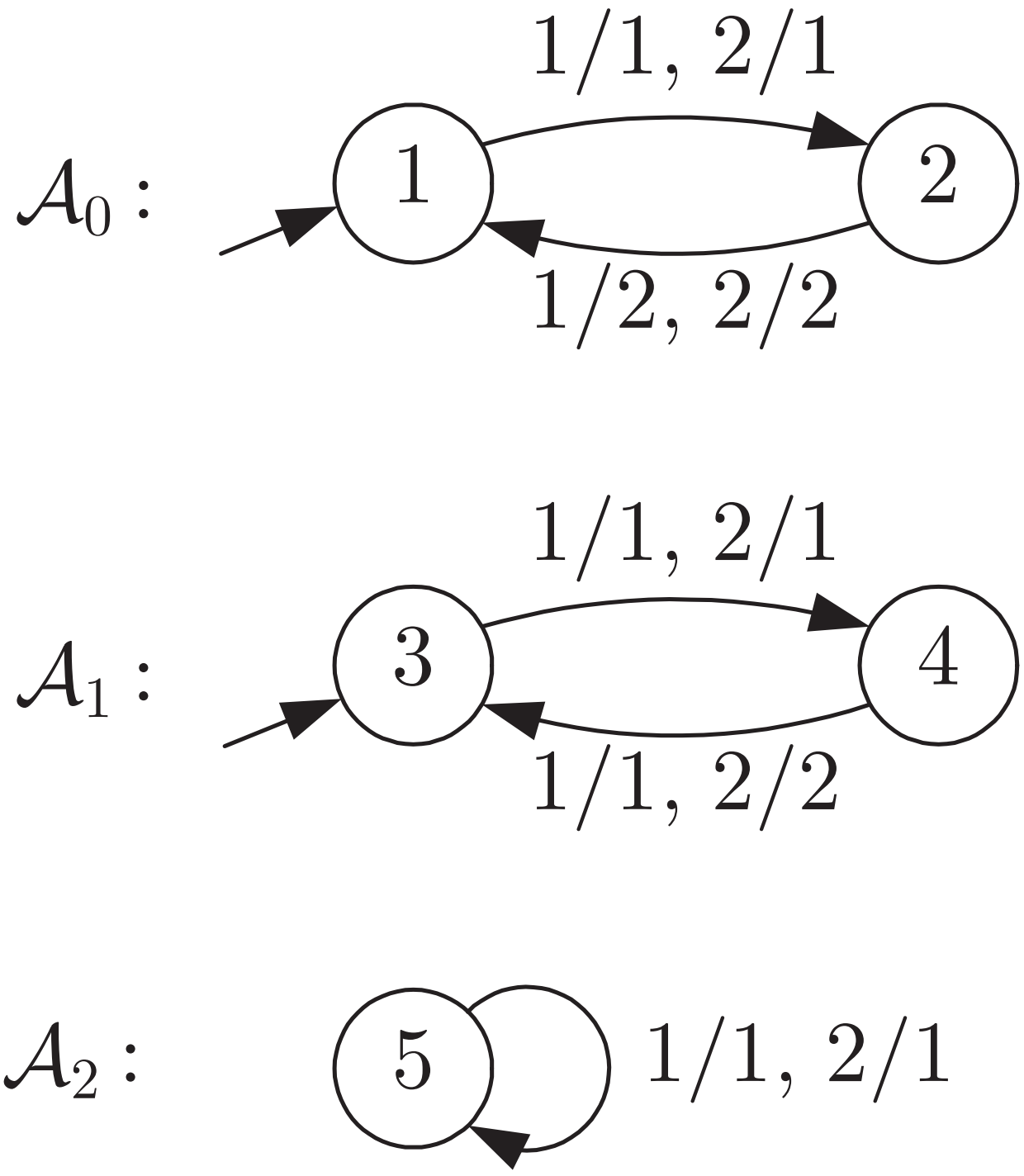

Fig. 11.20. Models of three fault cases

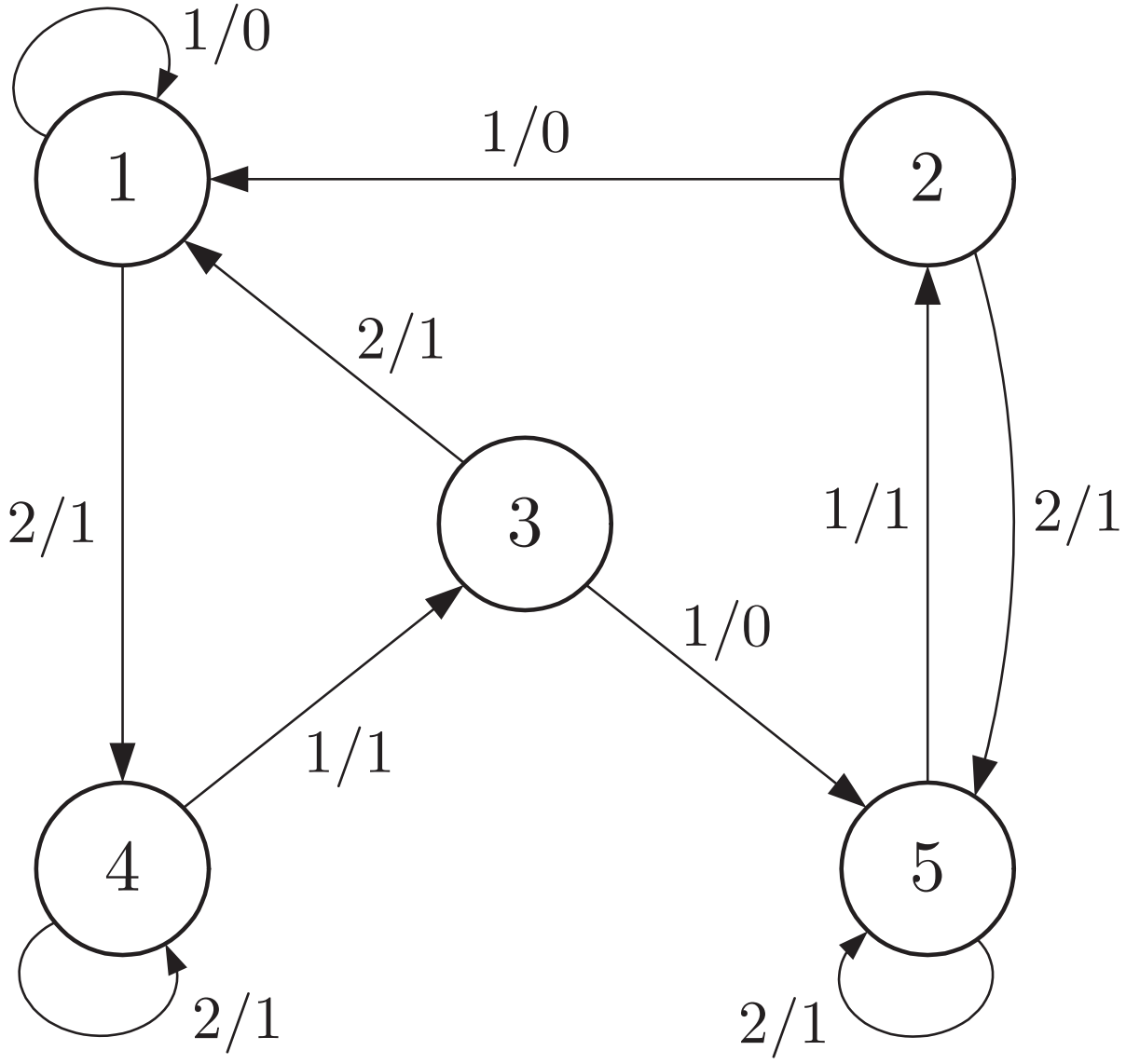

Fig. 11.21. Automaton

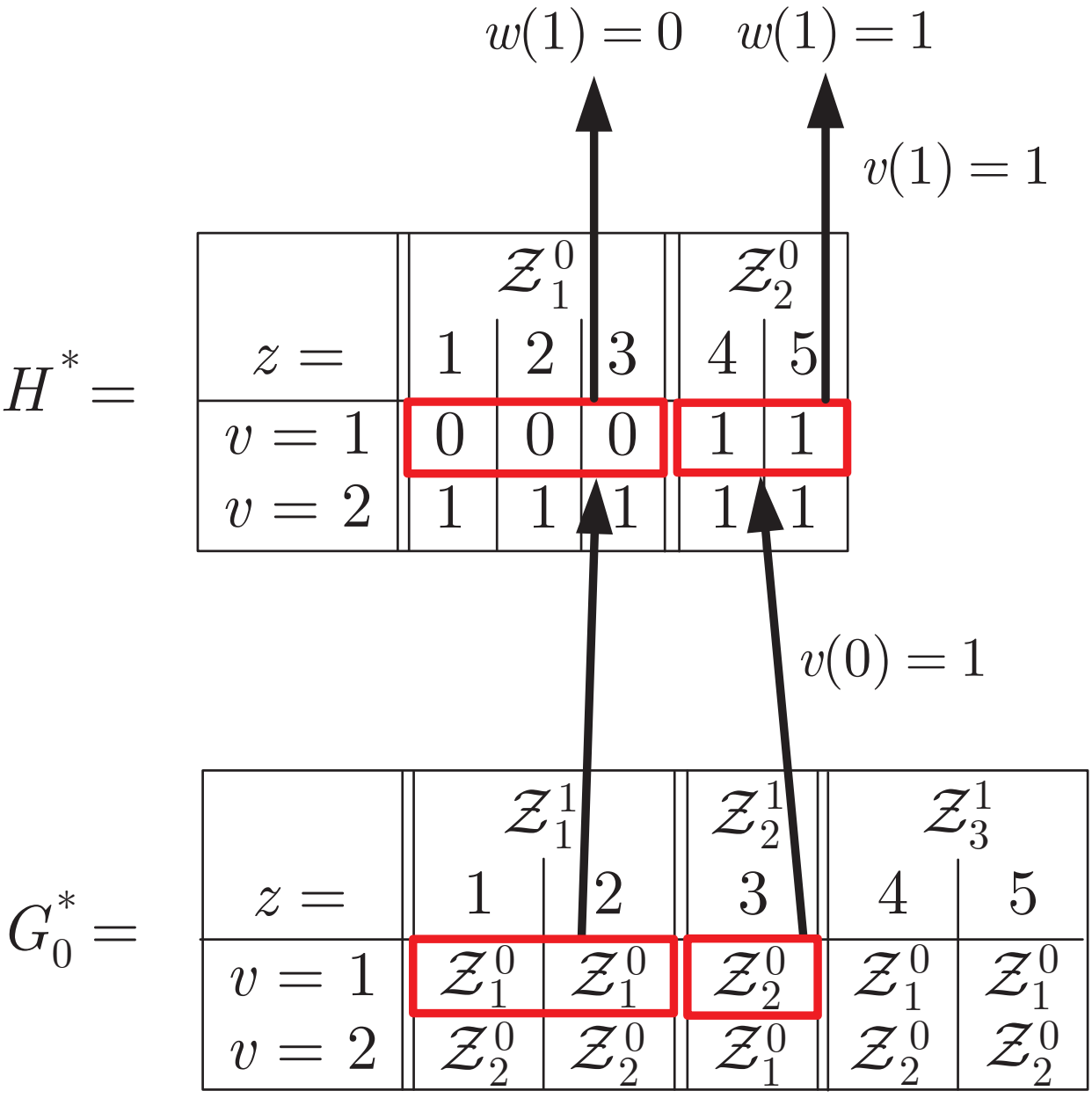

Fig. 11.22. Determination of the distinguishing input sequence of 1-distinguishing state pairs

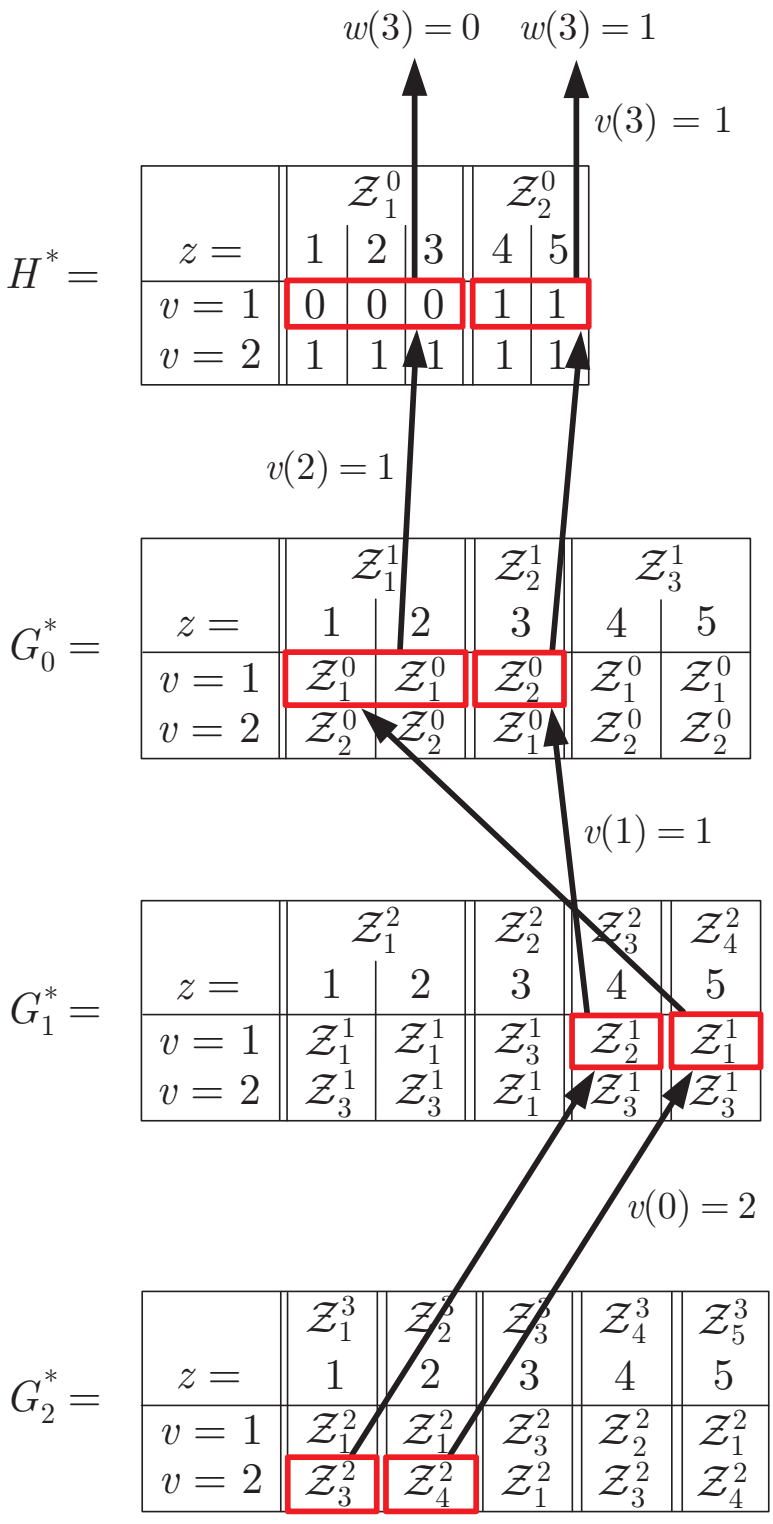

Fig. 11.23. Determination of the distinguishing input sequence of 3-distinguishing state pairs

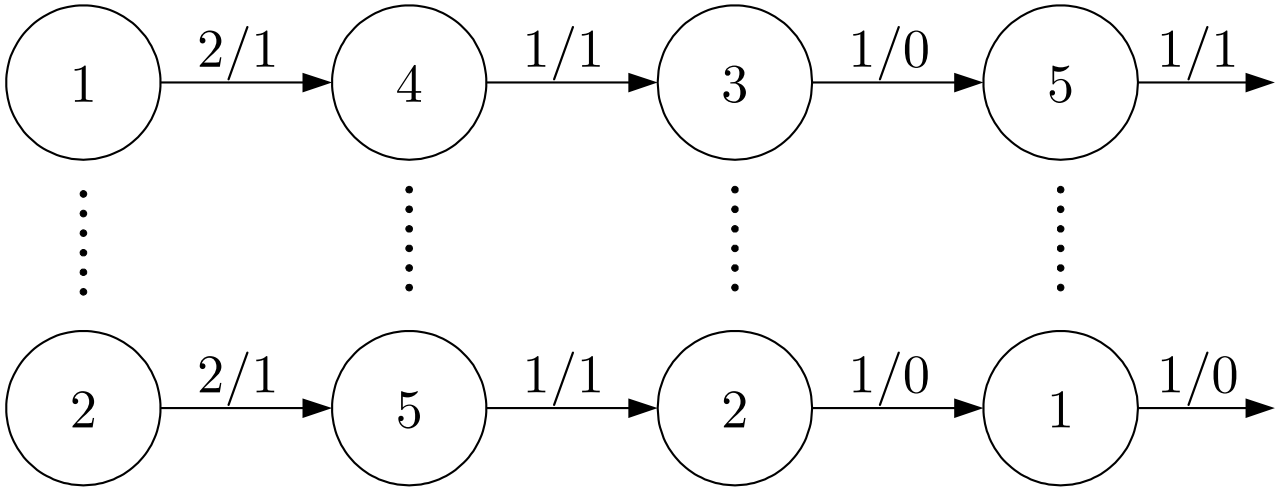

Fig. 11.24. State trajectories for determining whether the automaton is in the initial state 1 or 2

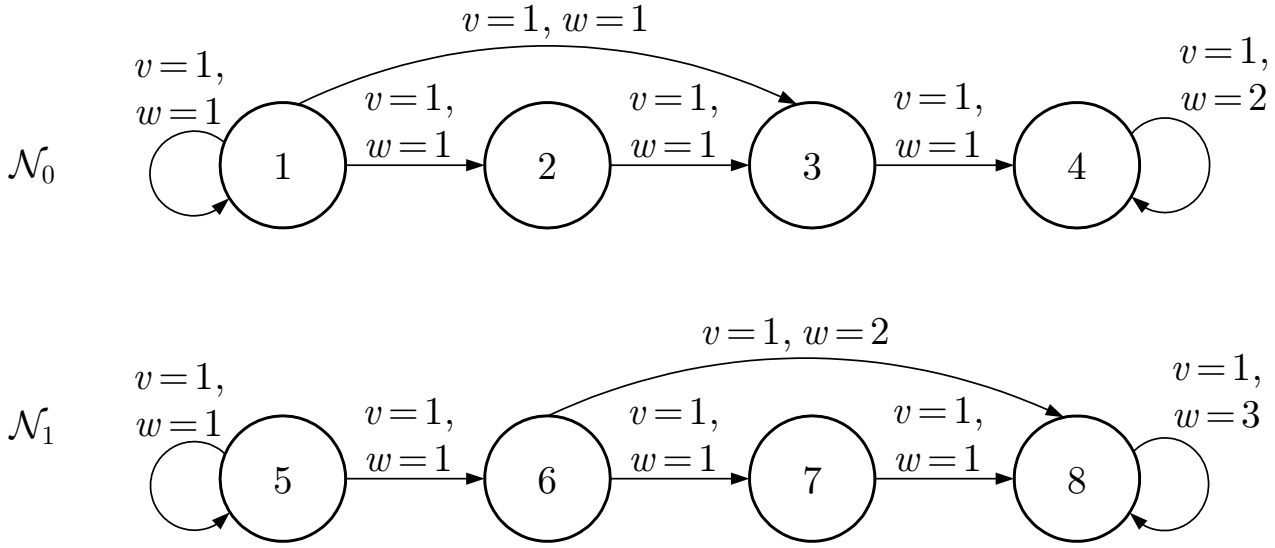

Fig. 11.25. Automaton graph of the example

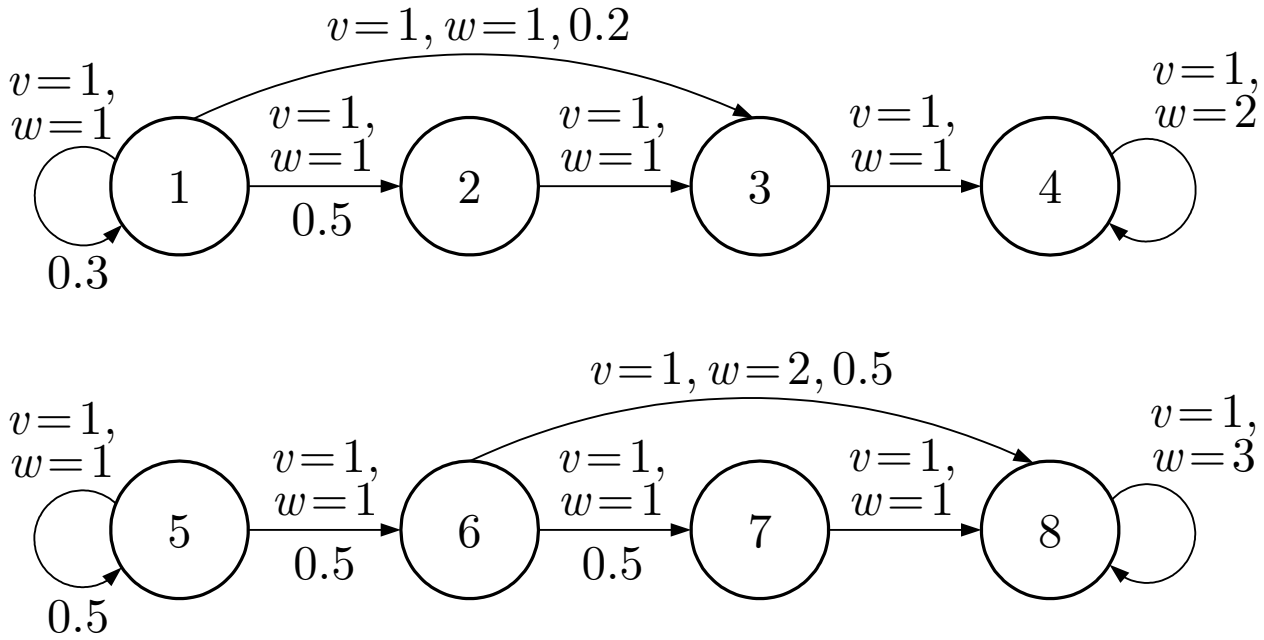

Fig. 11.26. Automaton graph of the example

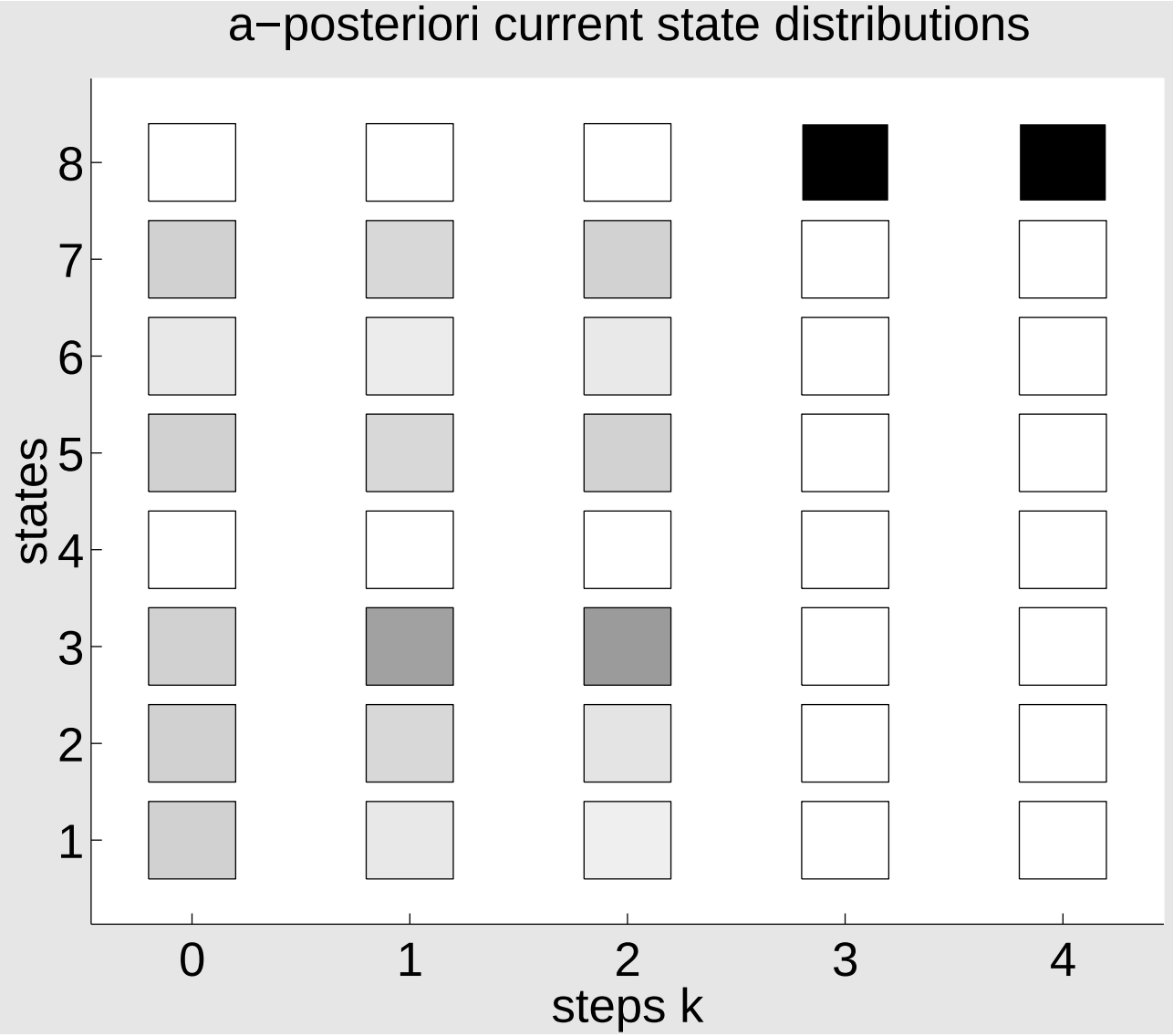

Fig. 11.27. Observation result

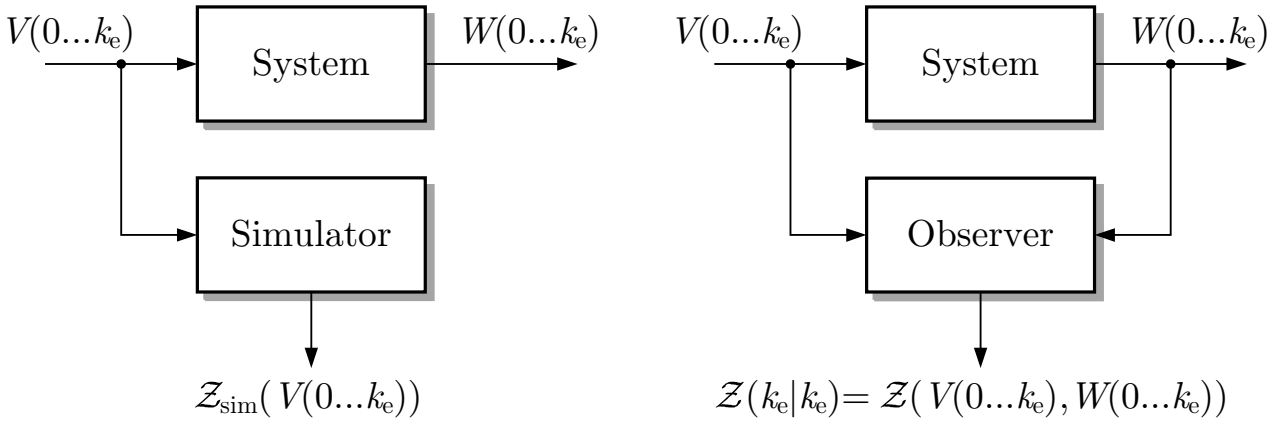

Fig. 11.28. Comparison of simulation and observation

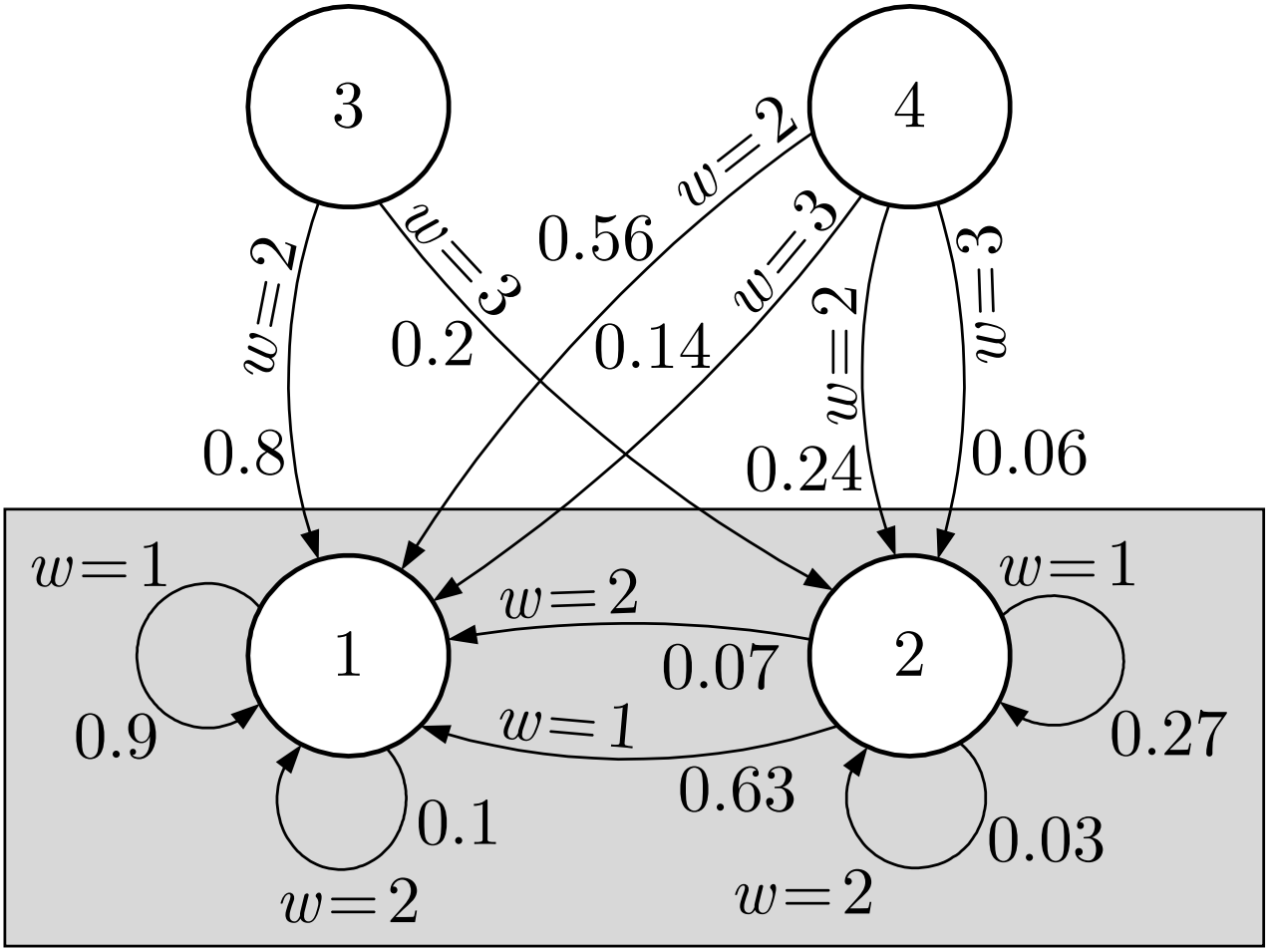

Fig. 11.29. Stochastic automaton with stochastically unobservable set $\{1, 2\}$

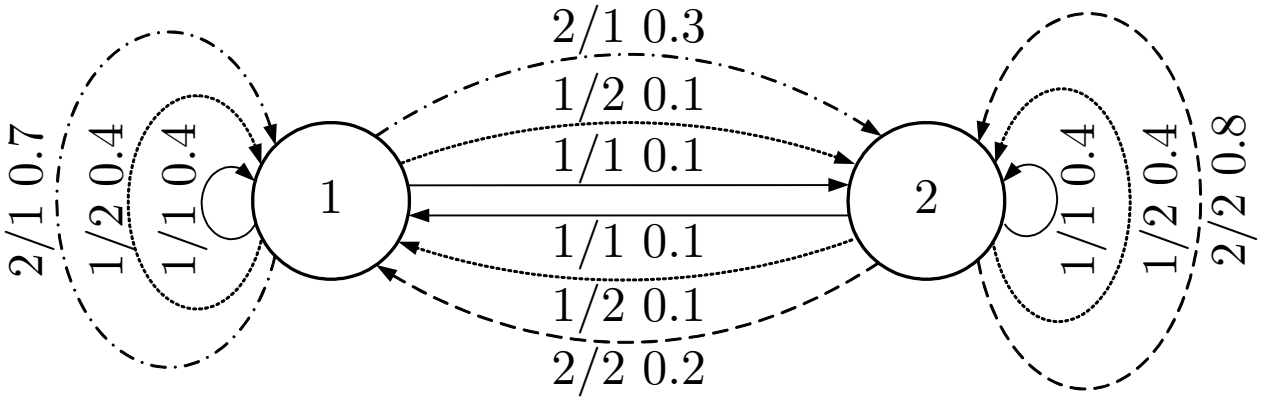

Fig. 11.30. Automaton graph of the example

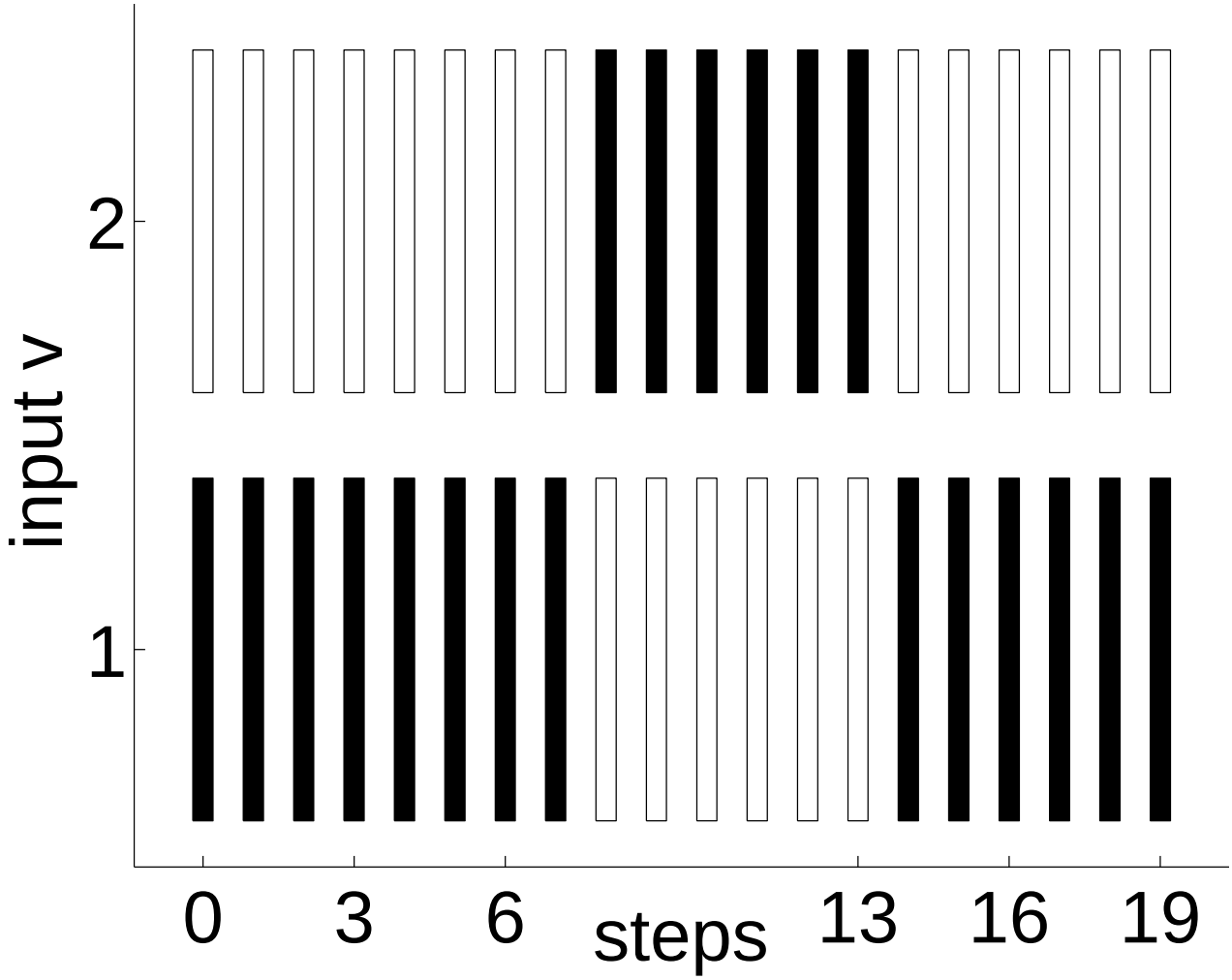

Fig. 11.31. Sequences of input symbols

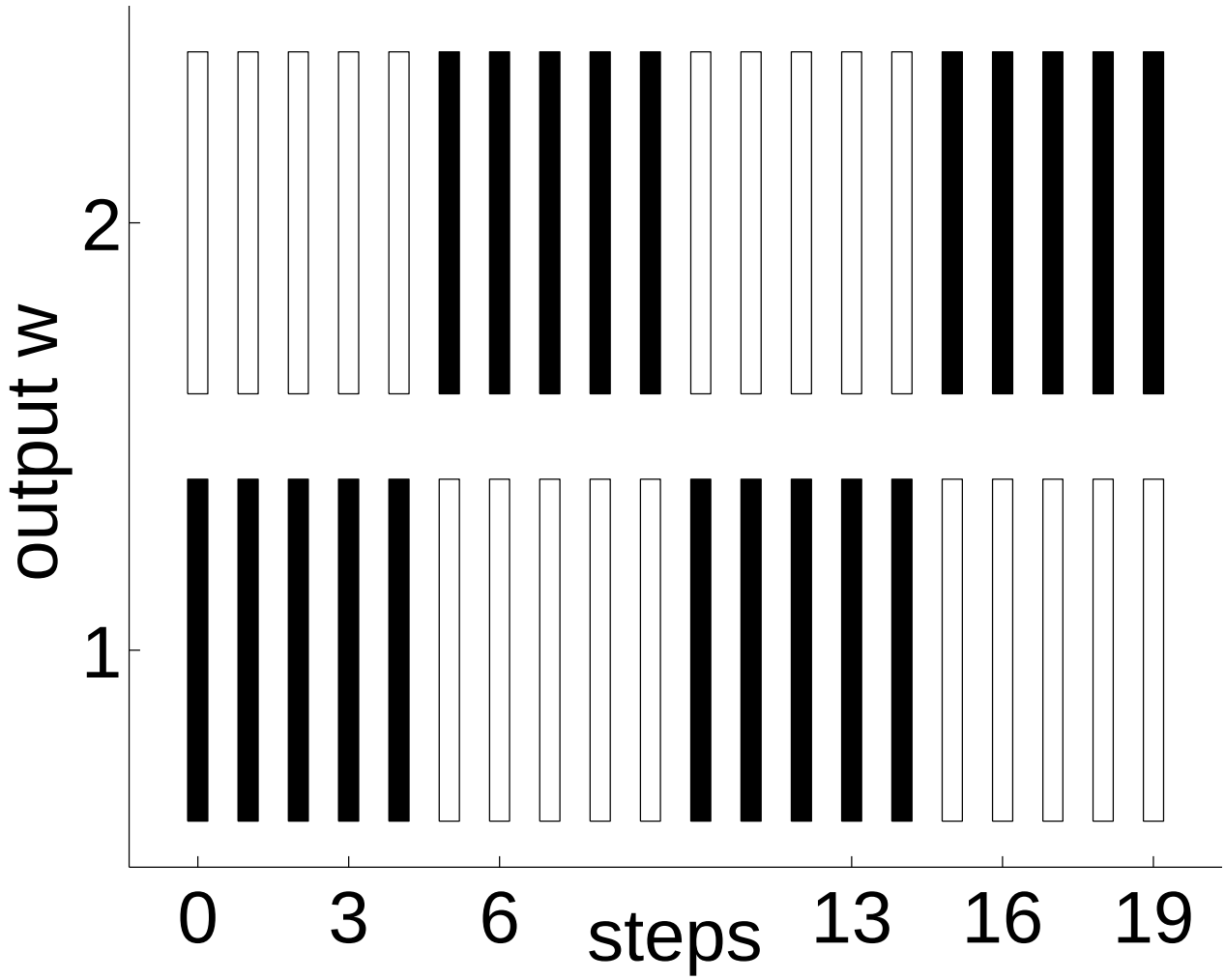

Fig. 11.31. Sequences of output symbols

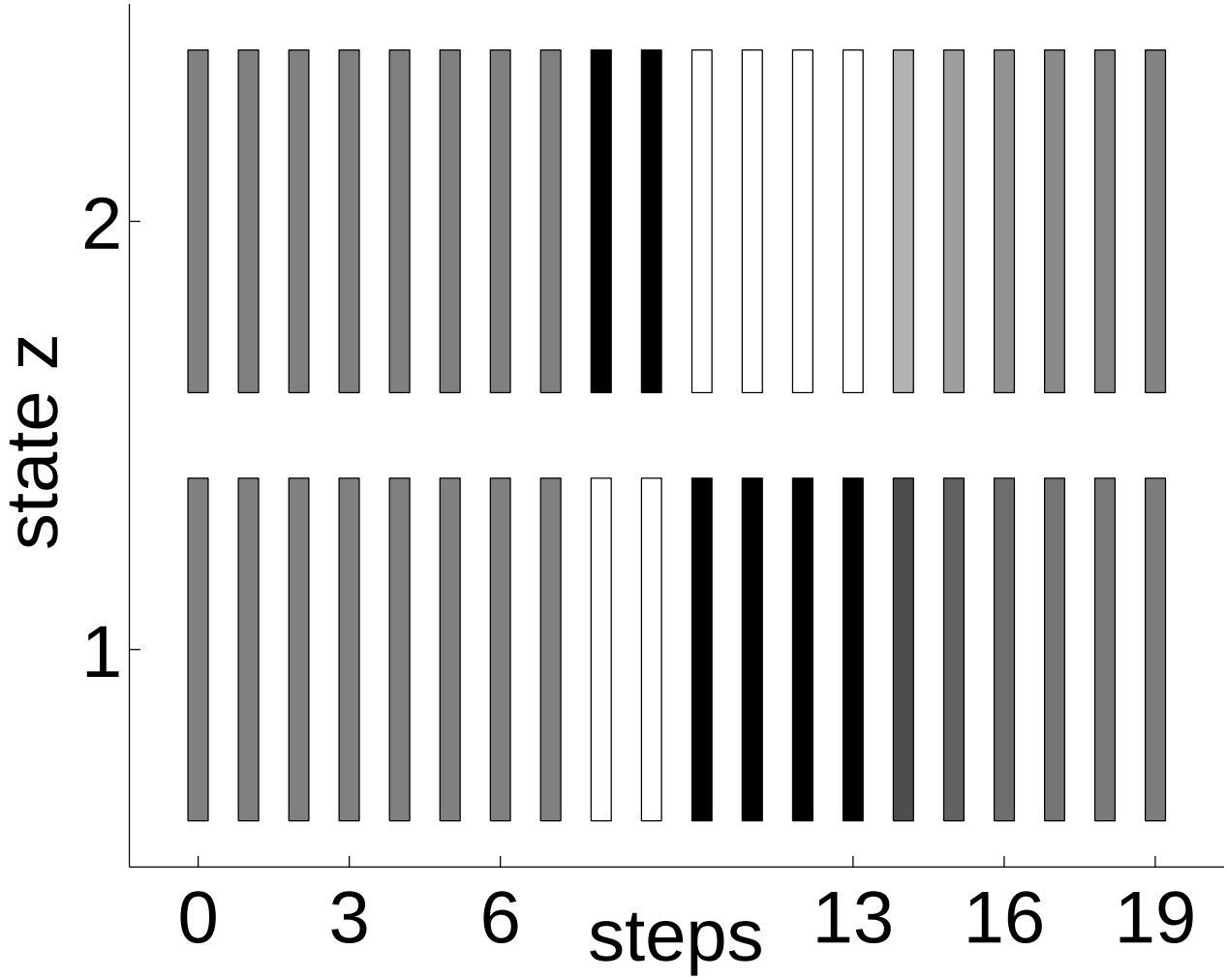

Fig. 11.32. Observation result

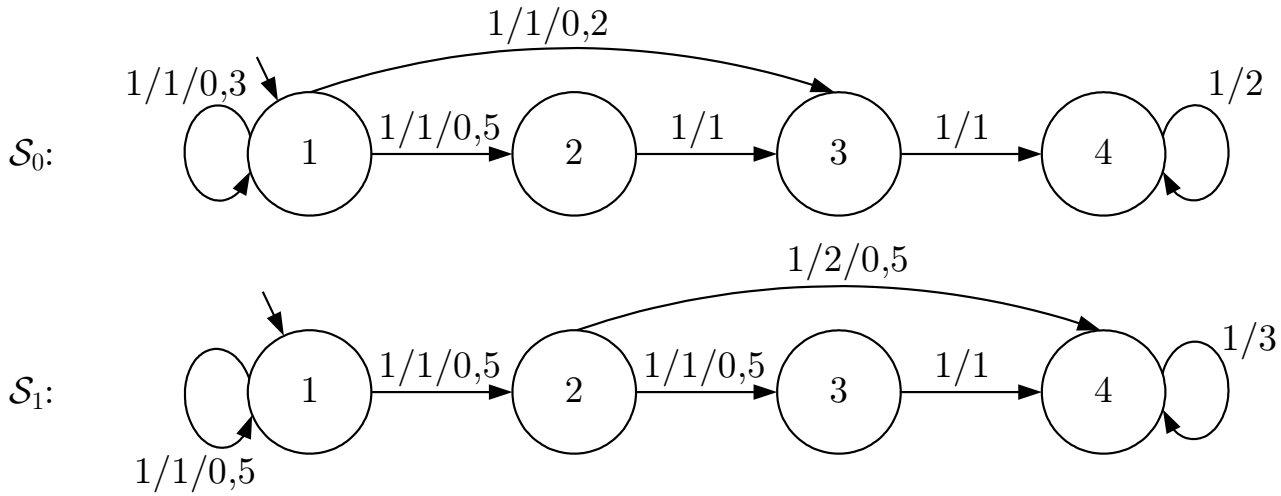

Fig. 11.33. Model of the faultless and the faulty system

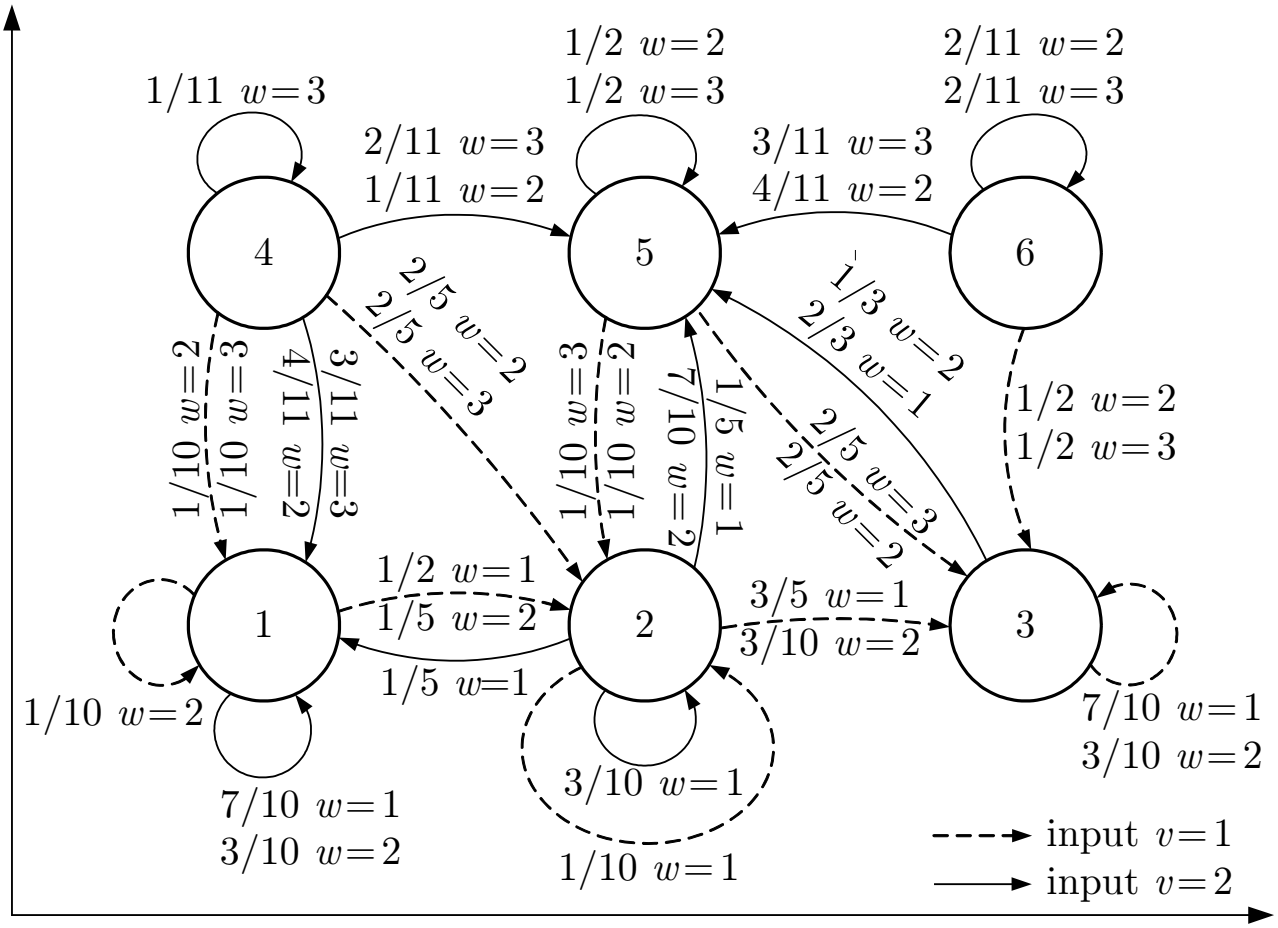

Fig. 11.34. Automaton graph for fault $f = 1$

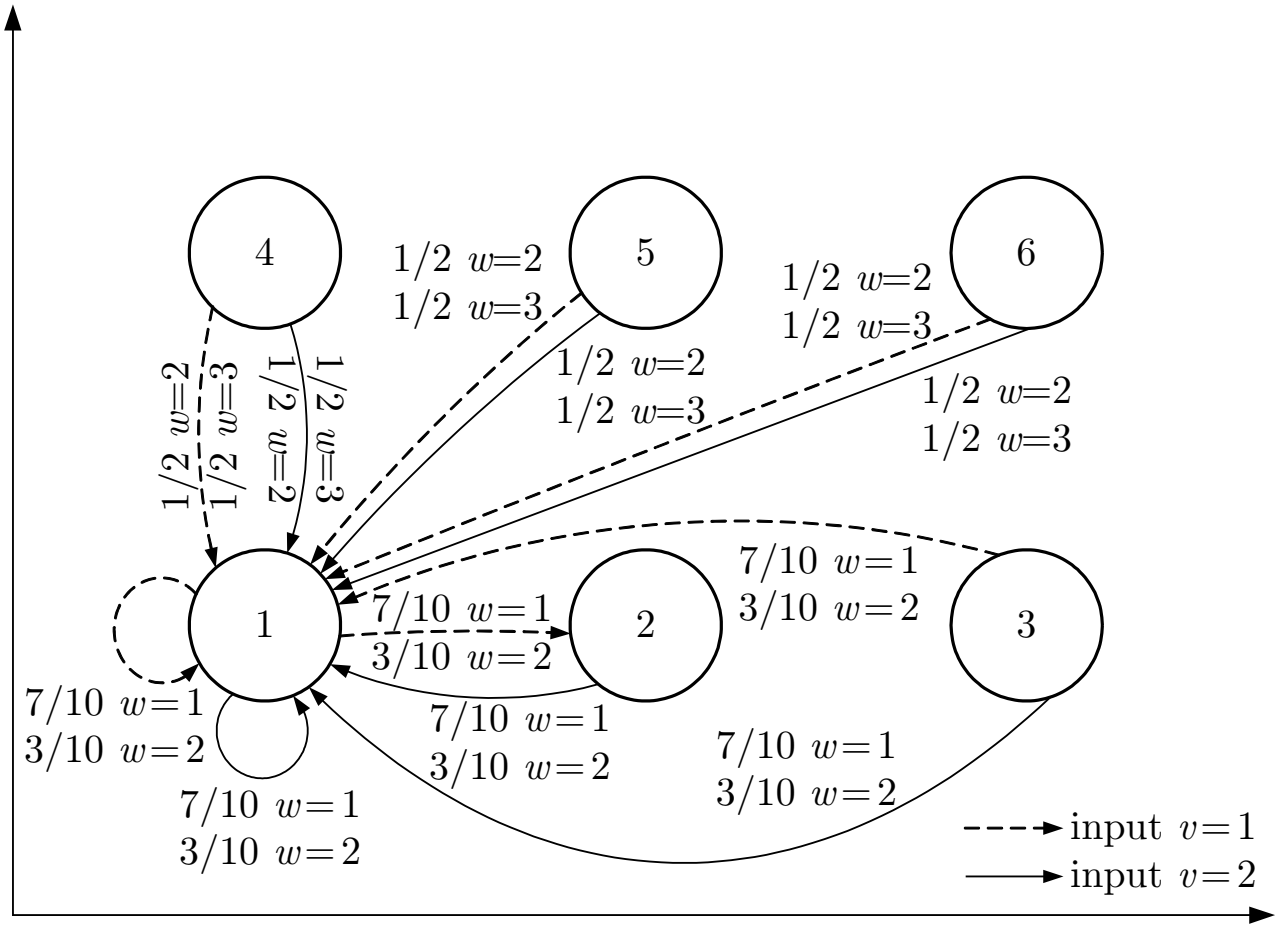

Fig. 11.35. Automaton graph for fault $f = 2$

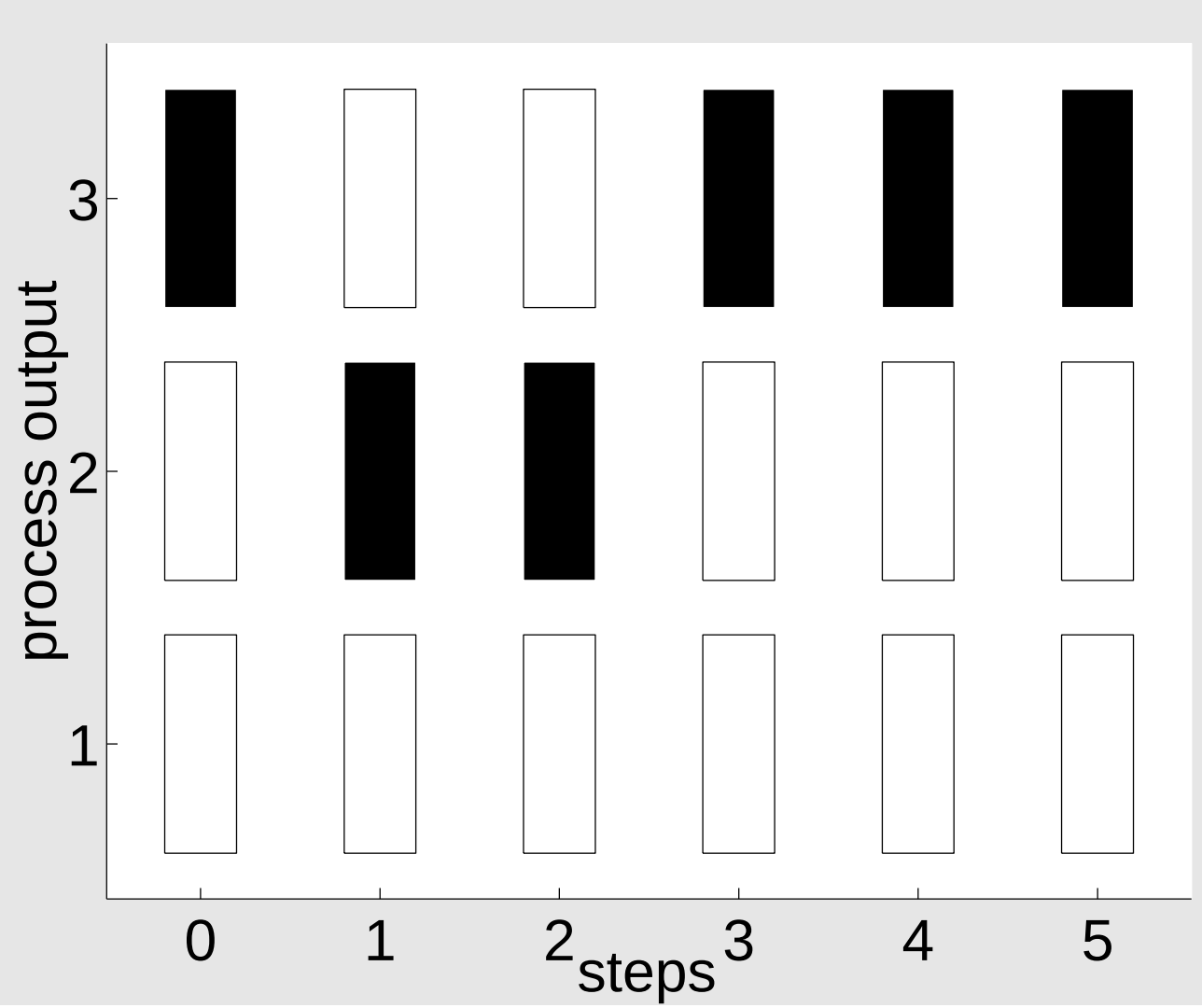

Fig. 11.36. Output sequences for $v = 2, f = 1$

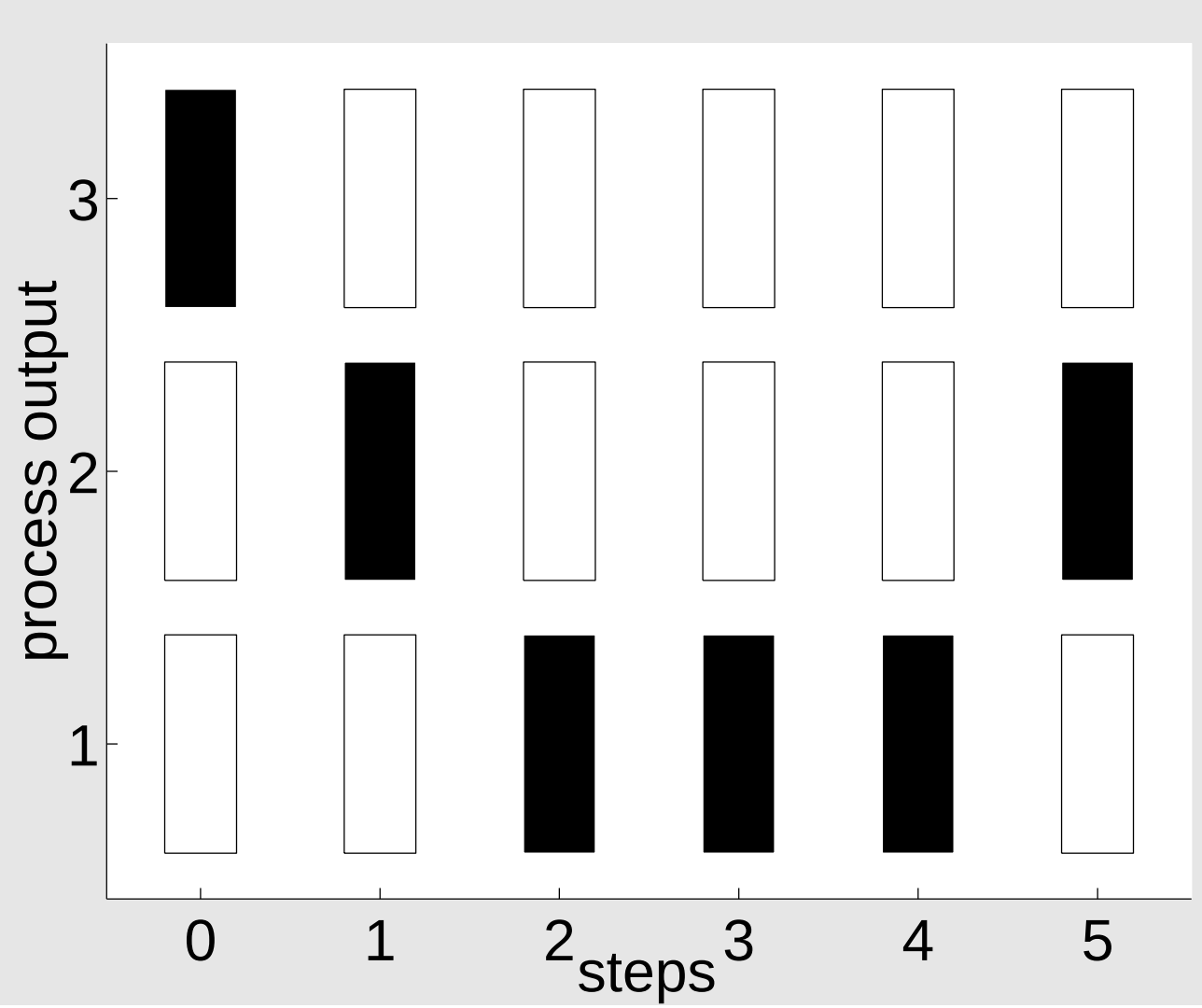

Fig. 11.36. Output sequences for $v = 2, f = 2$

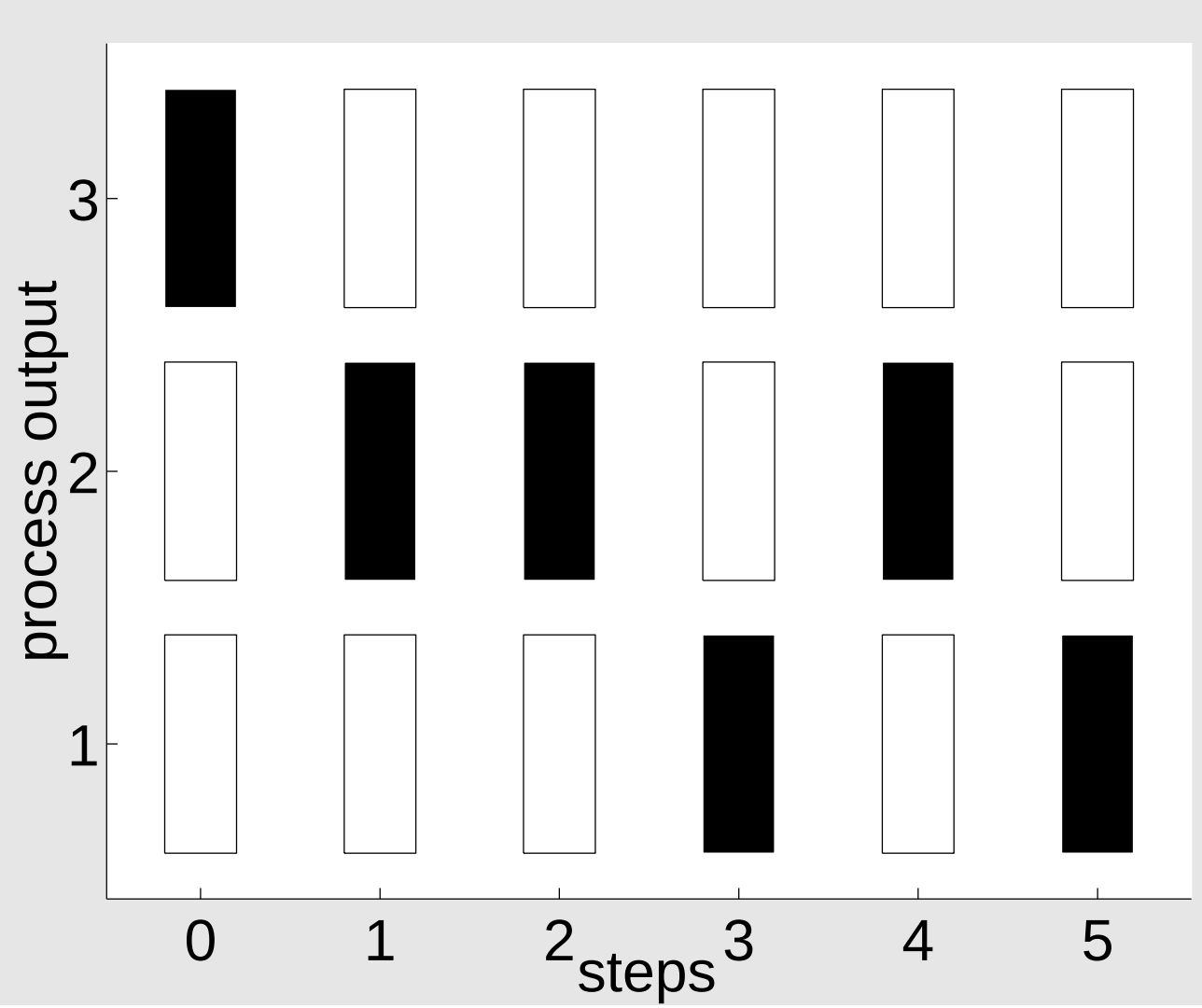

Fig. 11.36. Output sequences for $v = 1$, $f = 1$

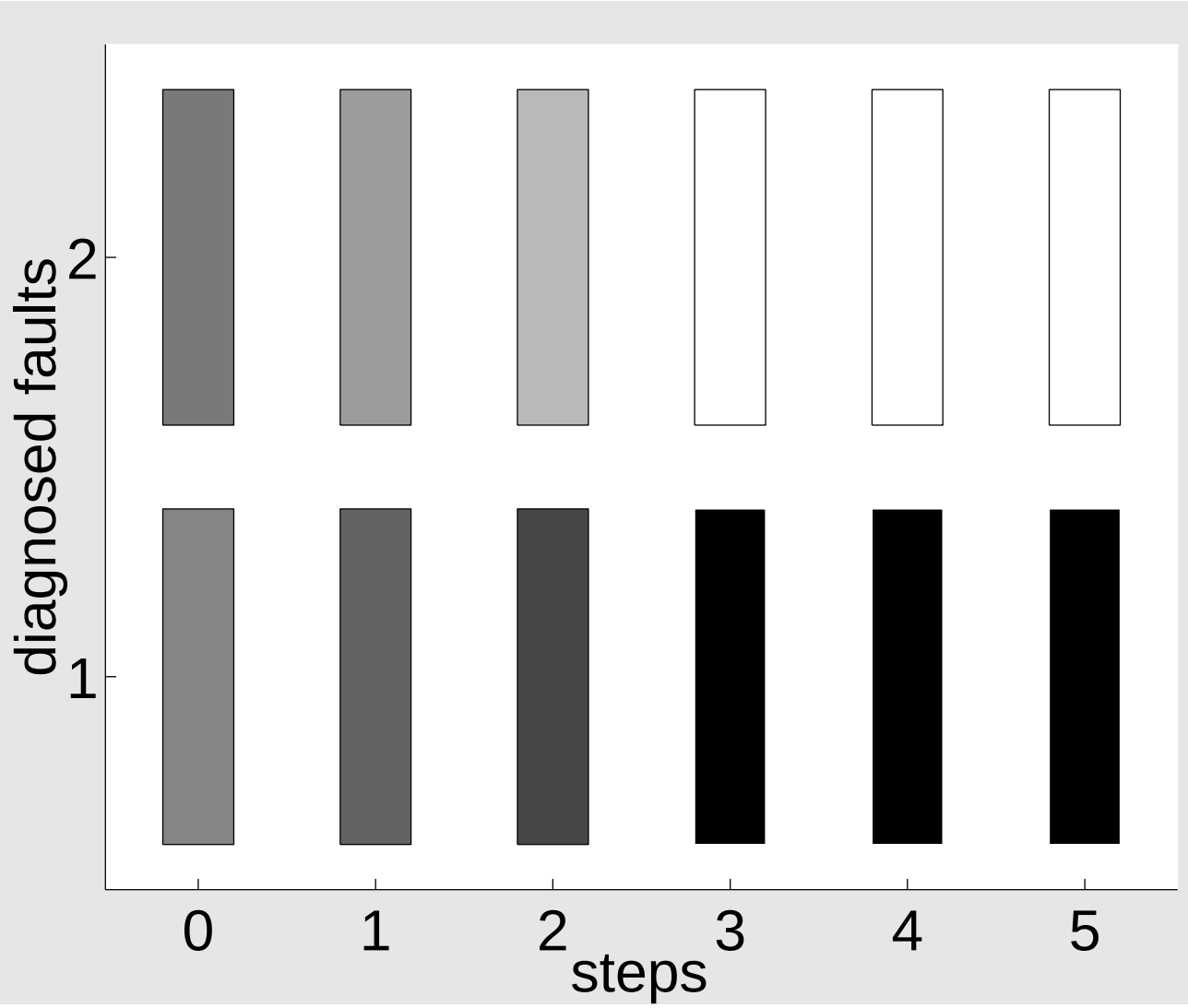

Fig. 11.37. Diagnostic results for the three experiments shown in Fig. 11.36 in the same order (Part 1)

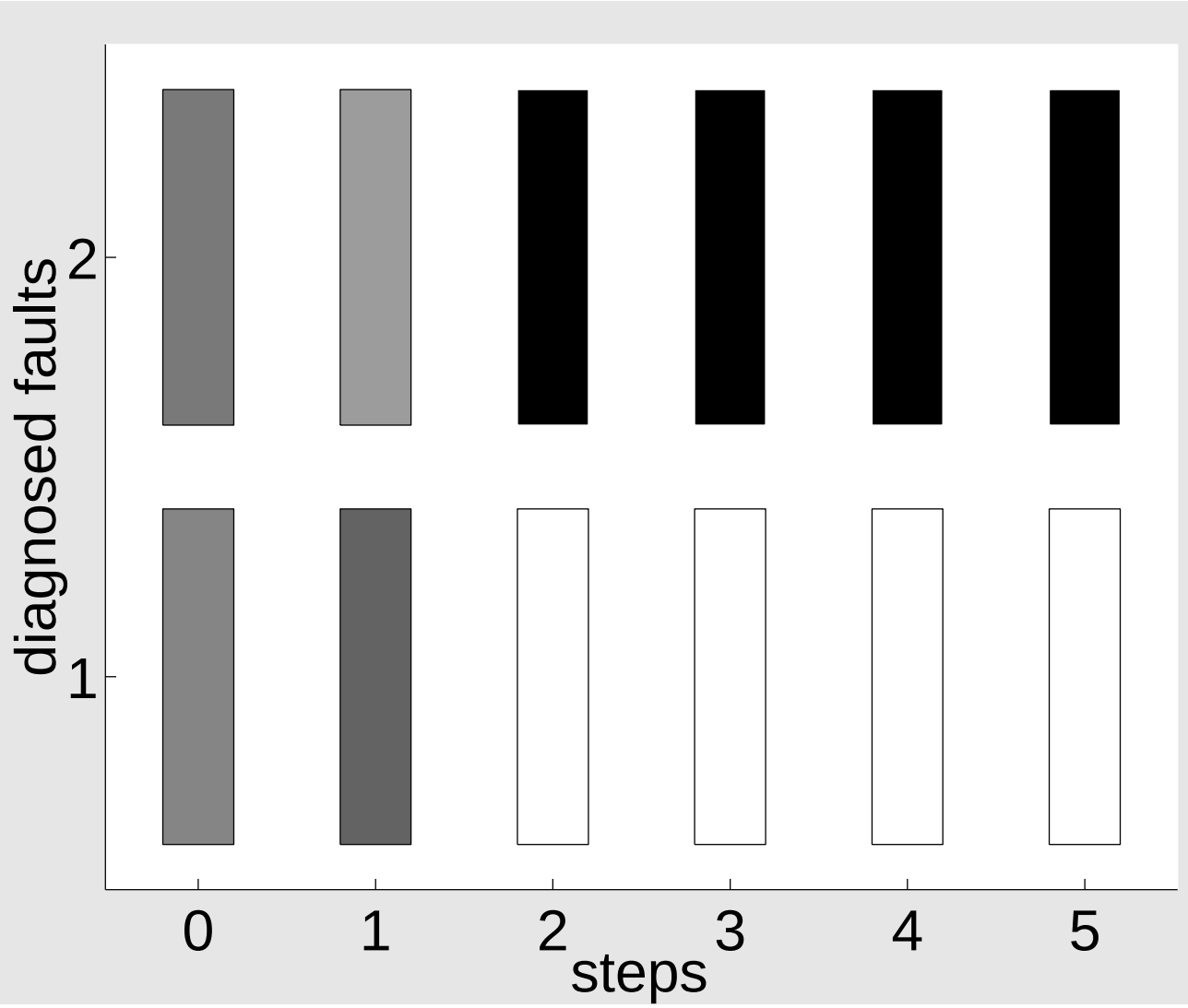

Fig. 11.37. Diagnostic results for the three experiments shown in Fig. 11.36 in the same order (Part 2)

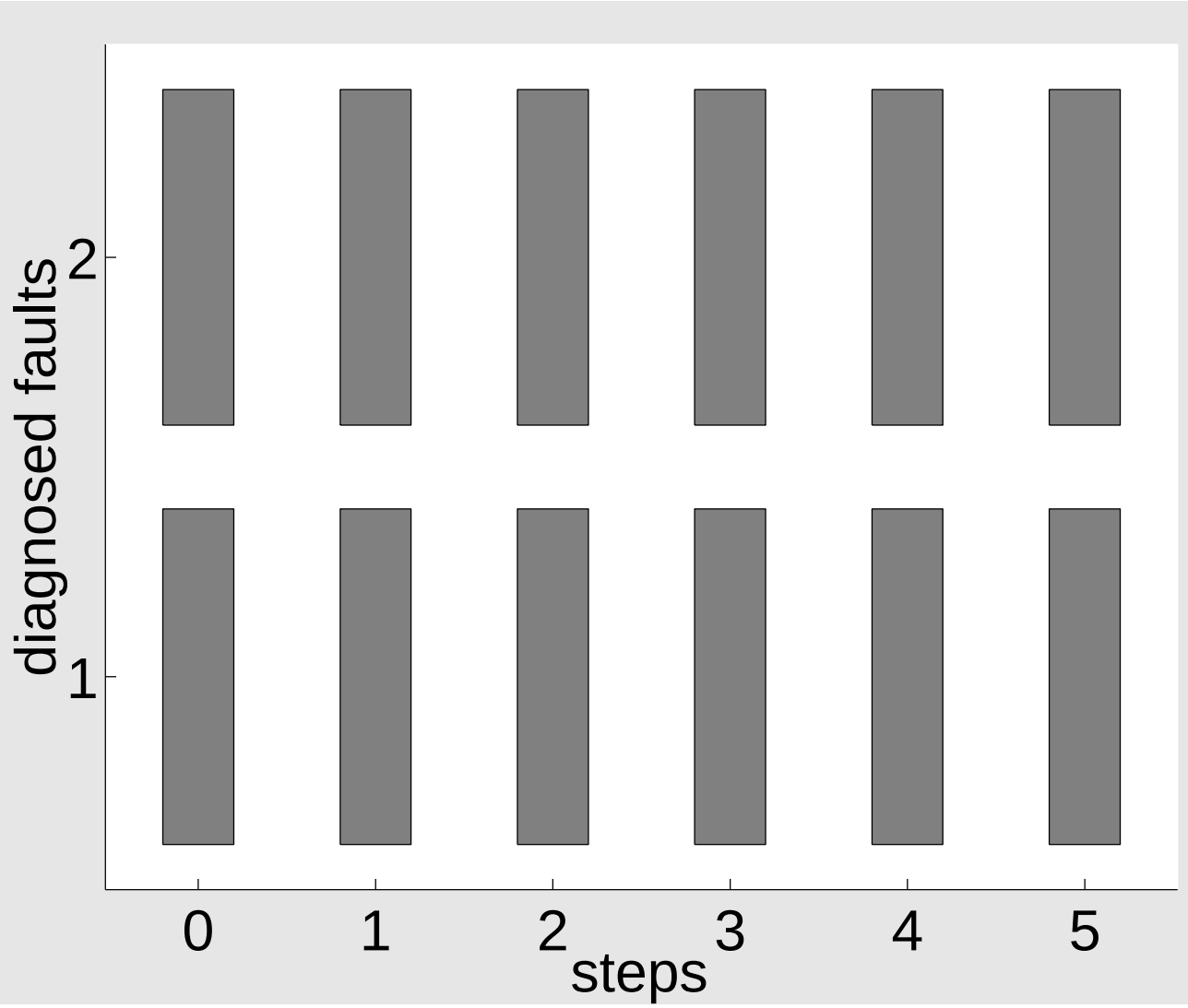

Fig. 11.37. Diagnostic results for the three experiments shown in Fig. 11.36 in the same order (Part 3)

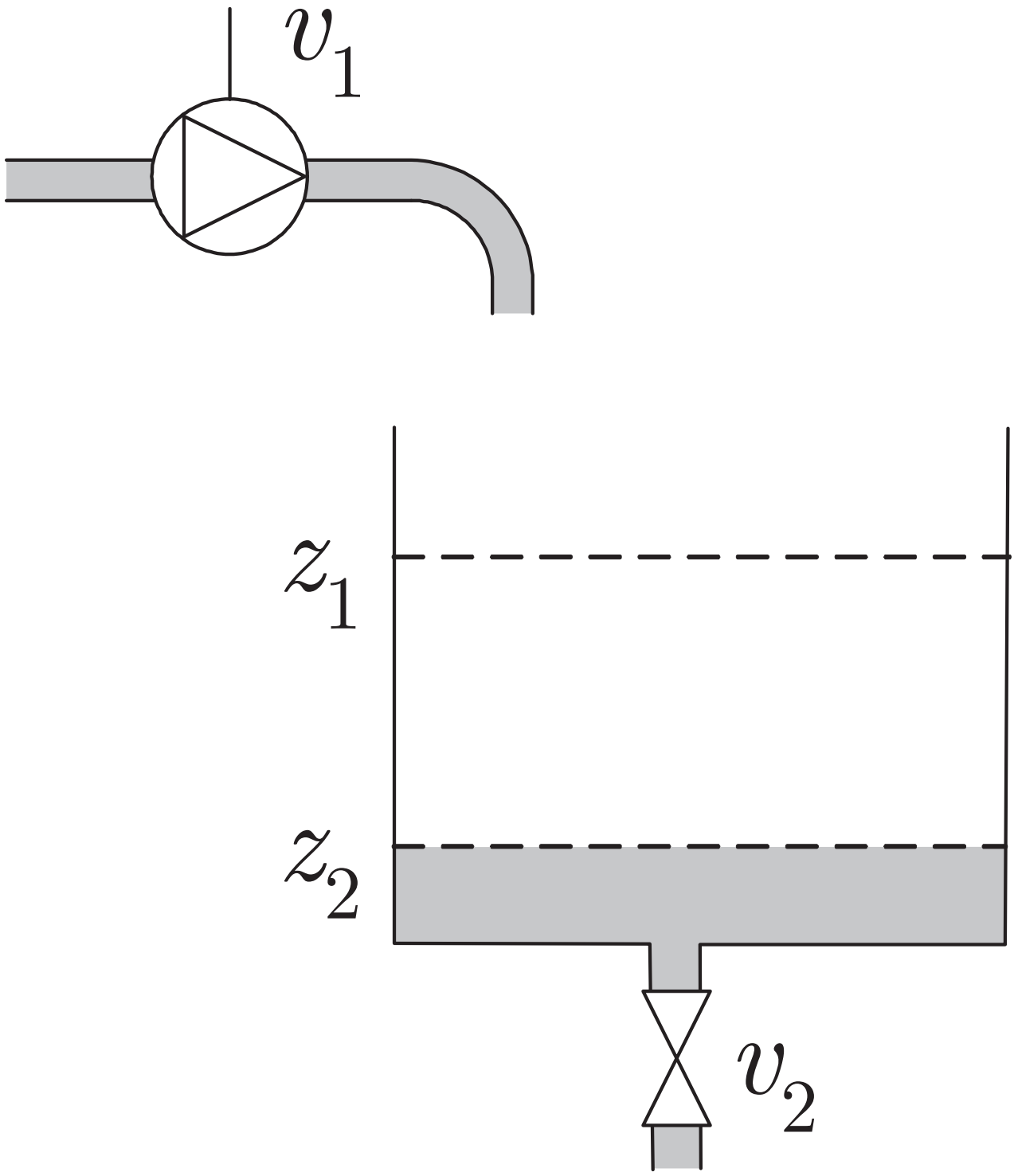

Fig. 11.38. Batch reactor

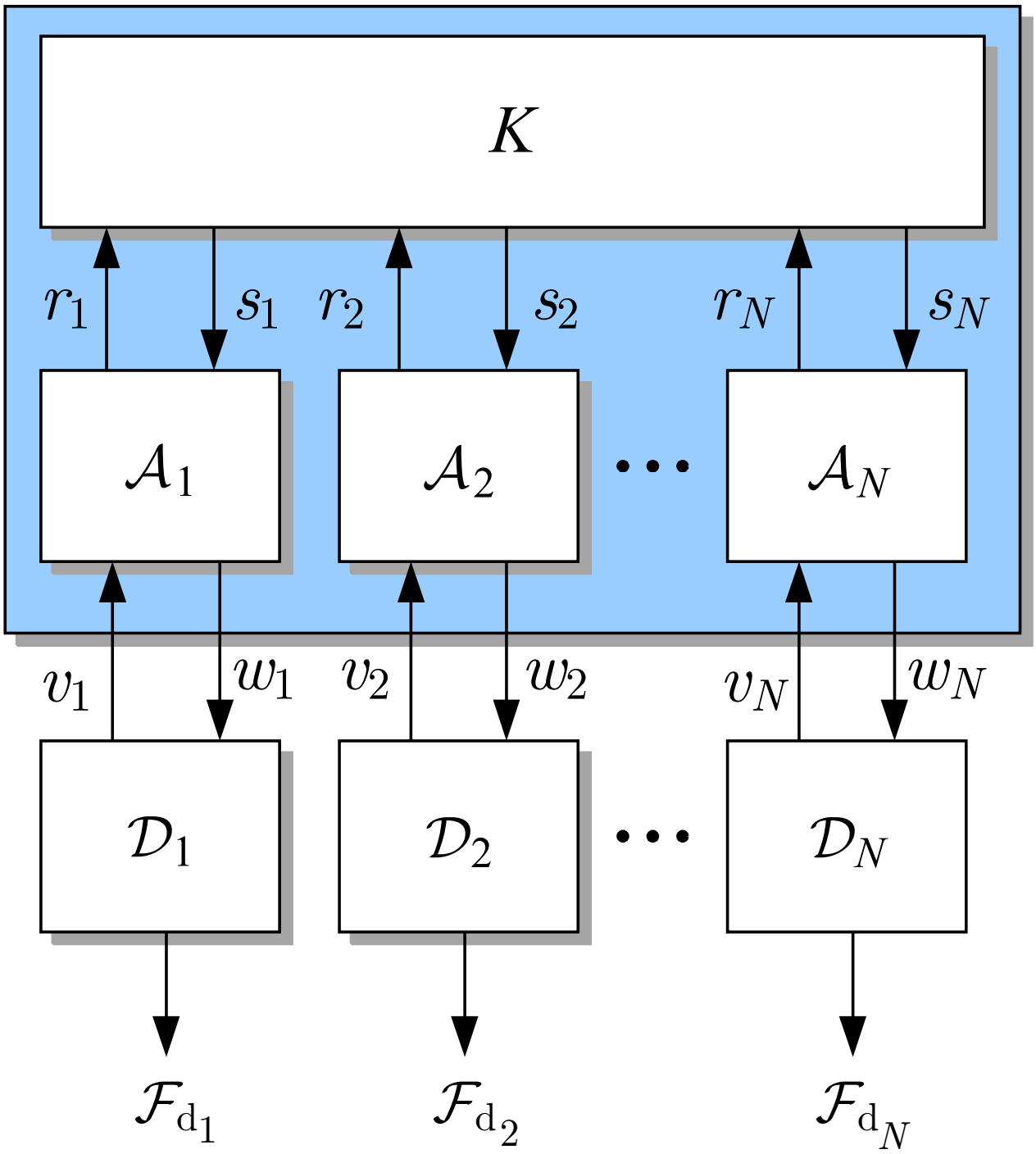

Fig. 12.1. Decentralised diagnosis of interconnected discrete-event systems

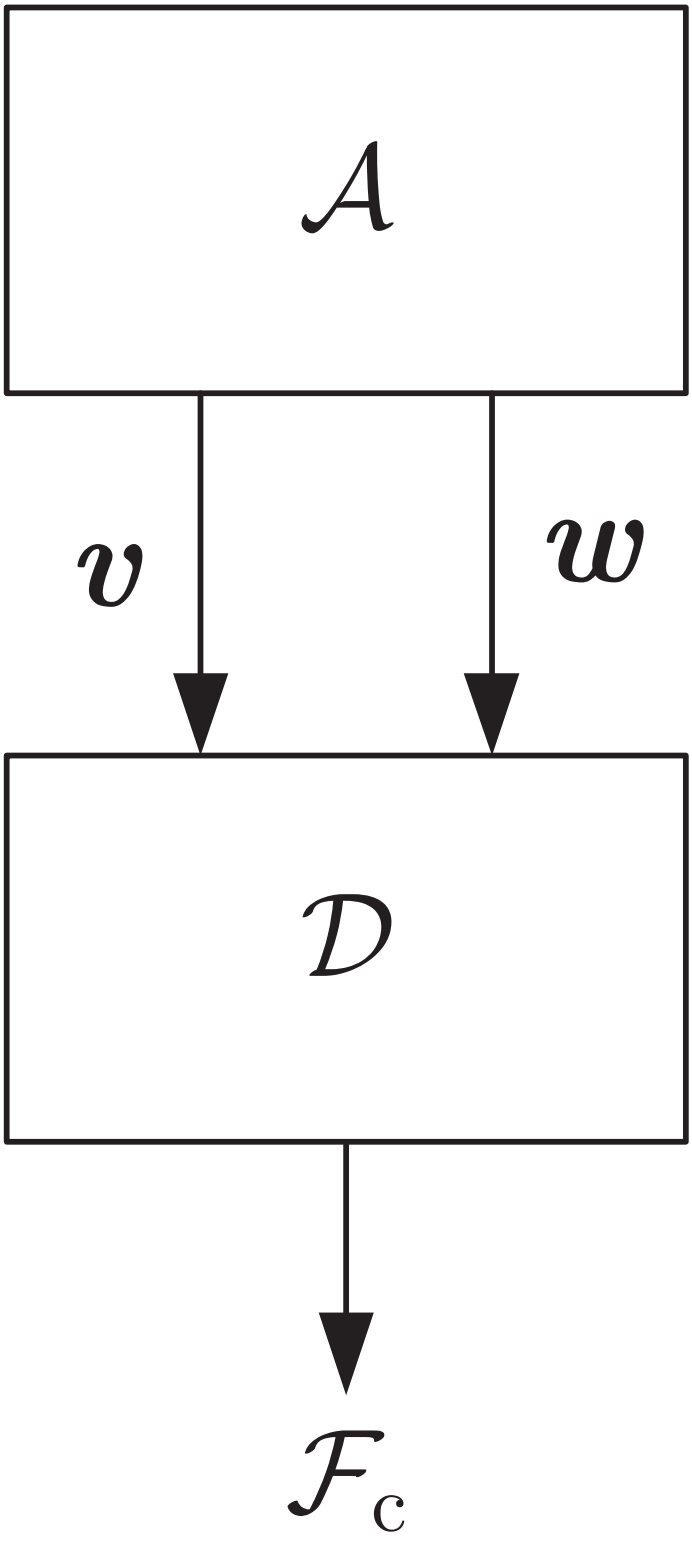

Fig. 12.2. Centralised diagnosis

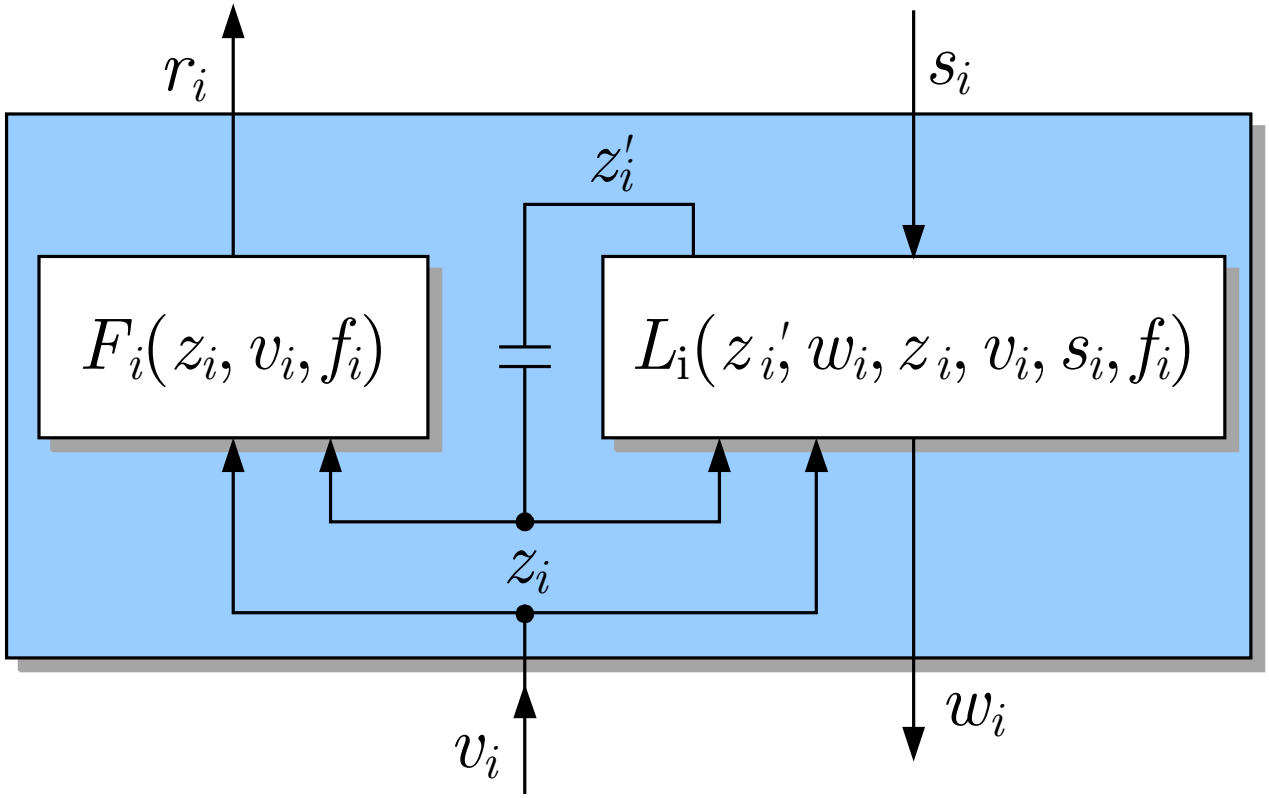

Fig. 12.3. Subsystem model

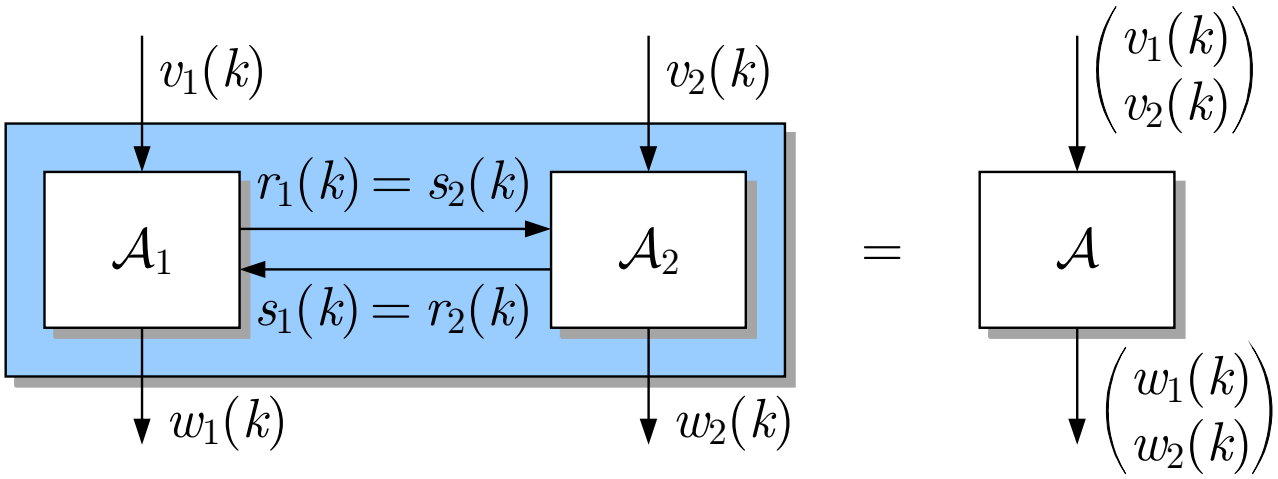

Fig. 12.4. Network with two I/O-automata

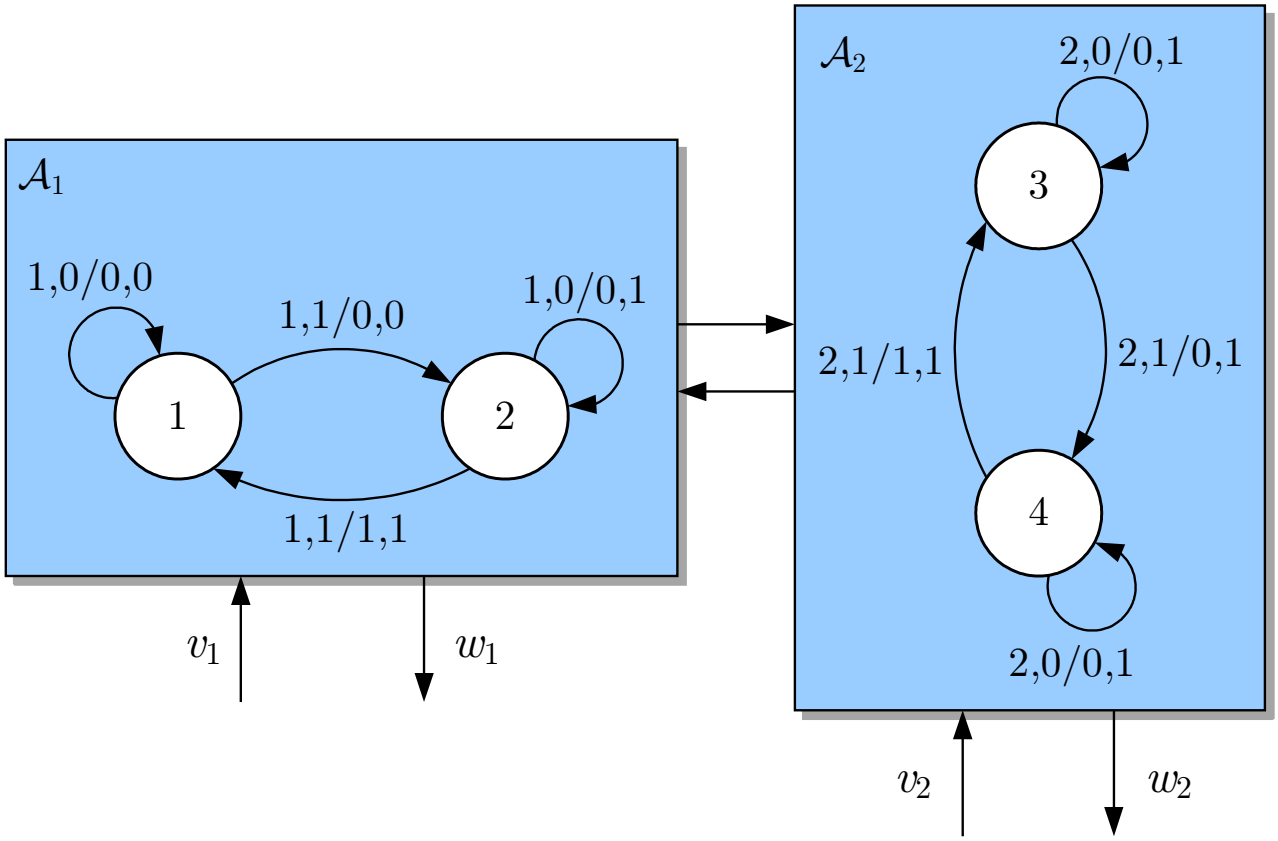

Fig. 12.5. Automata network

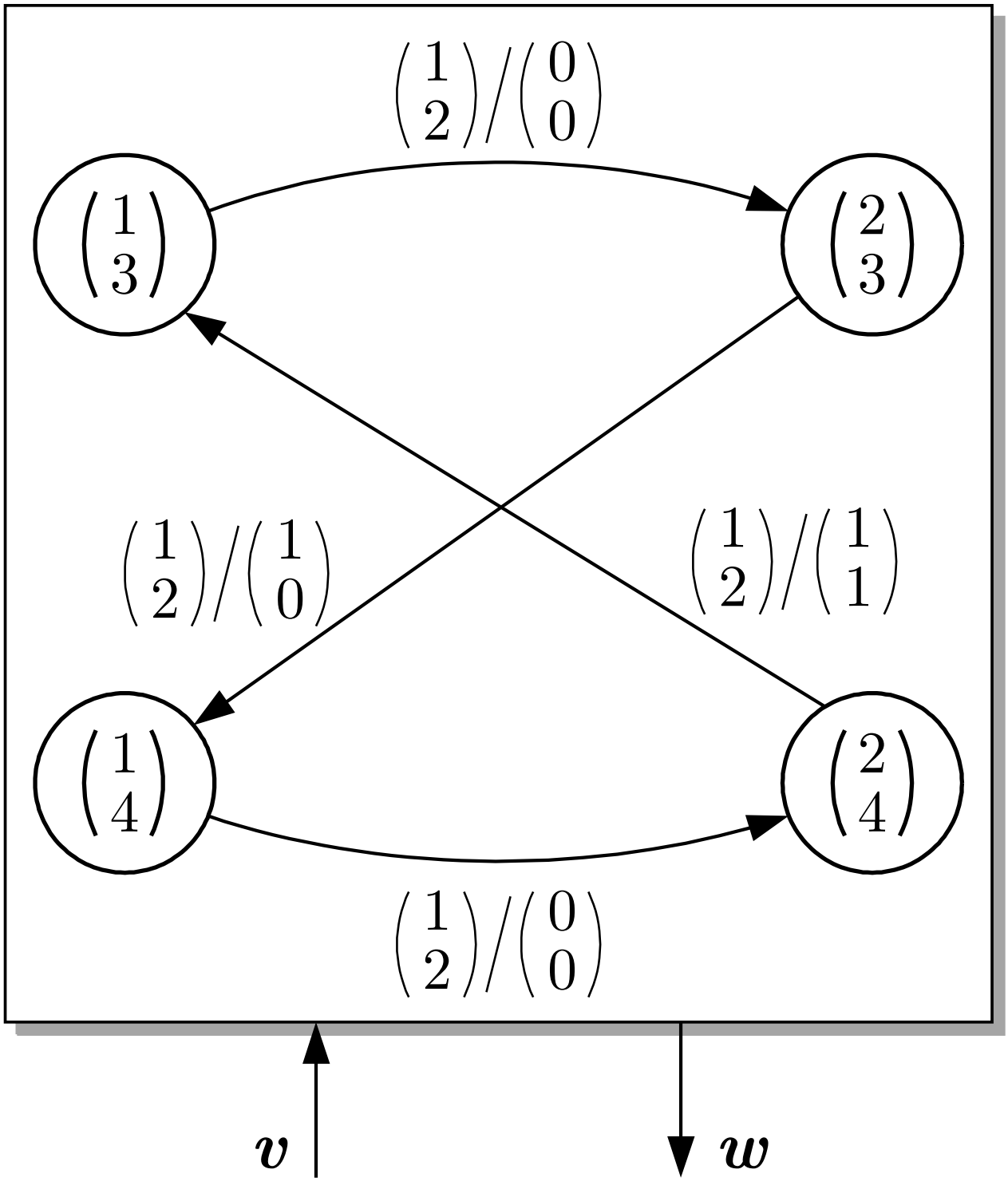

Fig. 12.6. Equivalent deterministic automaton

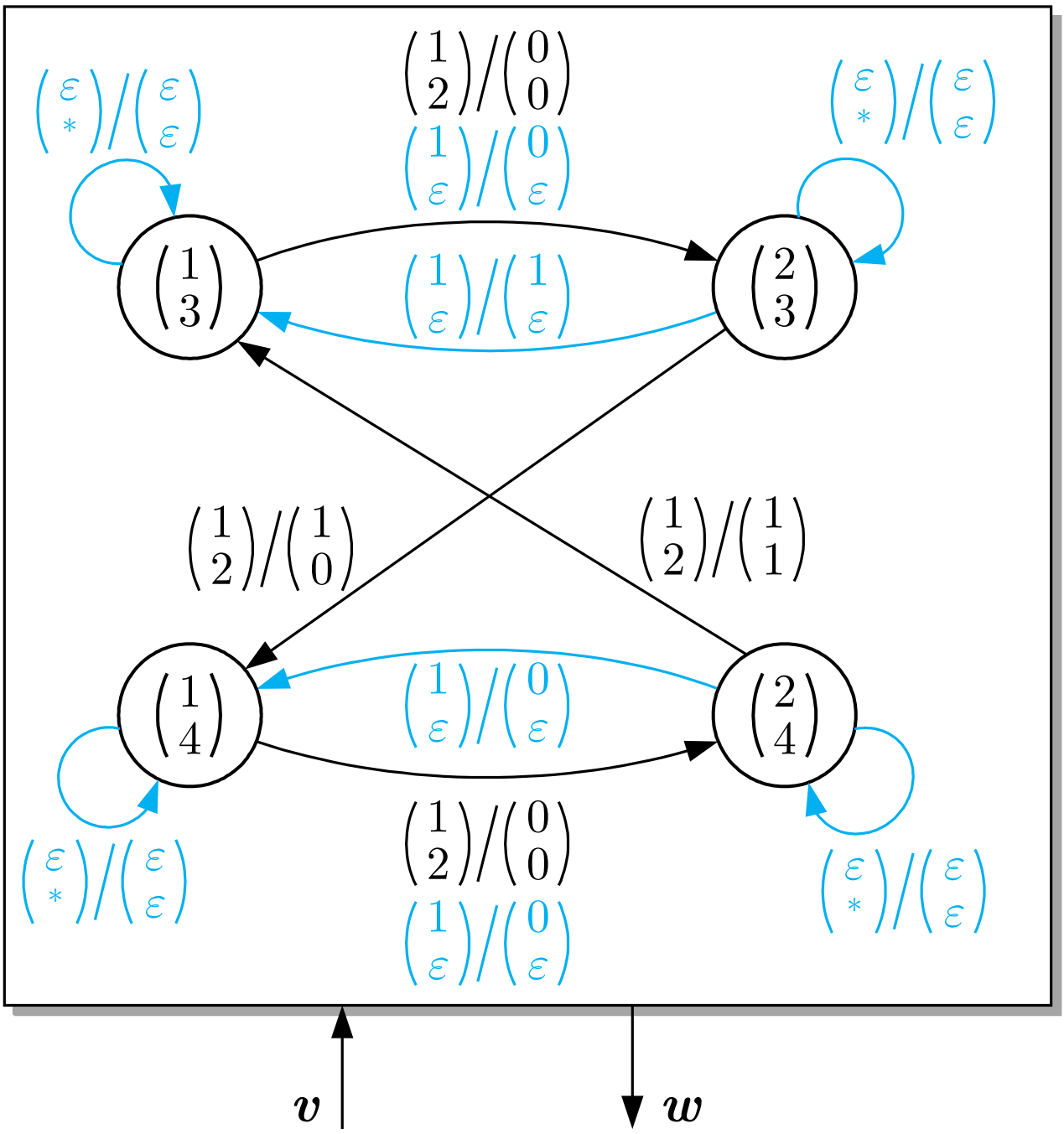

Fig. 12.7. Overall system with asynchronous state transitions

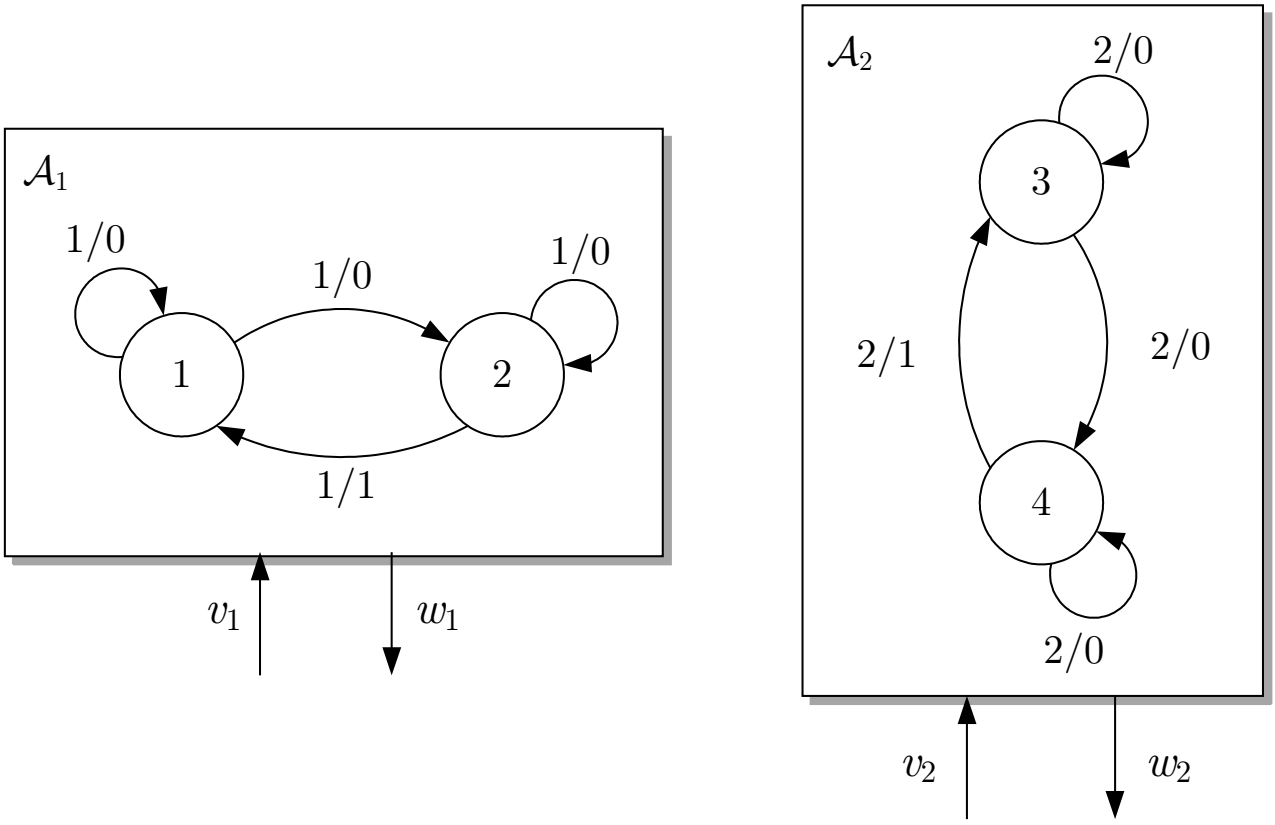

Fig. 12.8. Model of the isolated subsystems

Blanke/Kinnaert/Lunze/Staroswiecki:
Diagnosis and Fault-Tolerant Control, (3rd edition), Springer-Verlag 2015

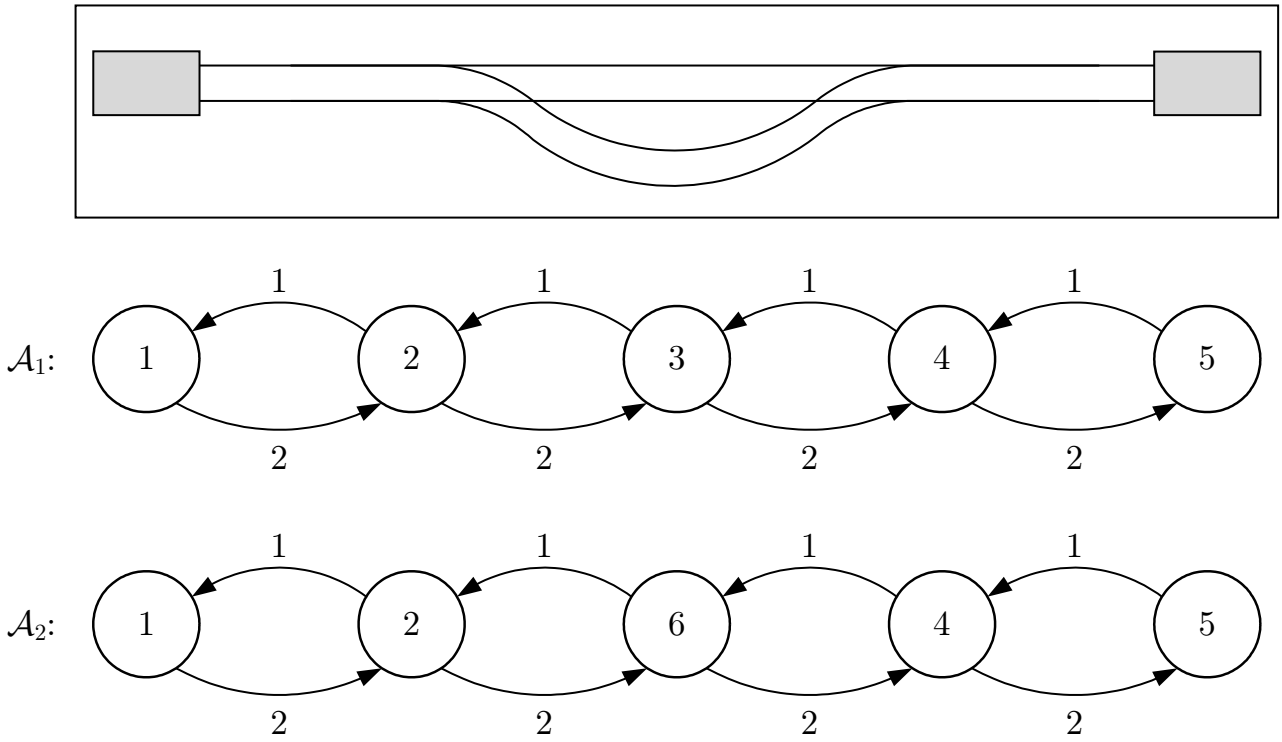

Fig. 12.9. Sketch and subsystem models of a mountain railway

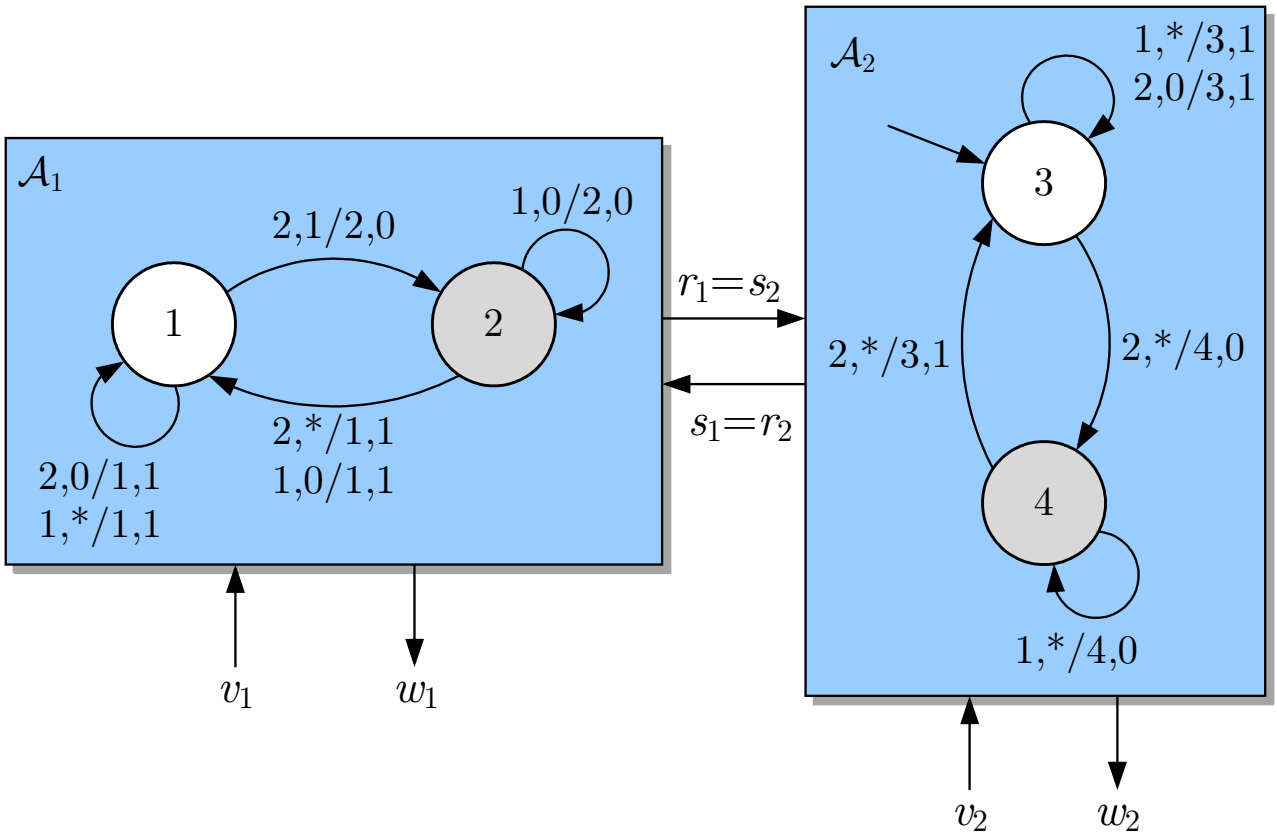

Fig. 12.10. Composite system model

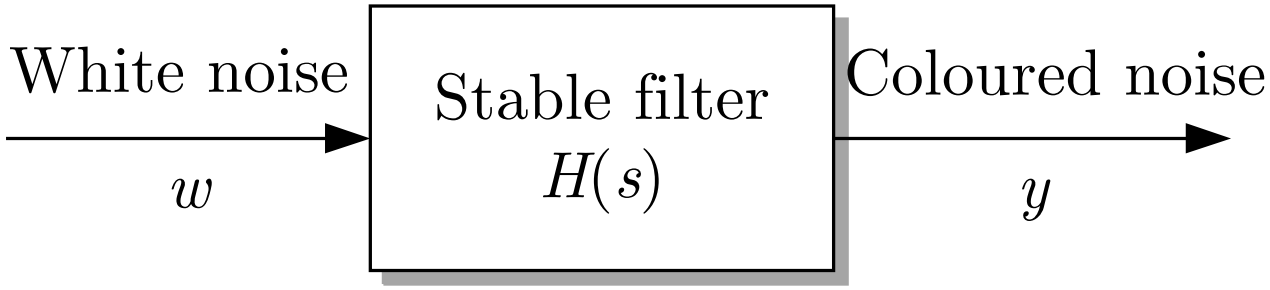

Fig. A2.1. Coloured noise generated by a filtered white noise